

CATALYSTS DEVELOPMENT FOR THE CONVERSION OF SYNGAS TO
HIGHER ALCOHOLS USING ALKALI-PROMOTED MoS₂-BASED
CATALYSTS OVER CARBON SUPPORTS

A Thesis Submitted to the College of
Graduate and Postdoctoral Studies
In Partial Fulfillment of the Requirements
For the Degree of Doctor of Philosophy (Ph.D.)
In the Department of Chemical & Biological Engineering,
University of Saskatchewan
Saskatoon

By:

PHILIP EFFAH BOAHENE

PERMISSION TO USE

In presenting this thesis/dissertation in partial fulfillment of the requirements for a Doctor of Philosophy Degree from the University of Saskatchewan, I agree that the libraries of the University of Saskatchewan may make this thesis freely available for inspection. I further agree that permission for copying of this thesis in any manner, in whole or in part, for scholarly purpose may be granted by Prof. Ajay Kumar Dalai who supervised my thesis work or, in their absence, by the Head of the Department or the Dean of the College of Graduate and Postdoctoral Studies in which the thesis work was done. It is understood that any copying or publication or use of this thesis or parts thereof for financial gain shall not be allowed without my written permission. It is also understood that due recognition shall be given to me and to the University of Saskatchewan in any scholarly use which may be made of any material in my thesis.

Requests for permission to copy or to make other use of material in this thesis in whole or parts shall be addressed to:

Head of the Department of Chemical & Biological Engineering

University of Saskatchewan

57 Campus Drive

Saskatoon, Saskatchewan S7N 5A9, Canada.

OR

Dean

College of Graduate and Postdoctoral Studies

University of Saskatchewan

116 Thorvaldson Building, 110 Science Place

Saskatoon, Saskatchewan S7N 5C9, Canada.

ABSTRACT

Conversion of syngas to mixed (C_1 - C_5) and higher (C_{2+}) alcohols over alkali-doped MoS_2 (ADM) catalysts, promoted with cobalt (Co) and rhodium (Rh), has exhibited great potential for commercial higher alcohols synthesis (HAS) reaction. Carbon-based supports with attractive physico-chemical and mechanical properties have immense potential to be explored for the HAS catalyst development. Due to their characteristic properties such as high surface area, thermal stability, and chemical inertness, this Ph.D study sought to explore three main carbon-based supports namely; multi-walled carbon nanotubes (MWCNTs), ordered mesoporous carbon (OMC) and carbon nanohorns (CNHs) for HAS catalyst formulation. The overall research objective was to explore options to develop novel carbon-supported ADM catalyst systems to effectively convert syngas to higher alcohols. The novelty of the work is in two folds: 1) to investigate the influence of binders incorporation, pelletization, and particle size on the HAS reactions using carbon (MWCNT, OMC and CNH)-supported $KCoRhMoS_2$ catalyst systems; and 2) to explore OMCs and CNHs as new support systems for the HAS reactions.

The influence of binders (bentonite clay, coal tar, and humic acid) addition, catalyst pelletization as well as the comparison of MWCNT and large-pore OMC-supported $KCoRhMo$ catalyst systems were investigated in phases 1 and 2, respectively. Extensive studies in phases 3, 4 and 5 are enumerated as: 3) the comparative study of chemical pre-treatments (acid and base) of OMC-supported $KCoRhMoS_2$ catalysts; 4) the optimization of binder (BC) loadings on OMC-supported $KCoRhMoS_2$ catalysts and their catalytic performance study; and 5) the synthesis, characterization and application of novel K-promoted $CoRhMo$ catalysts supported over CNH and its by-products (OCP_f & OCP) for the HAS reactions. Finally, the impacts of process parameters (temperature, pressure, and gas-hourly-space-velocity) were evaluated using the optimum

KCoRhMo/CNH catalyst. The power law model was then used to fit the experimental data in the kinetic study to ascertain the activation energies (E_a) of ethanol and propanol. Low values of E_a (54.4 and 92.2 kJ/mol, respectively) were obtained compared to those reported by other researchers. Long-term deactivation study of the sulfided KCoRhMo/CNH catalyst corroborated its durability over 500 h of continuous HAS reaction in a fixed bed reactor.

ACKNOWLEDGEMENTS

My sincere appreciation and gratitude goes to Professor Ajay Kumar Dalai for his exceptional supervision, constructive criticism and unlimited enthusiasm for intellectual growth which positively impacted my learning experience. I am also extremely grateful for his valued guidance and supervision throughout the planning, execution, and communication of my thesis work. I am also sincerely grateful to my co-supervisor, Dr. Ramaswami Sammynaiken, for his invaluable support, guidance and thoughtful suggestions throughout my program. Furthermore, I am most indebted to the members of my advisory committee: Drs. Meda Venkatesh, Medhi Nemati, Hui Wang, Jafar Soltan (Department of Chemical & Biological Engineering, University of Saskatchewan) and Dr. Lee Wilson (Department of Chemistry, University of Saskatchewan). I also want to be grateful to Dr. Burtron H. Davis for accepting to be the external examiner for my defense. My special thanks also go to Mr. Richard Blondin and Miss Heli Eunike for their constant technical support in the laboratory. Also, thanks are due to all members of the Catalysis and Chemical Reaction Engineering Laboratories (CCREL) for their support throughout my study. My gratitude also goes to the Natural Science and Engineering Research Council of Canada (NSERC) and BioFuelNet, Canada, for their much needed financial assistance. I would also like to thank all the professors and graduate students who have contributed to my studies at the University of Saskatchewan. I also thank my friends and colleagues of the CCREL at the Department of Chemical and Biological Engineering, University of Saskatchewan, for being cooperative and supportive.

Above all, I acknowledge the special grace, guidance and protection of Almighty God, without whom this accomplishment could not have been achieved.

DEDICATION

I dedicate this thesis to the following:

- ❖ Mrs. Trisha Effah Boahene, my lovely wife, my best friend and the solid woman behind this successful accomplishment. I wish I could find the appropriate words to adequately thank her for the candor and all the support she continues to provide.
- ❖ To our 4 months old lovely son, Philip Effah Boahene, Jr. You are so adorable and you've brought us so much joy.
- ❖ My dear mum, Miss Beatrice Kwofie, for the numerous sacrifices, years of support, encouragement and steadfast love.
- ❖ To the memory of my dad, Mr. Tonny Effah Gyamfi, for his good & disciplined upbringing. May his soul continue rest in the bosom of the Almighty.
- ❖ To my siblings and in-laws for their diverse supports throughout my studies.

TABLE OF CONTENTS

PERMISSION TO USE.....	i
ABSTRACT.....	ii
ACKNOWLEDGEMENTS.....	iv
DEDICATION.....	v
TABLE OF CONTENTS.....	vi
LIST OF TABLES.....	xiii
LIST OF FIGURES.....	xvi
NOMENCLATURE AND ABBREVIATIONS.....	xxii

CHAPTER 1

1. Introduction and Thesis Outline.....	1
1.1. Introduction.....	1
1.1.1. Ethanol and higher alcohols as motor fuels.....	3
1.2. Knowledge gaps.....	4
1.2.1. Hypotheses.....	5
1.2.2. Research objectives.....	6
1.3. Organization of the Thesis.....	8
1.4. Manuscript Content of the Thesis.....	9

CHAPTER 2

2. Literature review: Gas-to-Liquid technology and higher alcohols from syngas.....	13
2.1. Introduction.....	14
2.1.1. Synthesis gas production and cleaning.....	14
2.1.2. Syngas from biomass, coal and natural gas.....	15
2.2. Conversion of syngas to products.....	16
2.2.1. Fischer-Tropsch synthesis from syngas conversion.....	17
2.2.2. Higher alcohol synthesis from syngas conversion.....	18

2.3. Catalyst systems for higher alcohols synthesis.....	20
2.3.1. High-temperature methanol synthesis catalysts.....	20
2.3.2. Low-temperature methanol synthesis catalysts.....	21
2.3.3. Fe, Ni, Co-modified low temperature MeOH synthesis catalysts.....	22
2.3.4. Supported Rhodium-group catalysts.....	23
2.3.5. Alkali-modified molybdenum-based catalysts.....	24
2.4. Catalyst supports from higher alcohols synthesis.....	26
2.5. Catalyst preparation and pre-treatment conditions.....	29
2.6. Reaction mechanisms for higher alcohols synthesis.....	31
2.7. The Anderson-Schulz-Flory distribution.....	35

CHAPTER 3

3. Experimental methods and characterization techniques.....	37
3.1. Introduction.....	37
3.2. Synthesis and preparation of pristine supports.....	38
3.2.1. Synthesis of ordered mesoporous carbon support with F127 as template.....	38
3.2.2. Carbon nanohorns support and by-products syntheses.....	40
3.2.3. Chemical pre-treatments of pristine supports.....	42
3.2.4. Preparation of K-promoted supported catalysts.....	43
3.2.5. Preparation of binders-incorporated catalysts and pelletization.....	44
3.3. Characterization techniques of supports and catalysts.....	46
3.3.1. N ₂ -adsorption/desorption measurement.....	46
3.3.2. Wide-angle X-ray diffraction.....	47
3.3.3. Transmission electron microscopic analysis.....	47
3.3.4. Inductively Coupled Plasma Mass Spectroscopy.....	48
3.3.5. Fourier Transform Infra-red analysis.....	48
3.3.6. Boehm titration.....	49
3.3.7. Raman spectroscopic analysis.....	49

3.3.8. Thermogravimetric analysis.....	49
3.3.9. Temperature programmed reduction analysis.....	50
3.3.10. Mechanical strength analysis.....	50
3.4. Catalytic activity studies.....	51
3.5. Products sampling and composition analyses.....	52

CHAPTER 4

4. Influence of pelletization, particle size and incorporation of binders in the formation of KCoRhMoS₂/MWCNT catalysts for higher alcohols synthesis.....	54
4.1. Abstract.....	55
4.2. Introduction.....	56
4.3. Experimental.....	57
4.4. Results and Discussion.....	58
4.4.1. Physical catalysts characterizations.....	58
4.4.2. Chemical catalysts characterizations.....	65
4.5. Catalytic performance tests of MWCNT-supported KCoMoRh catalysts.....	72
4.5.1. Effect of particle size on CO conversion.....	73
4.5.2. Effect of binders on CO conversion.....	75
4.5.3. Effects of temperature on alcohol products distribution.....	76
4.6. Conclusions.....	80

CHAPTER 5

5. Comparative study of large-pore OMC and MWCNT-supported K-CoRhMoS₂ catalysts for higher alcohols synthesis.....	82
5.1. Abstract.....	83
5.2. Introduction.....	84
5.3. Experimental.....	86
5.4. Results and Discussion.....	86
5.4.1. N ₂ adsorption/desorption measurement.....	86
5.4.2. Elemental analysis.....	91

5.4.3. Wide-angle X-ray diffraction.....	92
5.4.4. Raman spectroscopic analysis.....	94
5.5. CO Hydrogenation Reaction for Higher Alcohol Synthesis.....	96
5.5.1. Alcohol Products Distribution and the Anderson–Schulz–Flory Plots.....	100
5.6. Conclusions.....	103

CHAPTER 6

6. Effects of chemical oxidative treatments (acid and base) of ordered mesoporous carbon-supported KCoRhMoS₂ catalysts for higher alcohols synthesis.....	104
6.1. Abstract.....	105
6.2. Introduction.....	106
6.3. Experimental.....	108
6.4. Results and Discussion.....	108
6.4.1. N ₂ -adsorption/desorption measurement.....	108
6.4.2. Elemental analysis.....	116
6.4.3. Wide-angle X-ray diffraction.....	116
6.4.4. Raman spectroscopic analysis.....	118
6.4.5. Fourier Transform Infra-red analysis.....	122
6.4.6. Thermogravimetric analysis.....	125
6.4.7. Temperature programmed reduction analysis.....	128
6.4.8. Transmission Electron Microscopic analysis.....	131
6.5. Catalytic Performance Tests of OMC-supported KCoMoRh Catalysts.....	133
6.5.1. Effect of chemical pretreatment of OMC supports on CO Conversion.....	133
6.5.2. Effects of chemical treatment on alcohol products distribution.....	135
6.5.3. Effects of temperature on alcohol products distribution.....	137
6.5.4. Alcohol products distribution and the ASF Plots.....	139
6.6. Conclusions.....	142

CHAPTER 7

7. Application of novel K-promoted CoRhMo catalysts supported over carbon nanohorns (CNHs) and its by-products (OCP & OCP_f) for higher alcohols synthesis.....	144
7.1. Abstract.....	145
7.2. Introduction.....	146
7.3. Experimental.....	148
7.4. Results and Discussion.....	148
7.4.1. N ₂ -adsorption/desorption measurement.....	148
7.4.2. Wide-angle X-ray diffraction.....	152
7.4.3. Raman spectroscopic analysis.....	154
7.4.4. Fourier Transform Infra-red analysis.....	157
7.4.5. Thermogravimetric analysis.....	160
7.4.6. Temperature programmed reduction analysis.....	162
7.4.7. Transmission Electron Microscopic analysis.....	164
7.5. Catalytic tests of CNH, OCP _f & OCP-supported KCoMoRh catalysts.....	165
7.5.1. Effect of temperature on CO Conversion.....	166
7.5.2. Alcohol products for CNH, OCP _f & OCP-supported catalysts.....	167
7.5.3. Arrhenius plot & activation energy calculations: Power law model.....	170
7.6. Conclusions.....	172

CHAPTER 8

8. Higher Alcohols Synthesis: Influence of bentonite clay incorporation, experimental and kinetic studies over CNH-supported KCoRhMo catalyst.....	173
8.1. Abstract.....	174
8.2. Introduction.....	174
8.3. Experimental.....	176
8.3.1. Experimental design for process parameters study.....	177
8.4. Results and Discussion.....	178
8.4.1. Effects of operating variables on higher alcohol synthesis.....	178
8.4.2. Effects of temperature on higher alcohol synthesis.....	178

8.4.3. Effects of pressure on higher alcohol synthesis.....	179
8.4.4. Effects of gas hourly space velocity.....	179
8.4.5. Effects of H ₂ -to-CO ratio.....	180
8.4.6. Quadratic models development by Design Expert for HAS reaction.....	180
8.4.7. Effects of temperature, pressure, and GHSV on CO conversion.....	181
8.4.8. Effects of temperature, pressure, and GHSV on STY of alcohols, hydrocarbons, and CO ₂	185
8.4.9. Effects of temperature, pressure, and GHSV on selectivity of alcohols.....	194
8.5. Process parameters optimization and reproducibility study.....	197
8.6. Conclusions.....	199

CHAPTER 9

9. Higher alcohols synthesis over carbon nanohorn-supported KCoRhMo catalyst: Pelletization and kinetic modelling.....	201
9.1. Abstract.....	202
9.2. Introduction.....	203
9.3. Experimental.....	205
9.4. Results and Discussion.....	206
9.4.1. Influence of bentonite clay and external mass transfer evaluations.....	206
9.4.2. Internal mass transfer diffusion evaluation.....	212
9.4.3. Intrinsic kinetic parameters analyses.....	213
9.4.3.1. Reaction scheme for higher alcohols synthesis.....	213
9.4.3.2. Assumptions for kinetic models development.....	214
9.4.3.2. Considerations for rate expressions development for the HAS reactions.....	215
9.4.4. Reactor modelling.....	216
9.4.5. Long-term stability studies over CNH-supported KCoRhMo catalyst.....	223
9.4.6. Comparison of activation energies of alcohols over MoS ₂ -based catalysts.....	226
9.5. Conclusions.....	227

CHAPTER 10

10. Conclusions and Recommendations.....	229
10.1. Overall project discussion and conclusions.....	229
10.2. Recommendations.....	233
10.3. Acknowledgment.....	235

REFERENCES	237
-------------------------	------------

APPENDIX A: Research Outcome.....	258
--	------------

A.1. Publications from Results of the Thesis.....	258
A.2. Refereed Conference Presentations.....	259

APPENDIX B: Experimental Calibrations.....	261
---	------------

B.1. Reactor temperature calibration.....	261
B.2. Mass flow controller calibration.....	261

APPENDIX C: Mass Balance Data.....	264
---	------------

APPENDIX D: Mass Transfer Calculations.....	267
--	------------

D.1. External mass-transfer limitation.....	267
D.2. Internal mass-transfer limitation.....	273

LIST OF TABLES

Table 4.1: Elemental compositions and CO uptake of KCoMoRh/MWCNT catalysts (with & without binders).....	58
Table 4.2: Textural properties of treated MWCNT supports and KCoMoRh/MWCNT catalysts (with & without binders) determined from N ₂ sorption analysis.....	62
Table 4.3: Boehm titration results of KCoMoRh/MWCNT catalysts (with & without binders).....	67
Table 4.4: The crushing strength of the KCoRhMo/MWCNT catalysts (with & without binders).....	72
Table 4.5: Products selectivities for KCoRhMo/MWCNT catalysts (with & without binders).....	79
Table 5.1: Textural properties of pristine and HNO ₃ treated MWCNT & OMC supports as well as KCoMoRh catalysts determined from N ₂ sorption analysis.....	90
Table 5.2: Elemental compositions and CO uptake of MWCNT and OMC-supported KCoRhMo catalysts.....	91
Table 5.3: Products selectivities for MWCNT and OMC-supported KCoRhMo catalysts.....	100
Table 6.1: Textural properties of untreated and chemically treated OMC supports & catalysts determined from N ₂ sorption analysis.....	113
Table 6.2: Elemental compositions and CO uptake of untreated as well as chemically treated OMC-supported KCoRhMo catalysts.....	116
Table 6.3: Products selectivities for OMC-supported KCoRhMo catalysts at T=330°C.....	137

Table 7.1: Textural properties of CNH, OCP _f , OCP supports & supported KCoRhMo catalysts.....	150
Table 7.2: Products selectivities for CNH, OCP _f and OCP-supported KCoRhMo catalysts at T=330°C.....	169
Table 7.3: Activation energies comparison for carbon-supported KCoRhMo catalysts for the HAS reaction.....	171
Table 8.1: Test of significance results for independent variables or interactions for the model derived for CO conversion.....	182
Table 8.2: Test of significance results for independent variables or interactions for the model derived for the STY of different products.....	186
Table 8.3: Test of significance results for independent variables or interactions for the model derived for the selectivities of different products.....	195
Table 8.4: The results of optimization studies (T=290-350°C; P=5.52-9.65 MPa; GHSV=2.4-4.8 m ³ (STP)/kg of cat-h, catalyst = 1g).....	198
Table 8.5: The results of reproducibility studies (T=325°C; P=9.1 MPa; GHSV=2.4 m ³ (STP)/kg of cat-h, catalyst = 1g).....	198
Table 8.6: Means and standard errors of data sets for reproducibility studies (T=325°C; P=9.1 MPa; GHSV=2.4 m ³ (STP)/kg of cat-h, catalyst = 1g).....	199
Table 9.1: Influence of particle size and binders on the external mass transfer diffusion.....	211
Table 9.2: Effects of gas flow on CO conversion and external mass transfer diffusion.....	212
Table 9.3: Experimental design for the estimation of net reaction rates of components in the HAS reaction (T=290-330°C; P=9.1 MPa; H ₂ /CO=1.25).....	218
Table 9.4: Computed values of kinetic parameters by the power law models.....	220

Table 9.5: Comparison of activation energies of alcohols over MoS ₂ -based catalysts for the HAS reaction.....	226
Table D.1: Summary of calculated gas properties at P=9.1 PMa.....	268
Table D.2: Summary of computed dimensionless quantities and mass transfer parameters.....	272

LIST OF FIGURES

Figure 3.1: Experimental set-up for ordered mesoporous carbon (OMC) supports synthesis.....	39
Figure 3.2: Experimental set-up for carbon nanohorn (CNH) supports synthesis.....	41
Figure 3.3: Single-pass downward flow fixed bed reactor system for higher alcohol synthesis.....	53
Figure 4.1A: N ₂ -adsorption isotherms of pelletized KCoMoRh/MWCNT catalysts (with & without binders) determined from N ₂ sorption analysis.....	59
Figure 4.1B: Pore size distribution of pelletized KCoMoRh/MWCNT catalysts (with & without binders) determined from N ₂ sorption analysis.....	60
Figure 4.2: Wide-angle X-ray diffraction patterns of KCoMoRh/MWCNT catalysts (with & without binders). (° graphite; * MoO ₃ ; † K ₂ Mo ₂ O ₇).....	64
Figure 4.3: FTIR patterns of KCoMoRh/MWCNT catalysts (with & without binders).....	66
Figure 4.4: Raman patterns of KCoMoRh/MWCNT catalysts (with & without binders).....	69
Figure 4.5: TGA profiles of KCoMoRh/MWCNT catalysts (with & without binders).....	70
Figure 4.6: Effect of particle size on CO conversion (P=8.3 MPa; T=300-340°C; GHSV=3.6m ³ (STP)/kg _{cat} -h; H ₂ :CO=1.25).....	74
Figure 4.7: Effect of binders on CO conversion (P=8.3 MPa; T=300-340°C; GHSV=3.6m ³ (STP)/kg _{cat} -h; H ₂ :CO=1.25).....	76
Figure 4.8: Alcohol products distribution for Cat-0 as a function of temperature (P=8.3 MPa; T=300-340°C; GHSV=3.6m ³ (STP)/kg _{cat} -h; H ₂ :CO=1.25).....	78

Figure 4.9: Alcohol productivity for Cats 0-4 as a function of carbon number (P=8.3 MPa; T=330°C; GHSV=3.6m ³ (STP)/kg _{cat} -h; H ₂ :CO = 1.25).....	79
Figure 5.1A: N ₂ -adsorption isotherms of MWCNT and OMC-supported KCoMoRh catalysts.....	87
Figure 5.1B: Pore size distribution of MWCNT and OMC-supported KCoMoRh catalysts determined from N ₂ sorption analysis.....	88
Figure 5.2: Wide-angle X-ray diffraction patterns of pristine OMC & MWCNT as well as supported KCoMoRh catalysts. (° graphite; * MoO ₃ ; † K ₂ Mo ₂ O ₇).....	93
Figure 5.3: Raman patterns of MWCNT and OMC-supported KCoMoRh catalysts.....	95
Figure 5.4: CO conversion as a function of time-on-stream for KCoMoRh-supported catalysts (P=8.3 MPa; T=330°C; GHSV=3.6 m ³ (STP)/h-k _g _{cat} ; H ₂ :CO=1.25).....	97
Figure 5.5: Alcohol composition as a function of carbon number (P=8.3 MPa; T=330°C; GHSV=3.6 m ³ (STP)/h-k _g _{cat} ; H ₂ :CO=1.25).....	99
Figure 5.6A: ASF plot for MWCNT-supported KCoRhMo catalyst.....	102
Figure 5.6B: ASF plot for OMC-supported KCoRhMo catalyst.....	102
Figure 6.1A: N ₂ -adsorption isotherms of untreated OMC support and acid/base treated supports.....	109
Figure 6.1B: N ₂ -adsorption isotherms of untreated and treated OMC-supported KCoMoRh catalysts	109
Figure 6.2A: Pore size distribution of untreated OMC support and acid/base treated supports determined from N ₂ sorption analysis.....	111
Figure 6.2B: Pore size distribution of untreated and treated OMC-supported KCoMoRh catalysts determined from N ₂ sorption analysis.....	112
Figure 6.3: Wide-angle X-ray diffraction patterns of pristine OMC & chemically	

<p>treated as well as untreated OMC-supported KCoMoRh catalysts. (°graphite; *MoO₃; †K₂Mo₂O₇)</p>	117
Figure 6.4A: Raman patterns of treated and pristine OMC supports.....	119
Figure 6.4B: Raman patterns of treated and untreated OMC-supported KCoMoRh catalysts	121
Figure 6.5A: FTIR profiles of chemically treated and untreated OMC supports.....	123
Figure 6.5B: FTIR profiles of chemically treated and untreated OMC-supported catalyst.....	124
Figure 6.6A: TGA patterns of chemically treated and untreated OMC supports.....	126
Figure 6.6B: TGA patterns of chemically treated and untreated OMC-supported catalyst.....	127
Figure 6.7: TPR profiles of chemically treated and untreated OMC-supported catalyst.....	129
Figure 6.8: TEM images of (A): Cat-UnOMC; (B) Cat-HNO ₃ ; (C) Cat-NH ₄ OH/H ₂ O ₂ ; (D) Cat-KOH.....	132
Figure 6.9: CO conversion as a function of time-on-stream for treated and untreated supported catalysts (P=8.3 MPa; T=330°C; Catalyst=2g; GHSV=3.6 m ³ (STP)/h-kg _{cat} ; H ₂ :CO =1.25).....	134
Figure 6.10: Alcohol composition as a function of carbon number (P=8.3 MPa; T=330°C; Catalyst=2g; GHSV=3.6 m ³ (STP)/h-kg _{cat} ; H ₂ :CO =1.25).....	135
Figure 6.11: Alcohol production as a function of temperature (P=8.3 MPa; T=300-340°C; Catalyst=2g; GHSV=3.6 m ³ (STP)/h-kg _{cat} ; H ₂ :CO = 1.25).....	138
Figure 6.12: ASF plots for OMC-supported KCoRhMo catalyst: (a) Cat-UnOMC; (b) Cat-HNO ₃ ; (c) Cat-NH ₄ OH/H ₂ O ₂ ; and (d) Cat-KOH.....	141

Figure 6.13: ASF plots comparing alcohol products distribution for all catalyst (untreated and chemically treated).....	142
Figure 7.1A: N ₂ -adsorption isotherms of pristine CNH, OCP _f & OCP supports as well as their functionalized forms.....	149
Figure 7.1B: N ₂ -adsorption isotherms of CNH, OCP _f & OCP-supported KCoMoRh catalysts.....	149
Figure 7.2: XRD profiles for CNH, OCP _f & OCP-supported KCoRhMo catalysts.....	153
Figure 7.3A: Raman spectra of pristine CNH, OCP _f & OCP as well as their functionalized supports.....	155
Figure 7.3B: Raman spectra for CNH, OCP _f & OCP-supported KCoRhMo catalysts.....	156
Figure 7.4A: FTIR profiles of pristine CNH, OCP _f & OCP as well as their functionalized supports.....	158
Figure 7.4B: FTIR profiles for CNH, OCP _f & OCP-supported KCoRhMo catalysts.....	159
Figure 7.5: TGA profiles for CNH, OCP _f & OCP-supported KCoRhMo catalysts.....	161
Figure 7.6: TPR profiles for CNH, OCP _f & OCP-supported KCoRhMo catalysts.....	162
Figure 7.7: TEM images of KCoRhMo catalysts supported on: d) CNH; (e) OCP _f ; and (f) OCP.....	164
Figure 7.8: CO conversion as a function of temperature for KCoMoRh-supported catalysts (P=8.3 MPa; T=300-340°C; GHSV=3.6 m ³ (STP)/h·kg _{cat} ; H ₂ :CO=1.25)	166
Figure 7.9: Alcohol composition as a function of carbon number (P=8.3 MPa; T=330°C; Catalyst=2g; GHSV=3.6 m ³ (STP)/h·kg _{cat} ; H ₂ :CO=1.25).....	168
Figure 7.10: Arrhenius plot & activation energy for CNH, OCP _f and OCP-supported catalysts.....	171

Figure 8.1 (a & b): 3-D surface response plots showing the interaction effects of temperature, pressure, and GHSV on CO conversion over KCoRhMo/CNH catalyst.....	183
Figure 8.2 (a & b): Effects of temperature, pressure, and GHSV on CO conversion over KCoRhMo/CNH catalyst. a) Perturbation plot; b) Parity plot.....	184
Figure 8.3: The effects of temperature, pressure, and GHSV on methanol STY over KCoRhMo/CNH catalyst: (a & b) 3-D surface responses; and (c) Perturbation plot.....	187
Figure 8.4: The effects of temperature, pressure, and GHSV on ethanol STY over KCoRhMo/CNH catalyst: (a & b) 3-D surface responses; and (c) Perturbation plot.....	189
Figure 8.5: The effects of temperature, pressure, and GHSV on total alcohols STY over KCoRhMo/CNH catalyst: (a & b) 3-D surface responses; and (c) Perturbation plot.....	190
Figure 8.6: The effects of temperature, pressure, and GHSV on hydrocarbons STY over KCoRhMo/CNH catalyst: (a & b) 3-D surface responses; and (c) Perturbation plot.....	192
Figure 8.7: The effects of temperature, pressure, and GHSV on CO ₂ STY over KCoRhMo/CNH catalyst: (a & b) 3-D surface responses; and (c) Perturbation plot.....	193
Figure 8.8: The effects of temperature, pressure, and GHSV on ethanol selectivity over KCoRhMo/CNH catalyst: (a & b) 3-D surface responses; and (c) Perturbation plot.....	196
Figure 9.1: Effects of different catalyst particle sizes and temperature on CO conversion and total alcohols selectivities over KCoRhMo/CNH catalysts.....	208
Figure 9.2: Effects of different catalyst particle sizes and temperature on higher alcohols space-time-yield (STY) over KCoRhMo/CNH catalysts.....	209

Figure 9.3: Plot of outlet ethanol mole fraction versus W/F at various temperatures for obtaining reaction rates (T=290-330°C).....	219
Figure 9.4: Arrhenius plots of alcohol products (C ₁ to C ₃ -OH) and by-products (CH ₄ and CO ₂).....	221
Figure 9.5A: Parity plot of the experimental and model flow rates for the different alcohols.....	222
Figure 9.5B: Parity plot of the experimental and model flow rates for the gaseous products.....	222
Figure 9.6: Profile of CO conversion as a function of time-on-stream for CNH-supported KCoRhMo catalyst (P = 9.1 MPa, T = 325°C, GHSV = 2.4 m ³ (STP)/h/(kg of cat.)/h, H ₂ -to-CO molar ratio = 1.25, wt. of cat. = 1 g).....	223
Figure 9.7: Profile of STYs of products as a function of time-on-stream for CNH-supported KCoRhMo catalyst (P = 9.1 MPa, T = 325°C, GHSV = 2.4 m ³ (STP)/h/(kg of cat.)/h, H ₂ -to-CO molar ratio = 1.25, wt. of cat. = 1 g).	225
Figure B.1: Axial temperature profiles for downward flow reactor.....	262
Figure B.2: Calibration curve for temperature controller.....	262
Figure B.3: Calibration curve - mass flow controller for 10 mol% Ar in syngas	263
Figure B.4: Calibration curve - mass flow controller for 10 mol% H ₂ S/H ₂ gas	263

NOMENCLATURE AND ABBREVIATIONS

ADM	Alkali-doped MoS ₂
AHM	Ammonium hepta molybdate
ASF	Anderson-Schultz Flory
BC	Bentonite clay
BET	Brunauer-Emmett-Teller
Cat	Catalyst
CT	Coal tar
E _a	Apparent activation energy
Fun	Functionalized
FTIR	Fourier-Transform Infra-red
HA	Humic acid
CNHs	Carbon nanohorns
GHSV	Gas hourly space velocity
HAS	Higher alcohol synthesis
MTBE	Methyl tertiary butyl ethers
MWCNTs	Multi-walled carbon nanotubes
NS _{BET}	Normalized specific surface area
OMC	Ordered mesoporous carbon
OCP	Other carbon particles
OCP _f	Other carbon particles (fine fractions)
PD	Desorption mesopore diameter
Pris	Pristine
PV	Pore volume
S _{BET}	Specific surface area calculated by the BET method.
SMI	Support-metal-interactions
STP	Standard temperature and pressure
TEM	Transmission Electron Microscopy
TGA	Thermogravimetric analysis
UnOMC	Unfunctionalized Ordered mesoporous carbon
WGS	Water-gas-shift

XRD X-ray diffraction

CHAPTER 1

Introduction and Thesis Outline

Contribution of this chapter to overall study

This chapter provides an overview of future energy demands resulting from population growth and the need for mixed alcohols as a potential alternative liquid transportation fuel resource to help meet this growing need. The chapter further discusses the importance of alcohols as alternative fuel and puts into perspective the application of ethanol and higher alcohols as motor fuel. In addition, the knowledge gaps, hypothesis, research scope and objectives are discussed along with organization and manuscript content on the thesis.

1.1. Introduction

Energy security for the future presents one of the most important challenges facing humanity as population grows. That notwithstanding, it is equally crucial to minimize the detrimental environmental impacts associated with the generation of needed energy to help save our planet (Key World Energy Statistics, 2016). The current world population of 7.3 billion has been projected by the Department of Economic and Social Affairs/Population Division (United Nations) to reach 8.5 billion by 2030, 9.7 billion in 2050 and 11.2 billion in 2100 (World Population Prospects: The 2015 Revision). The projected future population growth as well as high energy demands from emerging economies will also cause an upward surge in the demand of

energy. Though, efficient and prudent energy usage could help extend the world's energy supplies, the number of vehicles (cars/trucks) on our roads are also increasing. Thus, the demand for alternative energy resources to boost supplies of fossil-based liquid transportation fuels (World Energy Outlook, 2016).

Amongst the various interesting approaches for liquid transportation fuels production is the so-called synthesis gas route (Andersson, 2015). Using a wide range of carbon-containing feedstocks such as coal, natural gas, biomass, municipal solid wastes (MSW), etc., syngas can be produced and purified prior to their conversion to liquid fuels via the appropriate technology. Depending on the catalysts of choice as well as operation conditions, syngas can be converted to higher molecular weight hydrocarbons and mixed/higher alcohols via the Fischer-Tropsch Synthesis (FTS) or higher alcohol synthesis (HAS) routes prior to their upgrading premium liquid transportation fuels (Andersson, 2015).

Up to date, commercial success in the field of syngas conversion to higher alcohols has not yet been reality because of the low yield of higher alcohols from syngas and the decline in oil prices in recent years (Jie et al., 2016). However, with increasing concerns regarding global climate change, depletion of fossil fuel resources and unpredictability in crude oil prices, research activities in the field of alternative energy utilization and related areas has intensified over the years. In lieu of this scenario, alternative energy resources as opposed to petroleum-derived feedstocks and chemicals have become necessary options to further explore if improved air quality and increased energy security goals are to be met in the future. To achieve these goals, the development of novel technologies and catalytic systems to produce synthetic chemicals and green fuels via conversion of syngas ($\text{CO}+\text{H}_2$) needs to be further assessed. As part of the variety of product streams derived

from syngas conversion, mixed alcohols (C₁-C₆) production continues to exhibit great promise as far as gas-to-liquid (GTL) technology and subsequent products upgrading are concerned.

1.1.1. Ethanol and higher alcohols as motor fuels

Mixtures of methanol and higher (C₂₊) alcohols constitute valuable octane boosters for unleaded gasoline and may also be used as green fuels for internal combustion engines (Courty et al., 1987; Dhaundiyal, 2014). In addition, ethanol is environmentally friendly and relatively easier to be stored and transported. In this regard, ethanol and higher alcohols have the potential to store hydrogen in the liquid form for easier hydrogen transport, which can further be reformed in the presence of steam to provide readily available on-site hydrogen source for fuel cells applications (Davidson et al., 2014; Ferencz et al., 2014). Moreover, since blending of methanol into gasoline raises problems of phase separation, high volatility, and lowering of calorific value, higher alcohols would be more preferred for such purposes (Courty et al., 1987; Smith et al., 2014).

Higher alcohols have low vapor pressure, better solubility/miscibility with hydrocarbon compounds, improved water tolerance, and higher overall heating value (Subramani et al., 2008; Smith et al., 2014). In this context, higher alcohols, especially ethanol is being considered as a potential alternative synthetic fuel for automobiles application or as a potential source of hydrogen for fuel cells. Ethanol fuel is mainly used in Brazil and United States, and together both countries were responsible for 87.1% of the world's ethanol fuel production in 2011 (Dhaundiyal, 2014). In Canada, ethanol blended gasoline can be used in gasoline-powered vehicles manufactured since the 1980's and most gasoline-powered vehicles can run on a blend consisting of gasoline and up to 10% ethanol (National Resources Canada, 2016).

The incorporation of oxygenated compounds such as ethers and alcohols into gasoline contribute to the reduction of greenhouse gases and environmental footprints of other exhaust toxic

emissions (Tien-Thao et al., 2006). However, as a result of the ban imposed on the usage of octane enhancers such as methyl tert butyl ether (MTBE) as gasoline blends in North America, the demand for higher alcohols, particularly ethanol, for such applications has been on the rise. That notwithstanding, the catalytic conversion of syngas to ethanol still remains a daunting task and no economically viable commercial process exists as of today.

In this regard, the development of novel catalysts to enhance activity, total alcohol productivity and desired product selectivity has resorted to both homogeneous and heterogeneous catalytic systems studies. Even though, homogeneous catalytic processes are relatively more selective for ethanol production, the prohibitive cost of catalysts, high operating pressure, and the inherent difficulties involved in catalyst separation and recycling make these processes unattractive for commercial applications. On the contrary, the heterogeneous catalytic processes for converting syngas to ethanol suffer from low yield and poor selectivity due to relatively slow kinetics of the initial C-C bond formation and fast chain growth of the C₂ intermediate (Subramani et al., 2008). Nonetheless, various research conclusions point to the fact that in comparison to unsupported catalyst, supported catalyst systems would perform better for the CO hydrogenation reactions; and hence constitutes major aspect of the present investigation.

1.2. Knowledge gaps

Extensive literature survey (presented in Chapter 2) conducted on the catalytic conversion of syngas to higher alcohols showed knowledge gaps as enumerated below:

1. There is limited reported studies on the alkali-doped doubly promoted MoS₂-based catalyst supported on MWCNTs; however, no reports are currently available on the pelletized form of the catalysts and the influence of binders on such catalyst system for the HAS reactions.

Also, no such catalyst system supported on ordered mesoporous carbons (OMCs) and carbon nanohorns (CNHs) was found in the literature.

2. Study on the influence of large-pore OMC-supported KCoRhMo catalyst for the HAS reactions and how it compares with its MWCNT counterpart is missing in the literature.
3. The influence of chemical oxidation of ordered mesoporous carbon (OMC) using different oxidizing agents (acidic and basic) and their catalytic performance for HAS reactions has less been investigated in the literature.
4. Optimization of binder (bentonite clay) loadings on the OMC-supported catalysts for the HAS reaction is missing in the open literature.
5. Study on sulfided KCoRhMo catalysts supported on CNH and its byproducts (OCP_f and OCP) for HAS reactions has not been reported in the open literature.
6. The effects of operating conditions such as temperature, pressure, GHSV, and H₂/CO molar ratio and long-term stability behavior of such alkali-doped doubly promoted MoS₂ catalysts supported on CNHs and OMCs for HAS reactions is missing in the literature.

1.2.1. Hypotheses

1. The high surface areas and attractive textural properties of CNHs and OMCs as compared to MWCNT would enhance higher metals loading and also increase the propensity of obtaining highly dispersed supported metal species.
2. The mesoporous nature of these supports (MWCNTs, CNHs, and OMCs) would facilitate diffusion of higher molecular weight reaction products from the active sites (resident inside the pore structure) into the bulk medium so as to mitigate probable mass transport limitations.

3. The incorporation of binders (bentonite clay, humic acid, coal tar) would improve the mechanical strength of the formulated ADM-supported catalyst. Also, the variable catalyst pellet sizes and feed gas compositions would influence the alcohol product distributions.
4. The different oxygen-containing functional groups introduced by different oxidizing agents (acidic and basic) would greatly influence the surface chemistry of the carbon support, and hence the quantity and type of metal anchoring site generated on the surface of the OMC support.
5. Higher alcohols products distribution would be significantly affected on the different carbonaceous supports (MWCNTs and OMCs). Also, generated carbonaceous byproducts (OCP_f and OCP) during CNH synthesis could be active composite supports for the HAS reaction.
6. For a particular catalyst formulation, an optimal operating condition (T, P, GHSV, H₂/CO molar ratio) will be required to influence the kinetics of the HAS reaction toward achieving the optimum performance and long-term stability of the catalyst.

1.2.2. Research objective

The principal objective of this research is to develop novel catalysts for the conversion of syngas to higher alcohols using doubly-promoted alkali-doped MoS₂-based catalysts over MWCNTs, CNHs and OMC supports. Moreover, extensive characterization techniques such as Brunauer-Emmett-Teller (BET) analyses, transmission electron microscopy (TEM), X-ray diffraction (XRD), temperature programmed reduction (H₂-TPR), Thermogravimetric analysis (TGA), Fourier-infra red (FTIR) spectroscopy, Raman spectroscopy, etc., were employed to thoroughly characterize these catalysts prior to their catalytic evaluation via screening under typical reaction conditions for their CO hydrogenation capabilities.

The main objective was divided into six phases (i.e. sub-objectives) to help with careful experimental planning, execution, and progress monitoring throughout the span of the project:

Phase 1: *To investigate the influence of binders and catalysts pelletization on the HAS reaction.*

- ✓ Preparation of a series of KCoRhMo/MWCNT catalysts as well as binders (bentonite clay, coal tar, humic acid)-incorporated catalysts, characterization and screening tests.

Phase 2: *To investigate the catalytic performance of large-pore OMC and for the HAS reaction.*

- ✓ Synthesis of large-pore pristine OMC supports by the one-pot synthesis approach and characterization (BET, TEM, etc.).
- ✓ Catalysts preparation, characterization, and CO hydrogenation screening tests.

Phase 3: *To study the effects of acid and base treatments on the large-pore OMC-supported catalyst for the HAS reaction.*

- ✓ Synthesis of large-pore OMC supports, chemical pre-treatments (HNO₃, NH₄OH/H₂O₂, and KOH) and characterization (BET, TEM, etc.).
- ✓ Catalysts preparation, characterization, and CO hydrogenation screening tests.

Phase 4: *To investigate the catalytic performance of CNH and its by-products (OCP_f & OCP) for the HAS reaction.*

- ✓ Submerged arc discharge synthesis of CNH & its by-products and characterization (BET, TEM, etc.).
- ✓ Catalysts preparation, characterization, and CO hydrogenation screening tests.

Phase 5: *Optimization of binder (bentonite clay) loadings on the large-pore OMC catalyst for the HAS reaction.*

- ✓ Synthesis of large-pore OMC supports & preparation of a series of binder-incorporated KCoRhMo/OMC catalysts, characterization (BET, XRD, FTIR, Raman, etc.), and CO hydrogenation screening tests.

Phase 6: *Kinetics and long-term stability studies of optimum CNH catalyst for the HAS reaction.*

- ✓ Preparation of optimum binder-incorporated CNH catalyst, characterization, and CO hydrogenation screening tests.
- ✓ Study of the influence of kinetic parameters (T, P, GHSV) and long-term stability of KCoRhMo/CNH-catalyst on the higher alcohol synthesis reaction.

1.3. Organization of the Thesis

Organization of this Ph.D. thesis is aligned with the guidelines for manuscript-based thesis of University of Saskatchewan. In this regard, instead of presenting and coherently analyzing raw experimental data for the first time, discussions have been presented as a series of journal manuscripts. The major part of the thesis is composed of a series of literature publications of the research work carried out over the span of the project. In most cases, manuscripts were drafted and submitted to journals for peer review prior to their publications following the completion of the various stages of the project. As of the time of writing of this thesis, the manuscripts presented in Chapters 4, 5, 6, 7 and 8 have all been published in various international journals. It is intended that manuscripts for chapters 2 and 9 be prepared and submitted for review and possible publication.

In each manuscript-based chapter, two issues have been discussed in addition to the manuscript itself. These include the contribution of the Ph.D. candidate and the contribution of the manuscript to the overall study. Chapters 1 and 10 are original texts incorporated in this thesis to

introduce the subject matter and discuss the overall outcome of the project. The materials used and details on experimental methods as well as catalyst characterization techniques are presented in chapter 3. The relevant literature review is presented in each chapter to introduce the topic. The compiled reference lists as well as the relevant supplementary materials are presented in the references and appendices sections, respectively.

1.4. Manuscript Content of the Thesis

The specific topic of each chapter and the way in which it addresses the overall objectives of the thesis are detailed below. It deserves mentioning that the use of manuscript-based thesis may result in overlap of materials between chapters. However, attempts have been made to minimize such potential redundancies. The catalyst activity and selectivity of CO hydrogenation reactions were influenced by type of catalyst, binder incorporation as well as the nature of the carbon support matrix. It has been known that the promotion of group VIII metals, such as Co, Ni and Rh, to alkali-modified MoS₂ catalysts improved the activity and selectivity of higher alcohols synthesis due to the formation of new phases and improving the dispersion of catalytic species. Furthermore, in a previous Ph.D study on the development of Co and Rh-promoted alkali-modified molybdenum sulfide catalysts for higher alcohols synthesis by Surisetty et al., 2010, it was concluded that potassium promoted trimetallic CoRhMo catalyst supported on MWCNT showed superior catalytic performance for the CO hydrogenation reaction as compared to its AC and Al₂O₃ counterparts.

Thus, the first phase of the research looked at possibilities of consolidating the powdered form of the KCoRhMo/MWCNT catalyst by incorporating selected binders (bentonite clay, coal tar, and humic acid) and consequently pelletizing into different particle sizes. The trimetallic catalysts were prepared by the incipient wetness impregnation method and extensively

characterized for their physical, chemical and mechanical properties. The catalytic performance of the resulting three catalysts (binders-incorporated) was compared with binder-free catalyst for their higher alcohol synthesis capabilities under similar experimental conditions. Similarly, the fine powdered catalyst (88 μm) was also compared with the pelletized binder-free counterpart of (1700 μm) mesh size. The results and discussion are presented as a published manuscript in Chapter 4.

MWCNTs are new generation of carbon base supports with unique properties such as, inert graphite surface which is capable of hosting hydroxyl and carboxyl functional groups that are necessary for metals anchorage during catalyst preparation. Ordered mesoporous carbon (OMC) has superior physico-chemical properties as compared to its MWCNT counterpart. Thus, it was interesting to investigate the catalytic performance of the OMC-supported KCoRhMo catalyst for the HAS reaction as compared to the MWCNT counterpart under similar metal loadings, preparation and reaction conditions. The details of this study are presented as a published manuscript in Chapter 5.

Though the CNT-supported catalyst performed better than the OMC counterpart under similar metal loadings, it was interesting to study the influence of different chemical pretreatment of the latter support by subjecting the pristine material to both acidic and basic treatments. This oxidative treatment was intended to introduce different surface functional groups to enhance its metals anchorage properties. Similarly, the trimetallic catalysts were prepared by the incipient wetness impregnation method and extensively characterized for their physicochemical properties prior to catalytic performance evaluation HAS reaction. Chapter 6 presents the results and discussion as a published manuscript.

Though MWCNT and OMC have proven tendencies to produce alcohols, in our present research, it has been observed that carbon in the form of carbon nanohorns (CNH) can be a superior catalyst support for syngas conversion applications. Single-wall carbon nanohorn (SWCNH) is one of the most attractive new forms of nanocarbons (Ijima et al., 1999). These carbon nanoparticles were discovered by Ijima et al., 1999, and constitute a form of single-walled carbon nanostructures with graphitic tubes and cone-shaped caps, forming a cone angle of 20° at one end and individual SWCNH particles typically aggregating to form a spherical structure with diameters of 50-90 nm. Despite the fact that this novel porous carbon material (CNH) has recently attracted significant importance in the field of heterogeneous catalysis, it was gathered from our literature review that no work has yet been reported on CO hydrogenation reaction over these supports for higher alcohols synthesis, though, the CNH-supported NiMo catalysts proved successful in the hydrogenation of petroleum feedstock in hydrotreating reactions (Aryee et al., 2014). Thus, in chapter 7, the potential catalytic applications of CNH and its by-products (OCP_f and OCP) supports for higher alcohols synthesis via syngas conversion was explored.

The activity and selectivity of the higher alcohols synthesis from catalytic conversion of synthesis gas are affected by the operating conditions such as reaction temperatures, total pressures and GHSV. The effects of operating conditions as independent variables on the % CO conversion, STY of alcohols, hydrocarbons and CO_2 over CNH-supported catalyst have not yet been reported in the literature. Furthermore, the interaction effects of these parameters have also not been investigated. Moreover, no model exists that correlates STY and selectivity of alcohols with operating conditions in CO hydrogenation reactions. Therefore, a part of this Ph.D. research plan was allocated to develop models that correlate the interaction effects of temperature, pressure, and GHSV with that of % CO conversion, STY of alcohols, hydrocarbons and CO_2 , as well as

selectivity of alcohols in CO hydrogenation reactions using the H₂ to CO molar ratio of 1.25, using higher alcohols synthesis from synthesis gas over the sulfided KCoRhMo/CNH catalyst. The study also aimed to optimize the operating conditions to obtain maximum ethanol selectivity. The outcome of this study is discussed in Chapter 8. Chapter 9 discusses mass transfer considerations, kinetic modelling as well as the study of long-term catalyst stability of sulfided alkali-modified Co-Rh-Mo catalysts that are supported on CNH during continuous higher alcohols synthesis over 500 h in a fixed-bed micro reactor.

Chapter 10 gives the general discussion and overall conclusions on the catalyst development, different characterization techniques, optimization of process conditions, intrinsic reaction kinetics development and long-term deactivation studies of the catalyst for higher alcohols synthesis. Finally, the scope for future work is also discussed in this chapter as a recommendation section followed by the list of references used in the thesis. The research outcome in the form of publications and conference presentations is given as Appendix A. The experimental calibrations of temperature of this reactor and mass flow controllers are given in Appendix B. The example of mass balance data is given as Appendix C and mass transfer calculations are shown as Appendix D.

CHAPTER 2

Literature review: Gas-to-Liquid technology and higher alcohols from syngas

The content of this chapter is under preparation to be submitted for Journal publication as a review paper on higher alcohol synthesis.

Contribution of this chapter to overall study

This chapter provides an overview of the gas-to-liquid (GTL) technology, presents routes to produce synthesis gas from sources such as coal, biomass and natural gas as well as syngas cleaning/purification for various downstream applications. It also discusses the catalytic conversion of syngas to mixed Fischer-Tropsch products as well as higher alcohols. A brief historical background on the development of the HAS technology and potential industrial applications are also provided. Finally, catalyst systems, supports and preparation/pre-treatment conditions employed for the HAS reactions are discussed. The reaction mechanisms for higher alcohol synthesis as well as the Anderson-Schulz-Flory (ASF) distribution to provide insight about the chain growth probability during the HAS reaction is also provided in this chapter.

2.1. Introduction

The generation of “green” gasoline, diesel and alcohols as alternative liquid transportation fuels and fuel additives via Fischer-Tropsch synthesis (FTS) and higher alcohol synthesis (HAS) pathways have renewed the global interest of industry and academia for the gas-to-liquid (GTL) technologies (Jensen et al., 2014; de Klerk, 2011). These technologies provide promising pathways toward the production of clean liquid transportation fuels and derivative chemicals from syngas conversion (de Klerk, 2011). In the FTS process, syngas is converted into a range of hydrocarbon products, which are mainly composed of long-chain sulfur- and nitrogen-free normal paraffins and olefins, utilized to generate the liquid fuel. For the HAS process, depending on the catalyst used a product stream containing mixed alcohols (C₁-C₆) can be obtained (Subramani et al., 2008; de Klerk, 2011).

The synthesis of hydrocarbons and alcohols from syngas over selected group VIII transition metals by the FTS & HAS technologies involve surface catalytic reactions occurring in parallel with a series of surface polymerization reactions to generate the desired products in a required carbon range (van Steen et al., 1999). Despite the great technological successes achieved over the years, it is still faced with several challenges including the catalyst type and its specific design. In-depth insights of the FTS and HAS catalysis along with proper process operation conditions still remain cutting edge research for academia and related industries.

2.1.1. Synthesis gas production and cleaning

In a typical plant for the conversion of synthesis gas to liquid products (Fischer-Tropsch oils, alcohols, etc.) and related synthetic chemicals, a significant portion of the investment cost is used for the syngas production, cleaning and pre-conditioning. For instance, the conversion of natural gas-based syngas in a methanol plant represents about 2/3 of the investment cost

(Chaumette et al., 1988, Mills, 1993). Thus, economic viability of the entire gas-to-liquid (GTL) plant will be greatly dependent on the design of the syngas production part, which will have a direct correlation to the source and availability of feedstock as well as the downstream application of the generated syngas. That notwithstanding, the price of feedstock is also a factor that plays a critical role in the design, sizing, and overall economics of the plant. A good mix of all these factors, processes and energy utilization will constitute an integral part toward achieving overall efficiency and economy of the GTL plant product (Rostrup-Nielsen et al., 2011; de Klerk, 2011). Syngas cleaning removes contaminants such as sulfur (COS, H₂S), nitrogen (NH₃, HCN) and halogen compounds (HCl) as well as volatile metals (K, Na), particulates (soot, dust, char, ash) and tars (polyaromatics) from the gaseous (Kumar et al., 2009). For coal or biomass gasification, the generated syngas is H₂-lean and typically contains H₂/CO ratio in the range 0.45-1.5; however, H₂-rich syngas can be produced from a natural gas reforming (Göransson et al., 2011; Kalamaras et al., 2013).

2.1.2. Syngas from biomass, coal and natural gas

Biomass, coal and natural gas comprise components such as carbon, hydrogen and oxygen containing small proportion of nitrogen. The ultimate analysis of a fuel gives its elemental compositions represented as C, H, N, S and O as well as the ash content. The proximate analysis is presented in terms of moisture, volatiles and fixed carbon. The energy content of biomass is expressed in terms of heating value (HV) or calorific value (CV). HV or CV of a material is the energy released when a material is burnt in air and is presented in terms of energy content per unit mass or volume. This energy is measured with respect to a reference state as it cannot be measured directly (Surisetty, 2010; Sikarwar et al., 2016).

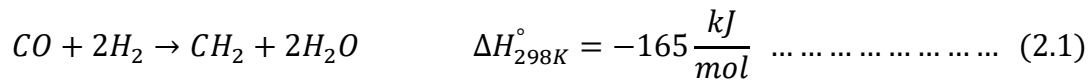
Syngas can be generated using different feedstock ranging from biomass, coal and natural gas. The main technology for syngas production can typically be categorized into two namely; gasification and reforming. The term gasification describes the conversion of solid/heavy feedstock (biomass, coal, etc.) to syngas. Reforming can be categorized into steam methane reforming (SMR), partial oxidation (POX), or autothermal reforming (ATR) and can commonly be used to describe the conversion of gaseous (natural gas) or liquid feedstock (naphtha) to syngas (Sikarwar et al., 2016). In the gasification process, the carbon-rich feedstock is reacted with steam and/or oxygen to convert the elemental carbon present to a gaseous mixture containing mainly hydrogen, carbon monoxide, carbon dioxide and methane. The quantity as well as quality of syngas generated will be dependent on factors including the source of feedstock (moisture content, elemental compositions), gasification medium (steam, oxygen and/or air) and reaction conditions (temperature, pressure). The type of gasifier used and gasification reaction technology employed also contributes to the quality of syngas produced (Siedlecki et al., 2011).

2.2. Conversion of syngas to products

Syngas can be converted to a wide product range using various processes. Syngas is a crucial intermediate resource for production of hydrogen, ammonia, methanol, synthetic hydrocarbon fuels (Fischer-Tropsch synthesis), and higher molecular weight alcohols (higher alcohols synthesis). Though the pursuit of catalytic processes for the production of synthetic fuels and chemicals via syngas conversion has been ongoing for decades, the quest for efficient catalysts for higher alcohols and hydrocarbons through the FTS approach share a common history.

2.2.1. Fischer-Tropsch synthesis from syngas conversion

Fischer-Tropsch synthesis (FTS) is a series of processes which converts syngas (mainly, H₂ and CO) to synthetic liquid fuels and valuable chemicals (Steynberg, 2004; Andersson, 2015). German scientists Franz Fischer and Hans Tropsch patented the FT process for the catalytic conversion of H₂ and CO to heavier hydrocarbons in the 1920s (Steynberg, 2004). Catalyst metals with activity towards the FTS reaction include iron, cobalt, nickel and ruthenium. Among these metals, iron and cobalt have gained commercial interest due to their relative cost and availability as compared to Ruthenium and Nickel. (Aasberg-Petersen et al., 2004, de Klerk, 2011). The FTS reaction is exothermic as depicted in eq. 2.1.



For Fe or Co-based catalysts, typical pressures for industrial FT reaction is the range of 20-40 bar and products distribution are affected by the operation temperatures as well as the catalyst metal of choice (Steynberg, 2004; de Klerk, 2011). Depending on the catalyst metal employed, the FTS reaction can be performed in two temperature regimes: low-temperature (i.e. LTFT: 200-240°C) or high-temperature (i.e. HTFT: 300-350°C). Fe-based catalysts are commonly used in latter applications, with linear low molecular weight olefins, gasoline and oxygenate forming the main FT products (Dry, 2002).

When high-molecular weight linear hydrocarbons (waxes) are the desired FT products, Fe or Co-based catalysts could either be a preferable choice; however, the reaction needs to be performed in the low-temperature regime (Dry, 2002). Typically, Fe catalysts have high water-gas shift activity while its Co-based counterpart exhibits poor water-gas shift activity (Dry, 2004; Steynberg, 2004). Thus, syngas mixture with low H₂/CO ratio would work better with Fe catalyst

as compared to a Co-based catalyst due to the simultaneously water-gas shift (WGS) reaction occurring during the FT reaction. After the FT reaction, the synthetic crude generated can be further upgraded via hydrocracking, isomerization, catalytic reforming and alkylation to achieve a premium fuel such as diesel or gasoline (de Klerk, 2011).

2.2.2. Higher alcohols synthesis from syngas conversion

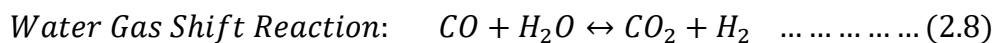
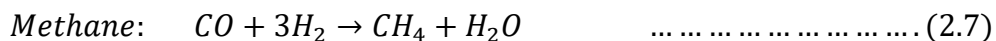
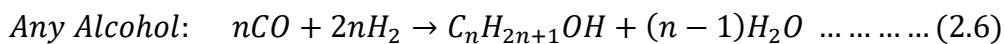
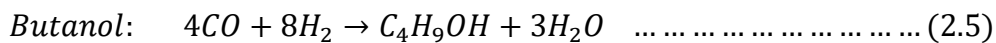
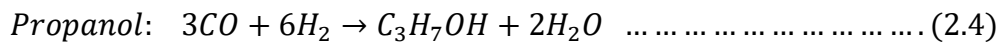
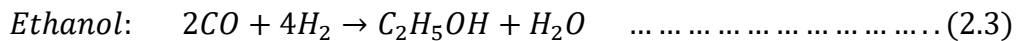
The process of converting syngas to a mixture containing hydrocarbons, alcohols, aldehydes, ketones, acids and other organic compounds using alkalized oxides of cobalt and osmium as catalysts was patented by Badische Anilin und Soda Fabrik (B.A. & S.F.) in 1913 (Fischer et al., 1922). Experimental runs with these catalysts was performed at 10 – 20 MPa and 300-400°C. In the 1923-24s, the research work of German scientists, Frans Fischer and Hans Tropsch, to directly convert syngas to higher alcohols using alkalized iron oxide catalyst was recognized (Fischer et al., 1923). A product mixture containing alcohols, aldehydes, ketones, fatty acids, and esters was formed when the catalytic CO hydrogenation reaction was performed at pressures and temperatures in the range of 10 - 15 MPa and 400 - 450°C, respectively. The Synthol process was then developed when the resulting mixture was named as Synthol (Fischer et al., 1923 & Fischer et al., 1924). In 1930, Frolich and Cryder used a mixed oxide catalyst with molar composition Zn:Mn:Cr, 1:1.1:1.03 to produce higher alcohols from syngas. It was reported that the pathway for methanol formation was via the formaldehyde intermediate and higher alcohols are formed from methanol through a stepwise condensation reaction (Frolich et al., 1930).

In the 1940s, Du Pont developed an alkalized Mn-Cr catalyst to synthesize methanol and higher alcohols from syngas for commercial purposes (McCutchen et al., 1922). A modified Synthol process was developed by Farbenindustrie in the 1940s to produce higher alcohols from

syngas using low reaction pressures and temperatures of 2 MPa and 190-200°C, respectively. A modified Fischer-Tropsch alkalized iron catalyst was used in their study to enhance the higher alcohol selectivity, with olefins and paraffins forming the greater portion of the remaining product (Haensel et al., 1943). The crucial role of incorporating substantial amounts of strong basic substances in catalyst formulation for higher alcohols synthesis applications was underscored by Natta and coworkers by assessing catalysts for the direct conversion of syngas to higher alcohols (Natta et al., 1957).

The renewed interest of academia and industry in the HAS technology during the 21st century is not only because of its environmental friendly nature, but also to reduce our overdependence on diminishing fossil fuel reserves. Mixing alcohols with gasoline produces a mixture commonly known as gasohol, which helps to reduce local air pollution (e.g. CO and ozone) as well as enhancing the anti-knock properties of the fuel in internal combustion engines.

Typical series of exothermic reactions taking place during the HAS reaction include the following (eqs. 2.2-2.6):



The formation of hydrocarbons, normally dominated by methane, together with short paraffins and olefins form the main side products during the HAS reaction. Oxygenated by-products such as aldehydes, esters and ethers might also be formed depending on catalyst and operation conditions used. The water-gas shift (WGS) reaction (eq. 2.8) occurs simultaneously with catalysts having water-gas shift activity. The MoS₂-based catalysts are known to display very high WGS activity (Andersson, 2015).

2.3. Catalyst systems for higher alcohols synthesis

From the consideration of available literature on catalysts for higher alcohols synthesis, a variety of catalyst formulations have been adopted for this complex reaction. However, for the purposes of this thesis, the two main categories of catalyst systems discussed for higher alcohol production include:

a) Alkali modified methanol synthesis catalysts

- i) High-temperature methanol synthesis catalysts
- ii) Low-temperature methanol synthesis catalysts

b) Modified Fischer-Tropsch catalysts

- i) Fe, Ni, or Co-modified low-temperature and pressure MeOH synthesis catalysts
- ii) Supported Rhodium-based catalysts
- iii) Alkali-modified molybdenum-based catalysts.

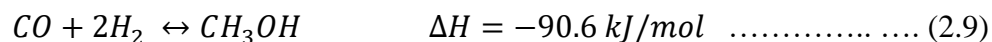
2.3.1. High-temperature methanol synthesis catalysts

It should be noted that various researchers investigating this field (GTL) agree on the role of active basic promoters like Cs, Rb, and K on the production of higher alcohols (Smith et al., 1983; Forzatti et al., 1991; Campos-Martin et al., 1996; Minahan et al., 1998). With alkalized methanol synthesis catalysts, the synthesis of higher alcohols typically occurs at temperature

above 400°C (Natta et al., 1957). For instance, alkali-modified ZnO/Cr₂O₃ methanol synthesis catalysts were prepared and applied for the conversion of syngas to alcohols using high temperatures and pressures of 400-450°C and 20.3-25.5 MPa, respectively. The authors remarked that alkali metals: Cs, Rb, and K, were the most active promoters for the production of higher alcohols (Natta et al., 1957). Campos-Martin and coworkers investigated the promoter effect of Cs on C-C bond formation during alcohol synthesis from CO/H₂ over Cu/ZnO/Cr₂O₃ catalysts. It was concluded that the incorporation of Cs resulted in a substantial improvement of C₂₊OH selectivity. In a different study using Cs and K promoter on Zn/Cr spinel catalyst for higher alcohols production, Minahan and coworkers observed improvements in the higher alcohol production rate and selectivity with the addition of these promoters. Superior performance was achieved for the Cs promoter in comparison to its K counterpart. The authors reported that amongst all the modified alkali promoted methanol synthesis catalysts screened for HAS application, the 3 wt.% Cs/Zn/Cr catalyst with excess ZnO yielded the highest isobutanol production rate of 171 g/kg h using high temperatures and pressures of 440°C and 10.3 MPa, respectively (Minahan et al., 1998).

2.3.2. Low-temperature methanol synthesis catalysts

Conventional conversion of syngas to methanol is temperature dependent due to the exothermicity of the reversible reaction:



Methanol is conventionally produced in a gas-solid phase process, which is operated at 250°C and 7-8 MPa of pressure in the presence of Cu/ZnO-based catalysts (Bo et al., 2014). Under these conditions, thermodynamic limitations mitigate the production of higher alcohols (Forzatti et al., 1991). That notwithstanding, Cu-based catalysts promoted with alkali resulted in the

production of higher alcohols at lower operating temperature and pressures. The incorporation of K_2CO_3 precursor in the formulation of commercial Cu/ZnO methanol catalysts increased the formation of ethanol, n-propanol and isobutyl alcohol (Smith et al., 1983). They concluded that the promoter concentration, temperature and pressure, as well as the H_2/CO feed ratio were important parameters in the determination of the higher alcohol selectivity. Typical low pressure and temperature methanol synthesis catalyst systems produce mainly branched C_{2+} alcohols along with methanol. However, in comparison with the high temperature methanol synthesis catalysts, relatively high conversions of syngas to higher alcohols with poor selectivity can be achieved from the former catalyst systems (Surisetty, 2010).

2.3.3. Fe, Ni, or Co-modified low temperature MeOH synthesis catalysts

Fe, Co, and Ni constitute the main catalysts commonly employed for the Fischer-Tropsch synthesis reactions (Arsalanfar et al., 2012; Ding et al., 2008). Whereas Fe and Co are the two reasonable choices for FTS, Ni is a known Fischer-Tropsch element with strong methanation tendency in CO hydrogenation reaction (Surisetty et al., 2013). Due to their relatively low cost and high water gas shift reaction activity, Fe-based catalysts have been successfully applied in industrial processes with syngas of low H_2/CO ratios (Lox et al., 1988; van der Laan et al., 1999). Though cobalt-based catalysts produce high yields of long chain hydrocarbons in FTS reactions (Madon et al., 1993), it also enhances the C_1 to C_2 homologation in higher alcohols formation (Santiesteban, 1989). Incorporation of alkali promoters to these FT catalysts was found to improve the production of higher alcohol synthesis (Anderson, 1984).

Both high-temperature methanol synthesis catalysts (based on ZnO/Cr_2O_3) and low-temperature counterparts (based on Cu/ZnO) react to the incorporation of alkali promoters and operating parameters in a different manner. For instance, while numerous studies using Cu-based

methanol synthesis catalyst showed that the most applicable temperature range for higher alcohol formation was 270-310°C, it is also noteworthy to mention that higher temperatures (>310°C) can result in the deactivation of the catalyst (Spivey et al., 2007). Catalysts deactivation resulting from sintering tends to destroy the spinel structures of Cu and Co, Ni or Fe. Furthermore, severe carbon deposition can be enhanced at high temperatures leading to the deactivation of these group catalyst. Low-temperature Fe and Co containing FT catalysts for HAS applications favor higher alcohols production under decreased operating temperatures and increased reactant stream contact time, which tends to reduce the formation of hydrocarbons (Xiaoding et al., 1987).

2.3.4. Supported Rhodium-group catalysts

Rhodium-based catalysts have been known to exhibit higher oxygenate activity and selectivity from synthesis gas (Balakos et al., 1991). During the synthesis of alcohols from syngas, iron group metal components are known to enhance the formation of linear higher alcohols, with Co-containing catalysts leading to the formation of large amounts of ethanol (Santiesteban et al., 1988). That notwithstanding, other metals of Group VIII, (e.g., rhodium), also promotes the formation of C₂ oxygenates from syngas, especially, ethanol (Herman, 2000). Alkali doping over Rh-based catalysts inhibit methanol formation and favours the formation of ethyl alcohol. In higher alcohols synthesis, Rhodium-based catalysts, with other iron group metal promoters increase the catalytic activity and shifts selectivity towards ethyl alcohol production. Rh-based catalysts can usually be operated at low temperatures (150-300°C) and pressures (0.1-1 MPa); hence catalyst deactivation by sintering is quite minimal during CO hydrogenation reaction (Surisetty, 2010).

Sachtler et al., investigated the catalytic site requirements for elementary steps in syngas conversion to oxygenates using promoted Rh-based catalysts. It was concluded that the

incorporation of highly oxophilic ions (Mn, Ti, Zr, and Nb) to the Rh-based catalyst enhanced CO dissociation (Sachtler et al., 1986). Nonetheless, Fe and Zn ions were found to block sites responsible for CO dissociation reaction on the Rh surface; thus, inhibiting the formation of hydrocarbons during the HAS reaction. Depending on the reaction conditions, properties of alkali promoters, and support, Rh-species in catalysts are capable of catalyzing dissociation, insertion, and hydrogenation of CO (Li et al., 2003). The CO conversion and yield of oxygenates over Mo-Rh/Al₂O₃ catalysts was higher than its Rh/Al₂O₃ counterpart. The interaction of rhodium with molybdenum affects the oxidation state of the rhodium species, which affects CO adsorption (DeCanio et al., 1991). Though the addition of Fe and Mo was reported to enhance the chain growth properties of the Rh/ZrO₂ catalyst and improve the formation of C₂₊ components in one study (Guglielminotti et al., 1994), and opposing effects was reported by Guglielminotti and coworkers in their study on the effects of iron on the activity and the selectivity of Rh/ZrO catalysts in the CO hydrogenation (Guglielminotti et al., 1995). The authors remarked that the addition of Fe to Rh/ZrO₂ catalysts produced two opposing effects namely; the decrease of Rh sites available for both CO and H₂ chemisorption; and also the increase of doubly bonded CO (Rh-CO-Fe) moieties, adjacent to Rh sites and enhanced the formation of C₂₊ oxygenates during the CO hydrogenation reaction.

2.3.5. Alkali-modified molybdenum-based catalysts

Molybdenum-based catalysts in the form of alkali-promoted molybdenum disulfide (MoS₂) catalysts have shown high selectivity to mixed alcohols (Surisetty, 2010). With the incorporation of iron group metals, especially Co, the activity and product distribution of MoS₂ catalyst can be significantly enhanced. In comparison to the low and high-temperature modified methanol and FT catalysts, the MoS₂ based catalysts have high tendency to resist catalyst

poisoning by the presence of sulfur component in the syngas and also exhibits high activity towards water gas shift reaction. Thus, the cost of ultra-desulfurization unit for sulfur removal from syngas feedstock as well as separation of water can be eliminated in the process design (Mills, 1992). Alkali-modified MoS₂ catalysts can be used to produce alcohols from syngas. Synthesis of higher alcohols from syngas was first patented by the DOW Chemical Company and the Union Carbide Corporation using the alkali metal impregnated MoS₂ catalyst (Quarderer et al., 1984; Kinkade, 1986; Stevens, 1988; Cochran et al., 1988; Cochran et al., 1989). In the absence of alkali promoters, the unpromoted MoS₂ catalyst produced only hydrocarbons, predominantly, methane. With the addition of alkali promoter, the selectivity of the catalyst dramatically shifted towards mixed alcohols production (Santiesteban et al., 1988; Surisetty, 2010).

The alkali additive increases active sites for alcohols formation by inhibiting the hydrogenation ability of adsorbed alkyl species on the surface of the catalyst to produce alkanes (Tatsumi et al., 1989). The alcohol products stream over these catalyst systems consists of linear alcohols with carbon numbers typically in the range of 1-6. The addition of Ni and/or Co promoter to the alkali-modified MoS₂ catalysts increased the alcohol yield and selectivity towards higher alcohols (Liu et al., 1997). Whereas the addition of Co into the formulation of alkali-modified MoS₂ catalysts enhanced the C₁→C₂ homologation step, leading to the formation of ethanol as the primary alcohol product, Ni addition to K/MoS₂ catalysts enhanced the methanation reaction (Santiesteban et al., 1988). Also, the impacts of different alkali metals (K, Rb, and Cs) addition on MoS₂ catalyst formulation for the HAS application is dependent on the alkali/Mo ratio (Qi et al., 2003). The promotional effect of K was greater than Cs for alcohol synthesis over the Co-MoS₂/clay catalyst (Iranmahboob et al., 2003).

The influence of operation conditions (T, P, GHSV, etc.) as well as syngas feed composition is also crucial for higher alcohol productivity. The presence of CO₂ in the syngas feed can enhance the production of greater amounts of water, which can inhibit higher alcohol formation; however, the presence of H₂S increases the formation of hydrocarbons in unpromoted MoS₂ catalyst (Iranmahboob et al., 2003). Addition of Co to alkali-modified MoS₂ catalysts increased the alcohol ratios of C₂₊/C₁ in the products relative to that for the un-promoted sample. Co species exhibited relatively stronger interaction with the Mo component in the form Co-Mo-S structure than in Co-Mo-O structure (Gang et al. 1997; Surisetty, 2010). For supported Rh-Mo-based catalyst matrix, the formation of alcohols can be catalyzed by electron deficient sites as opposed to electron-rich sites that are needed for hydrocarbons formation (Sudhakar et al., 1987). The incorporation of rhodium into the Mo-K/Al₂O₃ samples increased the catalytically active surfaces that are responsible for increasing the activity for alcohol synthesis. As a result of the co-existence of cationic and metallic Rh species, stabilized by the interaction of Rh with Mo species, the selectivity to the formation of higher alcohols is enhanced (Li et al., 1999; Surisetty, 2010).

Considering the potential reviewed catalysts for the HAS reaction, it is obvious that alkali-modified molybdenum sulphide catalysts are quite promising candidate due to their excellent resistance to sulfur poisoning and high activity for the water-gas shift reaction. With the incorporation of Co and/or Rh metal promoters to the catalyst formulation, the higher alcohol selectivity can be increased significantly.

2.4. Catalyst supports for higher alcohols synthesis

In heterogeneous catalytic hydrogenation reactions, where metal dispersed on a support serves as catalyst, the support plays a crucial role in the overall performance of the designed

catalyst (Tauster et al, 1981). The catalyst support material is a solid substrate that provides high surface area for the homogeneous or non-uniform dispersion of the catalyst metals. Apart from its high surface area, the catalyst support also possesses a degree of surface acidity, basicity or neutrality that can influence its catalytic properties such as metal dispersion and reducibility. Furthermore, the thermal stability of the catalyst support plays a crucial role in the preparation and operation of the catalyst since it can influence the sintering properties of the active phases generated on the support.

It is well known that supported metal catalysts are of immense significance when hydrogenation reactions are concerned due to the probable hydrogen spillover effect (Tauster et al, 1981; Hindermann et al., 1983). The atomic hydrogen forming as a result of dissociative adsorption on the metallic site migrates onto the support (hydrogen spillover); hence, the chemical reaction proceeds not only on the metal surface but also on the support (Hindermann et al., 1983). Typical supports such as carbon, alumina, silica, zirconia, etc. have been used for catalytic conversion of synthesis gas to higher alcohols (Kohl et al., 2002; Wang et al., 2002; Zurita et al., 2003). To be applied in the CO hydrogenation reaction for the HAS reaction, the catalyst support needs to be either neutral or basic with the incorporation of alkaline precursors. That notwithstanding, for catalyst supports with high surface acidities such as metal oxides (e.g. Al_2O_3 and ZrO_2), the formation of alcohols is greatly suppressed due to the enhanced rate of hydrocarbon formation (Kim et al., 1994).

It is notable to mention that activated carbon possesses numerous attractive properties such as high surface area ($>1000 \text{ m}^2/\text{g}$), micro and mesoporosity, minimal metal-support interaction (due to the inertness of the graphitic surface), resistance to acidic or basic media, and high stability at severe reaction temperatures and pressures (Duchet et al., 1983). However, the

presence of microporosity in AC-supported catalysts makes them susceptible to pore blockage due to the potential formation of coke on catalyst materials (Yang et al., 2011). Thus, effective mass transfer of reactants to the active sites resident in the pores is hindered, hence affecting the rate of the overall reaction.

The family of carbon materials have long been applied as catalyst supports due to their diverse porous structure, resistance to acidic and basic environments, easy accessibility to their internal surface area, low density, and flexibility of material synthesis using a wide range of manufacturing, activation and carbonization methods (Yurum et al., 2009; Yang et al., 2011). The extraordinary versatility of the core chemical element carbon has given rise to a wide diversity of structural forms of solid carbon, known as polymorphs which are composed entirely of carbon but have different physical structures. Two variants are amorphous carbons and crystalline carbons. For example, activated carbon is amorphous in nature, carbon nanotubes and nanohorns are crystalline (Bonard et al., 2002; Yang et al., 2011).

Following their discoveries by Ijima in 1991 and 1999, respectively, carbon in the form of multi-walled carbon nanotubes (MWCNTs) and carbon nanohorns have been considered as potential catalyst supports for syngas conversion applications (Shuihua et al., 2010). Like AC, MWCNTs and CNHs share common physico-chemical properties such as inert graphitic nature that minimizes the metal phase interaction and formation of mixed compounds with the support (Zhang et al. 2005). Based on performance, MWCNT is superior to activated carbon as catalyst support since the former displays unique meso/macro-porosity, mitigating reactants and products transport drawbacks prevalent in AC supports. Also, the uniform and straight pore channels of MWCNTs allow better dispersion of active metal species on this support (Che et al., 1999). Moreover, MWCNTs display exceptionally high mechanical strength, high thermal and electrical

conductivity, characteristic electronic properties, as well as medium to high specific surface areas, which renders this nano-structured carbon as a novel catalyst/support. Contrary to MWCNTs, the latest member of the carbon family tree, carbon nanohorns can be synthesized in large quantities, and the products, unlike nanotubes, does not need any further purification (Che et al., 1999). These two key factors make them promising candidates for large scale applications in catalysis and related fields, even though various methods exist for their synthesis.

The mesoporous nature of these carbon nanomaterials makes them attractive to be explored for catalyst support applications. Another porous carbon material that has attracted significant importance in the field of heterogeneous catalysis is the ordered mesoporous carbon (OMC). It is worthy to mention that even though activated carbons possess high surface area, their applications related to syngas conversion to higher alcohol is limited by the significant presence of micropores. Though carbon nanotubes are successfully applied for such as reactions, their potential could be restrained by the limited surface area (Surisetty et al. 2011). Ordered mesoporous carbon materials on the other hand have better surface area than carbon nanotubes, larger pore volume and diameter than activated carbon and it can be a reasonable candidate as a catalyst support for the CO hydrogenation reaction.

2.5. Catalyst preparation and pre-treatment conditions

Supported metal catalysts preparation with physico-chemical properties required for their practical application in chemical reactions is quite a daunting task. Indeed, the overall catalytic performance of the final working catalyst will be dependent on the method of preparation. That notwithstanding, other desired properties such as active metal species, particle sizes, metals dispersion, adequate acidity or basicity, thermal stability, etc., will also contribute to the overall performance (high activity and selectivity) of the catalyst. Moreover, the activity and selectivity

of products in heterogeneous chemical reaction also depends on the selection of metal precursors for the catalyst preparation, which has a direct impact on the cost and availability of the chemicals. The active metal species dispersed on the support substrate have to be accessible to the reactants to enhance the conversion of the reactants to products. To achieve great dispersion of active species on the support, the metal precursor is mostly dissolved in a solvent and impregnated on the support by either the incipient or wet impregnation technique.

The impregnation technique involves the wetting of the solid support matrix of high surface area with a liquid solution containing the dissolved metal oxide precursors. The support matrix may be either a siliceous, carbonaceous, metal oxide, crystalline, amorphous, etc., and the impregnating solution can be aqueous or organic depending on the solubility of the metal precursors. Depending on the correlation between the impregnating liquid volume (V_{liq}) and support pore volume (V_{supp}), the technique can either be described as wet or incipient (Geus et al., 1997; Che et al., 1997; Knowles et al., 2007). When the amount of impregnating solution is approximately the same as the support pore volume ($V_{\text{imp}} \approx V_{\text{supp}}$), the technique is often described as dry or incipient wetness (IW); however, in cases where much more impregnating solution is required ($V_{\text{imp}} \gg V_{\text{supp}}$), the process becomes the wet impregnation. Due to its simplicity and ease of carrying out, most synthesis methods for supported metal oxides preparation employs the impregnation technique (Knowles et al., 2007).

The supported MoS_2 -based catalysts for higher alcohols synthesis can be prepared by sequential pore volume impregnation or incipient wetness method (Surisetty et al., 2010). Though the MoS_2 catalytic species can be prepared from either the decomposition of $(\text{NH}_4)_2\text{MoS}_4$ precursor or by the reaction of ammonium hepta molybdate tetrahydrate (AHM) with aqueous ammonium sulfide or gaseous hydrogen sulfide, the MoS_2 species prepared by the

sulfidation of MoO_3 have been reported to be less selective towards hydrocarbons formation as compared to the decomposition of its ammonium tetrathiomolybdate counterpart (Naumann et al., 1982; Gherardi et al., 1983; Shen, 1997). Nevertheless, the prepared catalysts in its oxidic form needs to be pre-treated in-situ into the active sulfided form prior to the HAS reactions. Pre-treatment conditions such as temperature, pressure, gas flow rate and heat ramping rate can affect the physico-chemical properties as well as the catalytic performance of the final catalyst (Surisetty et al., 2010). All the catalysts prepared for the HAS study were subjected to sulfidation/reduction using gas mixture containing 10 mole% H_2S in H_2 at 450°C and 3.44 MPa at a gas flow and heat ramp rates of 50 mL/min and $2^\circ\text{C}/\text{min}$, respectively, for 6 h.

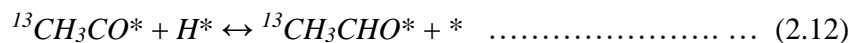
2.6. Reaction mechanism for higher alcohol synthesis

For alkali promoted sulfided catalysts, the retention of the C-O bond is enhanced during the CO hydrogenation. This is due to the electropositive nature of the alkali species which tend to stabilize the electronegative oxygen containing intermediates form during the CO hydrogenation reaction. The resulting stabilized intermediate then guides the hydrogenation to oxygenates rather than hydrocarbons (Christensen, 2011). In a study conducted on the co-feeding of syngas and lower alcohols ($\text{C}_1\text{-C}_2$) by Murchison et al., 1988 and Santiesteban et al., 1988, it was reported that for supported sulfide catalysts, readsorption and elongation of smaller alcohols contributed to the chain-growth of the final alcohol products. Moreover, Santiesteban et al., 1988 used isotopic labeling to elucidate the general mechanism in the synthesis of higher alcohols over MoS_2 based catalysts. These authors injected ^{13}C -labeled methanol into the syngas feedstock and passed it over K/Co/MoS_2 and Cs/MoS_2 catalysts.

It was reported that for the initial chain-growth step (i.e. C₁→C₂), the labelled ¹³C in the ethanol product occupied the β-position of the ethanol molecule relative to the hydroxyl-carbon (Santiesteban et al., 1988):

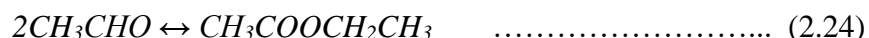
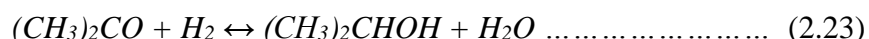
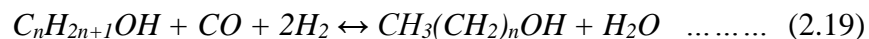
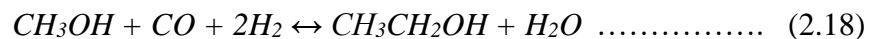


The authors explained the observation as a mechanism of CO migratory insertion into a methyl precursor (CH₃*), derived from the ¹³C-labelled methanol, to form the acyl (CH₃CO*) intermediate which further undergoes a series of hydrogenation steps on the catalyst surface to form ethanol:



It is also worth mentioning that depending on the process conditions and catalyst used, alcohols are synthesized using iso-synthesis (a step-wise CO insertion reaction and a condensation reaction). Conversely, alcohol production by the oxo-synthesis approach uses the FT synthesis pathway, whereby alcohols are generated by the reaction of olefins with one molecule each of CO and H₂ and subsequent hydrogenation of the resulting aldehyde. This involves the hydroformylation of olefins and homologation of lower molecular weight alcohols to generate higher alcohols (Surisetty et al., 2010). Primary and secondary alcohols of linear and branched carbon chains can be present in the product stream along with other oxygenates such as esters, aldehydes, and ketones.

Various chemical reactions taking place during the CO hydrogenation reaction in the HAS reaction include:

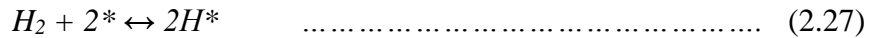
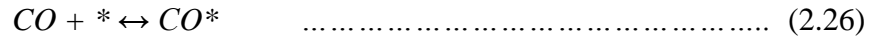


The water gas shift reaction, (eq. 2.17), is assumed to be in thermodynamic equilibrium. According to the reaction stoichiometry, the optimum H₂/CO ratio is 2; however, the simultaneous occurrence of water gas shift reaction means that the optimum ratio is closer to 1. The undesired side reactions such as hydrocarbon formation can occur during the HAS reaction and leads methane formation (eq. 2.25). Due to the exothermic nature of the HAS reaction, from a thermodynamic point of view, lower temperatures and higher pressures are advantage for the formation of alcohols.

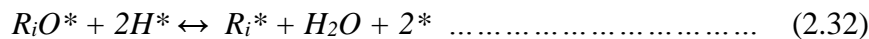
In the work of Santiesteban and coworkers, a reaction system was developed for the production of mixed alcohols over alkali-modified MoS₂ catalysts based on CO insertion

mechanism. The reactions scheme involved three main processes namely; chain initiation, propagation and termination (Surisetty, 2010):

Chain Initiation:



Chain Propagation:



Chain Termination:



where * represents the active sites located on the surface of the catalyst and R indicates an alkyl group (i.e., $R_i = C_iH_{2i+1}$, where $i = 1, 2, 3, \dots$). In the series of reaction schemes above, alcohols are formed by the respective hydrogenation of their precursors (R_iO^*). Similarly, hydrocarbons and esters are formed from R_i^* and R_iCOO^* precursors, respectively, by the CO insertion and hydrogenation mechanism. Reactions represented by eqs. (2.26) to (2.30) are

assumed to be in equilibrium due to the formation of intermediate precursors prior to the chain propagation step to take place.

2.7. The Anderson-Schulz-Flory (ASF) distribution

In the higher alcohol synthesis reaction, alcohols and hydrocarbon products distribution over alkali-promoted or unpromoted MoS₂ catalysts have often been deemed to approximately follow the so-called ASF (Anderson-Schulz-Flory) distribution. (Park et al., 1997). Derivation of the ASF distribution is based on the polymerization kinetics with C₁ monomers and is valid when the probability of chain growth (α) is independent of chain length (Friedel et al., 1950; Flory, 1977). This suggests that irrespective of the mechanism of the carbon chain growth, it occurs by a step-by-step addition of one carbon species derived from the CO molecule, and also the probability of chain growth is independent of the length of the growing carbon chain (Andersson, 2015)

Using the ASF model, the product distribution can be represented with the chain growth probability (α) defined as:

$$\alpha = \frac{R_p}{R_p + R_t} = \frac{k_p}{k_p + k_t} \dots\dots\dots (2.39)$$

where R_p and R_t are the rates of propagation and termination, respectively, with $R_p = k_p \theta_n$, $R_t = k_t \theta_n$. k_p and k_t are the rate coefficients for propagation and termination, respectively, and θ_n is the surface concentration of the chain with n carbon atoms.

Similarly, the probability of chain termination can be represented by:

$$1 - \alpha = \frac{R_t}{R_p + R_t} = \frac{k_t}{k_p + k_t} \dots\dots\dots (2.40)$$

The mathematical representation of the ASF distribution is given by:

$$S_n = n \cdot (1 - \alpha)^2 \alpha^{n-1} \dots\dots\dots (2.41)$$

where S_n is the carbon selectivity for chains with n carbon atoms and α is chain growth probability. Thus, plotting the $\ln (S_n/n)$ vs. n gives the ASF plot which results in a straight line when the chain growth probability (α) is independent of n .

$$\ln \frac{S_n}{n} = n \ln \alpha + \ln \frac{(1-\alpha)^2}{\alpha} \dots\dots\dots (2.42)$$

CHAPTER 3

Experimental methods and characterization techniques

Contribution of this chapter to overall study

This chapter provides detailed description of experimental methods and characterization techniques employed during the project. Detailed descriptions of the syntheses procedures for the pristine ordered mesoporous carbon, carbon nanohorns and its by-products have also been presented in this chapter. Also, methods employed for the preparation of all the carbon-supported KCoRhMo catalysts, their respective characterization techniques as well as their catalytic activity studies have been provided. Finally, the section also gives schematic designs of set-ups used throughout the studies.

3.1. Introduction

In this section, experimental methods and characterization techniques employed in the course of the project have been presented in four subsections: 1) Syntheses and chemical pre-treatments of pristine supports; 2) Preparation of supported KCoRhMo catalysts; 3) Characterization techniques of supports and catalysts; and 4) Catalytic activity studies for the HAS reaction. Also, addressed in this section are the detailed experimental procedures carried out in the project as well as the underlying principles considered in the various sections of the research.

Finally, the section is designed to enhance understanding of the entire project by providing basic descriptions of all the laboratory work that contributed to the conclusions reached in this thesis.

3.2. Synthesis and preparation of pristine supports

The main carbon supports investigated in this research for the HAS reaction include MWCNT, OMC, and CNH. Other support formulations with binders incorporated include BC-MWCNT, CT-MWCNT, HA-MWCNT, and BC-CNH; designated for bentonite clay (BC), coal tar (CT), humic acid (HA), respectively. The pristine MWCNT of 95% purity were purchased from M.K. Nano, Canada, and pretreated with nitric acid under reflux conditions. The two other pristine supports (OMC and CNH) were synthesized in-house using different synthesis methods and further chemically pre-treated to purify the materials and also introduce oxygen functional groups for metal anchorage. In the subsequent subsections, the syntheses of the pristine OMC and CNH supports as well as their chemical pre-treatment are discussed.

3.2.1. Synthesis of ordered mesoporous carbon support with F127 as template

Synthesis of the pristine OMC support followed procedure described in the literature 20 with some modification (Liu et al., 2010). Figure 3.1 provides schematic of the experimental set-up employed for the synthesis of OMC supports.

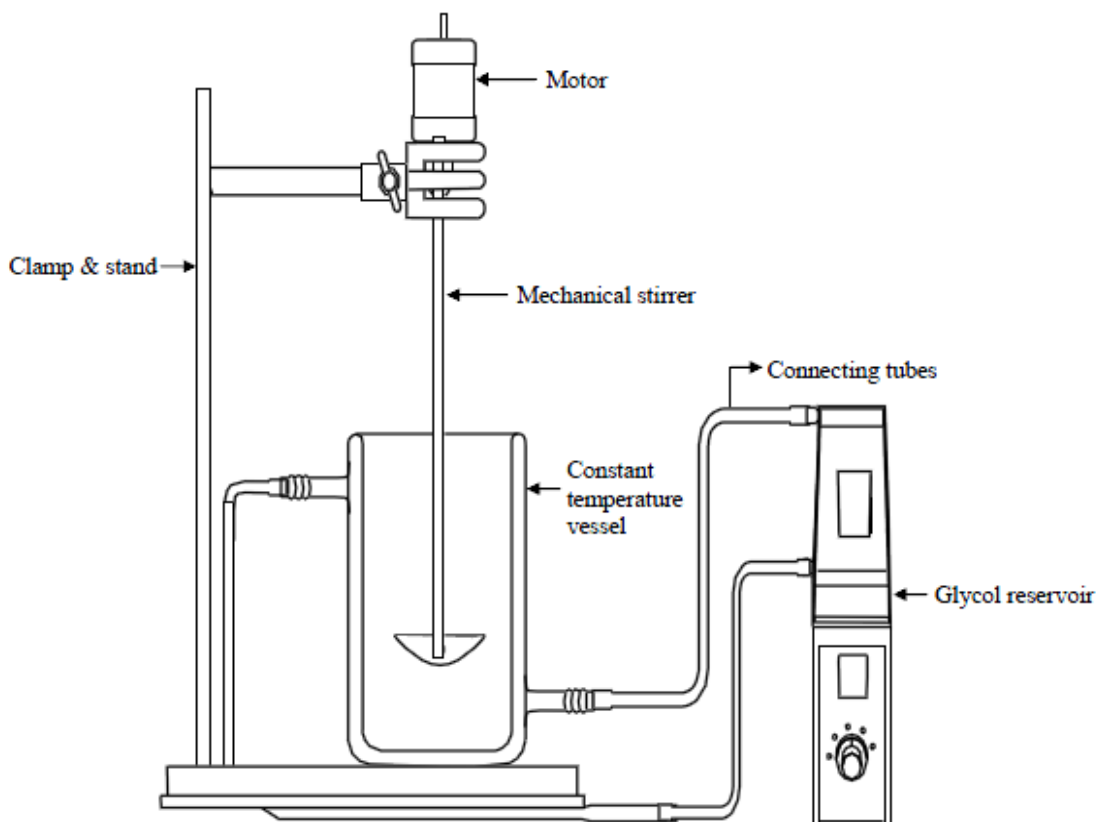


Figure 3.1: Experimental set-up for ordered mesoporous carbon (OMC) supports synthesis

The set-up consisted of a constant temperature vessel (CTV) equipped with ethylene glycol cooling system to control drastic temperature fluctuations. The accuracy of this CTV cooling system can be as high as $\pm 0.1^\circ\text{C}$. Due to its high degree of accuracy, its content was easily maintained at the desired temperature of 15°C for all experimental runs performed. Circulation of the glycol was facilitated by a circulatory pump and a tubing system which connected the CTV to the bulk glycol reservoir. The stirring rate of the disc-shaped mechanical stirrer was controlled by a digital motor assembly supported by means of a clamp and stand apparatus. The motor and circulatory pumping apparatus was powered by a DC (direct current) source for the duration of each experimental run.

In the synthesis of the OMC supports, poly(ethylene oxide)-poly(propylene oxide)-poly(ethylene oxide) block copolymer (F127) was used as the starting soft template, which served as the structure-directing agent (SDA). Phloroglucinol was employed as the phenolic compound to enhance the polymerization reaction of phenols with formaldehyde under acidic conditions (Gardziella et al., 2000). The block copolymer Pluronic F127 ($M_{av}= 12600$, $EO_{97}PO_{67}EO_{97}$) and phloroglucinol were procured from Sigma-Aldrich and used as received. The nominal molar ratio of the chemicals used in the synthesis medium was 0.0008 F127: 0.008 Phloroglucinol: 0.0099 Formaldehyde: 0.004 HCl: 0.435 Ethanol. In a typical synthesis protocol, 1.0 g each of phloroglucinol and F127 template were dissolved in 20 g of ethanol solution at 15°C under mechanical stirring. After the solid was completely dissolved, 0.39 g of 37% HCl was added to the solution as a catalyst and stirring continued at the same temperature for an additional 2 h until a light pink color appeared. Subsequently, 0.8 g of 37 % formaldehyde solution was added to the obtained solution and stirring continued for approximately 50 min until the mixture turned turbid.

The solution was then poured into petri dishes to facilitate the evaporation of ethanol at room temperature (for about 12 h), followed by heating in an oven at 100°C for 24 h. The as-made products were scraped out of the petri dishes and crushed into chunks. To carbonize the obtained product, the sample was pyrolyzed in a tubular furnace at 600°C for 4 h using a heating rate of 1°C/min under N_2 atmosphere (at a flow rate of 50 mL/min). To obtain the fine powdered pristine OMC support, the pyrolyzed sample was pulverized and then passed through vertically arranged sieves so as to obtain the required particle size for catalyst preparation.

3.2.2. Carbon nanohorn support and by-products syntheses

Carbon nanohorns can be generated using different synthesis techniques such as CO_2 laser ablation of graphite without a metal catalyst, laser ablation of Ni/Co doped graphite, chemical

vapor deposition (CVD), and submerged arc discharge method (Kasuya et al., 2002; Sano et al., 2004; Suehiro et al., 2006; Antolini et al., 2009). The submerged arc in liquid nitrogen technique is quite simple and economical as compared to other conventional techniques used to generate carbon nanostructures such as fullerenes and nanotubes (Wang et al., 2004). For the present study, the arc discharge method was employed due to the simple and easy to control design set-up. Figure 3.2 provides schematic of the experimental set-up employed for the synthesis of pristine CNH supports. It should be mentioned that in the synthesis of the pristine CNH support, other carbon byproducts are produced. In this work, these byproducts were designated as other carbon particles (OCP) and fine fraction of the other carbon particles (OCP_f).

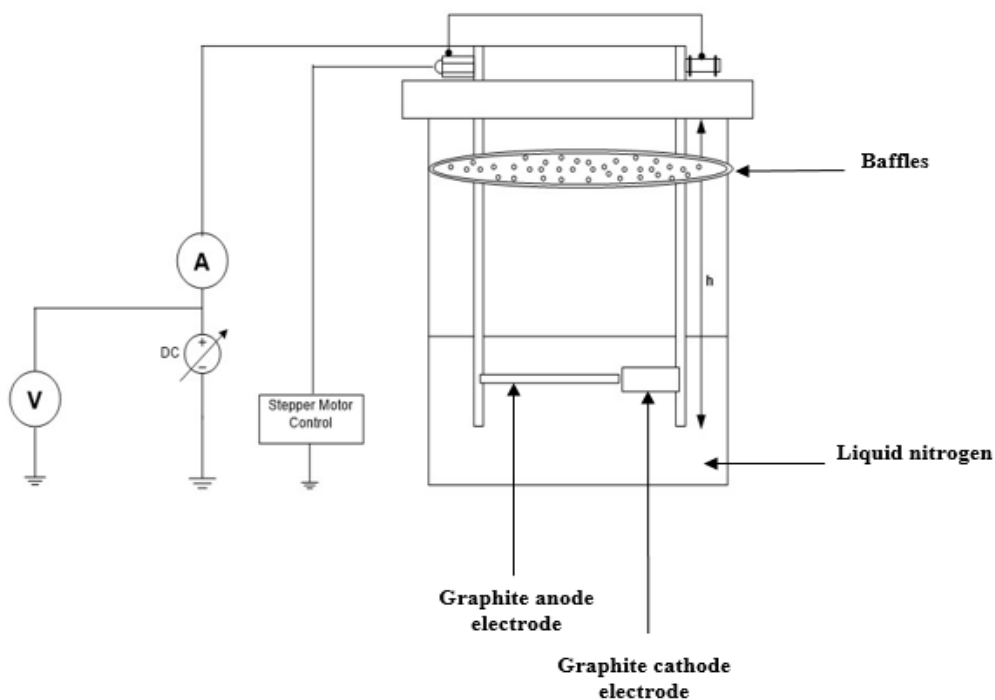


Figure 3.2: Experimental set-up for carbon nanohorn (CNH) supports synthesis

The pristine supports (CNH, OCP_f and OCP) were synthesized by the submerged arc discharge in liquid nitrogen technique as described by Wang, 2004 at a fixed current of 90A and

34V. This method requires a direct current (dc) power supply, carbon electrodes and liquid nitrogen. In a typical synthesis, two pure graphite (99.99% purity) electrodes were submerged in an insulated 2 L stainless steel Dewar flask containing liquid nitrogen. The cathode and anode tip diameters were maintained at 12 and 3 mm, respectively, throughout the experiments. The gap between the two electrodes was controlled manually by a control box equipped with a button to increase or decrease the gap distance. At a gap distance of ~1 mm, an arc was initiated in the liquid nitrogen, which was accompanied by turbulence and dense black smoke. The consumed graphite anode was immediately quenched into the liquid nitrogen solution, forming various carbon products including MWCNTs, amorphous carbon and CNHs.

After the CNH generation process, the content of the Dewar flask was kept for 12 h for the evaporation of the remaining liquid nitrogen. Subsequently, deionized water was used to thoroughly wash the Dewar flask prior to solution settling, decantation, and filtration procedures. The decanted portion of the solution formed the top floating carbon particles, mostly CNHs. The suspended particles in the solution as well as the chunky parts settling at the bottom of the flask were filtered, air dried, and designated as OCP_f and OCP, respectively, prior to HNO_3 functionalization.

3.2.3. Chemical pre-treatments of pristine supports

In this work, a total of five pristine carbon supports namely: MWCNT, OMC, CNH, OCP_f , and OCP were investigated for their performance in the conversion of syngas to higher alcohols. Chemical pretreatment/functionalization of the pristine carbon materials was a necessary step towards modification of the surface chemistry and the creation of functional groups for metal anchorage (Saito et al., 2002; Datsyuk et al., 2008). Treatments of these materials are crucial since different treatment conditions are required accordingly. For the MWCNT and OMC supports, prior

to co-impregnation of metal (Co, Mo, Rh) precursors, the pristine carbon supports were subjected to nitric acid pretreatment using 30 % HNO₃ refluxed at 110°C for 12 h, washed with distilled water multiple times until attainment of a neutral filtrate pH prior to drying at 120°C for 6 h. For the CNH support and its byproducts (OCP_f and OCP), HNO₃ treatment was carried out for 30 mins due to the nature of CNH material.

Other oxidizing agents aside from HNO₃ that was employed for chemical treatment of the OMC support were KOH and a mixture of NH₄OH/H₂O₂. For that study, the pristine OMC support treatments followed procedure described in the literature with modification (Datsyuk et al., 2008). In a typical NH₄OH/H₂O₂ treatment, 2 g of pristine was dispersed in 215 mL of a mixture of 25 wt% NH₄OH and 30 wt% H₂O₂ (in ratio 50:50) in a 500 mL flat bottom flask equipped with a condenser and immersed in an oil bath maintained at 110°C. The mixture was kept under reflux condition with magnetic stirring for 12 h and subsequently diluted with de-ionized water, filtered, and washed multiple times until a neutral filtrate pH was attained. The resulting solid sample was then oven dried at 120°C for 12 h. Finally, for the KOH treatment, 30 wt% KOH solution was prepared by dissolving the required amount of KOH pellets in 500 mL of de-ionized water in a flat bottom flask and reaction proceeded as described above. The chemically treated OMC supports were designated as OMC-HNO₃, OMC-NH₄OH/H₂O₂, and OMC-KOH for the HNO₃, NH₄OH/H₂O₂, and KOH treatments, respectively.

3.2.4. Preparation of K-promoted supported catalysts

Prior to metals (Co, Mo, and Rh) loading, the functionalized carbon supports were subjected to alkalization procedure using the required amount of aqueous solution of K₂CO₃. This was followed by supports stabilization at 300°C in argon flow of 50 mL/min at a heating rate of 10°C/min for 4 h, and consequently, the co-impregnation of respective metal (Co, Mo, Rh) species

using ammonium heptamolybdate tetra hydrate (Alfa-Aesar, Canada), potassium carbonate (Sigma-Aldrich, Canada), cobalt acetate tetra hydrate (Alfa-Aesar, Canada), and rhodium chloride hydrate (Sigma-Aldrich, Canada) as precursors for Mo, K, Co, and Rh, respectively. The oxidic form of the dried powder K-doped CoRhMo samples were obtained after 4 h of oven drying at 120°C, followed by stabilization at 450°C under argon flow of 50 mL/min at a heating rate of 10°C/min for 12 h. The final catalyst composition (wt.%) of 9% K, 15% Mo, 4.5% Co and 1.5% Rh, respectively, was to be attained.

To maintain clarity and consistency with published sections of this thesis as manuscript, the designations used in the published manuscripts have not been altered. In this regard, Cat-1 represents the fine powder form of the KCoRhMo/MWCNT catalyst sample. Similarly, the fine powder forms of the OMC-supported catalysts were designated as follows: KCoRhMo/Untreated OMC (Cat-UnOMC), KCoRhMo/OMC-HNO₃ (Cat-HNO₃), KCoRhMo/OMC-NH₄OH/H₂O₂ (Cat- NH₄OH/H₂O₂) and KCoRhMo/OMC-KOH (Cat-KOH), respectively. Finally, the fine powder form of the CNH, OCP_f and OCP-supported KCoRhMo catalyst samples were designated as Cat-CNH, Cat-OCP_f and Cat-OCP, respectively.

3.2.5. Preparation of binders-incorporated catalysts and catalyst pelletization

The three selected binders investigated in the present work include bentonite clay (BC), coal tar (CT) and humic acid (HA). For each binder studied, catalyst-binder matrix formulation followed preparation regimen reported in the literature with modifications (Zhongren et al., 2006). For instance, in a typical formulation of the humic acid-MWCNT catalyst (HA-MWCNT) matrix, a mixture of 1 g of 30 % HA (balance fine powdered catalyst, Cat-1) was mixed together with 2 mL of de-ionized water and allowed to dry for 12 h at room temperature. Subsequently, the caked mixture was crushed, packed into a 1 cm die and subjected to a load of 5,000 N for 10 min to

produce pellets with diameter of 1 cm. The casted pellet (in the die) was then heat treated (50 % variac power, 34 V), under a mechanical load of 2,000 lb for 1.5 h. The cylindrical pellet obtained was then stabilized at 600°C under Ar flow (50 mL/min) for 2 h using a vertical quartz tube housed in a furnace and a temperature control set up. A similar approach was followed in the preparation of the coal tar incorporated catalyst (denoted as CT-MWCNT). However, for the formulation of the bentonite-incorporated catalyst, a mixture of 1 g of 30 % bentonite (balance fine powdered catalyst, Cat-1) was mixed with 10 mL deionised water at 60°C for 1.5 h. In cases, where the weight percentage of bentonite used changed, the volume of deionised water added was changed proportionately. The obtained wet paste was dried at room temperature for 12 h, packed into a 1 cm die and pelletized as per aforementioned description.

Apart from this procedure, all other steps were similar to that employed for the other two binders. In the preparation of catalyst pellets of specific particle sizes, the heat treated sample was allowed to cool down at room temperature, pulverized and then passed through vertically arranged sieves so as to obtain particles of 1,700 μm size. In the first phase of study where MWCNT was the support of interest investigated, the binders incorporated catalyst samples were denoted as Cat-2, Cat-3, and Cat-4 to represent BC-MWCNT, CT-MWCNT, and HA-MWCNT-supported KCoRhMo catalysts, respectively; the binder-free counterparts were denoted as Cats-0 & 1, respectively. In phase three, the optimization of bentonite clay was conducted using OMC support. Catalysts prepared in that phase of study were denoted as Cat-1, Cat-2, and Cat-3. All prepared oxidic catalyst samples were characterized by N_2 -adsorption/desorption, inductively coupled plasma (ICP), powder X-ray diffraction (XRD), Raman spectroscopy, Boehm titration, and other characterization techniques. The sulfide catalyst samples were obtained by in-situ heating of the oxide catalysts in a flow of 10 % $\text{H}_2\text{S}/\text{H}_2$ gas at 450°C, at a heating rate of 2°C/min for 4 h.

3.3. Characterization techniques of supports and catalysts

Several characterization techniques were applied to the as-synthesized carbon supports and corresponding KCoRhMo-supported catalysts. Relevant techniques were selected to help ascertain the structure, morphology, textural properties, as well as to give insight about the catalytic behavior of materials produced.

3.3.1. N₂-adsorption/desorption measurement

The textural properties of catalysts were ascertained with a Micromeritics ASAP 2020 analyzer at liquid nitrogen temperature of 77 K. The fully computerized analysis allows the estimation of the specific surface area, pore volume, and average pore diameter of prepared samples using the Brunauer–Emmett–Teller (BET) method in the standard pressure range 0.05–0.30 P/P₀. Typically, nitrogen adsorption on the material is analyzed under liquid nitrogen conditions. Based on the amount of N₂ physically adsorbed by the materials, the specific surface area (m²/g), average pore diameter (nm), and pore volume (cm³/g) can be estimated.

Briefly, 0.2 g of sample was used for each analysis. The sample (support or catalyst) was degassed in sealed tube under vacuum at 200°C for 4 h prior to analysis until the static pressure remained <6.6*10⁻⁴ Pa. The value of 0.1620 nm² was taken for the cross-section of the physically adsorbed N₂ molecule. The pore diameter and pore size distributions were calculated from the adsorption and desorption branches of the isotherms using the Barrett–Joyner–Halenda (BJH) method. The mesopore volume was determined from the N₂ adsorbed at a P/P₀ = 0.4. The total pore volume was calculated from the amount of nitrogen adsorbed at P/P₀ = 0.95, assuming that adsorption on the external surface was negligible compared with adsorption in pores.

3.3.2. Wide-angle X-ray diffraction

Powder X-ray diffraction analysis is a powerful tool which employs X-rays of known wavelength incident on sample in order to identify its crystal structure. The wave nature of the X-rays facilitates diffraction by the lattice of the crystal to give characteristic diffraction peaks at differing angles and intensities. The diffracted beams from atoms in successive planes cancel out unless they are in phase, and the condition for this is given by the Bragg relationship:

$$n\lambda = 2d\sin\theta \dots\dots\dots (3.1)$$

where λ = wavelength of the X-rays; d = distance between different plane of atoms in the crystal lattice; and θ = angle of diffraction.

Wide-angle X-ray diffraction patterns of the powder carbon samples were recorded on a Rigaku diffractometer using high intensity Cu K α radiation source ($\lambda=0.1541$ nm). Scanning of each sample was performed at a rate of 0.05°/s within a 2θ range of 10 to 80°. The phases present were identified using the JCPDS diffraction files by matching the corresponding diffraction peaks or patterns.

3.3.3. Transmission Electron Microscopic analysis

Transmission Electron Microscopy (TEM) was used to study the morphological features of the support and catalysts. Electron micrographs were obtained using a JEOL 2011 scanning transmission electron microscope equipped with Gatan Imaging Filter (GIF 2000) to facilitate imaging at 200 keV using low to high magnifications, in the range of 20-500k times magnification. Prior to sample analysis, the powder samples were sonicated in ethanol using an ultrasonic bath for 1h, followed by deposition of the resultant solution on a 200 mesh carbon-coated copper grid. This technique provides a means by which the inner pore diameter, structural morphology, as well as the particle size of catalyst materials can be determined. A beam of incident electrons are

transmitted through an ultra-thin sample as a result of interaction with the sample. This produces an image which possesses a degree of transparency that allows the inner pore diameter and shape of the material as well as the dispersed catalyst particles to be determined.

3.3.4. Inductively Coupled Plasma-Mass Spectrometry

The main principle governing the inductively coupled plasma mass spectrometry (ICP-MS) method of analysis is by applying ICP to produce ions from the sample and MS to separate and detect the ions. Since there is always a difference between the targeted and actual amount of metal contents impregnated, the ICP-MS technique provides the necessary tool to determine the exact metal content of each catalyst sample. Thus, this technique was utilized to quantify the metal composition in the catalysts.

Inductive coupled plasma-mass spectroscopic (ICP-MS) analysis was utilized to quantify the metal composition in the catalysts. The content of Mo, Co, and Rh of the oxide catalysts were determined using a Perkin-Elmer ELAN 5000 ICP-MS instrument. Approximately 0.05 g of the catalyst sample was dissolved in hydrofluoric acid (48–51 %) at a temperature of 100–150°C for 3 days. Following cooling to room temperature, samples were further dissolved in concentrated HNO₃ to ensure the complete dissolution of the metals. The final solution was prepared using 0.2N HNO₃ and analyzed with a mass spectrometer. Furthermore, an energy-dispersive X-ray (EDX) analysis was also used for local compositional analysis using a system attached to the electron microscope which was operated at 25 kV. The chemical composition determination was based on the average analytical data of individual particles.

3.3.5. Fourier Transform Infra-red (FTIR) analysis

The Fourier transform infra-red (FTIR) spectra were recorded in the range 400–1,400cm⁻¹ wave numbers with JASCO FT-IR 4100 instrument using pellets prepared with spectroscopic

grade potassium bromide (KBr). Surface functional groups present on the samples were qualitatively determined by this technique using 64 scans with a nominal resolution of 4 cm^{-1}

3.3.6. Boehm titration

The concentration of oxygenated surface functional groups was evaluated using the Boehm titration method (Boehm, 1966). In a typical procedure for the determination of total number of acidic or basic groups, 25 mL of a solution prepared with 0.05 N of either NaOH or NaHCO₃ and 0.2 g of each of the sample was mixed together in sealed vials under mechanical agitation using shaker apparatus for 24 h. Subsequently, 5 mL of each filtrate was pipetted and titrated with 0.02 N HCl. The numbers of acidic sites were calculated under the assumption that NaOH neutralizes acidic groups and HCl neutralizes basic groups. The amount of HCl consumed was used to calculate the quantity of total acidic groups (carboxylic, lactonic and phenolic groups) reacted with NaOH.

3.3.7. Raman spectroscopic analysis

Laser Raman analyses of the carbon supports were carried out using a Raman imaging equipment (Renishaw Invia Raman Microscope) running WiRE software - version 1.3, with the following pre-set parameters to determine the quality of carbon structure: wave length of laser excitation, $\lambda = 514\text{ nm}$, laser power = $\sim 1\text{ mW}$, exposure time = 30 s, microscope objective = 50, and 1800 l/mm grating.

3.3.8. Thermogravimetric analysis (TGA)

Thermal degradation of the material was studied using the Thermogravimetric analysis (TGA). This technique uses controlled heating of the catalyst sample in the presence of air flow to monitor reactions and physical changes in materials. TGA provides quantitative measurement of

mass change in materials associated with transition and thermal degradation. It records change in mass from dehydration, decomposition, and oxidation of a sample with time and temperature.

Determination of the thermal stability of the freshly prepared catalysts samples was performed using 5 mg of each catalyst sample by employing the thermogravimetric analysis (TGA) technique. Using a Perkin-Elmer (Pyris Diamond) TGA instrument, data was collected at 0.5 s intervals as the sample was heated to 600°C at a rate of 10°C/min under Ar flow at 100 mL/min.

3.3.9. Temperature programmed reduction analysis

The H₂ -TPR profiles of the catalyst samples were obtained in order to study the reducibility of the metal species in the catalysts. In all cases for catalysts analysis, the stabilized catalyst sample (0.2 g) was first purged in a flow of argon at 170°C to remove traces of water, and then cooled to 40°C. Then the TPR of each sample was performed using 3.1% H₂ in He gas stream at a flow rate of 30 mL/min at atmospheric pressure using an automated Quanta chrome gas sorption instrument (AUTOSORB IQ TPD-TPR analyzer) equipped with a thermal conductivity detector, heating at a linearly programmed rate of 10°C /min up to 700°C. The amount of chemisorbed hydrogen was measured using the AUTOSORB IQ TPD-TPR analyzer system. The stabilized catalyst sample (0.2 g) was first purged in a flow of argon at 170°C to remove traces of water. The temperature was then raised to 700°C at a linearly programmed rate of 10°C /min and the temperature reduction profiles of the catalyst samples were recorded.

3.3.10. Mechanical strength analysis

It is desirable for the pelletized catalyst samples to exhibit sufficient mechanical strength so as to reduce losses during charging into the fixed bed reactor. In this regard, mechanical strength determination by means of catalyst crushing strength analysis was conducted using a Texture Expert Exceed Analyzer (version 2.6.4). Broken pieces and fines (fine powder) lost during

handling or produced during commercial use can represent a significant expense, especially for catalysts containing precious metals such as Rh (Haber, 1991). A catalyst pellet was tested for its crushing strength by first placing the pellet between two flat metal surfaces, applying a required compressive load, and measuring the force required to crush the piece.

3.4. Catalytic activity studies

The feedstock used in this study was the commercially available syngas mixture procured from Praxair, Saskatoon, Canada. The CO conversion and selectivity of desired products for the catalysts studied were evaluated using the as-received syngas molar composition (50% H₂:40% CO:10% Ar). Figure 3.3 shows the experimental set-up used for the HAS reaction. The higher alcohol synthesis experiments were conducted in a single-pass downward flow fixed bed reactor system (22 mm ID; 450 mm length) made of Inconel ^[18]. In brief, approximately 2 g of catalyst was diluted with 12 mL of 90 mesh size silicon carbide particles as diluents so as to enhance heat and mass transfer along the length of the reactor. An initial sulfidation/reduction of the oxidic catalyst was necessary prior to catalytic activity study. This was accomplished by first pressurizing the reactor to 3.44 MPa with helium followed by sulfidation/reduction at 450°C (rate of 20°C/min) for 6 h using a gas mixture containing 10 mol % H₂S (balance H₂) at a flow rate of 50 mL/min. The temperature was then lowered to the reaction temperature and the system pressurized to the reaction conditions. The synthesis gas mixture was then introduced via mass flow controllers and the higher alcohols synthesis reaction conducted under steady-state at reaction conditions of 300-340°C, 8.3 MPa, and a gas hourly space velocity (GHSV) of 3.6 m³ (STP)/(h.kg_{cat}) over a period of 24 h.

3.5. Products sampling and composition analyses

The product gas was cooled to 0°C in a cold trap to separate it into gaseous and liquid phases at the reaction pressure (Surisetty et al., 2010) The CO conversion and other gaseous products were monitored hourly by venting the exit gas through an online Shimadzu gas chromatograph instrument equipped with an integrated thermal conductivity detector (TCD) via a sampling valve. Using Ar as an internal standard, the CO conversion was calculated and the overall mass balance of the reaction was determined. The liquid products were collected after 24 h reaction period and analyzed with a Varian 3400 gas chromatograph equipped with a Stabil Wax capillary column and a flame ionization detector (FID). The volume and weight of liquid products were measured to check the mass balance. The experiments were repeated at least twice to check reproducibility.

Mass balance calculations, similar to those proposed by Bahome et al., 2005, were used to calculate the % CO conversion, % CO₂ produced, product STY, and alcohol selectivity (wt. %), and are given as follows:

$$CO\ conversion\ (mole\%) = \frac{Moles(CO_{in} - CO_{out}) * gas\ contraction}{Moles\ (CO_{in})} * 100 \dots\dots (3.2)$$

where the gas contraction was determined from Ar_{in}/Ar_{out} calibration.

$$CO_2\ produced\ (mole\%) = \frac{Moles\ of\ CO_2\ produced}{Moles\ of\ CO_2\ converted} * 100 \dots\dots\dots (3.3)$$

$$Alcohol\ selectivity\ (wt.\%) = \frac{Wt.\ of\ alcohol\ produced}{Total\ wt.\ of\ alcohol\ produced} * 100 \dots\dots\dots (3.4)$$

$$Product\ STY\ \left(\frac{g}{g_{cat} - h}\right) = \frac{Wt.\ of\ the\ product\ produced}{Wt.\ of\ catalyst\ used * reaction\ time} \dots\dots\dots (3.5)$$

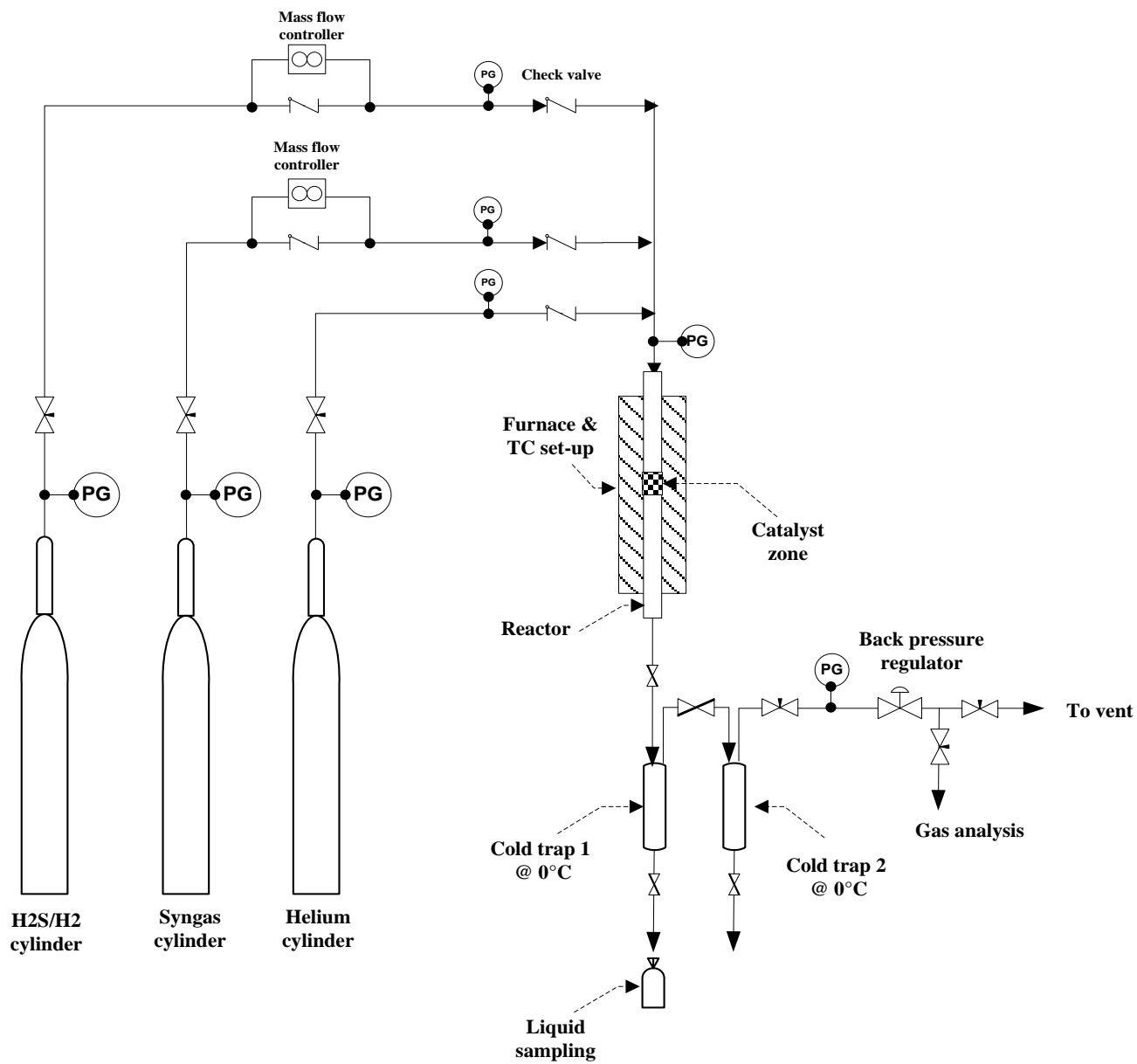


Figure 3.3: Single-pass downward flow fixed bed reactor system for higher alcohol synthesis

CHAPTER 4

Higher Alcohol Synthesis Using K-Doped CoRhMoS₂/MWCNT Catalysts: Influence of Pelletization, Particle Size and Incorporation of Binders

The contents of the manuscript provided in this chapter is very similar to the one published in the Journal: Topics in Catalysis.

Citation:

Boahene P. E.; Surisetty V. R.; Sammynaiken, R.; Dalai, A. K., Higher Alcohol Synthesis Using K-Doped CoRhMoS₂/MWCNT Catalysts: Influence of Pelletization, Particle Size and Incorporation of Binders. Top. Catal., 57, 6, 2014, 538-549.

Contribution of the Ph.D. Candidate

Setting up of the fixed-bed microreactor for experimental runs, development of the catalysts as well as their extensive characterizations and catalytic studies were performed by Philip Effah Boahene. Data collection, analysis and interpretations were performed by Philip Boahene with assistance from Drs. Ajay Kumar Dalai, Venkateswara Rao Surisetty and Ramaswami Sammynaiken. Dr. Sammynaiken was my co-supervisor throughout the program. All the writing submitted manuscript was done by Philip Effah Boahene and discussed with Drs. Sammynaiken and Dalai. Dr. Dalai provided editorial guidance regarding the style and content of the paper.

Contribution of this chapter to overall study

This chapter addresses the challenge of the first phase of the project: to investigate the influence of binders and KCoRhMo/MWCNT catalysts pelletization on the HAS reaction. In this regard, the research explored possibilities of consolidating the powdered form of the KCoRhMo/MWCNT catalyst by incorporating selected binders (bentonite clay, coal tar, and humic acid) and consequently pelletizing into different particle sizes. The trimetallic catalysts were prepared by the incipient wetness impregnation method and extensively characterized for their physical, chemical and mechanical properties. The catalytic performance of the resulting three catalysts (binders-incorporated) was compared with binder-free catalyst for their higher alcohol synthesis capabilities under similar experimental conditions. Finally, the fine powdered catalyst (88 μm) was also compared with the pelletized binder-free counterpart of (1700 μm) mesh size.

4.1. Abstract

In this study, alkalized MWCNT supported MoS_2 catalysts have been doubly-promoted with Co and Rh. Catalysts were prepared by the conventional co-impregnation method and stabilized under argon atmosphere. Characterization of the oxidic samples by BET revealed that the mesoporosity of the pristine MWCNT support was not compromised after loading a combined total of 30 wt% metals (9wt.% K, 4.5wt.% Co, 1.5wt.% Rh, and 15wt.% Mo) on the support; however, a significant decrease in specific surface area was observed. Broad angle XRD analysis confirmed the homogenous dispersion of catalyst metals on the support. Two catalyst grain sizes were first investigated to elucidate the effect of particle size: a finely ground powder (88 μm) and a pelletized form (1780 μm). Despite the total alcohol yield of 0.261 g/(g cat h) observed by conducting higher alcohol synthesis reaction at $T=330^\circ\text{C}$, $P=8.3\text{MPa}$, $\text{H}_2/\text{CO}=1.25$, and $\text{GHSV}=3.6\text{ m}^3_{\text{STP}}/(\text{kg cat/h})$ for the fine powdered sample, the relatively higher pressure drop

could be minimized by using the pelletized form of the catalyst. Finally, a systematic study of variety of selected binders was conducted to gain insight of catalyst's applicability for industrial purposes. Three selected binders namely: Bentonite clay, coal tar, and humic acid were thus investigated; taking into consideration significant factors such as melting point and binder requirement per catalyst support. The CO conversions evaluated for the two binder-free catalysts (88 μm and 1700 μm) showed that the catalyst with fine particle sizes (88 μm) performed better than that in the pelletized form (binder-free, 1700 μm); yielding a maximum ethanol selectivity of 38.5% at steady-state reaction conditions.

4.2. Introduction

By reason of its potential utilization in automobiles with environmental benign footprints, the conversion of syngas to higher alcohols has garnered much attention in recent years (Muramatsu et al., 1992; Herman, 2000). Development of novel catalysts to enhance activity, total alcohol productivity and desired product selectivity has resorted to both homogeneous and heterogeneous catalytic systems studies; though, the latter is unattractive for commercial applications as of present. That notwithstanding, the heterogeneous catalytic processes for higher alcohols synthesis (HAS) via the conversion of syngas suffers from low yield and poor selectivity due to relatively slow kinetics of the initial C-C bond formation and fast chain growth of the C_2 intermediate (Courty et al., 1987).

Of the numerous research attempts to improve the rather low productivity and poor selectivity to desired products using heterogeneous catalytic approach, a range of catalyst systems namely: 1) modified methanol synthesis catalyst (based on $\text{Cu-ZnO/Al}_2\text{O}_3$ and $\text{ZnO/Cr}_2\text{O}_3$); 2) modified Fischer-Tropsch synthesis catalysts (based on Co, Fe, and Ru); 3) modified Mo-based catalysts; and 4) modified MoS_2 -based catalysts have been explored (Herman, 2000). Outstanding

candidate of the enumerated catalytic systems investigated for higher alcohols synthesis is the alkali-doped molybdenum sulfide (ADM) catalysts, which has attracted special attention of commercial significance due to their excellent resistance to sulfur poisoning and high activity for water gas shift (WGS) reactions (Forzatti et al., 1991).

Furthermore, Surisetty et al., 2010, concluded from their comparative study of K-doped CoMoS₂ supported on both activated carbon (AC) and multi-walled carbon nanotube (MWCNT) and co-promoted with Rh that the selectivity toward higher alcohols was much enhanced on the latter support due to its desirable textural properties; and also shows high economic prospects (Surisetty et al., 2010). Nonetheless, the influence of binder incorporation and pelletization of the powdered catalyst into a consolidated form to enhance its applications in the higher alcohol synthesis was not studied. Thus, the main focus of chapter was to investigate the influence of selected binders and catalyst pelletization on the HAS reaction.

4.3. Experimental

The pristine MWCNT support (purity > 95%) used in the preparation of the K-doped MoS₂ catalysts for this study was obtained from M.K. Nano, Canada. The detailed description of the supported KCoRhMo catalysts preparations (with or without binders) and their respective pelletization can be found in Chapter 3, sections 3.2.4 & 3.2.5 of thesis. Furthermore, characterization techniques employed as well as the CO hydrogenation experimental procedures have also been discussed in Chapter 3.

4.4. Results and discussion

4.4.1. Physical catalysts characterizations

Elemental analysis, nitrogen-adsorption/desorption and wide angle XRD analyses were performed. The calcined oxidic KCoRhMo catalysts were analyzed for their respective elemental compositions. The actual percentage of Co, Mo, and Rh were identified using inductively coupled plasma - mass spectrometer (ICPMS). The results of ICP-MS of KCoRhMo catalysts with targeted compositions are presented in Table 4.1. The elemental compositions obtained from ICP-MS and EDX correlate well with each other, as well as with targeted values.

Table 4.1: Elemental compositions and CO uptake of KCoMoRh/MWCNT catalysts (with & without binders)

Sample ID	Composition (wt.%)			CO uptake ($\mu\text{mol/g}$)
	Co	Mo	Rh	
Cat-1	4.5* (4.4)	15* (15.1)	1.5 (1.4)	39
Cat-2	4.5* (4.4)	15* (14.9)	1.5 (1.3)	28
Cat-3	4.5* (4.3)	15* (14.8)	1.5 (1.4)	19
Cat-4	4.5* (4.3)	15* (14.9)	1.5 (1.3)	14

* Targeted composition

The physisorption of nitrogen is a technique commonly used to determine the textural properties of porous materials (Khodakov et al., 2001). Figs. 4.1A & 4.2B show the N₂-

adsorption/desorption isotherms examined at liquid nitrogen temperature of -196°C for the supports and corresponding catalysts. As can be seen in the figures, the supports and catalysts exhibited type IV isotherms with H1 hysteresis loop; indicative of the presence of textural mesoporosity with uniform cylindrical pores (Tanev et al., 1996).

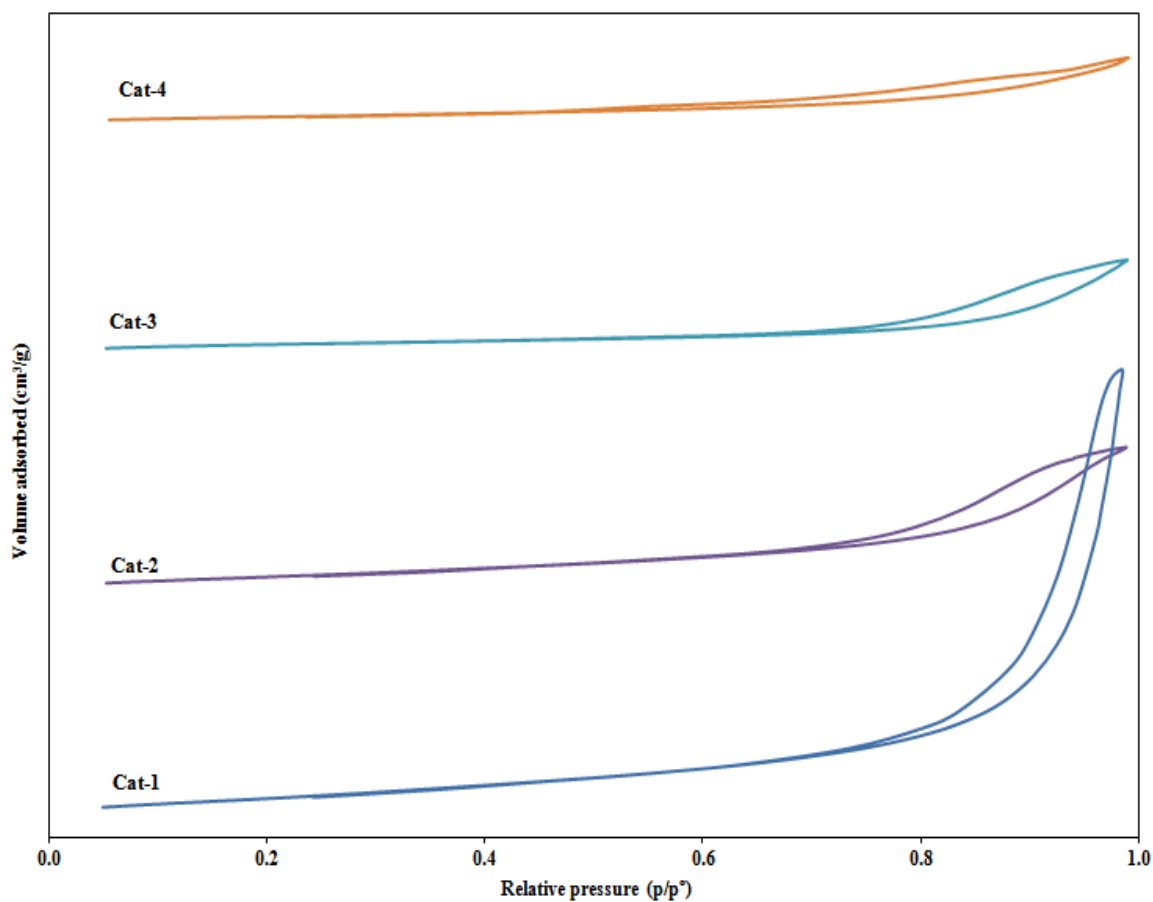


Fig. 4.1 (A): N_2 -adsorption isotherms of pelletized KCoMoRh/MWCNT catalysts (with & without binders) determined from N_2 sorption analysis.

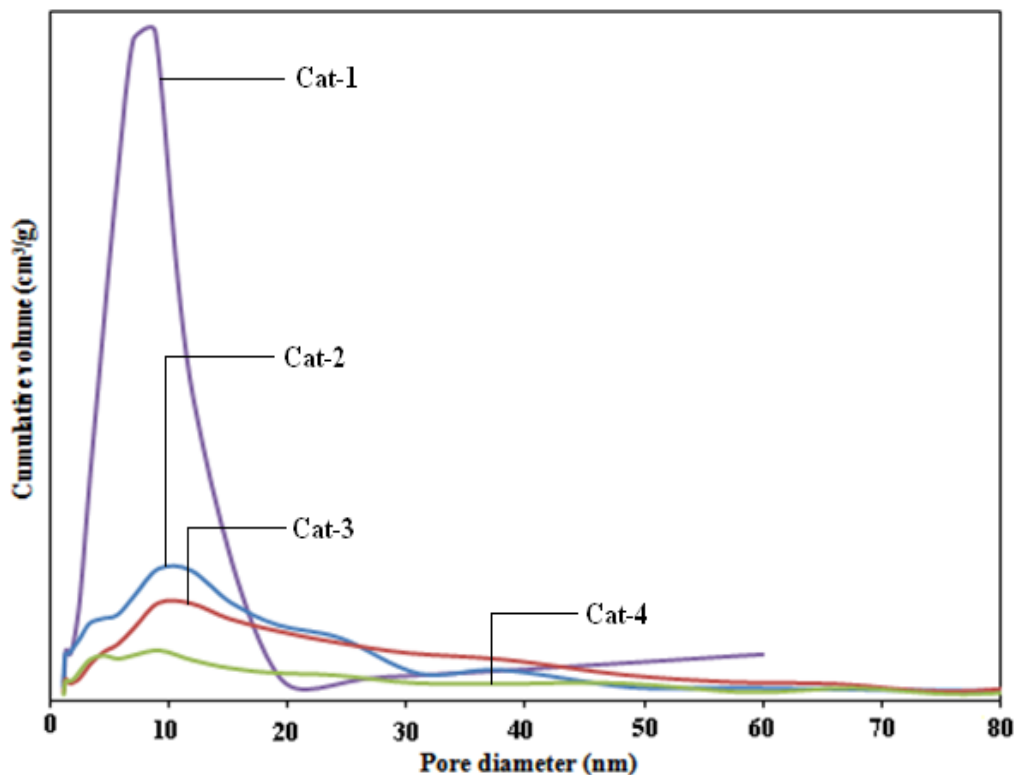


Fig. 4.1 (B): Pore size distribution of pelletized KCoMoRh/MWCNT catalysts (with & without binders) determined from N₂ sorption analysis.

In the catalysis of porous materials, the presence of textural mesoporosity is crucial due to inherent diffusional limitations during adsorption of reactants, surface reaction and desorption of products. The specific surface area (S_{BET}), cumulative pore volume (V_p) and pore diameter of MWCNT supports (with & without binders) and MWCNT-supported KCoMoRh catalysts are listed in Table 4.2. An increase in the specific surface area of the pristine MWCNT support was observed following its pre-treatment with 30wt.% HNO₃, refluxed at 100°C overnight. HNO₃ treatment of CNT supports has been reported to open closed ends and caps of pristine the material (Surisetty, 2010; Sigurdson, 2010). It could be reasoned that the etching effect of the acid on the close-ended pores of the support must be responsible for the increase in surface area as observed. The reduction in specific surface area of supports as a result of co-impregnation of Co, Mo, and

Rh metal precursors was expected. With the incorporation of binders into the fine powder KCoMoRh/MWCNT catalyst, a monotonic decrease in both the surface area as well as pore volume was observed to follow the order: MWCNT-BC > MWCNT-CT > MWCNT-HA; however, changes in the pore diameter of the supports was minimal. This trend is consistent with that observed for corresponding pelletized catalysts, formulated from these supports; except for Cats-0 & 1, which are binder-free and pelletized, respectively. Marginal changes in textural properties can be observed in Cats-0 & 1 (binder-free). The decrease in specific surface as a result of co-impregnation of Co, Mo, and Rh metal precursors on the MWCNT support studied could have resulted in the inhomogeneous dispersion of metal species on the surface of the supports, as corroborated by the X-ray powder diffraction analysis.

For the catalysts studied the NS_{BET} decreases with the deposition of metal species on the supports; the values of NS_{BET} following the order: Cat-0 \approx Cat-1 > Cat-2 > Cat-3 > Cat-4. One can conclude that the incorporation of binders influenced the porosity and the overall textural properties of the final catalysts as was evidenced from the NS_{BET} values; giving an indication of minimal pore blockage in the catalysts formulated without the incorporation of binders.

All catalysts exhibited the type IV isotherm with H1 hysteresis loop, with the shape of the loop changing with the incorporation of binders and metals loading. This indicates that prepared catalysts exhibit uniform textural porosity, which is also in agreement with XRD results. The height of the hysteresis loop is decreased after metals loading into MWCNT due to a decreased pore volume indicating the introduction of metal species within the mesopores of the support. Moreover, the surface area and pore volume of the MWCNT decreased significantly after metal loading. The sharpness of the desorption branches is indicative of the narrow mesopore size distribution.

Table 4.2: Textural properties of treated MWCNT supports and KCoMoRh/MWCNT catalysts (with & without binders) determined from N₂ sorption analysis.

Sample ID	Composition (wt.%)				BET analysis			
	K	Co	Mo	Rh	BJH _{ads}	PV	SSA	NS _{BET}
					(nm)	(cm ³ /g)	(m ² /g)	
Untreated MWCNT	-	-	-	-	12.2	0.541	178	-
HNO ₃ -treated MWCNT	-	-	-	-	10.6	0.662	199	-
30 wt.% BC-MWCNT	-	-	-	-	10.5	0.352	139	-
30 wt.% CT-MWCNT	-	-	-	-	10.9	0.237	131	-
30 wt.% HA-MWCNT	-	-	-	-	10.0	0.14	120	-
Cat-0 (Fine powder)	9	4.5	15	1.5	10.1	0.489	127	0.91
Cat-1 (Pellet - no binder)	9	4.5	15	1.5	10.2	0.497	125	0.90
Cat-2 (BC)	9	4.5	15	1.5	9.8	0.185	76	0.78
Cat-3 (CT)	9	4.5	15	1.5	10.7	0.151	71	0.77
Cat-4 (HA)	9	4.5	15	1.5	10.1	0.085	62	0.74

S_{BET}, specific surface area calculated by the BET method.

NS_{BET} (Normalized surface area) were calculated by using the equation, $NS_{BET} = (S_{BET} \text{ of the catalysts}) / (1-x) \cdot S_{BET} \text{ of the support}$

PV, pore volume determined by nitrogen adsorption at a relative pressure of 0.98.

PD_{ads}, mesopore diameter corresponding to the maximum of the pore size distribution obtained from the adsorption isotherm by the BJH method.

MWCNT, Multi-walled Carbon Nanotubes; **BC**, Bentonite Clay; **CT**, Coal Tar; **HA**, Humic Acid

The pore size distributions of the pelletized KCoMoRh/MWCNT catalysts (with & without binders) are given in Fig. 4.1 (B). As can be seen from this figure, Cat-1 showed a narrower pore size distribution profile as compared to its counterparts formulated with the incorporation of binders. This could be attributable to the introduction of pore sizes in the different size ranges,

with the pores in the smaller size range resulting from the blockage of the support's pore channels and with the pores in the mid-size pore range emerging from the collapse of smaller pores, probably during the calcination step. This characteristic broad pore size distribution may lead to pore blockage; hence, hindering diffusional characteristics of these catalysts during the higher alcohol synthesis reaction. The presence of dispersed metal species inside the mesopores of the MWCNT support was confirmed by estimating the normalized S_{BET} values of the catalyst using an equation proposed by Vradman et al., 2005:

$$NS_{BET} = \frac{(S_{BET})_{Cat}}{(1-x) \cdot (S_{BET})_{Sup}} \dots\dots\dots (4.1)$$

where NS_{BET} is the normalized S_{BET} and x is the weight fraction of the phases. The values of normalized NS_{BET} are given in Table 4.2. As a measure of the extent of pore blockage experienced by the catalyst support during the metals loading procedure, values of NS_{BET} of catalysts close to unity suggest less pore blockage. For instance, NS_{BET} of Cat-0 was computed to be 0.91, which is < 1 ; indicating that the introduction of the oxidic metal nanoparticles caused a minimal reduction in pore volume resulting in an insignificant decrease in the normalized surface area. Furthermore, these results also give an indication that impregnation of metal species on a catalyst support plays a vital role in the overall catalytic surface area required for a given chemical reaction.

Powder X-ray diffraction patterns of the stabilized KCoMoRh/MWCNT catalysts are shown in Fig. 4.2 for 2θ values in the range of 10-80°. The peaks generated by the XRD analysis are matched with the corresponding peaks using the JCPDS chemical spectra data bank (Calafata et al., 1998; Eswaramoorthi et al., 2008). The characteristic peaks occurring at 2θ values of 27.1 and 36.2 are due to the presence of crystalline graphitic carbon in the catalysts studied. Similarly, peaks occurring at 35.8, 41.4 and 64.3 can be attributed to the crystalline MoO_3 . This crystalline

MoO₃ phase was detected on the catalyst formulated with and without binders. Moreover, one could recount that with the incorporation of binders, other peaks are generated while the intensity of some existing peaks become heightened. Typically generated peaks can be found on the diffraction profile for catalyst formulated with humic acid incorporated as a binder.

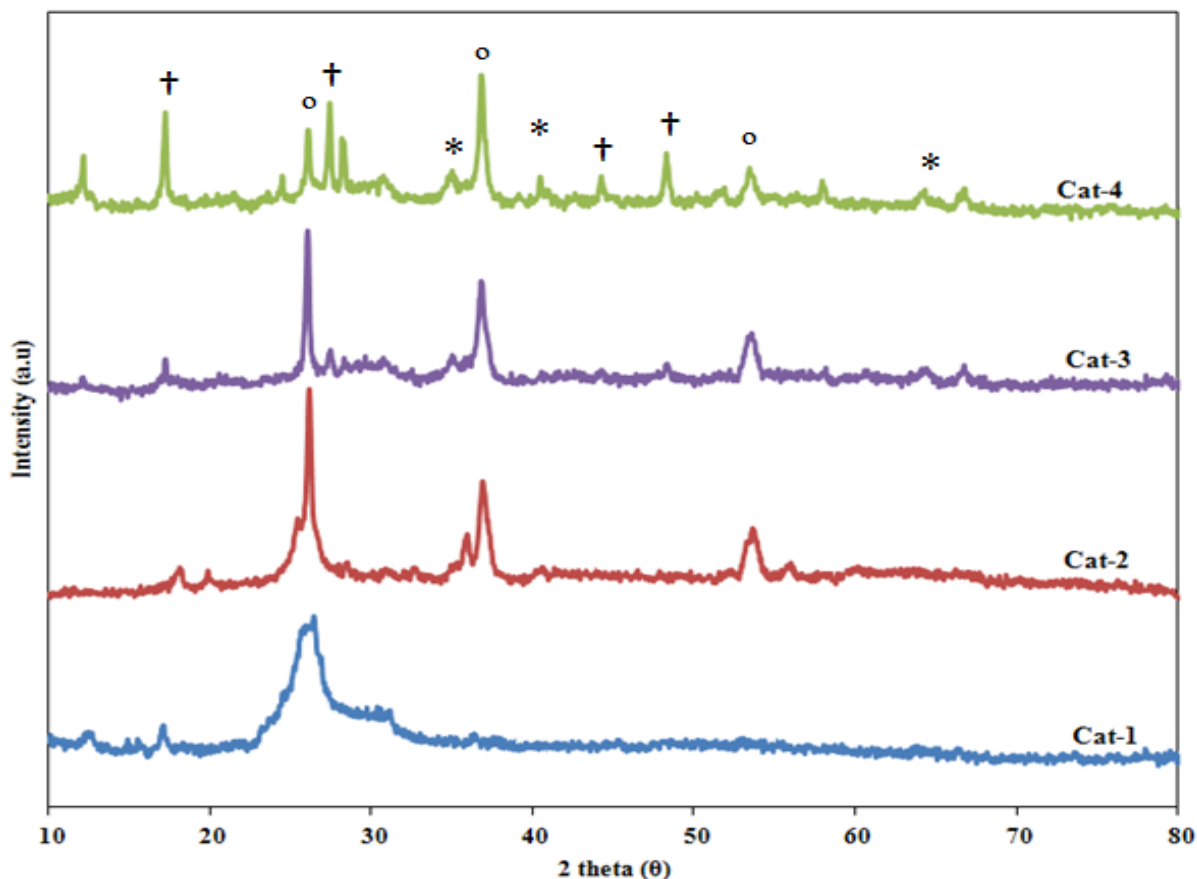


Fig. 4.2: Wide-angle X-ray diffraction patterns of KCoMoRh/MWCNT catalysts (with & without binders). (° graphite; * MoO₃; † K₂Mo₂O₇)

It could be reasoned that homogeneity of metal species deposited on the support for this catalyst was the least enhanced as compared to the catalysts formulated with bentonite and coal tar. The relatively low surface area (120 m²/g) of the HA-MWCNT support least favored dispersion of the active phases; thus, probably contributing to the formation of larger metal phases

in the resulting catalyst. Conversely, the relatively higher surface area of the binder-free support ($199 \text{ m}^2/\text{g}$) may have played a significant role by enhancing great dispersion of catalytic phases as confirmed by the XRD profile for Cat-1. The peaks occurring at 2θ values of 17.6, 20.9, 25.9 and 31.1 can be assigned to the presence of $\text{K}_2\text{Mo}_2\text{O}_7$ species in the samples (Surisetty et al., 2009). Calculation of the average MoO_3 particle size from the XRD spectra by the Debye-Scherrer's equation for the binder-incorporated catalysts showed MoO_3 crystallite size of 11.5 nm for Cat-4 as opposed to 8 nm for Cat-2. These results clearly suggest that the larger MoO_3 nanoparticles formed on the humic acid-incorporated catalyst contributed significantly in its lowest catalytic performance for syngas conversion to higher alcohols.

4.4.2. Chemical catalysts characterizations

Chemical characterization studies conducted include FTIR, Boehm titration and Raman analyses. The surface functional groups present in the catalysts studied were analyzed by the FTIR technique and are shown in Fig. 4.3. The bands occurring at 1642 cm^{-1} corresponds to the stretching modes of carboxylic groups and that at 2365 cm^{-1} can be assigned to the -OH stretching modes from strongly hydrogen-bonded -COOH (Faraj et al., 2010). It is noteworthy that these carboxylic groups can be generated due to the oxidation of some carbon atoms on the surface of the MWCNT support as a result of nitric acid pretreatment. Also, the FTIR spectra from all the catalysts showed a broad peak at $\sim 3450 \text{ cm}^{-1}$, which could be assigned to the -OH stretch of the hydroxyl group, indicating the oscillation of carboxyl groups (Jang et al., 2004). The IR bands occurring at $890\text{-}1091 \text{ cm}^{-1}$ for Cats-2, 3 & 4 could be due to the intrinsic properties of the binders which are not known as of present. As can be seen from the figure these functional groups were absent on the binder-free catalyst; however, they are generated as a result of binders incorporation.

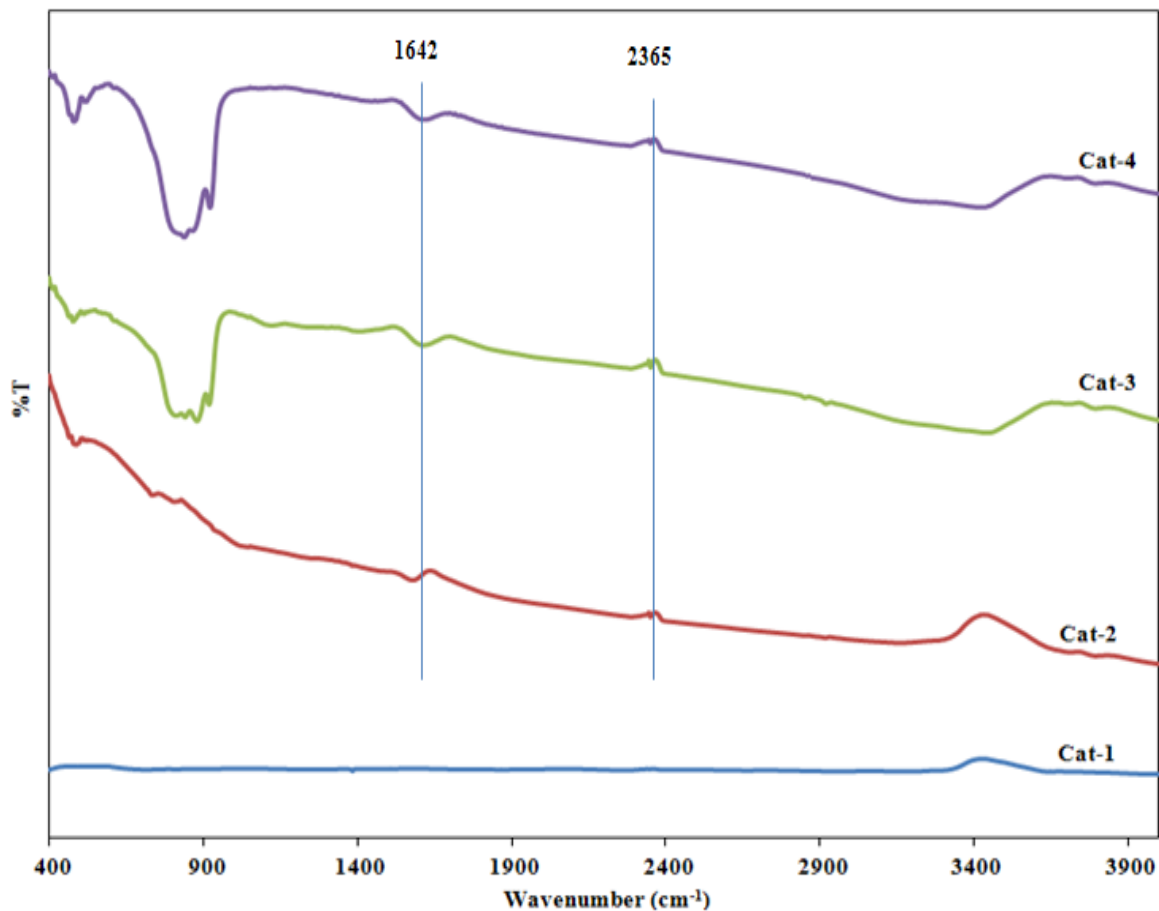


Fig. 4.3: FTIR patterns of KCoMoRh/MWCNT catalysts (with & without binders).

One could conclude that the incorporation of binders into the powder form of the KCoMoRh/MWCNT catalyst resulted in the creation of more –OH and –COOH groups in the catalyst; probably due to their acidic/basic properties. Even though the mechanical properties of the binder-incorporated catalysts were improved, their catalytic performance became counter affected.

Boehm titration, based on the principles of acid/base titration, is a widely used technique to characterize the surface chemistry of carbon materials (Boehm, 1966). This titration technique can effectively determine oxygen-containing functional groups present on the surface of carbon

materials to provide information of surface groups relevant for catalysis. The theory was premised on the fact that in aqueous solution, acid and base tend to react with various basic sites and acidic sites of the carbon material, which are derived from different oxygenated groups, respectively (Li, 2012).

Table 4.3 shows results obtained from Boehm titration conducted using 25mL of a solution prepared with 0.05N of either NaOH or NaHCO₃ and 0.2g of each of the catalyst sample.

Table 4.3: Boehm titration results of KCoMoRh/MWCNT catalysts (with & without binders).

Sample ID	Acidic functional groups (mmol/g)		Total acidity (mmol/g)	% Carboxylic groups (mmol/g)
	Carboxylic	Lactonic + phenolic		
Cat-1	0	0.01	0.01	0
Cat-2	0.02	0.01	0.04	66.7
Cat-3	0.02	0.01	0.04	66.7
Cat-4	0.02	0.00	0.02	100

It can be seen from Table 4.3 that of the four catalyst samples investigated, only a minimal amount of total surface acidity was present in these catalysts; with a greater portion (>66%) being present in the form of carboxylic acid groups (which was initially absent in the binder-free catalyst). It is known that NaOH can centralize carboxylic groups, lactonic groups and phenolic groups of carbon (eg. activated carbon) surfaces (Boehm, 1966); however, owing to the poorer basic property of NaHCO₃ as compared to NaOH, the for can selectively centralize only carboxyl groups and lactonic groups (Li, 2012). Moreover, the release of H⁺ ion or (the proton) in carboxylic

functional groups is much easier as compared to phenolic functional groups, making it easier for the carboxylic acid to donate a proton to make it a stronger acid (Korodi, 2012). As a result, one could reason that the oxygen functional groups present in carboxylic acid in the Cat-1 (binder-free) sample becomes readily available to be consumed for metal anchorage sites during the impregnation step; thus leaving only a mixture of phenolic and lactonic groups on the catalysts (Table 4.3), probably due to the differences in acid strength. It could also be deduced from this table that while the surface functional groups present on Cat-4 is predominantly carboxylic groups (100%), the groups present on Cats-2 and 3 are composed on a mixture of lactonic, phenolic and carboxylic groups. One can conclude that using humic acid as a binder in the catalyst formulation resulted in the introduction of excessive carboxylic acid groups, which is less desirable for the higher alcohol synthesis reaction.

Raman scattering is the inelastic scattering of light, which involves electron excitation from the valence energy band to the conduction via photon absorption; emission of phonons as a result of scattering of excited electron; and finally, the emission of the absorbed photon due to electron relaxation to the valence band (Dresselhaus et al, 2005). For carbon materials such as graphite and SWNTs, information such as electronic structure as well as sample imperfections can be derived from spectra obtained from Raman analysis. As shown in Fig. 4.4, the vibrational characteristics of MWCNT-supported KCoMoRh catalysts (with and without binders) were studied by Raman spectroscopy. The two major bands evidenced in the range of 1350-1360 cm^{-1} and 1575-1600 cm^{-1} can be attributed to the D-band (which characterizes the extent of disorderliness) and the G-band (which is due to C-C stretching mode) of the carbon material. While the G-band indicates the graphitic E_{2g} plane vibration, the D-band is due to the disordered parts such as grain boundaries (Shimodaira et al., 2002), which is indicative of the A_{1g} plane. It is known that the

intensity ratio of the D to G bands (I_D/I_G) is generally used to denote the extent of disorderliness present in the graphite layer of carbon material (Vinu et al., 2007).

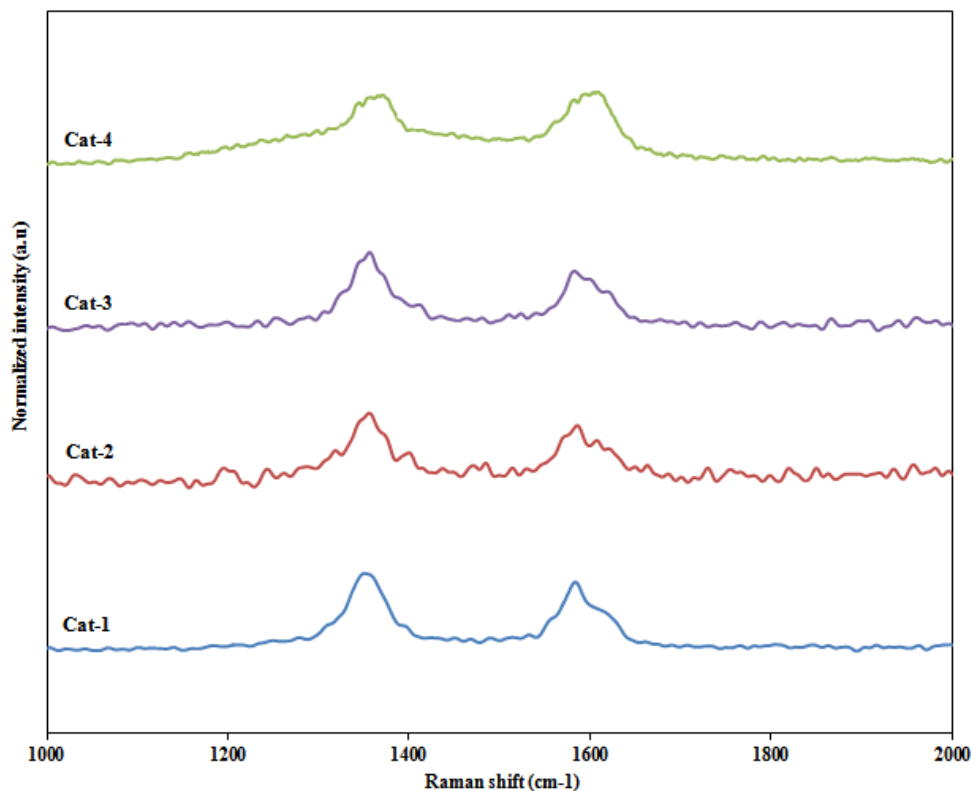


Fig. 4.4: Raman patterns of KCoMoRh/MWCNT catalysts (with & without binders).

As can be seen in Fig 4.4, Cat-4 exhibited the least I_D/I_G ratio indicating the existence of minimal defective sites for the HAS reaction. That notwithstanding, the observed trend for the other catalysts studied follow the order: Cat-3 > Cat-2 > Cat-1. Though the observed trend least explains any logical order, it could be attributed to the unique nature of the binders employed in the catalyst formulation. The noticeable excessive defective sites obtained in the coal tar incorporated sample (Cat-3) must have resulted in the creation of more functional groups which might be due excessive etching of the wall of the carbon material and increase in surface functional groups during functionalization with nitric acid of higher concentration.

The percent weight loss of the catalyst samples as a function of temperature was ascertained by TGA technique so as to determine the thermal stability of the impregnated catalysts during the HAS reaction. Fig. 4.5 shows the TGA profiles for Cats-1 to 4.

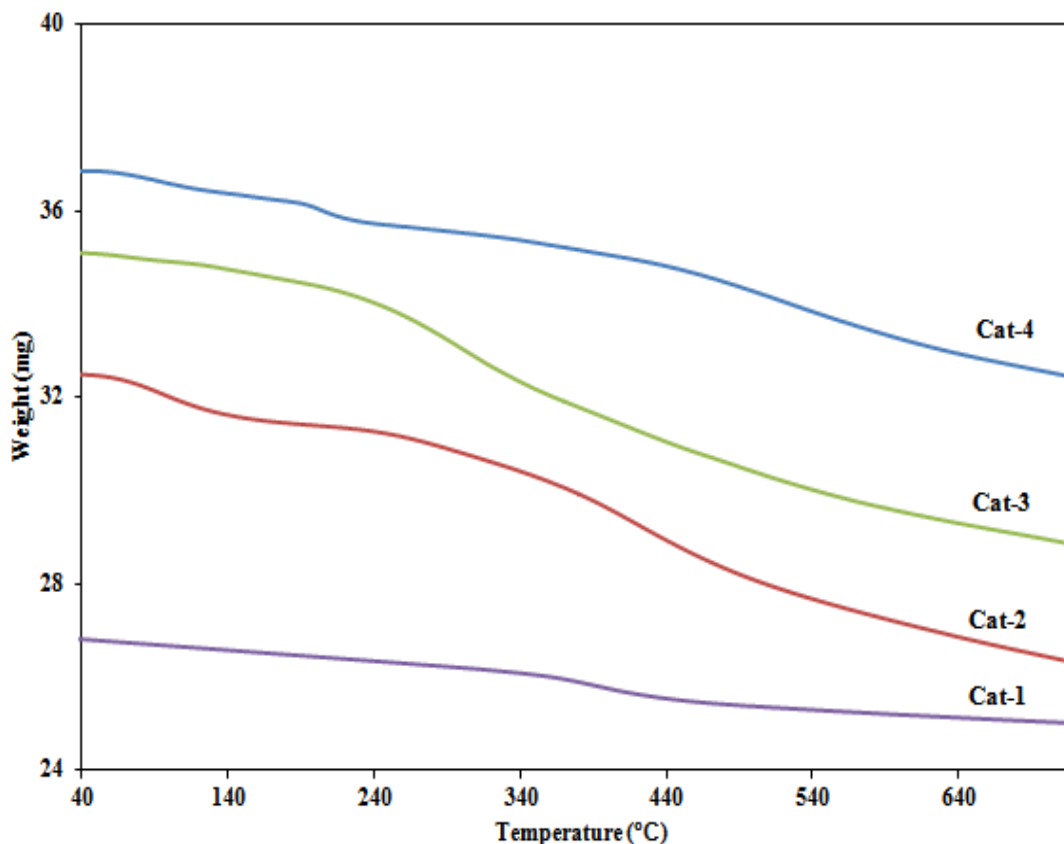


Fig. 4.5: TGA profiles of KCoMoRh/MWCNT catalysts (with & without binders).

It is clear from the patterns that with incremental temperature changes, a significant loss in weight was observed for all catalysts formulated with the incorporation of binders. That notwithstanding, the binder-free catalyst (Cat-1) exhibited quite stable thermal property as compared to its counterparts; thus would experience minimal weight loss under practical reaction conditions. The trend observed for weight loss in the temperature range of 240-540°C is as follows: Cat-3 (11.8%) > Cat-2 (11.5%) > Cat-4 (5.3%) > Cat-1 (3.1%). For instance, in a study conducted

by Stagnaro et al., 2012, on the influence of thermal treatment on bentonite used as adsorbent, it was observed from thermogravimetric analysis that a significant mass loss occurred between 200-500°C, after which only 4% mass lost was observed between 500 and 700°C. This observation is consistent with the profile of the bentonite-incorporated catalyst, which experienced about 11.5% mass loss in the range of 240-540°C. One could deduce from Fig. 4.5 that the rapid weight loss for binder-incorporated catalysts suggests a form of decomposition of these materials from the catalysts as temperature gradually increased, resulting in the generation of more pores, probably, due to the inherent collapse of pore walls contributing to the increase of cumulative pore volume as corroborated by results obtained from textural property analysis by the BET technique.

The mechanical strength of the pelletized KCoMoRh/MWCNT catalyst samples by means of crushing strength determination were ascertained to determine the extent to which these formed pellets could be subjected to a constant compressive load without failure. The measurements of this parameter will give an idea of the capabilities of the catalyst to maintain its physical integrity during handling and its subsequent use in the reactor. It is clear that the incorporation of binders improved the crushing strength of the plain catalyst. As can be depicted in Table 4.4, the crushing strength of the binder-incorporated catalysts followed the order: Bentonite clay > Coal Tar > Humic acid. It is obvious that the pelletized form of the catalysts studied showed that Cat-2 (with Bentonite Clay as a binder) could withstand a maximum load of ~340N before crushing into fines, with the pelletized binder-free catalyst (Cat-1) exhibiting the least crushing strength of 1.4N. As compared to the commercial γ -Al₂O₃ support, one could conclude that though the minimal distance that the applied compressive load needs to advance before crushing the pellet is very small for the binder-free catalyst as compared to the catalyst formulated with the incorporation of binders. This

gives an indication that the incorporation of binders provided some extent of mechanical strength to the formulated catalyst.

Table 4.4: The crushing strength of the KCoRhMo/MWCNT catalysts (with & without binders).

Sample ID	Force (N)	Distance (mm)
Cat-1	1.4	0.01
Cat-2	339.9	0.41
Cat-3	208.5	0.22
Cat-4	156.2	0.29
γ -Al ₂ O ₃	448.7	0.46

4.5. Catalytic performance tests of MWCNT-supported KCoMoRh catalysts

Evaluation of prepared catalyst samples for their performance in the HAS reaction using a high-pressure fixed-bed micro reactor was accomplished by screening Cats-1 to 4 using syngas as feedstock under conditions of pressure, temperature, H₂:CO, and GHSV of 8.3 MPa, 300-340°C, 1.25, and 3.6 m³ (STP)/kg_{cat.} h, respectively. The higher alcohol synthesis reaction was carried out prior to initial catalyst sulfidation/reduction step, which is necessary to transform the less active oxidic form of the catalyst to a more active sulfidic form. The metals loading intended for the formulation of these catalyst samples were maintained the same to help study the effect of particle size and binders incorporation on higher alcohols productivity.

4.5.1. Effect of particle size on CO conversion

In heterogeneous catalytic reactions, whereby the catalyst material is usually in a different phase from that of the reactant species, the nature of catalyst (fine powder or pelletized form) plays a vital role in the overall rate of reaction. For such a catalyzed reaction, the solid metal species are commonly dispersed on solid substrate of high surface area so as to increase the quantity of active sites, which are usually located inside the catalyst pores, needed for the reaction. For the CO hydrogenation reaction to occur, it is necessary for the reactant species to diffuse from the bulk reaction medium to the pore mouth and subsequently to the active sites resident inside the pores. Depending on the nature of generated phases present on the surface of the catalyst, the syngas molecules ($\text{CO}+\text{H}_2$) then adsorb dissociatively or undissociatively prior to surface chemical reaction of adsorbed species. Due to mass transfer considerations as a result of diffusion of reactants into the porous catalyst media, control of the size of the catalyst pellet becomes crucial since the particle size would influence alcohol product distribution.

Fig. 4.6 shows profiles of effect particle size on CO conversion investigated for two particle sizes (88 and 1700 μm). It is clear from the figure that CO conversion increased as a function of temperature; however, at similar temperatures, the catalyst with fine particle sizes (88 μm) performed better than that in the pelletized form (binder-free, 1700 μm). It is a general knowledge in heterogeneous catalysis that the overall rate of reaction is affected by the difference in effective mean free path, which is dependent on the catalyst particle radius (Fogler, 2006).

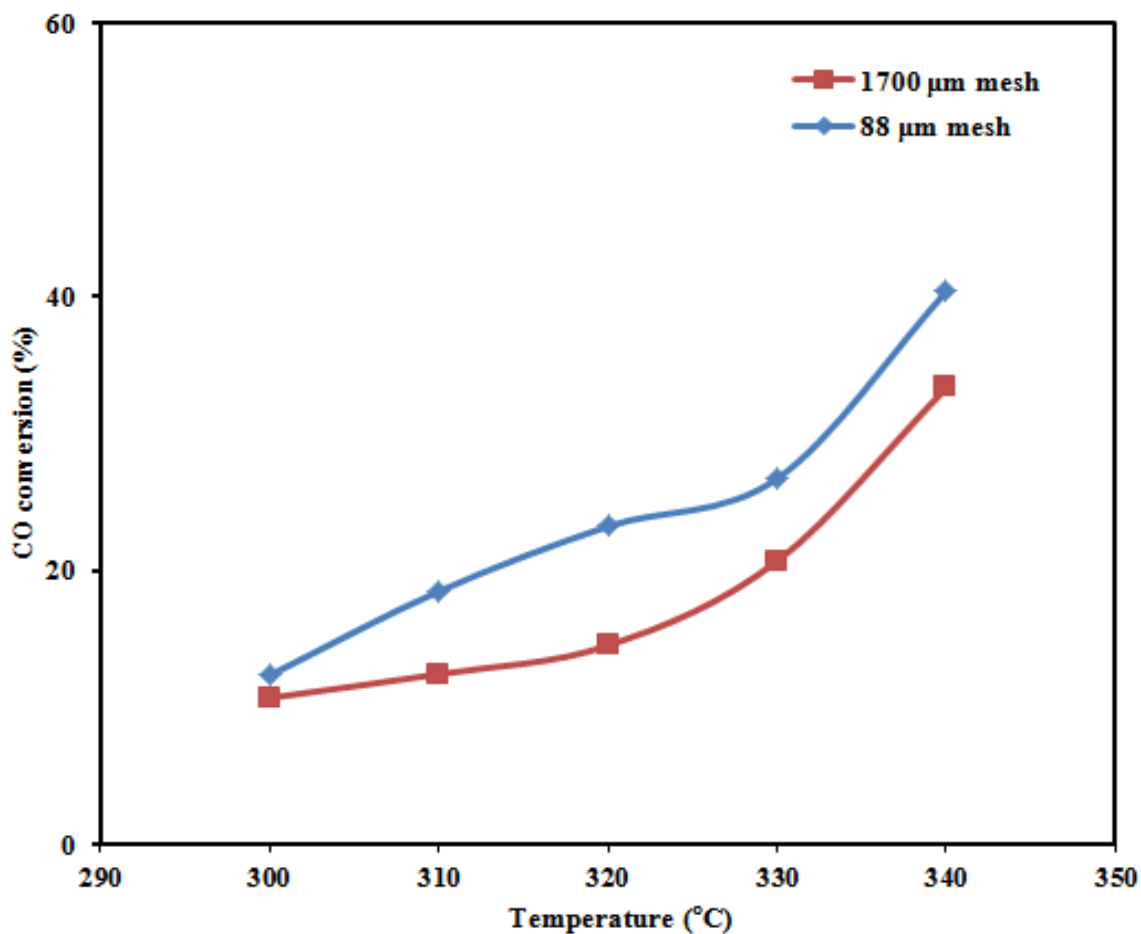


Fig. 4.6: Effect of particle size on CO conversion ($P=8.3$ MPa; $T=300-340^{\circ}\text{C}$; $\text{GHSV}=3.6\text{m}^3$ (STP)/ $\text{kg}_{\text{cat}}\text{-h}$; $\text{H}_2:\text{CO}=1.25$)

In this regard, the observed trend could be due to the difference in particle sizes. As compared to the pelletized catalyst, the transfer of reactants as well as reaction products in the fine powder catalyst seems to be easier, probably, due to differences in the minimum distance reactant species and products have to travel into and out of the internal catalytic active sites in the porous medium.

4.5.2. Effect of binders on CO conversion

The application of MWCNTs as a potential high-quality carbon support has been proven for CO hydrogenation reactions such as Fischer-Tropsch (Abbaslou et al., 2011) and higher alcohol synthesis (Surisetty et al., 2011). MWCNTs possess characteristic features that facilitate greater product selectivity, high mechanical strength; and better stability at high temperatures compared to more commonly used supports such as activated carbon (Surisetty et al., 2011). For a typical laboratory scale application, MWCNT-supported catalysts are screened in the form of fine powder in fixed-bed micro reactors. However, for a successful novel catalyst to be considered for industrial scale applications, it is more practical that these fine powders be consolidated into pellet forms to ensure easier handling and charging into reactors. Moreover, if not pelletized, these fine catalyst powder have the propensity to cause high pressure drops and possible channeling when used in large-scale reactors operated under high pressure gas flow rates. That notwithstanding, when applied in a slurry phase reactor, separation of fine catalyst solids formulated from expensive rare metals (such as Rh and Ru) can pose quite a challenge. To circumvent this issue, incorporation of suitable binders into the catalyst formulation and subsequent pelletization becomes the obvious choice. The consolidated pellet would provide remedy to the issues of pressure drop and catalyst separation as afore discussed.

The influence of binders on CO conversion as a function of temperature during the higher alcohol synthesis reaction was investigated for four different catalyst samples: Cat-1 (pelletized, binder-free) and Cats-2 to 4 (pelletized, binders-incorporated). The percentage CO converted into products gives a measure of catalyst's activity. As can be seen from Fig. 4.7, similar patterns were observed for all binders-incorporated catalysts as compared to the binder-free MWCNT-supported KCoMoRh catalyst.

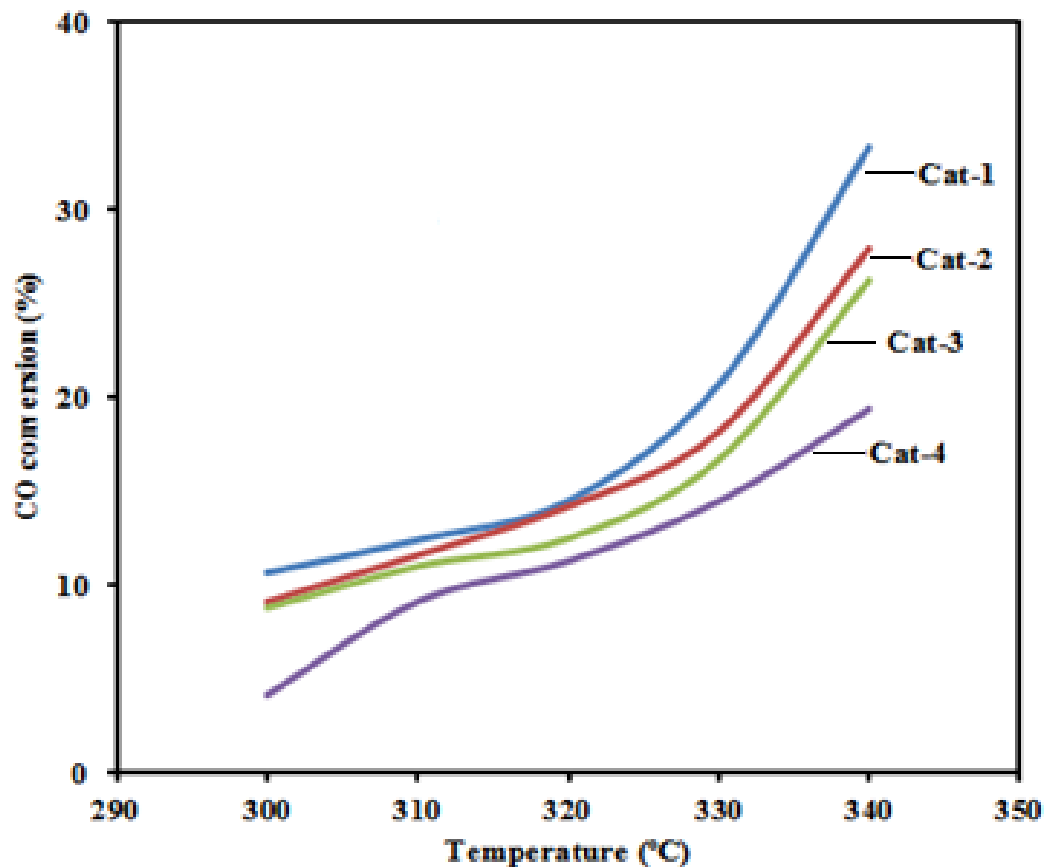


Fig. 4.7: Effect of binders on CO conversion ($P=8.3$ MPa; $T=300-340^{\circ}\text{C}$; $\text{GHSV}=3.6\text{m}^3$ (STP)/ $\text{kg}_{\text{cat-h}}$; $\text{H}_2:\text{CO}=1.25$).

One could observe a common trend at all temperatures studied for CO conversion, which follows the order: $\text{Cat-1} > \text{Cat-2} > \text{Cat-3} > \text{Cat-4}$. The superior activity of the binder-free catalyst could be attributed to its high surface area and pore volume as confirmed by results from the BET analysis. As a result, metal species were uniformly dispersed on the MWCNT support as corroborated by results from XRD profiles.

4.5.3. Effects of temperature on alcohol products distribution

As prevalent in all hydrogenation reactions, temperature plays a significant role in the conversion of syngas to higher alcohols. In practical terms, due to the complex nature of reactions

taking place during this process, the exothermicity/endothemicity of reaction systems could be affected. Moreover, the thermodynamics of the system could also be affected due to the reversible nature of some reactions (e.g. water-gas shift reaction), which could influence the equilibrium yield of the reaction products. It is also known that an easy and cost-efficient way of increasing CO conversion during the higher alcohol synthesis reaction is quite temperature-dependent. Nonetheless, it is noteworthy that excessively high operating temperatures may lead to rapid loss of activity and shortening of catalyst life due to agglomeration of nanocrystallites of the catalyst material (Speight, 2000). This leads to an accelerated catalyst deactivation as a result of sintering of nanocrystallite metal particles into larger less active phases. Moreover, there exists a high tendency of methanation reaction, resulting in coke formation, which is favored at high temperatures (Subramani et al., 2008). In this regard, the potential deposition and coverage of catalytically active phases by coke precursors can affect the performance of the catalyst.

Fig. 4.8 shows the alcohol products distribution as a function of temperature for the best performed catalyst (Cat-0). As can be seen from this figure, apart from selectivity toward methanol product, which tends to decrease with temperature, that for ethanol and other higher alcohols increased with temperature. The results suggest that the formation of various forms of alcohols is thermodynamically affected. However, considering the competition for available CO in the syngas feedstock for the formation of these products, it could be noted that methanol will be thermodynamically unfavorable. Also, the complexity of reactions occurring during the formation of these alcohols and their respective side products via CO hydrogenation does significantly affect the selectivities of products by the heats and free energies of the associated reactions (Chiang et al., 2012). Moreover, it should be noted that the formation of C₁ alcohol is exothermic in nature,

though the extent of exothermicity is less than that for C_{2+} alcohols formation (Mawson et al., 1993).

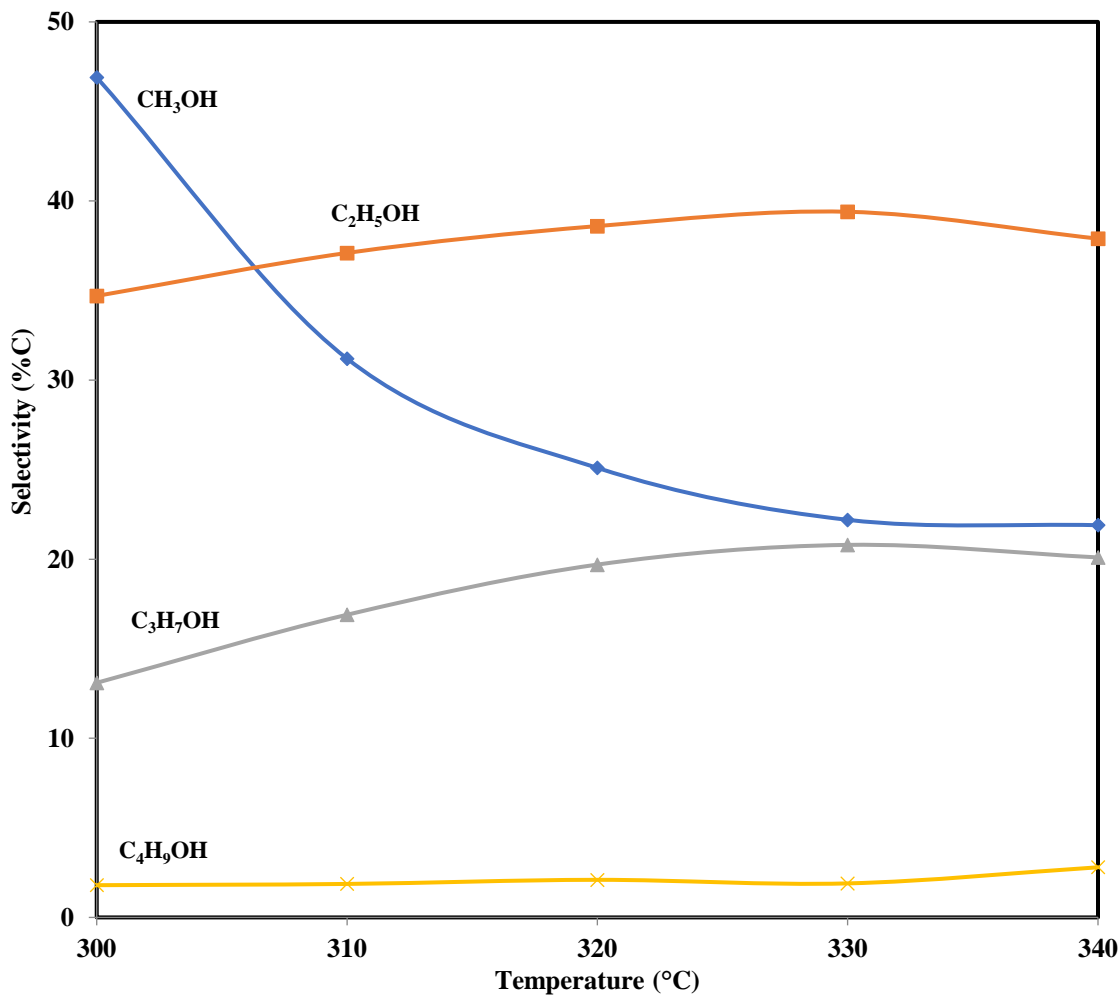


Fig. 4.8: Alcohol products distribution for Cat-0 as a function of temperature ($P=8.3$ MPa; $T=300$ - 340°C ; $\text{GHSV}=3.6\text{m}^3$ (STP)/ $\text{kg}_{\text{cat-h}}$; $\text{H}_2:\text{CO}=1.25$).

For all catalysts evaluated at the various temperatures, the main by-products observed for the CO hydrogenation reactions included carbon dioxide and hydrocarbons (mainly methane and ethane). These by-products tend to be more favorable at higher temperatures for these KCoRhMo catalysts studied.

Table 4.5: Products selectivities for KCoRhMo/MWCNT catalysts (with & without binders).

Catalyst	Product Selectivities (%)						
	Alcohol product Selectivities (%)					Main by-products	
	MeOH	EtOH	PrOH	BuOH	Total alc.	Hydrocarbons	CO ₂
Cat-0 (Fine powder)	22.1	38.5	21.7	3.4	85.7	5.9	8.4
Cat-1 (Pellet -No binder)	19.2	36.3	12.6	2.2	70.3	10.1	19.6
Cat-2 (BC)	13.1	32.5	3.9	0.1	49.6	26.3	24.1
Cat-3 (CT)	11.9	14.9	5.1	0.6	32.5	39.1	28.4
Cat-4 (HA)	6.3	12.1	8.2	2.1	28.7	44.2	27.1

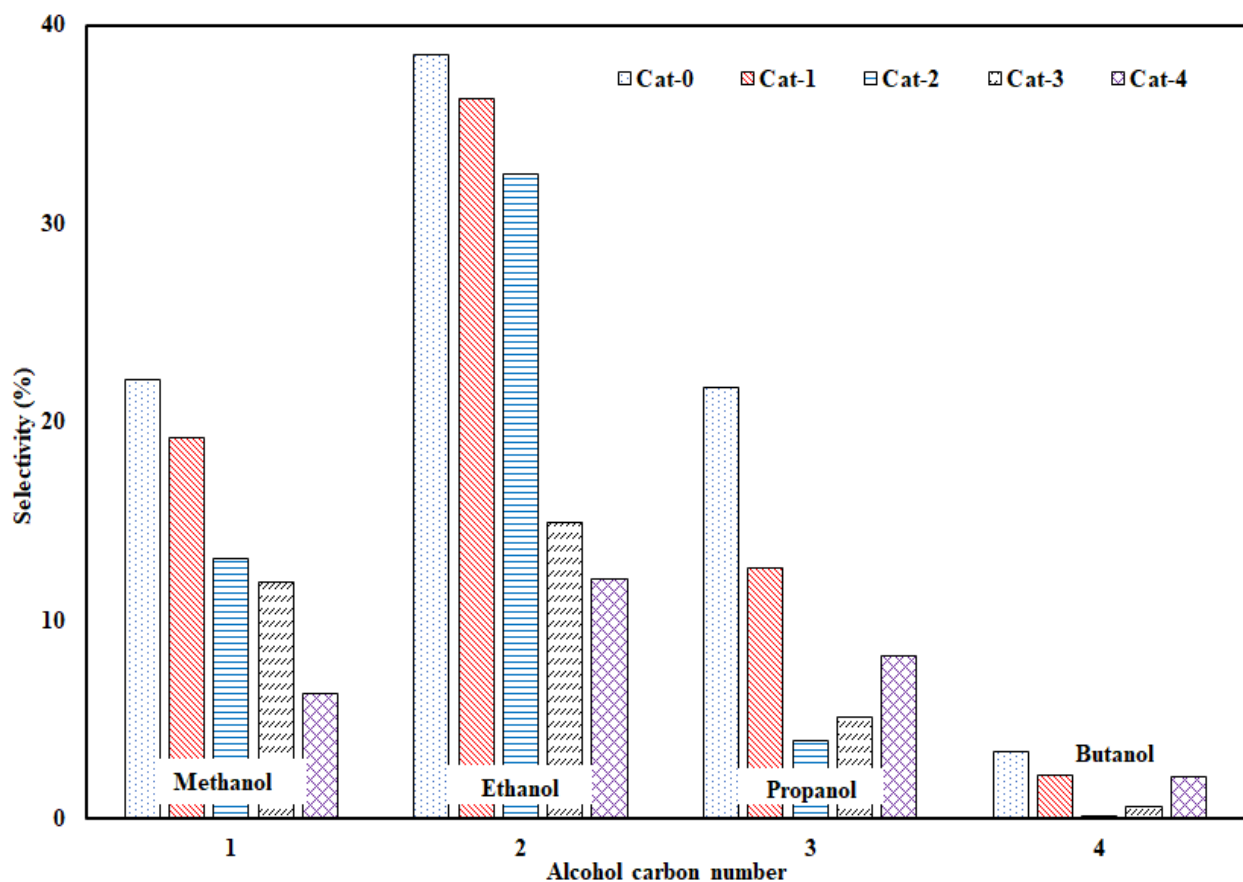


Fig. 4.9: Alcohol productivity for Cats 0-4 as a function of carbon number (P=8.3 MPa; T=330°C; GHSV=3.6m³ (STP)/kg_{cat}-h; H₂:CO = 1.25).

Table 4.5 shows the summary of both the gaseous and liquid products selectivities for all catalysts investigated. Similarly, the alcohol product selectivities as a function of their respective carbon numbers are also presented in Fig. 4.9. It can be concluded from Fig. 4.9 and Table 4.5 that the MoS₂-based catalysts investigated have high selectivity towards the production of higher alcohols, with ethanol being the most predominant higher alcohol product in the final liquid product stream with the main by-products constituting hydrocarbons and carbon dioxide.

4.6. Conclusions

In this work, the influence of pelletization and particle size as well as the incorporation of selected binders in the formulation of potassium promoted CoRhMoS₂/MWCNT catalysts was investigated using an equivalent binder loading of 30 wt. % in the preparation of all the binder-incorporated catalysts. BET analysis of catalysts studied suggested that the structural mesoporosity and orderliness were compromised with the incorporation of binders, resulting in the significant decrement in the pore volumes of these catalysts. Moreover, broader pore size distribution profiles for the binder-incorporated catalysts were obtained for the KCoRhMo/MWCNT catalysts in contrast to its binder-free counterpart.

Though the crushing strength of the binder-incorporated catalysts followed the order: Bentonite clay > Coal Tar > Humic acid, the pelletized catalyst formulated with bentonite clays as a binder (Cat-2) exhibited the best mechanical strength, which could withstand a maximum load of ~340N before crushing into fines as compared to the pelletized binder-free catalyst (Cat-1), exhibiting the least crushing strength of 1.4N. Also, CO conversion for the binder-free catalysts evaluated at the same temperature for two particle sizes (88 μm and 1700 μm) showed that the catalyst with fine particle sizes (88 μm) performed better than that in the pelletized form (binder-

free, 1700 μm); yielding a maximum ethanol selectivity of 38.5% at steady-state conditions of pressure, GHSV, and H_2/CO ratio of 8.3 MPa, 330°C, 3.6 m^3 (STP)/ $\text{kg}_{\text{cat}}\text{-h}$, and 1.25, respectively.

CHAPTER 5

Syngas Conversion to Higher Alcohols: A Comparative Study of Large-pore OMC and MWCNT-supported K-CoRhMoS₂ Catalysts

The contents of the manuscript provided in this chapter is similar to the one published as a book chapter in Fischer-Tropsch Synthesis, Catalysts, and Catalysis.

Citation:

Boahene P. E.; Sammynaiken, R.; Dalai A. K., Syngas Conversion to Higher Alcohols: A Comparative Study of Large-pore OMC and MWCNT-supported K-CoRhMoS₂ Catalysts. Fischer-Tropsch Synthesis, Catalysts, and Catalysis, 15, 2016, 275-294.

Contribution of the Ph.D. Candidate

Setting up of the fixed-bed microreactor for experimental runs, development of the catalysts as well as their extensive characterizations and catalytic studies were performed by Philip Effah Boahene. Data collection, analysis and interpretations were performed by Philip Boahene with assistance from Drs. Ramaswami Sammynaiken and Ajay Kumar Dalai. All of the writing of the submitted manuscript was done by Philip Effah Boahene and discussed with Drs. Sammynaiken and Dalai. Dr. Dalai provided editorial guidance regarding the style and content of this research.

Contribution of this chapter to overall study

Ordered mesoporous carbon (OMC) is a new generation of carbon base supports with unique properties such as, inert graphite surface which is capable of hosting hydroxyl and carboxyl functional groups that are necessary for metals anchorage during catalyst preparation. Ordered mesoporous carbon (OMC) has superior physico-chemical properties as compared to its MWCNT counterpart. Thus, it was interesting to investigate the catalytic performance of the OMC-supported KCoRhMo catalyst for the HAS reaction as compared to the MWCNT counterpart under similar metal loadings, preparation and reaction conditions.

5.1. Abstract

In the present investigation, the novel one-pot synthesis approach has been employed to synthesize large-pore ordered mesoporous carbon (OMC) support using Pluronic F127 as the starting template. A series of OMC & MWCNT-supported catalysts composed of 9%K, 4.5%Co, 15%Mo, & 1.5wt.%Rh metal species respectively, were then prepared and evaluated at similar catalytic reaction conditions for the conversion of syngas to higher alcohols. Catalysts were thoroughly characterized by N₂ adsorption analysis, XRD, Raman spectroscopy, SEM and TEM techniques. Results from SEM images evidenced that the MWCNT material is composed of arrays of interwoven nanotubules, whereas the OMC exhibited a composite of aggregated nanoparticles. Nonetheless, TEM and N₂ adsorption–desorption isotherms confirmed the presence of high mesoporosity in both materials. At this similar metals loading, CO hydrogenation experiments conducted at temperatures, pressure, GHSV, and H₂/CO ratio of 300-340°C, 8.3 MPa, GHSV=3600 mL (STP)/h.g_{cat}, and 1.25, respectively, revealed a superior alcohol productivity over the MWCNT-supported catalyst as compared to its OMC counterpart; probably due to the differences in their pore structure and morphology. Though the OMC-supported KCoMoRh

catalyst showed overall better textural properties, the MWCNT-supported catalyst showed the maximum (38.4%) total amount of higher alcohol produced as compared to its OMC counterpart (36.5%).

5.2. Introduction

In heterogeneous catalytic hydrogenation reactions, where metal precursors dispersed on a porous support serves as catalyst, the support plays a crucial role due to the probable hydrogen spillover effect (Tauster et al., 1981; Filikov et al., 1986). The atomic hydrogen forming as a result of dissociative adsorption on the metal migrates onto the support (hydrogen spillover); making the chemical reaction proceeds not only on the metal surface but also on the support (Tauster et al., 1981). In general terms, the support acts to: 1) stabilize the active species and promoters; 2) promote hydrogen or oxygen donation or exchange; and 3) modify the dispersion, reducibility, and electron-donating or accepting effects of metal particles among others (Subramani et al., 2008). That notwithstanding, in the CO hydrogenation reaction catalysis, interaction of the support and active metal components can significantly alter selectivity to ethanol and higher alcohols. For instance, over the unsupported Mo-based catalysts, Saito et al., 1980, observed that molybdenum species existed in a much reduced state; whereby the activity of the catalyst is found to be high on Mo species with lower oxidation state, causing the catalyst to be more selective towards hydrocarbons production. Murchison et al., 1988, investigated both alumina and activated carbon-supported MoS₂ catalyst for higher alcohol synthesis and found the latter catalyst to be superior for the CO hydrogenation reaction; showing alcohol selectivity of about six times that of the former catalyst.

Similarly, Surisetty et al., 2011, investigated the influence of different textural properties of activated carbon-supported potassium-doped Co-Rh/MoS₂ catalysts for higher alcohols

synthesis and compared selectivity to MWCNT-supported catalyst. A space time yield and selectivity of total alcohols of 0.296 g/(g of cat./h) and 35.6%, respectively, was reported for the K-Co-Rh-Mo/MWCNT catalyst compared to the AC-supported counterpart at similar metal loadings. They inferred that support textural properties (pore size and volume) directly influenced the synthesis of mixed alcohols from synthesis gas.

Another porous carbon material that has of recent times attracted significant importance in the field of heterogeneous catalysis and related area is the ordered mesoporous carbon (OMC). In fact, it is notable to mention that even though carbon nanotubes are successfully applied for such reactions, their potential could be restrained by the limited surface area (Surisetty et al., 2011). Ordered mesoporous carbon materials on the contrary possess better surface area than carbon nanotubes, larger pore volume and diameter than activated carbon and it can be a reasonable choice as a catalyst support for the CO hydrogenation reaction. While various authors (Hussain et al., 2009; Narayanasarma et al., 2011) have tested the catalytic performance of supported-OMC catalysts in hydrodesulfurization reactions (due to their reduced coking propensity and high resistance to sulfur poisoning) and selective hydrogenation of cinnamaldehyde to alcohols (Liu et al., 2012), the application of such catalyst support system for syngas conversion to products such as higher alcohols and hydrocarbons is rare in the open literature. For instance, CoMo catalysts dispersed on OMC were found to exhibit higher activity than the conventional CoMo/Al₂O₃ catalysts for the HDS of thiophene (Hussain et al., 2009). Moreover functionalized OMC-supported CoMo was found to exhibit a much higher HDS activity for thiophene than the pristine OMC (i.e. not functionalized) support due to a relatively large number of surface oxygen groups introduced on the carbon surface, which tend to act as anchoring site for interaction with metallic precursors (Calvo et al., 2005).

Thus, the motivation of the current investigation presented in this chapter was to explore the potential catalytic applications of large-pore OMC supports for higher alcohols synthesis via syngas conversion in a laboratory fixed bed reactor under industrial conditions and evaluate its performance with the known MWCNT counterpart at similar metals loading.

5.3. Experimental

In this study, the detailed description of the synthesis of large-pore OMC support using F127 as structural directing agent (SDA) can be found in Chapter 3, sections 3.2.1, 3.2.4 & 3.2.5 of thesis. Also, the preparations of K-promoted CoMoRh/MWCNT and CoRhMo/OMC catalysts as well as their extensive characterization procedures have been discussed in Chapter 3.

5.4. Results and discussion

5.4.1. N₂-adsorption/desorption measurement

Nitrogen sorption experiments conducted at liquid nitrogen temperature of -196°C is one of the generally used techniques for the textural properties assessment of porous materials (Khodakov et al., 2001). The isotherms for the MWCNT and OMC-supported KCoRhMo catalysts are shown in Fig. 5.1A. The presence of textural mesoporosity with uniform cylindrical pores can be confirmed from the profiles of the HNO_3 treated supports and catalysts; exhibiting the type IV isotherms with H1 hysteresis loop (Tanev et al., 1996; Boahene et al., 2014). In heterogeneous catalytic reaction in which the reaction of reactants predominantly proceeds on the surface of the catalyst, the porosity of the catalyst is of a great essence. This is due to the fact that the porosity of the material controls the mass transfer processes via diffusion, which occurs during the adsorption of reactants, surface reaction and subsequent products desorption into the bulk medium.

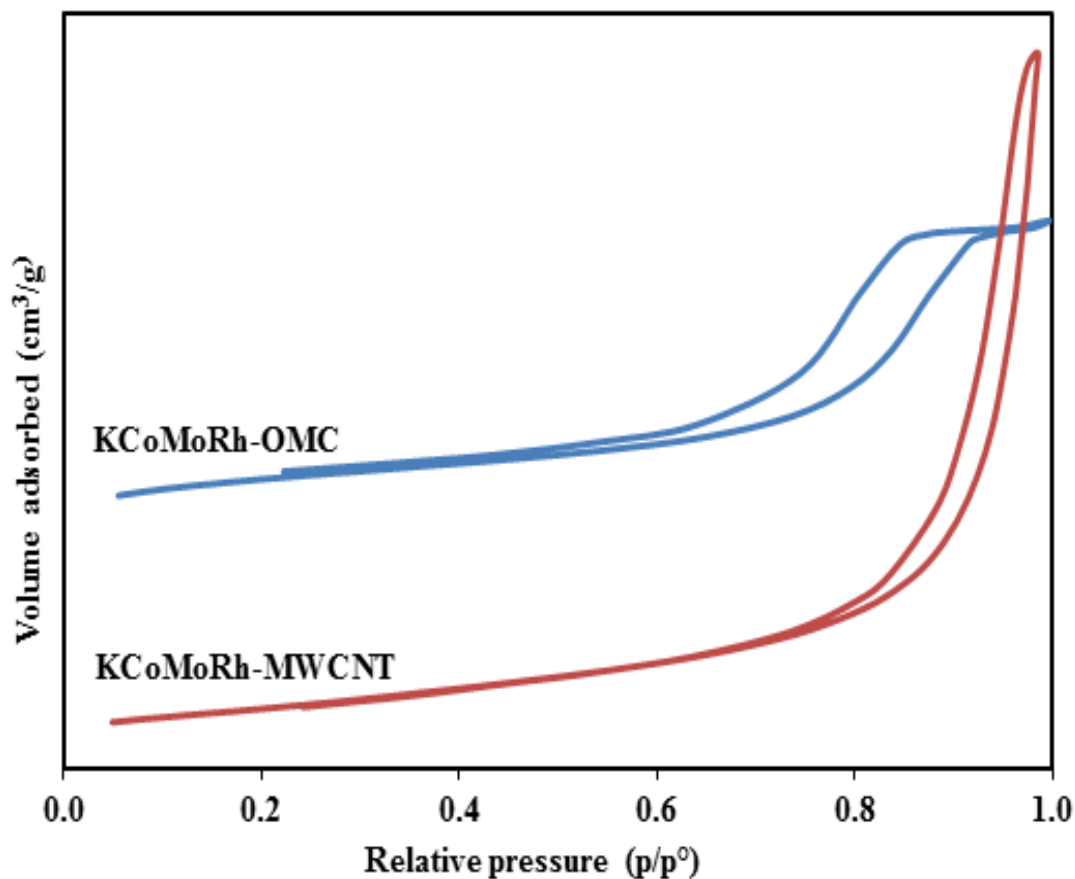


Fig. 5.1 (A): N₂-adsorption isotherms of MWCNT and OMC-supported KCoMoRh catalysts

It is clear from Fig. 5.1 (A) that the type IV isotherm with H1 hysteresis loop exhibited by both catalysts shows a slight change in the shape of the loops of the supports as a result of metals loading. This indicates that both supported catalysts exhibited uniform textural porosity, which is also in agreement with XRD results. The sharpness of the desorption branches is indicative of the narrow mesopore size distribution. This is important since it shows that the textural mesoporosity of the catalyst was not overly compromised following the introduction of metal species within the mesopores of the supports.

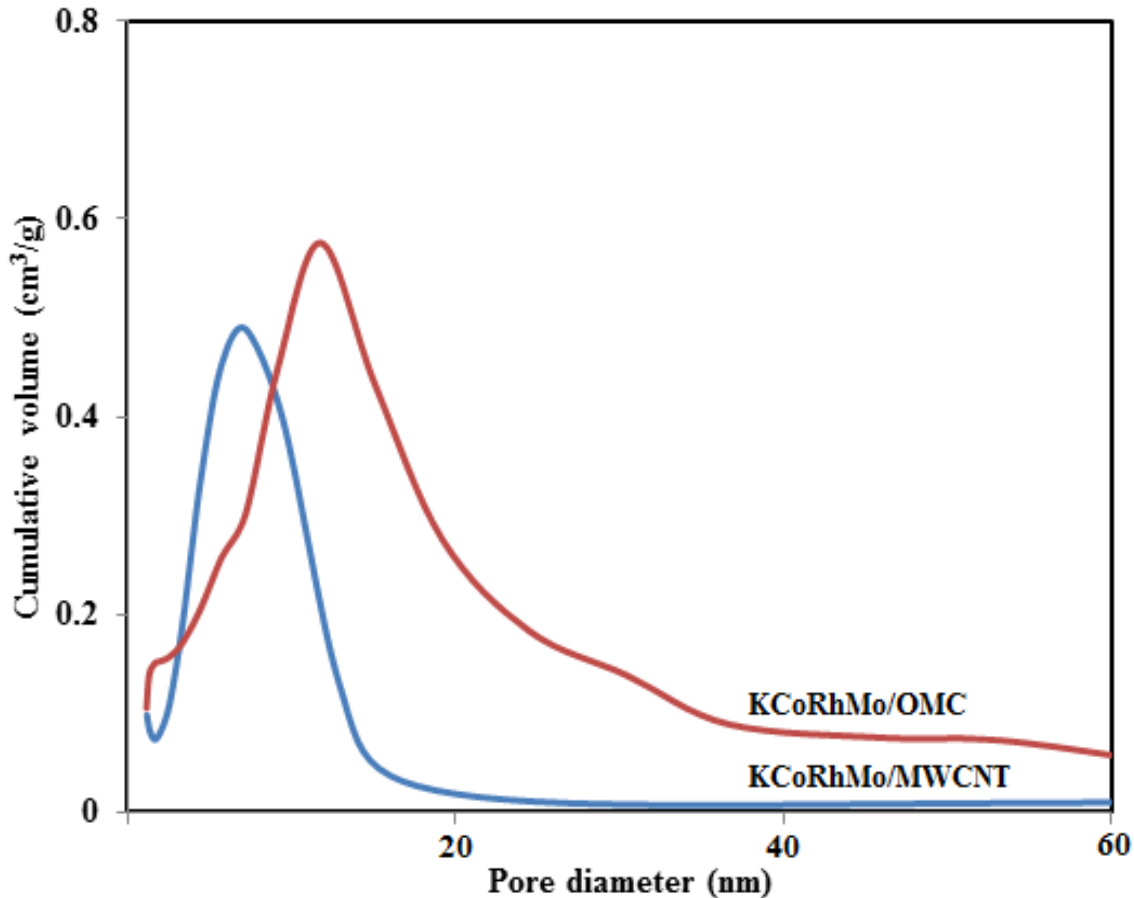


Fig. 5.1 (B): Pore size distribution of MWCNT and OMC-supported KCoMoRh catalysts determined from N₂ sorption analysis.

Also, the pore size distribution profiles for both MWCNT and OMC-supported KCoMoRh catalysts are given in Fig. 5.1 (B). As can be seen from this figure, the cumulative volume of N₂ desorbed by the latter catalyst is more than that of the former. On the contrary, the MWCNT-supported catalyst exhibited a narrower pore size distribution profile as compared to its OMC counterparts. One could reason that the OMC-supported catalyst experienced a significant merging of smaller pores into much larger ones, probably during the multi-step heat treatment of the pristine support prior to the final catalyst calcination step. This characteristic broader pore size distribution

may have contributed to the observed lower alcohol productivity exhibited by the OMC-supported catalyst during the higher alcohol synthesis reaction.

Table 5.1 is a summary of the textural properties of the pristine and HNO₃ treated supports as well as the KCoRhMo-supported catalysts. 30wt.% HNO₃ pre-treatment of the pristine MWCNT and OMC supports resulted in respective increases of the specific surface areas of these supports. It is worth mentioning that acid pre-treatment of pure MWCNTs has been noted to open the closed ends and caps of the pristine material and also significantly improves its textural properties (Surisetty et al., 2011; Sigurdson, 2010).

As can be seen from Table 5.1, one could conclude that the etching effect of the acid pre-treatment on the close-ended pores of the MWCNT support must be responsible for the increments observed in the surface area of the supports. With the incorporation of metal precursors onto the support matrix via the conventional co-impregnation method, a resultant decrease in both the surface areas and pore volumes of the catalysts was observed to follow the order: KCoRhMo/OMC > KCoRhMo/MWCNT; however, changes in the pore diameter of the supports was minimal. The monotonic reduction in textural properties (specific surface area and pore volume) of the supports as a result of metal (Co, Rh, Mo) precursors loading was expected. Nevertheless, the decrease in specific surface as a result of co-impregnation of Co, Mo, and Rh metal precursors on the supports did not have any significant influence on the homogeneity of dispersion of metal species on the surface of the supports, as corroborated by the X-ray powder diffraction analysis.

In addition, the normalized specific surface area (NS_{BET}) analysis of the prepared catalysts showed a decreasing trend with the deposition of metal species on the supports. The values of normalized NS_{BET} are given in Table 5.1.

Table 5.1: Textural properties of pristine and HNO₃ treated MWCNT & OMC supports as well as KCoMoRh catalysts determined from N₂ sorption analysis.

Sample ID	Composition (wt.%)				BET Analysis			
	K	Co	Rh	Mo	SSA	PV	BJH _{ads}	NS _{BET}
					(m ² /g)	(cm ³ /g)	(nm)	
Untreated MWCNT	-	-	-	-	178	0.541	12.2	-
HNO ₃ -treated MWCNT	-	-	-	-	199	0.662	10.6	-
K/MWCNT	9.0	-	-	-	158	0.549	10.4	0.98
KCoRhMo/MWCNT	9.0	4.5	1.5	15	127	0.489	10.1	0.91
Pristine OMC	-	-	-	-	373	0.439	13.7	-
HNO ₃ -treated OMC	-	-	-	-	459	0.785	13.3	-
K/OMC	9.0	-	-	-	405	0.700	13.4	0.97
KCoRhMo/OMC	9.0	4.5	1.5	15	302	0.545	13.0	0.94

S_{BET}, specific surface area calculated by the BET method.

NS_{BET} (Normalized surface area) were calculated by using the equation, NS_{BET} = (S_{BET} of the catalysts)/(1-x)·S_{BET} of the support

PV, pore volume determined by nitrogen adsorption at a relative pressure of 0.98.

PD_{ads}, mesopore diameter corresponding to the maximum of the pore size distribution obtained from the adsorption isotherm by the BJH method.

MWCNT, Multi-walled Carbon Nanotubes

OMC, Ordered Mesoporous Carbon

The NS_{BET} is parameter which gives a measure of the extent of pore blockage as experienced by the catalyst support during the metals loading procedure; with values of NS_{BET} close to unity suggesting less pore blockage suffered by the catalyst. For instance, NS_{BET} of KCoRhMo/OMC catalyst was computed to be 0.94, which is < 1; indicating that the introduction of the oxidic metal nanoparticles caused a minimal reduction in pore volume resulting in an insignificant decrease in the normalized surface area. Furthermore, these results also give an indication that impregnation of metal species on a catalyst support plays a vital role in the overall catalytic surface area required for a given chemical reaction.

The observed trend for the values of NS_{BET} of catalysts investigated follows the order: $KCoRhMo/OMC > KCoRhMo/MWCNT$. This could be attributable to the significantly higher specific surface area of the pristine OMC support as compared to its MWCNT counterpart. The specific surface areas of the support and their respective catalysts play a role in the computation of the NS_{BET} values. At this metals loading for the $KCoRhMo/MWCNT$ and $KCoRhMo/OMC$ catalysts formulation, one can conclude that the incorporation of metals precursors on the OMC support slightly affected the porosity and the overall textural properties of the final catalysts as compared to its MWCNT counterpart. This observation is quite evident from the NS_{BET} values, which gives an indication of minimal pore blockage in the OMC-supported catalyst as compared to the MWCNT-supported catalyst at similar metals loading.

5.4.2. Elemental analysis

Inductively coupled plasma-mass spectrometer (ICP/MS) technique was used to ascertain the respective elemental compositions (actual wt.%) of Co, Mo, and Rh present in the prepared $KCoRhMo$ catalysts in the oxidic state. Table 5.2 shows the ICP/MS results of $KCoRhMo$ supported catalysts with their corresponding targeted compositions. It was observed that the nominal metal loadings were consistent with the targeted compositions.

Table 5.2: Elemental compositions and CO uptake of MWCNT and OMC-supported $KCoRhMo$ catalysts.

Sample ID	Composition (wt.%)			CO uptake ($\mu\text{mol/g}$)
	Co	Mo	Rh	
Cat-1	4.5* (4.4)	15* (15.1)	1.5 (1.4)	39
Cat-2	4.5* (4.4)	15* (14.9)	1.5 (1.3)	35

* Targeted composition

5.4.3. Wide-angle X-ray diffraction

Wide-angle X-ray diffraction patterns of the pristine MWCNT and OMC supports as well as their corresponding KCoMoRh catalysts are shown in Fig. 5.2 for 2θ values in the range of 10-80°. Analyses of generated XRD peaks of these samples were matched with the corresponding peaks using the JCPDS chemical spectra data bank (Calafata et al., 1998; Eswaramoorthi et al., 2008). The characteristic peaks occurring at 2θ values of 27.1, 42.1 and 44.2 can be assigned to the presence of crystalline graphitic carbon in the catalysts studied. Similarly, peaks occurring at 19.8, 30.7, 35.8 and 40.1 can be attributed to the crystalline MoO₃. However, the more prominent graphitic peaks of the pristine MWCNT support as compared to the OMC counterpart suggest that the former support is highly graphitized as opposed to the latter. Moreover, with the incorporation of metal nanoparticles, the generated peaks on the MWCNT-supported catalyst becomes more heightened in intensity as compared to the OMC-supported catalyst, which displayed quite a uniform dispersion of metal nanoparticles. It could be reasoned that homogeneity of metal species deposited on the OMC support was better enhanced as compared to that for the KCoRhMo/MWCNT catalyst.

This could be attributed to relatively lower surface area (199 m²/g) of the HNO₃-treated MWCNT support as opposed to the higher surface area (459 m²/g) of the treated OMC counterpart. It is worth mentioning that a catalyst support with more desirable textural properties would better enhance the stabilization the active species and promoters as well as playing a vital role to modify the dispersion, reducibility, and electron-donating or accepting effects of metal nanoparticles (Hindermann et al., 1983).

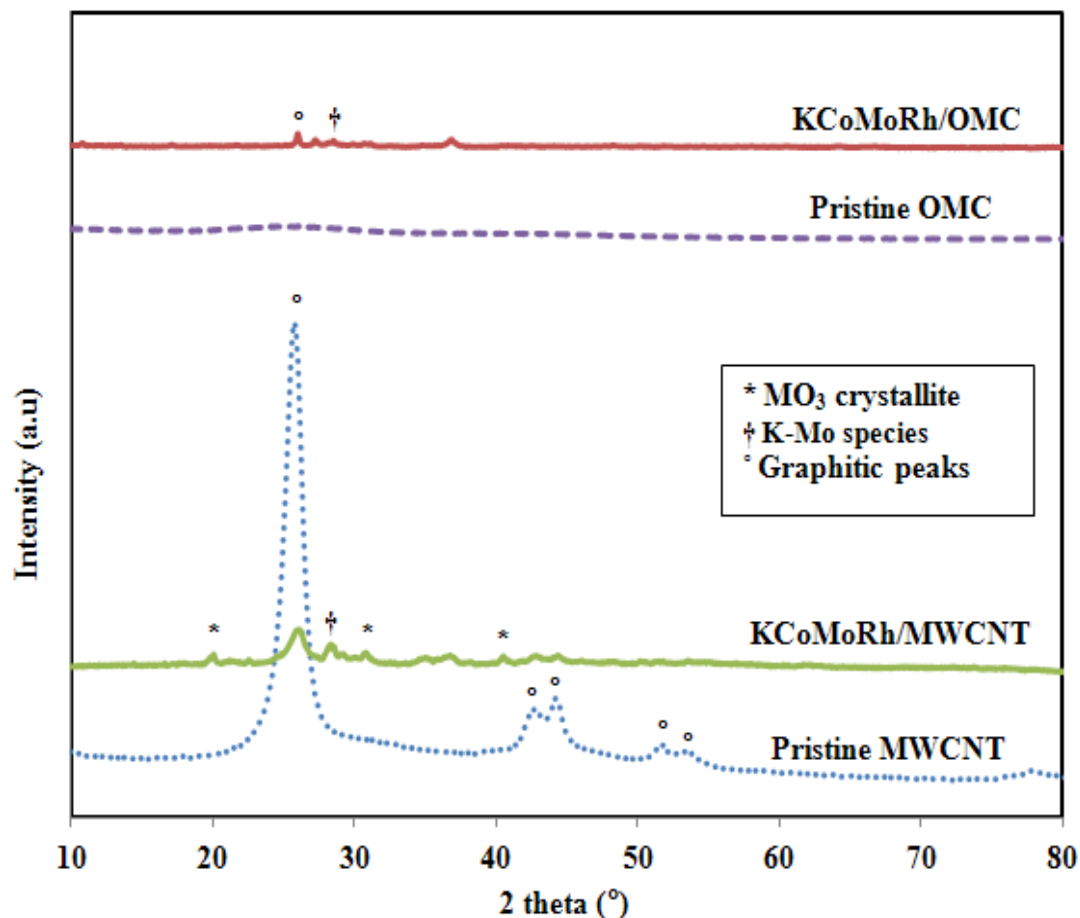


Fig. 5.2: Wide-angle X-ray diffraction patterns of pristine OMC & MWCNT as well as supported KCoMoRh catalysts. (° graphite; * MoO₃; † K₂Mo₂O₇).

Consequently, the relatively higher surface area of the HNO₃-treated OMC support may have played a significant role by enhancing great dispersion of catalytic phases as confirmed by the XRD profile for its corresponding catalyst. Also, the peaks occurring at 2θ values of 25.9 and 28.2 can be assigned to the presence of K₂Mo₂O₇ species in the samples (Haber et al., 1995). The average MoO₃ crystallite size from the full width at half maximum (FWHM) diffraction profile computed by the Debye-Scherrer's equation ($L=0.9\lambda/\beta\cos\theta$) for the KCoRhMo/MWCNT catalysts showed MoO₃ crystallite size of 8 nm as opposed to 6.4 nm for the OMC-supported catalyst. Both particle sizes favored the higher alcohols synthesis reaction. However, it should be noted that these

nanoparticles are liable to significant changes during higher alcohol synthesis reaction as result of time on stream under operation conditions of pressure and temperature.

5.4.4. Raman spectroscopic analysis

Carbon materials are predominantly composed of pure carbon atoms which exist in a variety of different nanostructure forms; however, from a molecular perspective, all of these nanomaterials are entirely made up of chains of C-C bonds, although the orientation of these bonds varies from material to material. Thus, in order to effectively characterize the slight changes in the orientation of the C-C bonds, a highly sensitive vibrational spectroscopic technique becomes an important tool (Dresselhaus et al, 2005). Raman spectroscopic analysis is a nondestructive technique and particularly well suited to detect small changes in structural morphology of carbon nanomaterials (Schwan et al., 2001). Raman scattering is the inelastic scattering of light, which involves electron excitation from the valence energy band to the conduction via photon absorption; emission of phonons as a result of scattering of excited electron; and finally, the emission of the absorbed photon due to electron relaxation to the valence band (Dresselhaus et al, 2004). Every band occurring in the Raman spectrum corresponds directly to a specific vibrational frequency of a bond within the molecule (Yang et al., 1990). For carbon materials such as graphite and SWNTs, information such as electronic structure as well as sample imperfections can be derived from spectra obtained from this technique.

As shown in Fig. 5.3, the vibrational characteristics of MWCNT and OMC-supported KCoMoRh catalysts were studied by Raman spectroscopy. The two major bands evidenced in the range of 1350-1360 cm^{-1} and 1575-1600 cm^{-1} can be attributed to the D-band (which characterizes the extent of disorderliness) and the G-band (which is due to C-C stretching mode) of the carbon material.

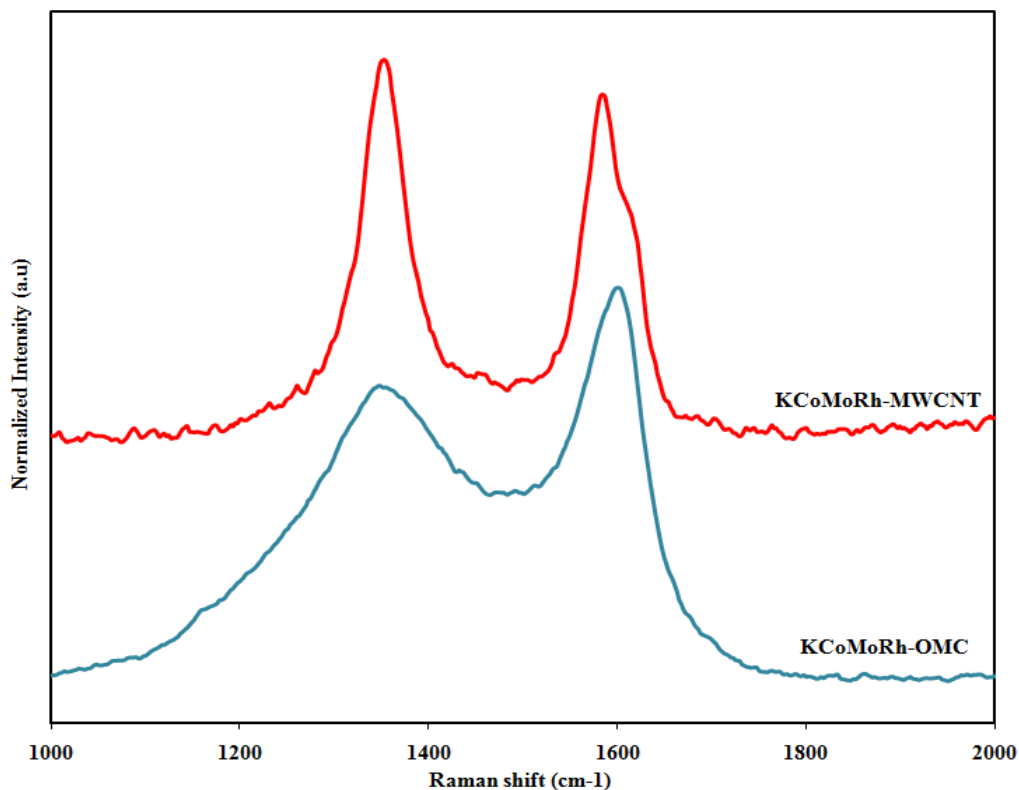


Fig. 5.3: Raman patterns of MWCNT and OMC-supported KCoMoRh catalysts

While the G-band indicates the graphitic E_{2g} plane vibration, the D-band is due to the disordered parts such as grain boundaries (Shimodaira et al., 2002; Boahene et al., 2014), which is indicative of the A_{1g} plane. It is known that the intensity ratio of the D to G bands (I_D/I_G) is generally used to denote the extent of disorderliness present in the graphite layer of carbon material (Vinu et al., 2007). The greater the value of this parameter, the more disordered the material becomes. As can be noted in Fig 5.3, OMC-supported KCoRhMo catalyst exhibited the least I_D/I_G ratio which is indicative of the existence of lesser defective sites for the HAS reaction as compared to the MWCNT-supported catalyst. Also, it can be noticed that for both samples the linewidth of the G mode is narrower than that of the D band, confirming that the G mode is related to the crystalline component in carbons (Jawhari et al., 1995). Moreover, the bandwidth of the D mode is clearly greater for the KCoRhMo/OMC catalyst sample than in the case of the MWCNT-

supported catalyst counterpart; suggesting that the extent of ordering of the former samples is lower than that of latter. This could also explain the more defective or active site as corroborated by the CO uptake analysis.

5.5. CO hydrogenation reaction for higher alcohol synthesis

At the start of the CO hydrogenation reaction, the activities of the MoS₂-supported catalysts are mostly at their best performance. As can be seen from Fig 5.4, the conversion of CO in the syngas feedstock for both catalysts studied tends to decline as a result of time on stream over the 24 h period of investigation. This could be due to the propensity of MoS₂-based catalysts undergoing initial coke deposition phase prior to attaining stable catalytic activity, as has been experienced by conventional MoS₂ catalysts applied for the hydrogenation of fossil feedstocks of carbon base (Narayanasarma et al., 2011). Moreover, the catalytic activities of both catalysts leveled off after 18 h time-on-stream; suggesting a stable activity for both catalysts after this time period on stream. The catalysts did not show any significant deactivation after this reaction time online. That notwithstanding, it could be noted that the MWCNT-supported KCoRhMo catalyst exhibited a higher CO conversion as opposed to its OMC counterpart. This could be explained by the fact that at similar metals loading, the concentration of active metal species on the former catalyst is more than that of the OMC-supported catalyst as can be corroborated by the CO uptake analyses of these catalysts (Table 5.2). The amount of CO uptake of the MWCNT-supported catalyst was 39 mmol/g as compared to that of 35 mmol/g for the OMC counterpart; giving an indication that more active sites were present on the former catalyst for the CO hydrogenation reaction as opposed to the latter.

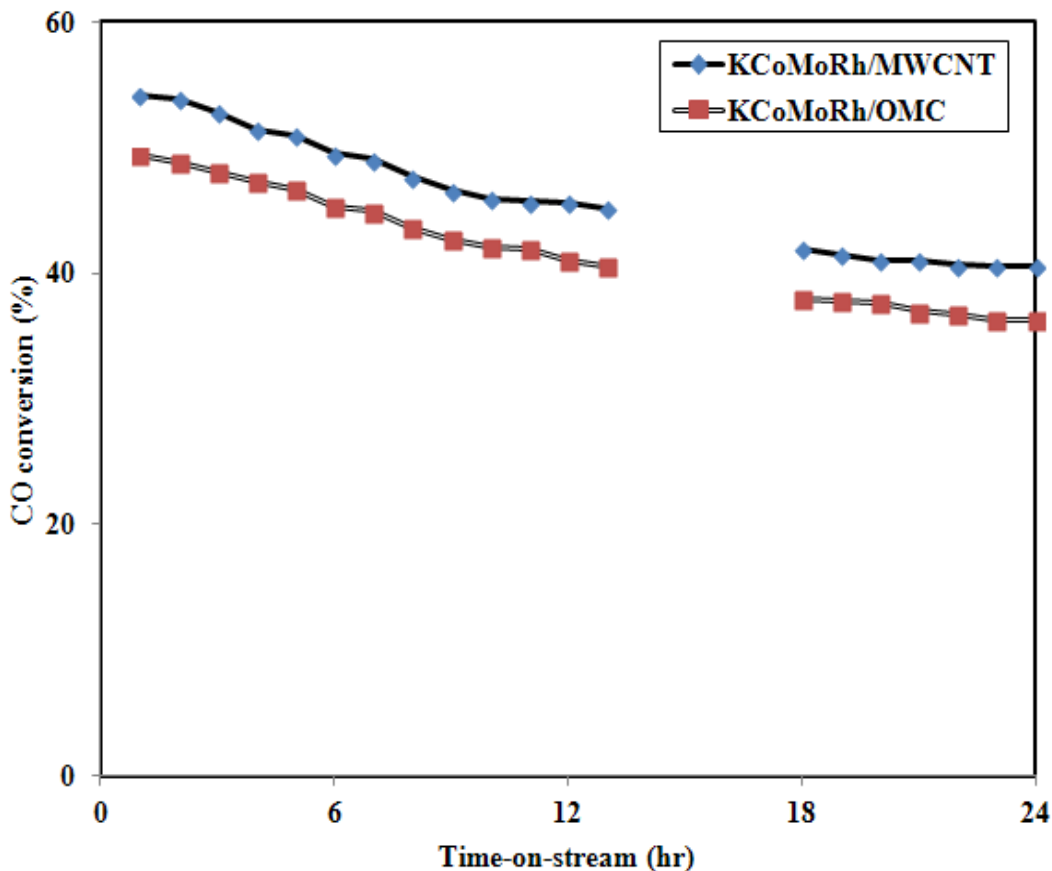


Fig 5.4: CO conversion as a function of time-on-stream for KCoMoRh-supported catalysts (P=8.3 MPa; T=330°C; Catalyst=2g; GHSV=3.6 m³ (STP)/h·kg_{cat}; H₂:CO=1.25)

The higher concentration of active catalytic species present in the MWCNT-supported KCoRhMo catalyst could also be attributed to the greater amount of metals species per unit area of the catalyst by reason of the fact that the OMC-supported catalyst had a much higher surface area (1.5 times) than that of its MWCNT counterpart. Though the higher surface area of the OMC support may have greatly enhanced the homogeneous distribution of the dispersed metal species, it also appears that at these metals loading, the sparse orientation of these metal species on the OMC support may have resulted in a probable least synergetic metal-metal phase interactions as well as reduced active phase-reactants interactions, thereby resulting in a slightly reduced catalytic activity.

The prepared oxidic form of the KCoRhMo-supported catalysts were evaluated using a high-pressure fixed-bed downward flow reactor system for catalysts screening so as to ascertain their performance in the HAS reaction. The syngas of molar composition of 50% H₂:40% CO:10% Ar was used as the feedstock. Typical reaction conditions evaluated include pressure, temperature, and GHSV of 8.3 MPa, 300-340°C, and 3.6 m³ (STP)/kg_{cat.} h, respectively. Prior to the onset of the higher alcohol synthesis reaction, an initial catalyst activation step was necessary in order to ensure the phase conversion of the rather less active oxidic catalytic species into a more active sulfidic form. This was achieved by subjecting catalysts to an initial catalyst sulfidation/reduction step using a sulfiding gas mixture of 10% H₂S/H₂ molar compositions. With the intended metals loading maintained constant for both catalysts preparation, the influence of variable supports on the higher alcohols productivity was investigated.

The extent of alcohol products distribution is crucial and supports dependent since the catalyst supporting matrices have the capabilities of facilitating the dispersion of the active metal species. In this regard, the influence of supports on alcohol products distribution has been presented in Fig 5.5.

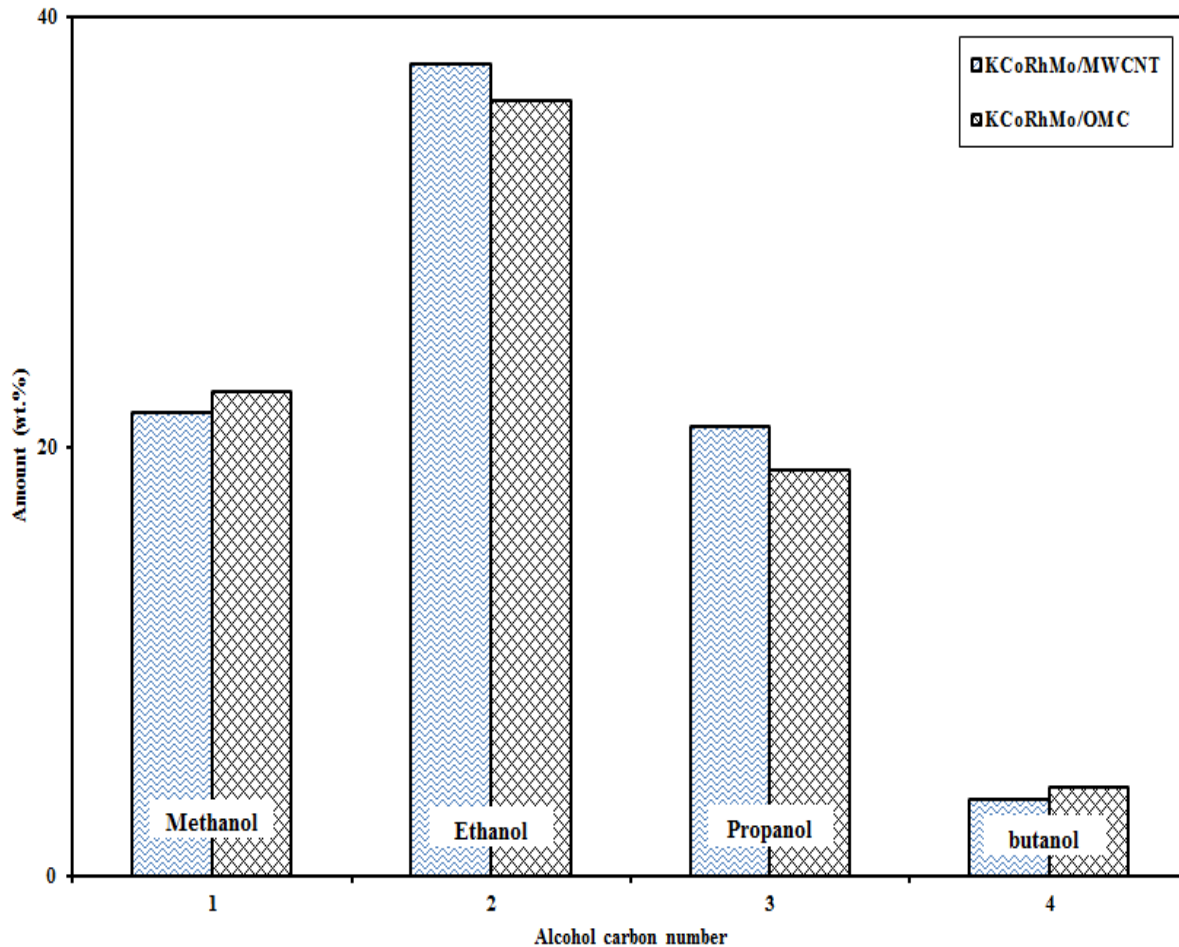


Fig. 5.5: Alcohol composition as a function of carbon number (P=8.3 MPa; T=330°C; Catalyst=2g; GHSV=3.6 m³ (STP)/h·kg_{cat}; H₂:CO=1.25).

It is quite obvious that alcohol products stream generated by the KCoRhMo catalysts constituted mostly linear alcohols with carbon numbers in the range of C₁ to C₄. Both support systems enhanced the production of these alcohols, mostly C₂ alcohols, with selectivities of about 38.4 & 36.5% for the MWCNT and OMC-supported systems, respectively.

Products selectivities for the gaseous and liquid streams of the CO hydrogenation reaction are summarized for both catalysts investigated and are presented in Table 5.3. As can be seen, the OMC-supported catalysts tend to produce more CO₂; suggesting its higher activity for the water-gas-shift reaction. That notwithstanding, the total alcohols productivities for these catalysts are

marginally different at this metals loadings; giving an indication that at a higher metals loading, the alcohol products selectivities could be improved due to the higher specific surface area of the OMC support. Thus, from Fig. 5.5 and Table 5.3, it becomes quite conclusive that both carbon supported (MWCNT and OMC) KCoRhMoS₂ catalysts investigated for higher alcohol productivity turned out to have high selectivity towards the production of higher alcohols, with ethanol being the most predominant higher alcohol product in the final liquid product stream with the by-products comprising mainly CO₂ and light hydrocarbons (methane and ethane).

Table 5.3: Products selectivities for MWCNT and OMC-supported KCoRhMo catalysts

Catalyst	Product Selectivities (%)						
	Alcohol product Selectivities (%)					Main by-products	
	MeO H	EtOH	PrOH	BuOH	Total alc.	Hydrocarbons	CO ₂
KCoRhMo/MWCNT	22.1	38.5	21.7	3.4	85.7	5.9	8.4
KCoRhMo/OMC	22.6	36.5	19.5	3.6	82.2	5.1	12.7

5.5.1. Alcohol products distribution and the ASF Plots

The term higher alcohols (C₂₊OH) is used to describe alcohols with carbon numbers greater than 1; thus, total alcohols constitutes a combination of C₁, C₂ as well as all C₂₊ alcohols put together. In the formation of C₂₊ alcohols over Mo-based catalyst, a generally accepted mechanism is the CO insertion (Santiesteban et al., 1988; Subramani et al., 2008) in which syngas reactant species (CO and H₂) associatively or dissociatively adsorb onto the catalyst's active sites; yielding adsorbed formyl (HC=O) and alkyl (CH_x) species. Consequently, hydrogenation of the former species can proceed to produce methanol (CH₃OH) via reaction of adsorbed H species with the carbonyl group. Conversely, the insertion of adsorbed CO into the surface alkyl bond can also occur to yield adsorb acetyl species (COCH_x), which can further undergo hydrogenation to form

ethanol (C₂H₅OH). Furthermore, this chain propagation mechanism can continue with the insertion of CO into surface alkyl species of high carbon numbers and their subsequent hydrogenation to yield corresponding high carbon number alcohols (Smith et al., 1990; Song-bai et al., 2011). During this chain polymerization HAS reaction, the selectivities of various alcohols can be depicted from the chain-growth probability (α) and carbon number (n) by the well-known Anderson-Schulz-Flory (ASF) model, represented as (Schulz, 1999; Spivey et al., 2007):

$$\ln W_n = n \ln \alpha + \ln \frac{(1 - \alpha)^2}{\alpha} \dots \dots \dots (5.1)$$

where W_n is the weight percent of a product containing n carbon atoms and α is the chain growth probability. Figures 5.6 (A & B) depict the ASF plots for the MWCNT and OMC-supported KCoRhMo investigated for the HAS reaction. It can be seen that alcohols products distribution for the various carbon numbers is consistent with the linear trend predicted by the ASF model; however, a deviation can be observed in the formation of methanol for both catalysts. Evaluation of the chain-growth probability from the slopes of the linear ASF plots yielded α values of 0.31 and 0.29, respectively, suggesting that the chain polymerization reaction for the formation of alcohols over both catalysts followed the classical CO insertion mechanism.

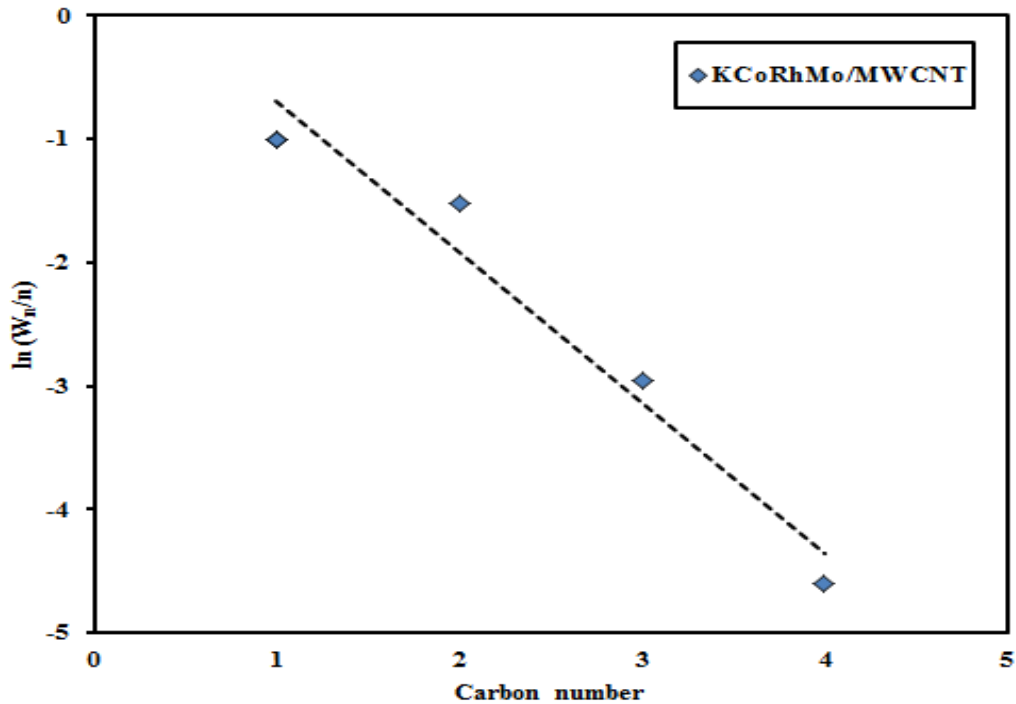


Fig. 5.6 (A): ASF plot for MWCNT-supported KCoRhMo catalyst

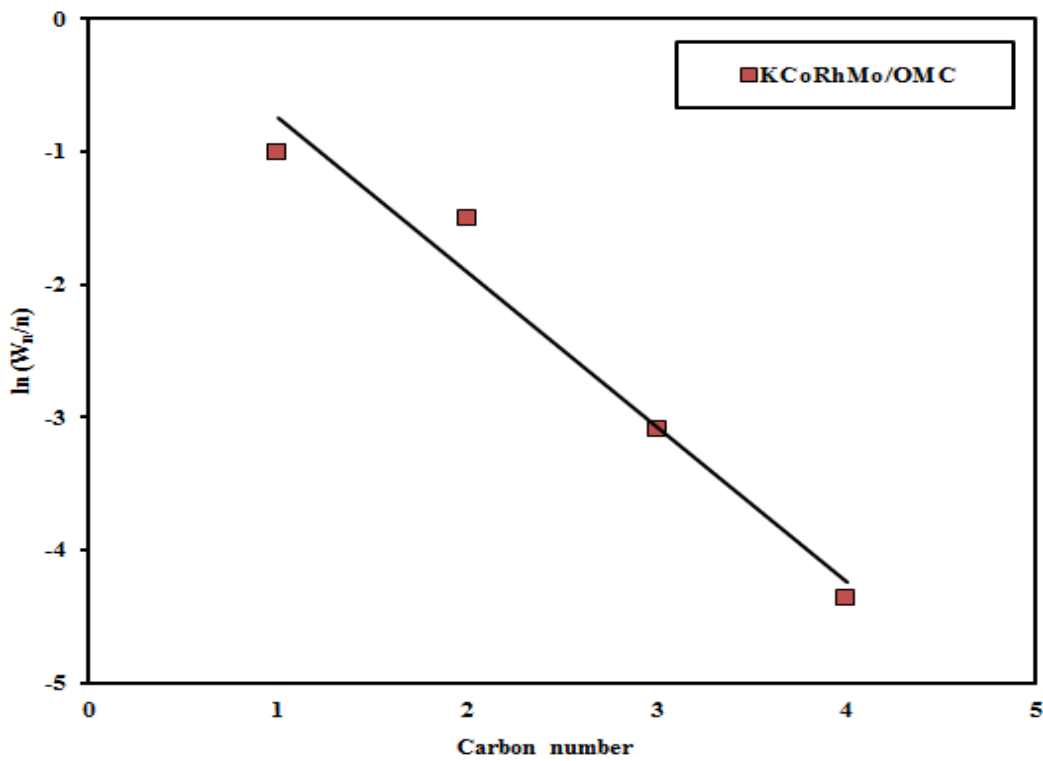


Fig. 5.6 (B): ASF plot for OMC-supported KCoRhMo catalyst

5.6. Conclusions

In summary, large pore diameter OMC support was synthesized by the soft-templating approach and compared with MWCNT support of similar pore diameter for the formulation of K-doped CoRhMoS₂ catalysts and subsequently evaluated for their performance in the HAS reactions. At similar metals loading, BET analysis of both catalysts evidenced significant structural mesoporosity and orderliness since the physical properties of the materials were not compromised; however, a lesser pore blockage was observed in the OMC-supported catalyst as confirmed by the NS_{BET} computations. Moreover, at similar metals loadings of 9%K, 4.5%Co, 15%Mo and 1.5wt.% Rh, XRD analysis evidenced a better metal nanoparticles dispersion on OMC-supported catalyst since less crystalline peaks were detected as confirmed by the TEM images. Both the OMC & MWCNT-supported catalysts exhibited high activities toward the production of alcohols, especially ethanol. Though the OMC-supported KCoMoRh catalyst showed overall better textural properties, the MWCNT-supported catalyst showed the maximum (38.5%) total amount of higher alcohol produced as compared to its OMC counterpart (36.5%). Evaluation of the chain-growth probability from the slopes of the linear ASF plots yielded α values of 0.31 and 0.29, respectively, suggesting that the chain polymerization reaction for the formation of alcohols over both catalysts followed the classical CO insertion mechanism.

CHAPTER 6

Syngas conversion to higher alcohols: A comparative study of acid and base-treated mesoporous carbon-supported KCoRhMoS₂ catalysts

The contents of the manuscript provided in this chapter is similar to the one published in the Journal: Catalysis Today.

Citation:

P.E. Boahene; R. Sammynaiken; A. K. Dalai., Syngas conversion to higher alcohols: A comparative study of acid and base-treated mesoporous carbon-supported KCoRhMoS₂ catalysts, Catal. Tod., Vol. 291, 2017, 106-123.

Contribution of the Ph.D. Candidate

Setting up of the fixed-bed microreactor for experimental runs, development of the catalysts as well as their extensive characterizations and catalytic studies were performed by Philip Effah Boahene. Data collection, analysis and interpretations were performed by Philip Boahene with assistance from Drs. Ramaswami Sammynaiken and Ajay Kumar Dalai. All of the writing of the submitted manuscript was done by Philip Effah Boahene and discussed with Drs. Sammynaiken and Dalai. Dr. Dalai provided editorial guidance regarding the style and content of this work.

Contribution of this chapter to overall study

In our previous study, it was observed that the MWCNT-supported catalyst performed better than the OMC counterpart under similar metal loadings. However, due to the superior textural properties of the latter support, it was interesting to study the influence of different chemical pretreatment on the OMC support by subjecting the pristine material to both acidic and basic treatments. This oxidative treatment was intended to introduce different surface functional groups to enhance its metals anchorage properties. Similarly, the trimetallic catalysts were prepared by the incipient wetness impregnation method and extensively characterized for their physicochemical properties prior to catalytic performance evaluation HAS reaction.

6.1. Abstract

Ordered mesoporous carbons (OMC) of desirable textural properties have been synthesized by the novel one-pot soft-templating synthesis approach. Prior to catalyst metals loading, the OMC supports were functionalized using the wet chemical oxidation technique to introduce surface oxygen-containing functional groups for metals anchorage. In this regard, the crucial role functionalizing agents (acidic and basic) on the morphology & structural integrity of the parent OMC support was also investigated. It was observed that the structural integrity of the parent OMC material remained intact as confirmed by the TEM analyses. Moreover, less defective sites were generated as evidenced from the Raman spectroscopic analysis; suggesting that non-acidic oxidative treatment could be a mild way of introducing oxygen functionalities as metal anchoring sites on the surface of pristine OMC support. Based on the defective sites generated on the OMC supports, the severity of chemical oxidative treatment was observed to follow the trend: $\text{HNO}_3 > \text{NH}_4\text{OH}/\text{H}_2\text{O}_2 > \text{KOH}$. The HNO_3 , $\text{NH}_4\text{OH}/\text{H}_2\text{O}_2$ and KOH treated-OMC supports were used to prepare a series of KCoRhMoS_2 catalysts with nominal compositions of 9%K, 4.5%Co,

15%Mo, & 1.5wt.%Rh, respectively. Catalytic performance evaluations of these catalysts for syngas conversion to higher alcohols were also studied at similar reaction conditions: T= 300-340°C, P=8.3 MPa, GHSV=3600 mL (STP)/h.g_{cat}, and H₂/CO =1.25). The HNO₃-treated OMC-supported KCoRhMoS₂ catalyst showed superior total alcohol productivity as compared to its NH₄OH/H₂O₂ and KOH counterparts; probably due to the greater number of surface oxygen-containing functional groups, thereby, enhancing its metal-oxygen anchorage properties in the catalyst formulation. All catalysts showed an increase in CO conversion with incremental temperature with a maximum of 40.2% recorded for the KCoRhMo/OMC-HNO₃ catalyst at T=330°C as opposed to 26.1 and 19.6% for the catalysts with KOH and NH₄OH/H₂O₂ treatment, respectively.

6.2. Introduction

Carbon-based supported MoS₂ catalysts, promoted with Co and Rh have garnered immense attention in the conversion of syngas to higher alcohols via the Fischer Tropsch synthesis process (Abbaslou et al., 2011; Surisetty et al., 2011). Carbonaceous materials such as ordered mesoporous carbons (OMC) have received considerable focus due to their potential applications in a wide range of fields including catalysis, adsorption or sensor technology. Though, these porous carbon materials possess desirable textural properties (tunable pore sizes, high surface areas, and large pore volumes), applications in catalysis becomes limited as a result of their chemical inertness, minimal surface functionality and their hydrophobic nature (Ryoo et al., 2001). Thus, to enhance their surface chemistry for practical catalysis application, carbon materials are usually subjected to post-synthesis treatment techniques including chemical oxidation (liquid or gas phase), polymer coating and grafting in order to improve their hydrophilicity as well as generate the necessary surface oxygen groups for interacting with catalytic species (Chen et al., 2003; Bazula et al., 2008).

Regarding surface chemistry modification via oxidation, the most studied carbon-based materials include activated carbon and carbon nanotubes (Bazula et al., 2008).

To a large extent, the introduced oxygen-containing groups play the role as weak acids or bases, which possess ion exchange properties. For instance, acidic groups such as carboxyl, phenolic hydroxyl, lactone and quinone can be introduced to the surface of the carbon material leading to significant changes of the surface chemistry; hence, its application as catalyst support or adsorbent (Li et al., 2005). Commonly used treatment protocols include oxidative treatment (wet or dry), plasma treatment, and electrochemical modifications (Pradhan et al., 1998; Lu et al., 2005), whereas dry chemical oxidation employs gaseous oxidizing agents (e.g. oxygen, ozone and carbon dioxide), its wet counterpart uses individual solutions of nitric acid, sulfuric acid, phosphoric acid or a mixture with hydrogen peroxide, sodium hypochlorite, permanganate etc., to accomplish a similar purpose (Pradhan et al., 1999; Li et al., 2005; Lu et al., 2005; Bazula et al., 2008).

Among the series of different oxidants studied (including HNO_3 and H_2O_2), Pradhan and coworkers observed HNO_3 treatment as the most effective regarding modification of the surface area and porosity of activated carbons (Pradhan et al., 1999). Also, treatment of CNT with 68% HNO_3 under reflux conditions introduced carboxylic groups on the surface and ends of the nanotubes as reported by Tsang et al., 1994. Similarly, chemical oxidation treatments as reported recently by Ryoo and coworkers evidenced that the carbon framework remained intact after surface modification of CMK-1 and CMK-5 by oxidation with concentrated nitric acid at 110°C for 15 min (Ryoo et al., 2003). Moreover, the same workers reported in a previous study that OMC can maintain an ordered structure even in boiling 5 M aqueous solution of NaOH, KOH, or H_2SO_4 over a week, showing strong resistance to attack by acids and bases (Ryoo et al., 2001). However,

Lu and co-workers modified the surface chemistry of CMK-5 carbon using the mild oxidizing agent H_2O_2 in order to introduce surface oxygen groups while its ordered structure was maintained, but surprisingly a structural collapse occurred (Lu et al., 2005).

In the work presented in this chapter, the surface modification (via wet chemical oxidation treatments) of the pristine OMC supports was performed using HNO_3 , $\text{NH}_4\text{OH}/\text{H}_2\text{O}_2$, and KOH . The catalytic performances of their respective catalysts were investigated for the HAS reaction at similar metals loading using laboratory-scale fixed bed reactor under industrial conditions. In addition, the untreated OMC-supported-KCoRhMo catalyst were also evaluated at similar conditions to benchmark performance via screening with syngas feedstock for the HAS reaction.

6.3. Experimental

The pristine ordered mesoporous carbon (OMC) support used in this work prepared in-house using the soft-templating nanocasting approach with F127 as the template. The detailed description of the chemical pre-treatments of the pristine support as well as their corresponding supported KCoRhMo catalysts can be found in Chapter 3, section 3.2.1, 3.2.3 & 3.2.4 of thesis. Furthermore, characterization techniques employed as well as the CO hydrogenation experimental procedures have also been discussed in Chapter 3.

6.4. Results and discussion

6.4.1. N_2 -adsorption/desorption measurement

Figures 6.1 (A & B) show the isotherms of the four supports (untreated or chemically treated) and their respective OMC-supported KCoRhMo catalysts.

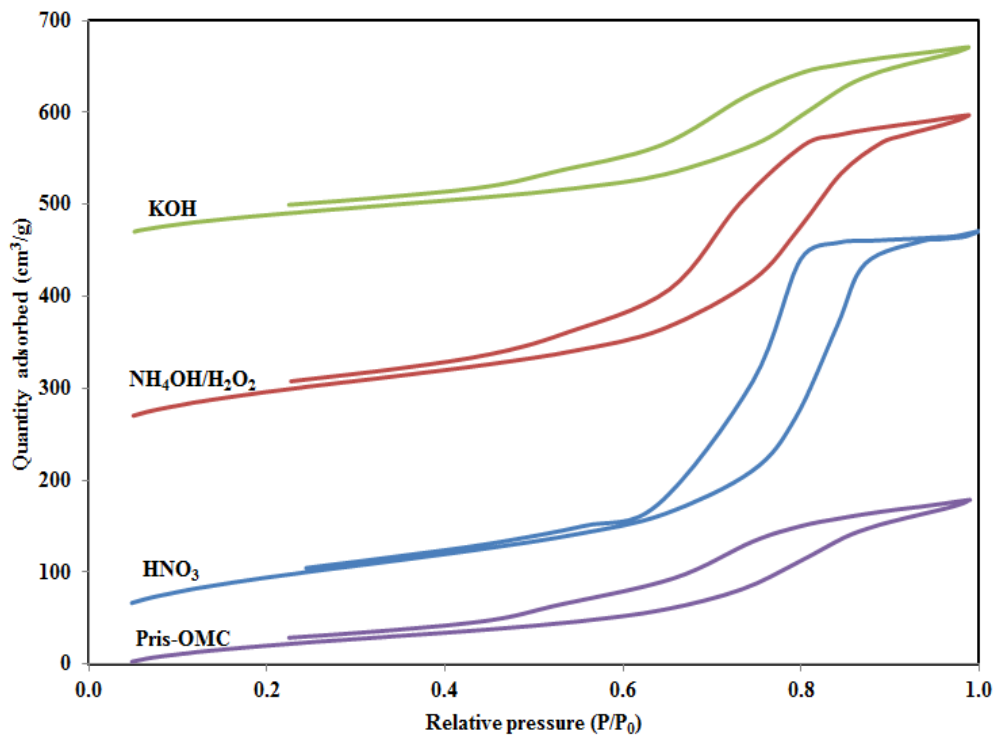


Fig. 6.1 (A): N₂-adsorption isotherms of untreated OMC support and acid/base treated supports

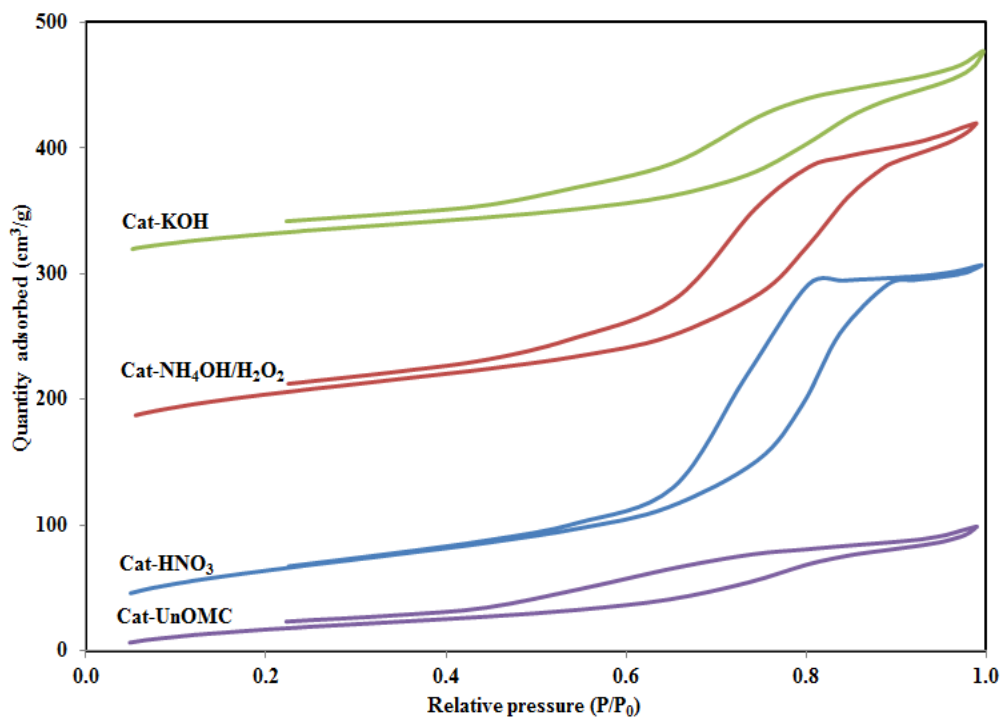


Fig. 6.1 (B): N₂-adsorption isotherms of untreated and treated OMC-supported KCoMoRh catalysts

As evidenced in these figures, the occurrence of textural mesoporosity with uniform cylindrical pores can be confirmed from the profiles of the chemically treated supports and catalysts; exhibiting the type IV isotherms with H1 hysteresis loop (Tanev et al., 1996; Khodakov et al., 2001). For the untreated support and Cat-UnOMC catalyst, the isotherms appear not to be prominently distinct as compared to its treated counterparts; probably due to the presence of carbon impurities prior to chemical treatment. For the application of these catalysts in CO hydrogenation reactions, which is predominantly a surface phenomenon, the porosity as well as the surface area of the catalyst is of a great essence. This is due to the fact that the porosity of the material controls the mass transfer processes via diffusion, which occurs during the adsorption of reactants, surface reaction and subsequent products desorption into the bulk medium.

It is clear from Figures. 6.1 (A & B) that co-impregnation of metal precursors onto the various supports did not significantly change the shape of the type IV isotherms as depicted in these figures. This indicates that supported catalysts exhibited uniform textural porosity after metals loading, as corroborated by TEM results. The sharpness of the desorption branches is indicative of the narrow mesopore size distribution. This is important since it shows that the textural mesoporosity of the catalyst was not overly compromised following the introduction of metal species within the mesopores of the supports (Boahene et al., 2014).

Also, the pore size distribution profiles for the OMC supports and supported KCoMoRh catalysts are given in Figures 6.2A and B, respectively. It is clear that the cumulative volume of N₂ desorbed by the OMC supports (both untreated and treated) is more as compared to their respective catalysts; suggesting that incorporation of metal precursors partially filled portions of the pore volume. In contrast, a much broader pore size distribution profile was evidenced in the pristine support and its corresponding catalysts as compared to the treated counterparts of the same.

One could reason that chemical treatments of the OMC supports resulted in the removal of impurities from the carbon structure during its synthesis; thus, contributing to the narrower pore size distribution profile observed in both the treated supports as well as their corresponding catalysts.

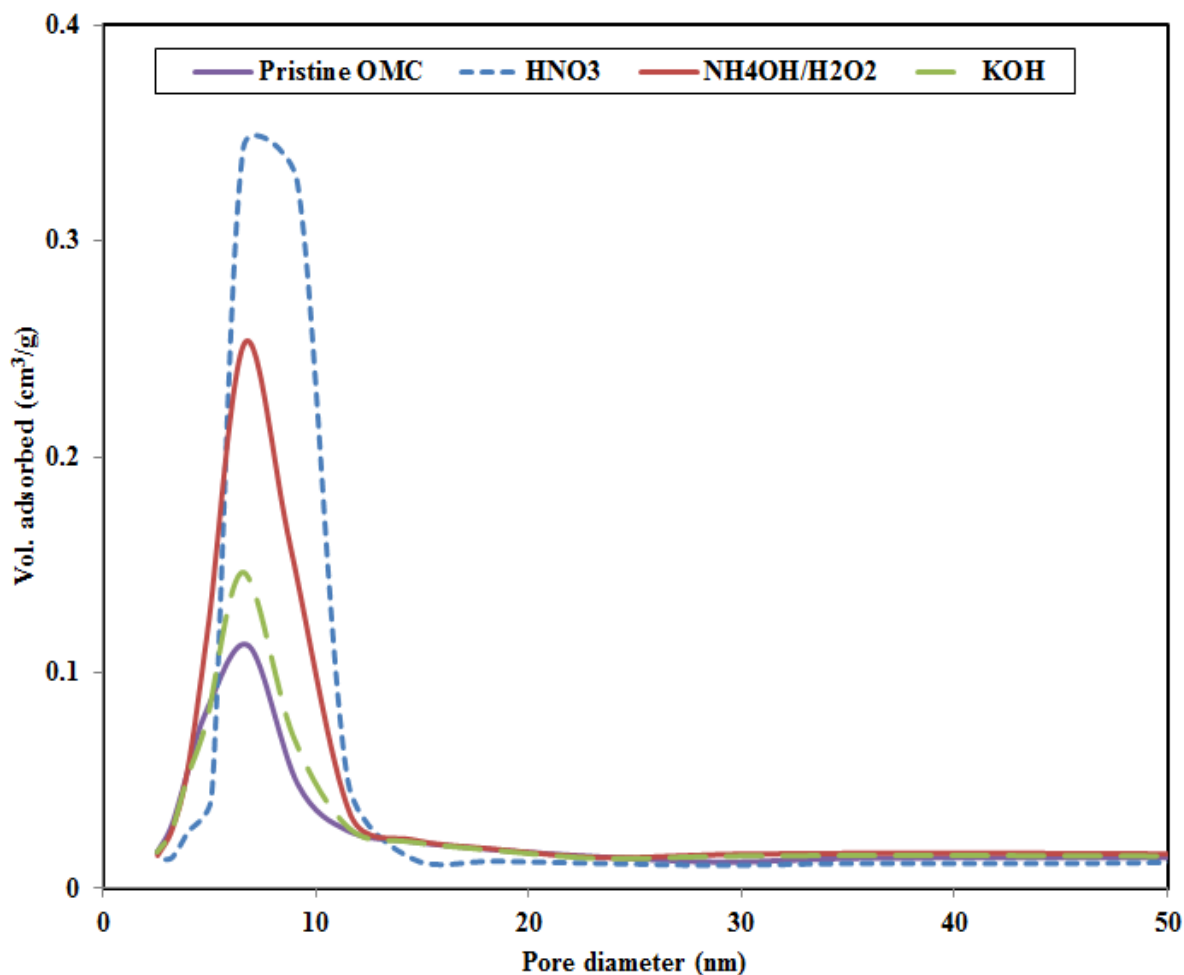


Fig. 6.2(A): Pore size distribution of untreated OMC support and acid/base treated supports determined from N₂ sorption analysis

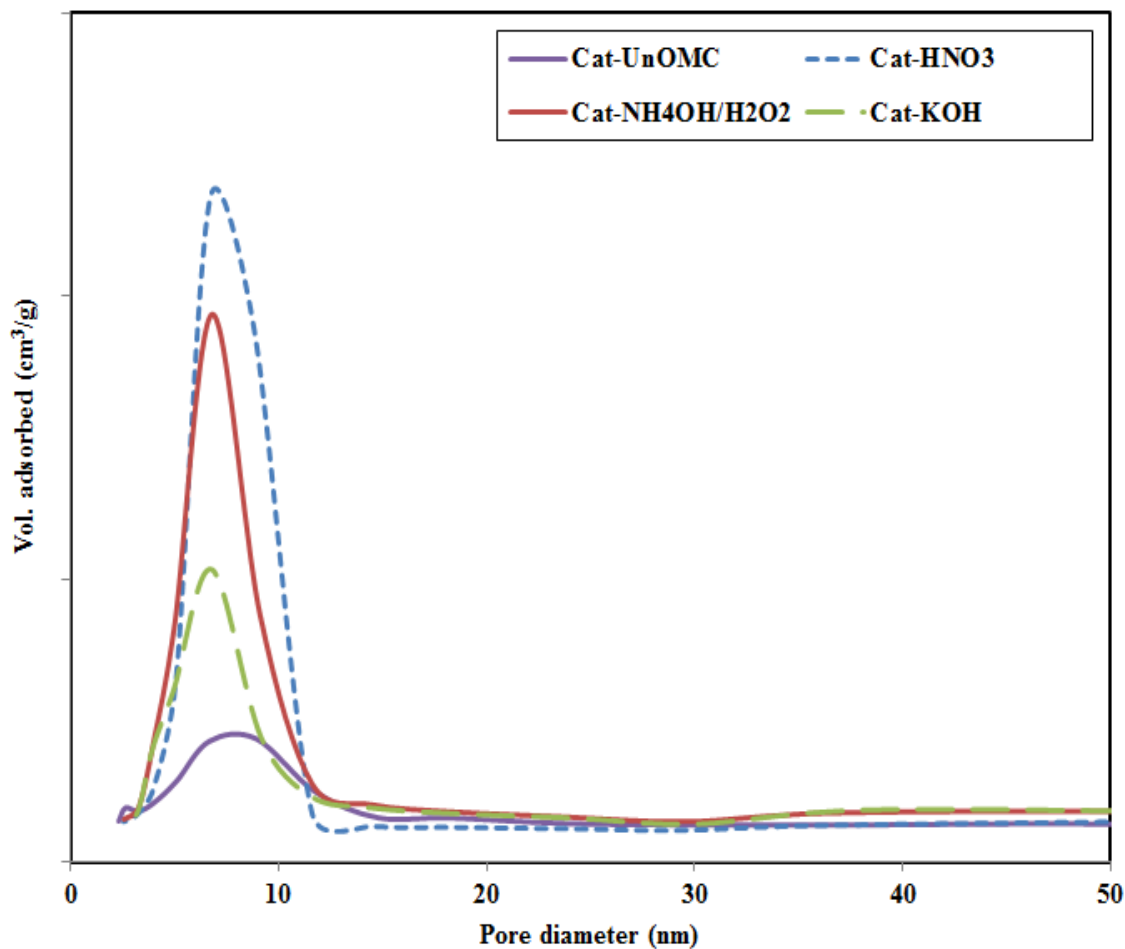


Fig. 6.2 (B): Pore size distribution of untreated and treated OMC-supported KCoMoRh catalysts determined from N₂ sorption analysis.

In addition, a significant merging of smaller pores into much larger ones could be observed and attributed to the sudden one-step heat treatment of the pristine supported catalyst during the calcination step. It is known that the presence of catalysts metals in carbon materials may affect its porosity during the calcination step (Surisetty et al., 2010). This characteristic broader pore size distribution resulting from the merging of smaller pores may have contributed to the observed lower alcohol productivity exhibited by Cat-UnOMC during the HAS reaction.

Table 6.1 gives a summary of the textural properties of the pristine OMC and chemically treated supports as well as the OMC-supported KCoRhMo catalysts.

Table 6.1: Textural properties of untreated and chemically treated OMC supports & catalysts determined from N₂ sorption analysis.

Sample ID	BET Analysis			NS _{BET}	Increments (%)	
	SSA (m ² /g)	PV (cm ³ /g)	BJH _{ads} (nm)		SSA	PV
<u>SUPPORTS</u>						
Pristine OMC	481	0.472	7.4	-	-	-
OMC-HNO ₃	577	0.812	8.6	-	20.0	72.0
OMC-NH ₄ OH/H ₂ O ₂	515	0.734	7.7	-	7.1	55.5
OMC-KOH	494	0.493	7.4	-	2.7	4.4
<u>CATALYSTS</u>						
Cat-UnOMC	279	0.256	6.8	0.83	-42.0	-45.8
Cat-HNO ₃	375	0.521	8.4	0.93	-35.0	-35.8
Cat-NH ₄ OH/H ₂ O ₂	316	0.503	8.1	0.88	-38.6	-31.5
Cat-KOH	268	0.331	8.1	0.78	-45.7	-32.9

NS_{BET}, specific surface area calculated by the BET method.

NS_{BET} (Normalized surface area) were calculated by using the equation, NS_{BET} = (S_{BET} of the catalysts)/(1-x)·S_{BET} of the support

PV, pore volume determined by nitrogen adsorption at a relative pressure of 0.98.

PD_{ads}, desorption mesopore diameter corresponding to the maximum of the pore size distribution obtained from the adsorption isotherm by the BJH method.

OMC, Ordered Mesoporous Carbon

It is worth mentioning that acid pre-treatment of pristine carbon materials such as MWCNTs resulted in the opening of the closed ends and caps of the pristine material and also significantly improved its textural properties (Khodakov et al., 2001). In the case of OMC materials studied, chemical treatments of the supports resulted in increases in surface area, pore volume and pore diameters in comparison to the pristine OMC support. Specific surface area and pore volume increments in the ranges of 2.7-20% and 4.4-72%, respectively, were recorded for the chemically treated supports as compared to the untreated support. The HNO₃ treated support

showed the highest surface area as well as pore volume, while the least of the parameters were recorded by the KOH treated support. For the catalysts, decreases in surface area and pore volumes were recorded for all supports (either untreated or chemically treated), with Cat-HNO₃ recording the least surface area decrement of 35%. Similarly, Cat-HNO₃ showed a 35.8% pore volume decrement as compared to 45.8% as recorded by Cat-UnOMC. This suggests that between the best treated supported catalysts (Cat-HNO₃) and the untreated catalyst (Cat-UnOMC), the recorded 10% difference in pore volume was quite significant for the loading of metal precursors. This is also the case for the specific surface area difference of 7% between the same materials.

It can be deduced from Table 6.1 that the oxidizing agents used for chemical treatment evidenced different oxidizing power; thus, contributing to the significant changes in textural properties observed. It should be noted that apart from opening the closed end caps and incorporation of oxygen-containing groups on to the walls and ends of carbon nanotubes, Sigurdson et al., 2010, also observed an etching effect on the surface of the tubes; thus, enhancing its surface chemical properties. For the OMC supports, the added etching effect of HNO₃ pre-treatment must be responsible for the increments observed in the surface area of the supports. That notwithstanding, with the incorporation of metal precursors onto the support matrix, a resultant decrease in both the surface areas and pore volumes of the catalysts was observed to follow the order: Cat-HNO₃ > Cat-NH₄OH/H₂O₂ > Cat-UnOMC > Cat-KOH; however, changes in the pore diameter of the supports did not follow a particular trend. The monotonic reduction in textural properties (specific surface area and pore volume) of the supports as a result of metal (Co, Rh, Mo) precursors loading was expected. Nonetheless, the decrease in specific surface area as a result of co-impregnation of Co, Mo, and Rh metal precursors on the supports did also significantly

influenced the homogeneity of dispersed metal species on the surface of the supports, as corroborated by the X-ray powder diffraction analysis.

In addition, the normalized specific surface area (NS_{BET}) analysis of the prepared catalysts showed a similar trend (as shown above) with the deposition of metal species on the supports. The NS_{BET} of Cat- HNO_3 and Cat-KOH were computed to be 0.93 and 0.78, respectively, which is < 1 ; indicating that while the introduction of the oxide metal nanoparticles caused a minimal reduction in pore volume for the former catalyst, the latter catalyst experienced quite a significant pore blockage. Furthermore, these results also give an indication that impregnation of metal species on a catalyst support plays a vital role in the overall catalytic surface area required for a given chemical reaction. Thus, the activity and alcohol products selectivities could be affected by the available surface areas of the respective catalysts during the surface-catalyzed HAS reaction.

Similarly, the observed trend for the values of NS_{BET} of catalysts investigated followed the order: Cat- HNO_3 $>$ Cat- NH_4OH/H_2O_2 $>$ Cat-UnOMC $>$ Cat-KOH. This could be attributable to the significant changes in specific surface area of the pristine OMC support following the various chemical oxidation treatments. The specific surface areas of the support and their respective catalysts play a role in the computation of the NS_{BET} values. At this similar metals loading for catalysts formulation (4.5%Co, 1.5%Rh & 15%Mo), one can conclude that the incorporation of metals precursors on to the OMC supports (treated and untreated) affected differently the porosity as well as the overall textural properties of the final catalysts. This observation is quite evident from the NS_{BET} values, which gives an indication of minimal pore blockage in the HNO_3 treated OMC-supported catalyst as compared to its KOH counterpart.

6.4.2. Elemental analysis

Inductively coupled plasma-mass spectrometer (ICP/MS) technique was used to ascertain the respective elemental compositions (actual wt.%) of Co, Mo, and Rh present in the prepared KCoRhMo catalysts in the oxide state. Table 6.2 shows the ICP/MS results of KCoRhMo supported catalysts with their corresponding targeted compositions as well as CO uptake of the catalysts determined by CO chemisorption analysis.

Table 6.2: Elemental compositions and CO uptake of untreated as well as chemically treated OMC-supported KCoRhMo catalysts.

Sample ID	Composition (wt.%)			CO uptake ($\mu\text{mol/g}$)
	Co	Mo	Rh	
Cat-A	4.5* (4.1)	15* (13.7)	1.5* (1.3)	25
Cat-B	4.5* (4.3)	15* (14.3)	1.5* (1.4)	37
Cat-C	4.5* (4.2)	15* (14.7)	1.5* (1.2)	30
Cat-D	4.5* (4.1)	15* (13.9)	1.5* (1.3)	16

* Targeted composition; **Cat-A:** Cat-UnOMC; **Cat-B:** Cat-HNO₃; **Cat-C:** NH₄OH/H₂O₂; **Cat-D:** Cat-KOH

6.4.3. Wide-angle X-ray diffraction

The crystal phase of the sample was analyzed by X-ray diffraction (XRD). Diffraction patterns of the pristine OMC & chemically treated as well as the untreated OMC-supported KCoMoRh catalysts are shown in Fig. 6.3 for 2 θ values in the range of 10-80°.

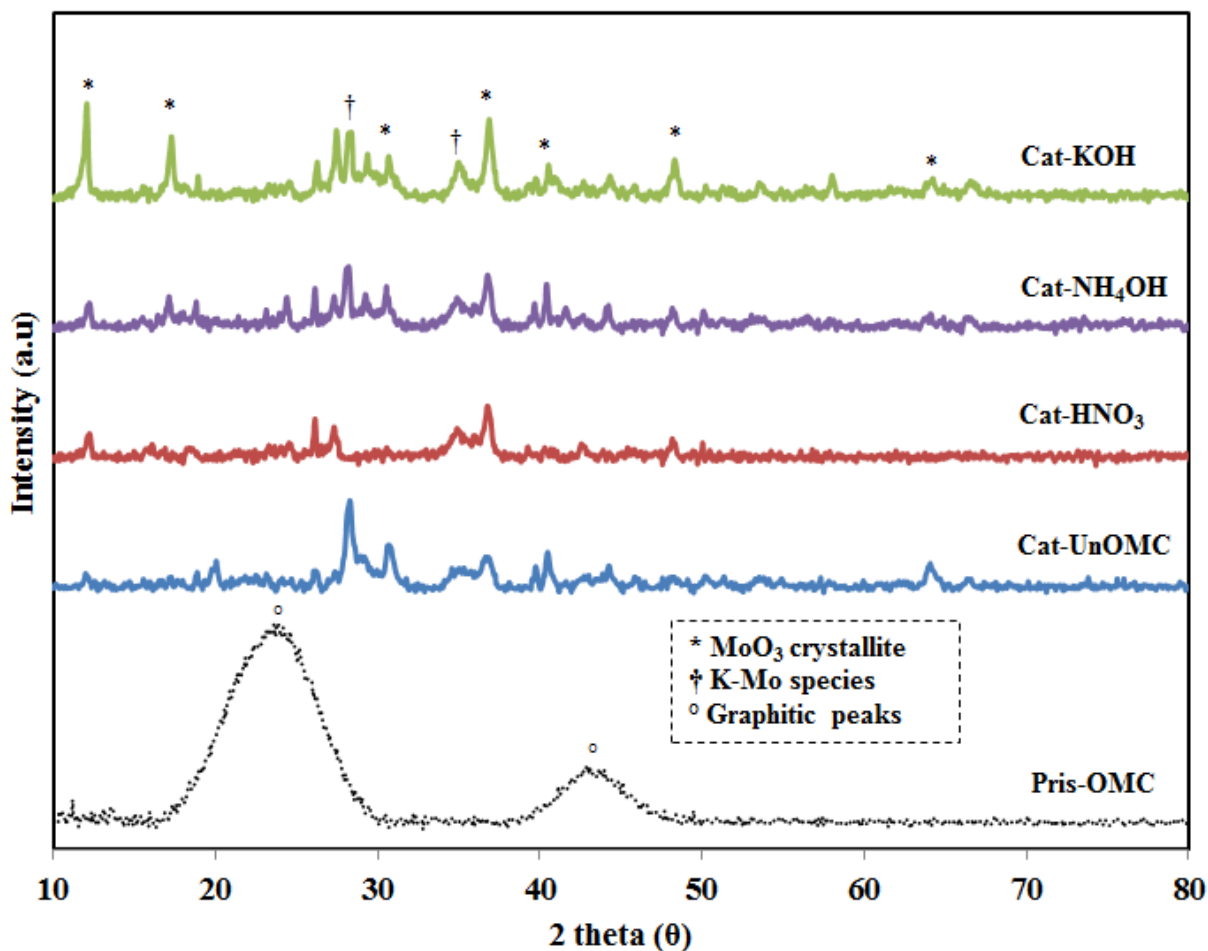


Fig. 6.3: Wide-angle X-ray diffraction patterns of pristine OMC & chemically treated as well as untreated OMC-supported KCoMoRh catalysts. (° graphite; * MoO₃; † K₂Mo₂O₇)

The characteristic peaks occurring at $2\theta = 24.2^\circ$ and 43.7° can be assigned to the presence of amorphous carbon (corresponding to (002) and (100) reflection, respectively) in the pristine OMC support. The broad diffraction peaks demonstrate the existence of amorphous phase in the as-made OMC (Calafata et al., 1998). Similarly, peaks occurring at 17.1° , 30.4° , 36.8° and 40.6° can be attributed to the crystalline MoO₃. However, the more prominent graphitic peaks of the pristine OMC support diminishes in the all catalysts; suggesting that chemical treatment resulted in the purification of the carbon matrices. With the incorporation of metal nanoparticles, the generated peaks on the Cat-KOH showed sharper spikes with heightened intensities as compared to its HNO₃

and $\text{NH}_4\text{OH}/\text{H}_2\text{O}_2$ counterparts; suggesting a more crystalline metal phases on the former catalyst. It could also be reasoned that homogeneity of metal species deposited on the HNO_3 treated supported catalyst was superior as compared to the remaining catalysts investigated. This could be attributed to relatively lower surface area ($268 \text{ m}^2/\text{g}$) of Cat-KOH as opposed to the higher surface area ($375 \text{ m}^2/\text{g}$) of Cat- HNO_3 . It is worth mentioning that a catalyst support with more desirable textural properties would better enhance the stabilization the active species and promoters as well as playing a vital role to modify the dispersion, reducibility, and electron-donating or accepting effects of metal nanoparticles (Hindermann et al., 1983).

Consequently, the relatively higher surface area of the HNO_3 -treated OMC support may have played a significant role by enhancing great dispersion of catalytic phases as confirmed by the XRD profile for its corresponding catalyst. Also, the peaks occurring at 2θ values of 26.2, 28.3 and 34.8 can be assigned to the presence of $\text{K}_2\text{Mo}_2\text{O}_7$ species in the samples (Surisetty et al, 2009; Surisetty, 2010). The average MoO_3 crystallite size from the full width at half maximum (FWHM) diffraction profile computed by the Debye-Scherrer's equation ($L=0.9\lambda/\beta\cos\theta$) for the chemically treated OMC catalysts showed MoO_3 crystallite size in the range 6-9 nm as opposed to 12 nm for the untreated supported catalyst. Nonetheless, both particle sizes quite favored the higher alcohols synthesis reaction. However, it should be noted that these nanoparticles are liable to significant changes during higher alcohol synthesis reaction as a result of time on stream under operation conditions of pressure and temperature.

6.4.4. Raman spectroscopic analysis

Raman spectroscopy is a powerful tool for identifying carbon materials and detecting heteroatoms present in carbon matrix (Zhang et al., 2013; Ansari et al., 2011; Mao et al., 2012). It is a nondestructive vibrational technique and particularly well suited to detect small changes in

structural morphology of carbon nanomaterials (Schwan et al., 2001; Yang et al., 2013; Silva et al., 2012). Every band occurring in the Raman spectrum corresponds directly to a specific vibrational frequency of a bond within the molecules of the specimen investigated (Yang et al., 1990; Dresselhaus et al., 2004). For carbon materials such as graphite, carbon nanotubes, ordered mesoporous carbons, etc., information such as electronic structure as well as sample imperfections can be derived from spectra obtained from this technique (Xiong et al., 2015).

Figures 6.4 (A & B) show characteristics vibrational profiles of both treated and untreated OMC supports as well as their corresponding KCoMoRh catalysts as ascertained by Raman spectroscopic studies.

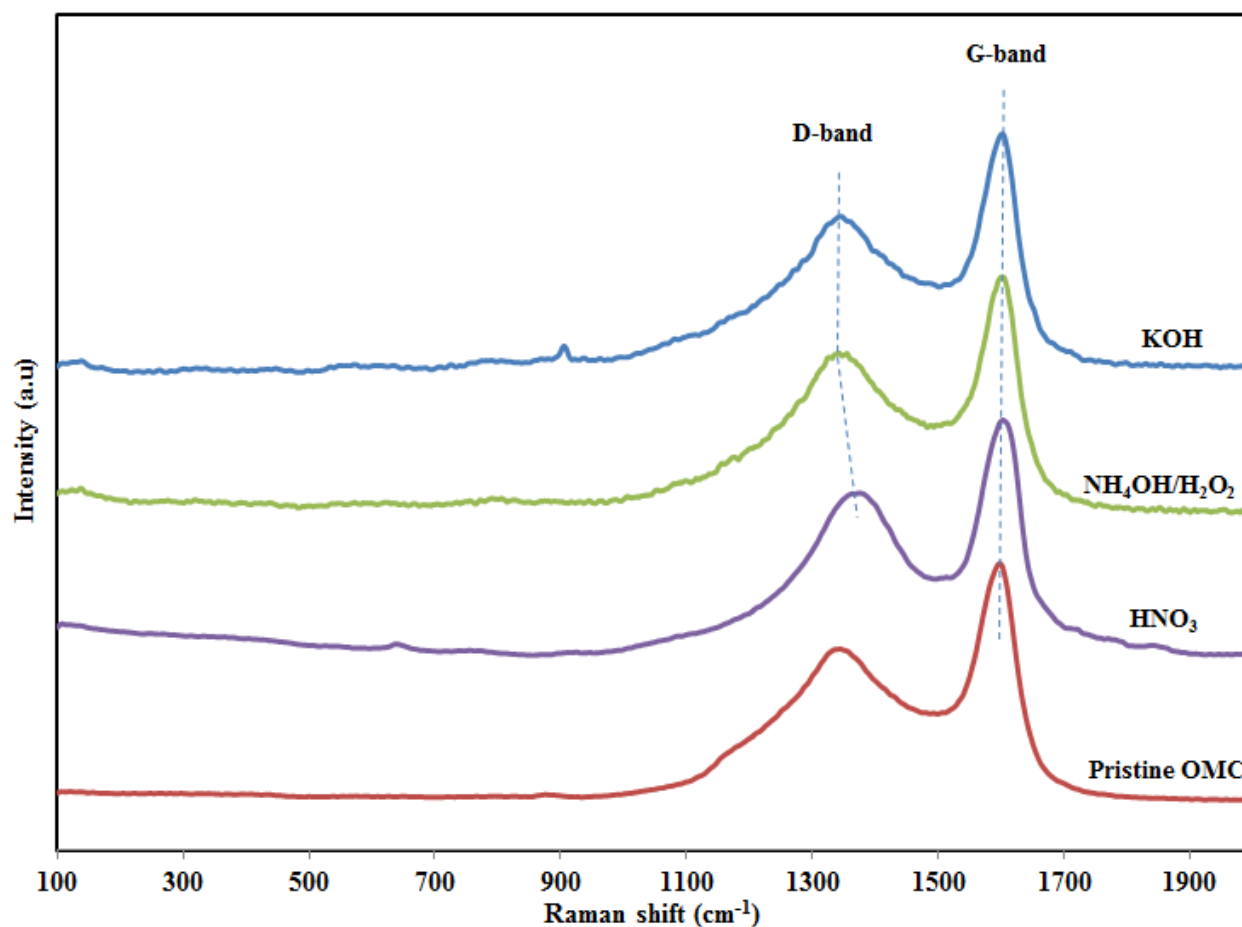


Fig. 6.4 (A): Raman patterns of treated and pristine OMC supports.

Raman spectra evidenced two distinct peaks in the range of 1340-1365 cm^{-1} and 1575-1600 cm^{-1} , and can be attributed to the so called D- and G-bands, respectively. The former is characteristic of the extent of disorderliness in the carbon matrix and the latter is due to the C-C stretching modes present in the material. While the G-band indicates the graphitic E_{2g} plane vibration, the D-band is due to the disordered parts such as grain boundaries (Shimodaira et al., 2002; Boahene et al., 2014) which is indicative of the A_{1g} plane. It is known that the intensity ratio of the D to G bands (I_D/I_G) is generally used to denote the extent of disorderliness present in the graphite layer of carbon material. The greater the value of this parameter, the more disordered the material becomes (Vinu et al., 2007). For instance, using the ratio of peak intensities (I_D/I_G), the level of disorder in the Raman spectra of graphene was characterized by Lucchese and co-workers (Lucchese et al., 2010). The authors observed that as the extent of disorder in the graphene material increased, I_D/I_G displays two different behaviors: a regime of “low” defect density, where I_D/I_G ratio increases and a regime of “high” defect density, where I_D/I_G ratio decreases. The former is as a result of higher defect density creating more elastic scattering; and the latter can be a result of an increasing defect density resulting in a more amorphous carbon structure (Lucchese et al., 2010). These two regimes are referred to as “nanocrystalline graphite” and “mainly sp² amorphous carbon” phases, respectively (Ferrari et al., 2000; Ferreira et al., 2011; Cançado et al., 2011).

As can be noted in Fig 6.4A, apart from the band position of the HNO₃-treated support, which appears to be shifted towards the right (a Raman shift from 1340 to 1366 cm^{-1}), the D-bands for all others can be located at the same position; suggesting that chemical treatment of the OMC support with HNO₃ might have caused more defective sites as compared to its NH₄OH/H₂O₂ and KOH counterparts. The respective I_D/I_G ratios for the untreated and chemically treated supports followed the order: NH₄OH/H₂O₂ (0.76) > HNO₃ (0.73) > KOH (0.65) > Pristine OMC (0.61);

however, the corresponding trends for the supported catalysts is as follows: Cat-UnOMC (0.77) > Cat-KOH (0.68) > Cat-NH₄OH/H₂O₂ (0.59) > Cat-HNO₃ (0.57). It can also be deduced that the I_D/I_G ratios of the respective chemically treated supports and their corresponding catalysts decreased. For instance, following the various chemical treatments, the I_D/I_G ratios changes as follows: NH₄OH/H₂O₂ (0.76 to 0.59), HNO₃ (0.73 to 0.57), KOH (0.65 to 0.68) and UnOMC (0.61 to 0.77). This observed trend can be explained by the fact that initial chemical treatment by NH₄OH/H₂O₂ and HNO₃ modified the surface chemistry of the OMC support and created the needed defective sites (“high” defect density) via oxygen-functional groups anchorage.

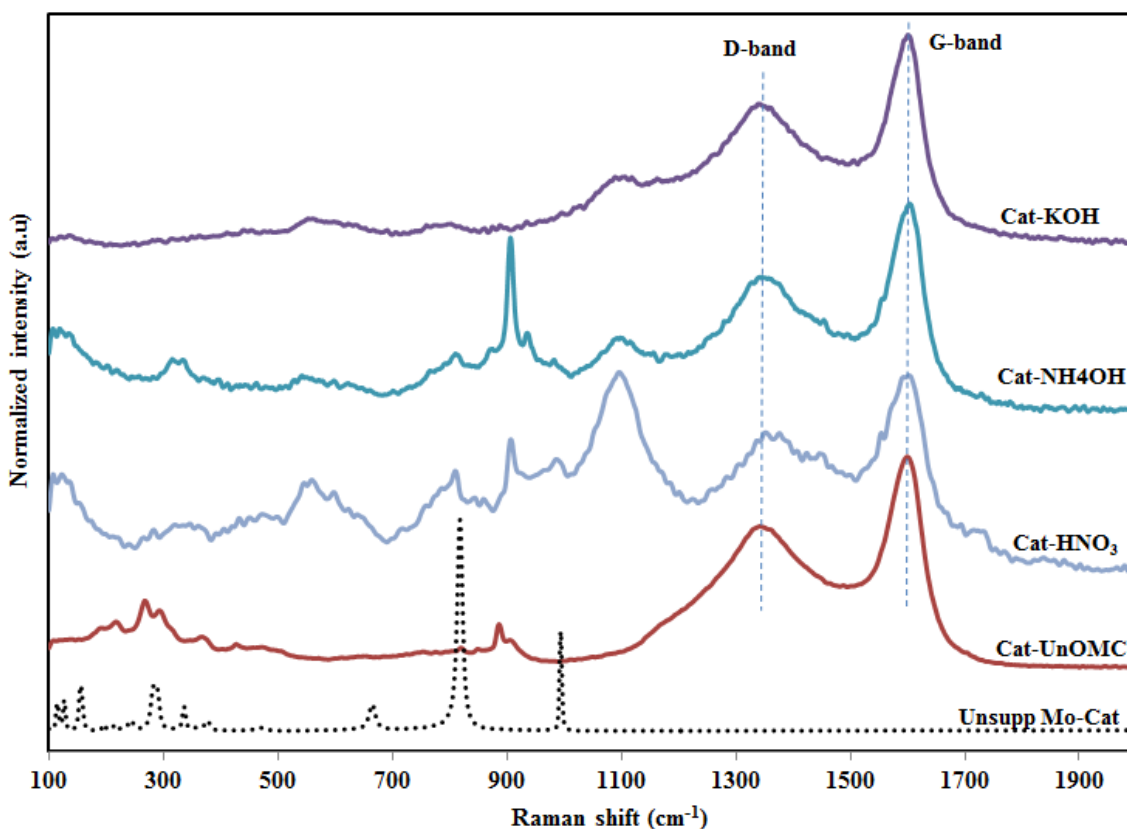


Fig. 6.4 (B): Raman patterns of treated and untreated OMC-supported KCoMoRh catalysts

The incorporation of metal precursors via co-impregnation on to these chemical treated supports and subsequent catalyst calcination caused a shift from a regime of “high” defect density

to that of “low” defect density, characterized by a decrease in I_D/I_G ratio as evidenced in a similar study conducted by Lucchese et al., 2010. Similarly, the increase in I_D/I_G ratio as observed in KOH (0.65-0.68) and UnOMC (0.61-0.77) can be due to the vigorous treatment resulting from KOH functionalization and the direct one-step calcination of Cat-UnOMC; probably suggesting creation of more amorphous carbon in the Cat-KOH and Cat-UnOMC catalyst materials. As can be seen in Fig 6.4B, other peaks located at 261, 540, 789, 904, 967, and 1080 can be attributed to metal-oxygen species formation in the catalysts studied, probably of the forms; O-Mo-O, K-Mo-O, and Co-Mo-O, bonds. One can conclude from the present work that not only did the chemical oxidation treatment of the OMC support cause the generation of defective sites, but also the direct metal precursor impregnation on to the support (without chemical pre-treatment) and the concomitant one-step calcination can also contribute to the creation of defective sites as corroborated by Raman analysis.

6.4.5. Fourier Transform Infra-red analysis

The FTIR technique was employed to analyze the surface functional groups present on all the carbon materials studied. The resulting spectra of samples are shown in Figs. 6.5A & B. The spectrum of the pristine OMC carbon support shows bands related to oxygen and carbon groups, located at 3450 and 1615 cm^{-1} , respectively. The peak at 3450 cm^{-1} is due the stretching vibration of O-H groups in the material, indicating the oscillation of carboxyl groups (Jang et al., 2004). This peak can also be seen in the chemically treated supports; however, it becomes more prominent for the HNO_3 treated support. The other peak located at 1615 cm^{-1} as observed for the pristine OMC support can be attributed to the stretching skeletal vibration of C=C (polynuclear aromatic structure) bond which could also been seen in all the supports (Lazaro et al., 2007).

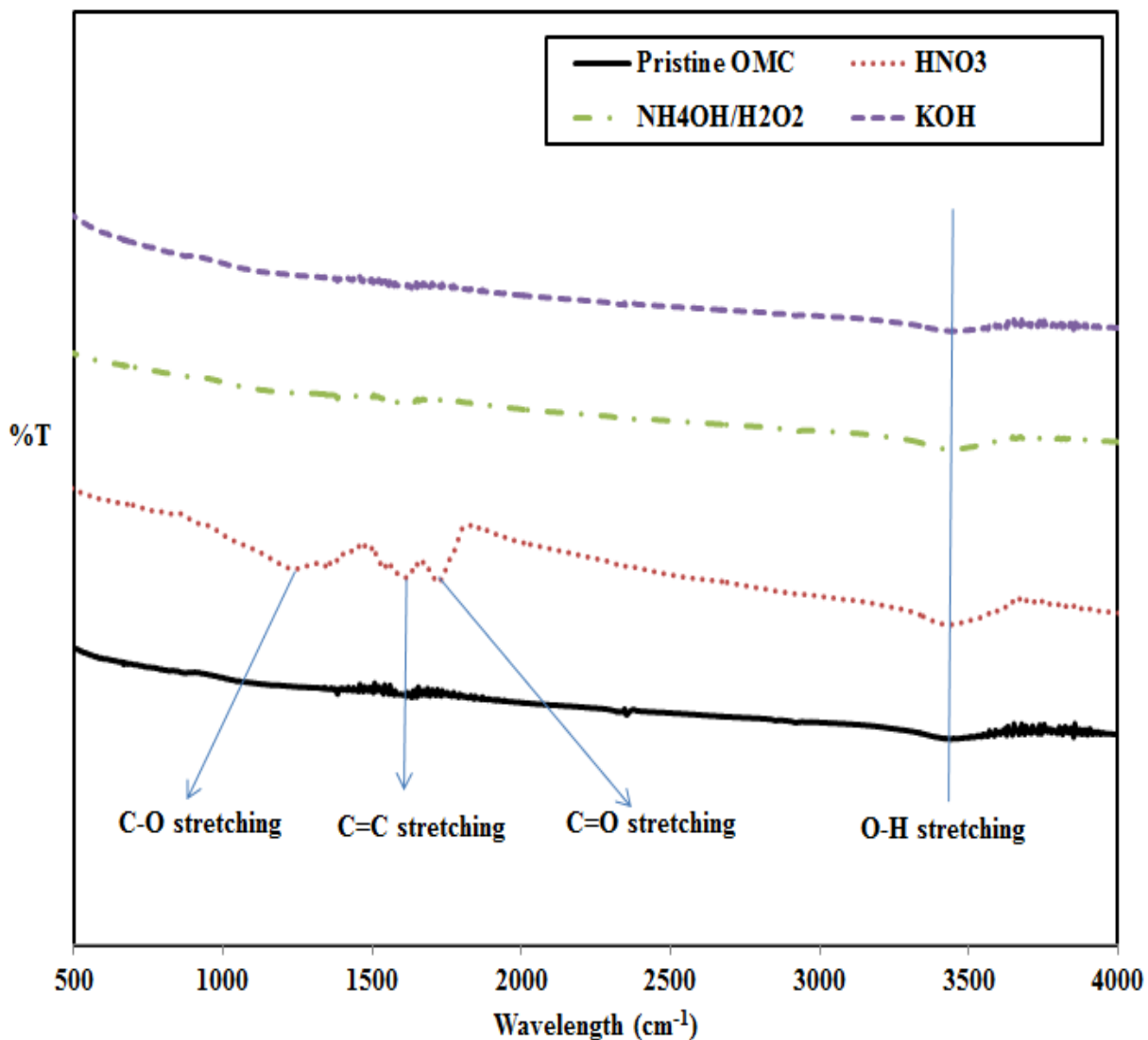


Fig. 6.5 (A): FTIR profiles of chemically treated and untreated OMC supports

For the treated supports, additional distinct peaks located at 1245 and 1720 cm⁻¹ were observed on the spectrum of the HNO₃ treated support. The band at 1245 cm⁻¹ can be assigned to contributions from stretching C–O–C vibrations (in ether and lactone structures or other single bonded oxo-group, C–O–R) and that observed at 1720 cm⁻¹ can be assigned to C=O stretching vibrations from carbonyl or carboxyl groups, respectively (Bazula et al., 2008). It is noteworthy to mention that these carboxylic groups can be generated due to the oxidation of some carbon atoms

on the surface of the OMC support as a result of the chemical pretreatment (Boahene et al., 2014). Furthermore, two more prominent peaks occurring at 1350 and 1535 cm^{-1} on the same HNO_3 spectrum can be assigned to stretching vibrations (asymmetric and symmetric, respectively) of nitro group (NO_2), indicating the simultaneous occurrence of nitration reactions during the intended HNO_3 chemical oxidation treatment (Lazaro et al., 2007).

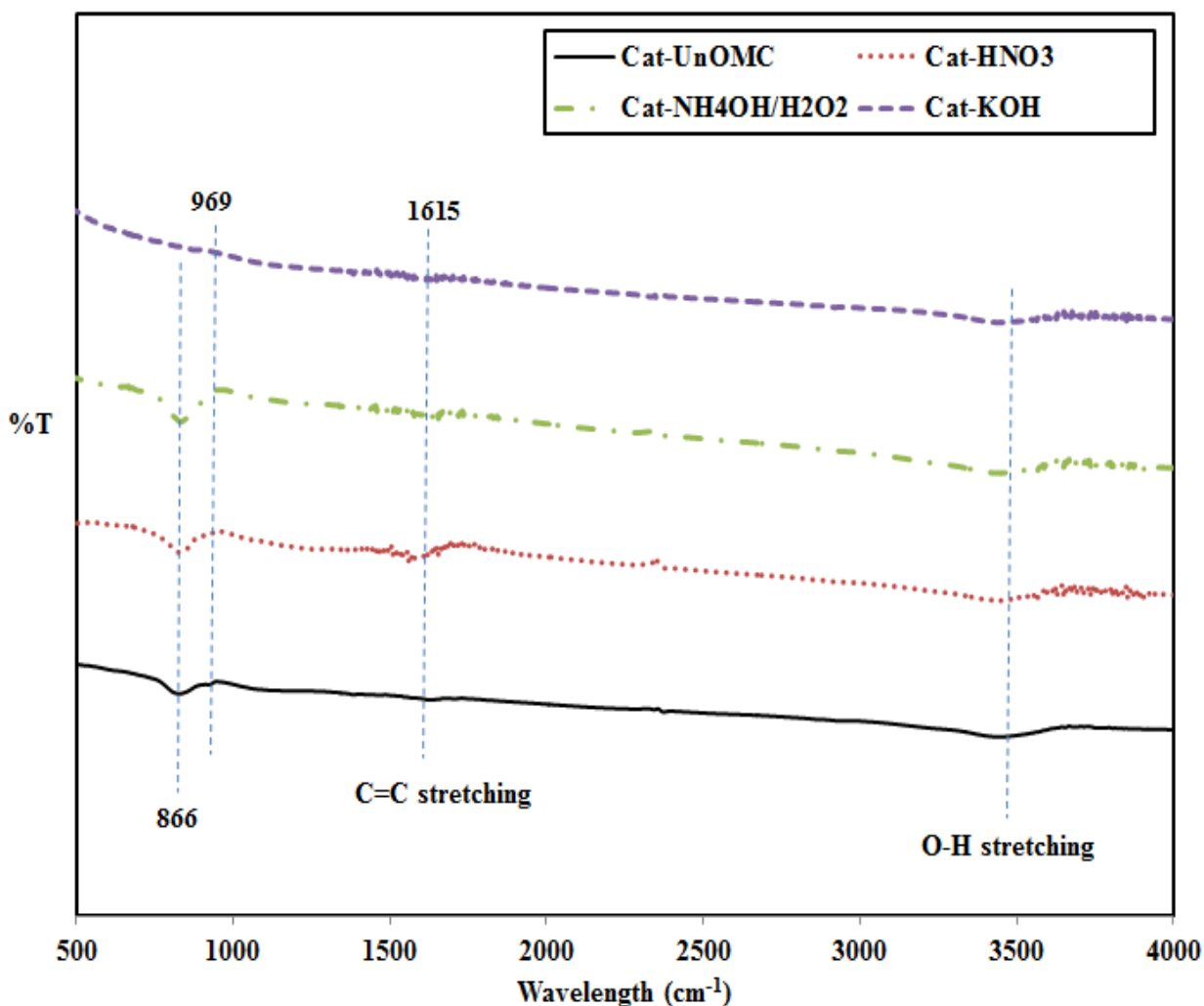


Fig. 6.5 (B): FTIR profiles of chemically treated and untreated OMC-supported catalyst

These peaks were absent in the $\text{NH}_4\text{OH}/\text{H}_2\text{O}_2$ and KOH treated supports; suggesting that the chemical composition of the carbon network in the OMC support is changed considerably during

oxidation with nitric acid. In Fig 5B, it can be observed that most of the peaks disappeared due to their consumption in metal-oxygen bond formation, following metal precursor impregnation and subsequent calcination in N₂ atmosphere. All catalysts showed peaks at 866 and 969 cm⁻¹, which could be ascribed to out-of-plane deformation of C-H bonds, possibly via the formation of metal species moiety (Lazaro et al., 2007; Bazula et al., 2008).

6.4.6. Thermogravimetric analysis

The percent weight loss of the supports and catalyst samples as a function of temperature were ascertained by TGA technique so as to determine the thermal stability of the impregnated catalysts during the HAS reaction. Figs. 6.6 (A & B) show the TGA profiles for the supports and catalysts, respectively. It shows that prior to chemical oxidation, the pristine OMC support did not have much oxygen-containing functional groups; indicated by the fairly stable thermal characteristics as depicted by its profile. However, after chemical oxidation of the pristine support, the thermogravimetric (TG) profiles of the chemically treated supports (especially, HNO₃ and NH₄OH/H₂O₂) evidenced significant changes in their respective profiles; suggesting the incorporation of functional groups during the pretreatment step. Typically, the existence of surface functional groups can be confirmed due to the significant mass loss during the controlled heat treatment experiment. Thus, an increase in the mass loss during the TG analysis can be correlated to an increased amount of functional groups present on the carbon surfaces by the oxidation treatment. This is consistent with the results from FTIR spectroscopy in which chemical treatment resulted in the appearance of more distinct peaks for example the HNO₃ treated support.

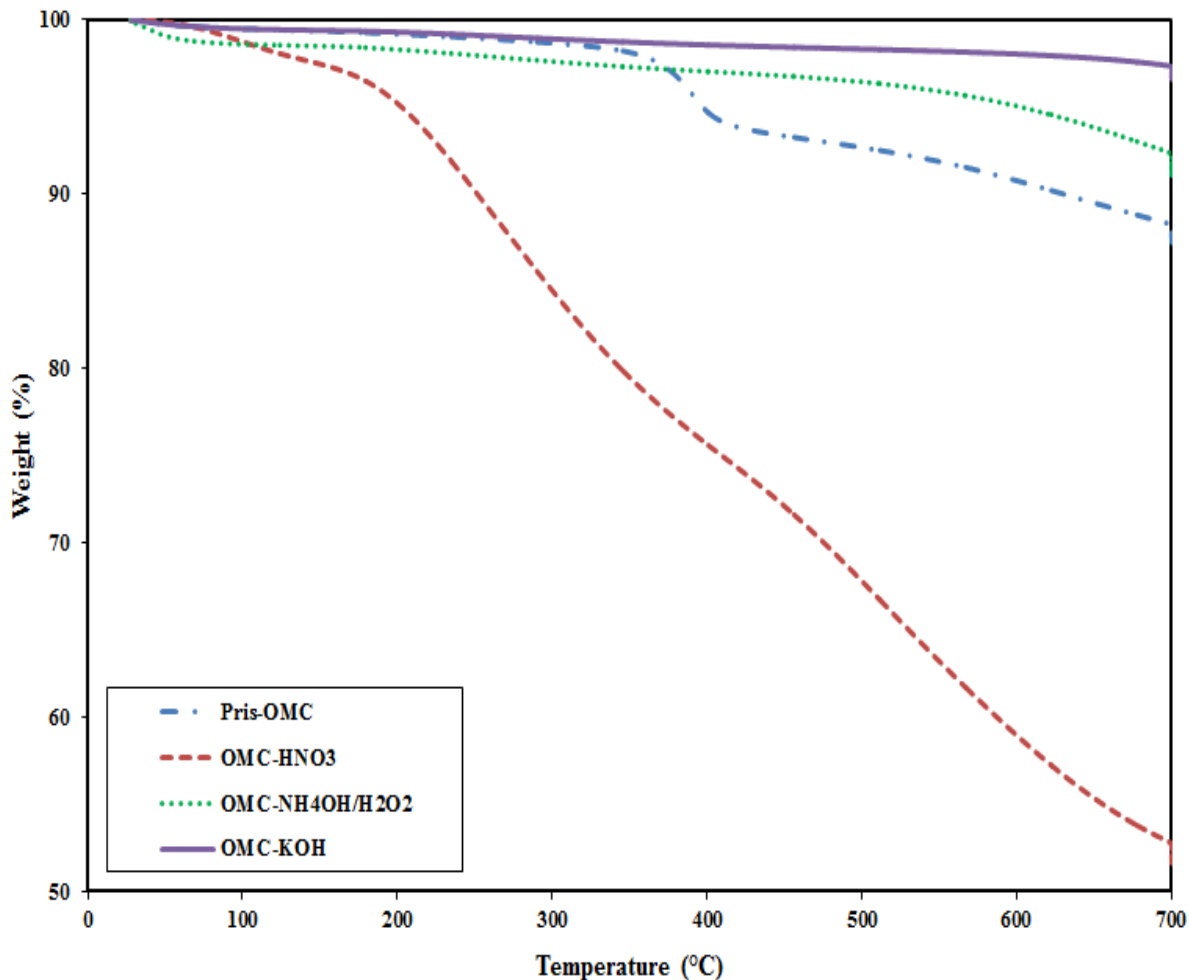


Fig. 6.6 (A): TGA patterns of chemically treated and untreated OMC supports

In addition, during the TG analysis, thermal degradation of the surface functional groups occurs in the chemically oxidized samples. The evolved gaseous species is quantifiable if TG setup is equipped with mass spectrometer (MS). For instance, within the range of temperature for the TG analysis (150-700°C) for typical carbon materials, a significant amount of CO₂ (resulting from the decomposition of carboxyl groups) together with other compounds such as methane, butane and butanol (resulting from the decomposition of the carbon framework) have observed in the MS traces (Bazula et al., 2008). At low-temperature, CO₂ evolution may be the result of carboxyl groups decomposition; however, at high-temperature, the decomposition of anhydride and lactone

groups have been reported (Otake et al., 1993). Moreover, whereas CO₂ evolution mostly occurs below 500°C and CO evolution proceeding above this temperature, both physisorbed and chemisorbed water are mostly released in the range of 100–450°C (Arnoldy et al., 1985; Teng et al., 1993; Cheng et al., 2003). However, in the present work, quantitative evaluation of the corresponding evolved gaseous species was not determined. Nonetheless, the corresponding % mass loss for the supports investigated in the temperature range of 200–500°C followed the trend: HNO₃ (32.4%) > Pristine OMC (7.9%) > NH₄OH/H₂O₂ (1.1%) > KOH (0.1%)

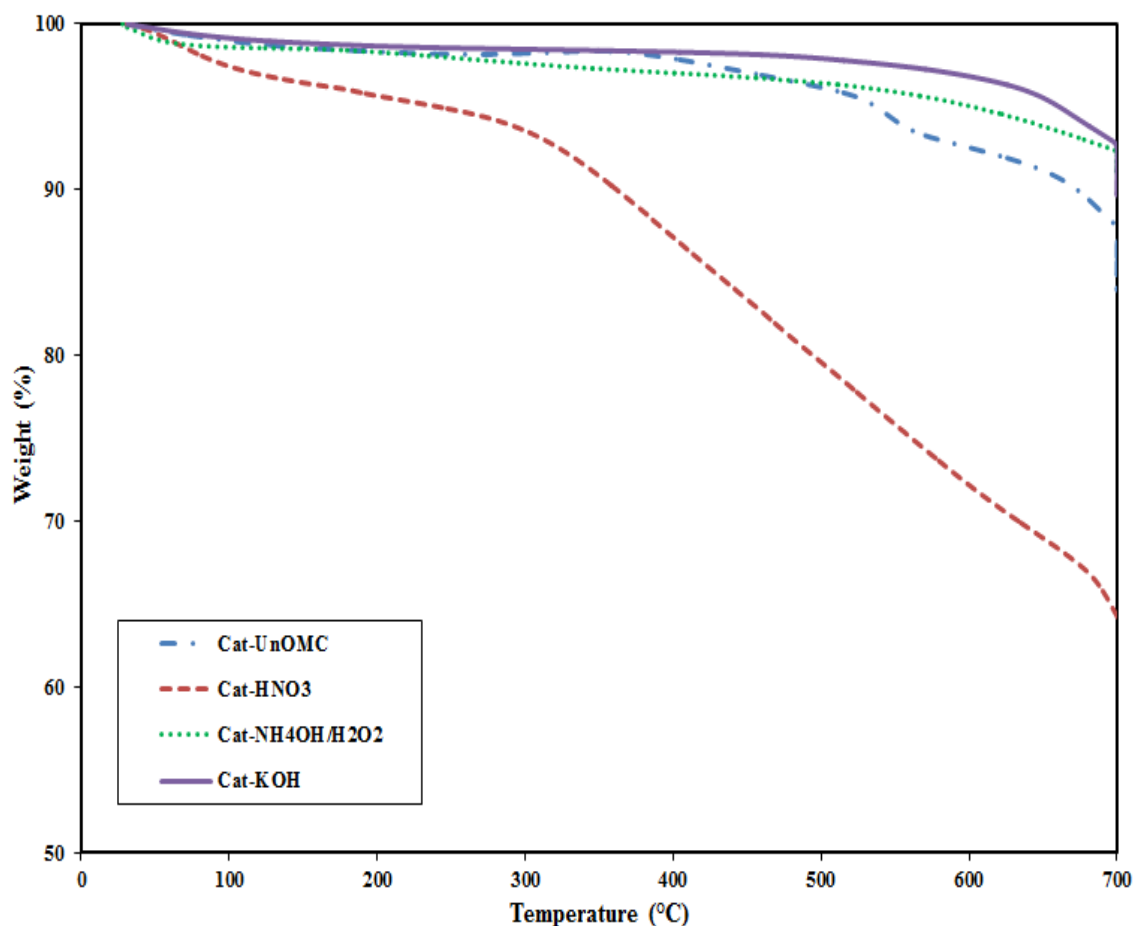


Fig. 6.6 (B): TGA patterns of chemically treated and untreated OMC-supported catalyst

For the supported catalysts, it is clear from profiles in Fig 6.6B that a similar weight loss pattern was observed for all chemically treated catalysts. That notwithstanding, the untreated-supported KCoRhMo catalyst (Cat-UnOMC) exhibited quite a stable thermal property as compared to its HNO₃ counterparts; thus, would still survive the practical reaction conditions though it was not chemically pretreated. It also deserves mentioning that Cat-HNO₃ is thermally stable up to 400°C after which temperature it undergoes significant rapid weight loss as a function of increasing temperature. However, since the actual HAS reaction does not go beyond 400°C, it should be within reasonable error margin. Thus, the trend observed for weight loss in the temperature range of 200–500°C for the catalysts is as follows: Cat-HNO₃ (16.3%) > Cat-UnOMC (7.1%) > Cat-NH₄OH/H₂O₂ (2.7%) > Cat-KOH (1.2%). One could deduce from these trends and Figures 6A & B that the rapid weight loss as a function of temperature for the HNO₃-treated support and its supported catalysts suggests a form of decomposition of chemical species in this material as temperature gradually increased; resulting in the generation of their unique defective sites that favored the HAS reaction. As shown in Table 6.1, the decreases in the specific surface areas and pore volumes associated with catalysts preparation from their respective supports are in the range of 35–45% and 31–46%, respectively. This reduction is due to the increased additional mass after metal precursors co-impregnation, as corroborated by the TG measurements. TG analyses (Figs. 6.6A & B) showed that above 400°C, some of the oxidized catalyst samples exhibited higher mass loss; thus, providing useful information regarding the thermal stability of the investigated catalysts for a typical HAS reaction.

6.4.7. Temperature programmed reduction analysis

Metal-support interactions describe changes that occur in the chemisorption properties of catalyst metals when dispersed on its support material. The nature of metal-support interaction was

critical for this work since metal oxide supports like $\gamma\text{-Al}_2\text{O}_3$ tend to form complexes with dispersed metals (e.g. Co) that are quite difficult to sulfide; thus, reducing the overall activity of the catalyst. In this regard, temperature programmed reduction (TPR) was used to study the reducibility of metal species in the catalyst formulation using hydrogen gas as the probe gas. H_2 -TPR profiles for the supported catalysts are presented in Fig. 6.7. All four catalysts evidenced the typical hydrogen consumption peaks corresponding to the reduction of octahedrally coordinated MoO_3 species (Mo^{6+}) to the tetrahedrally coordinated MoO_2 species (Mo^{4+}), which undergo further reduction to lower oxidation state molybdate moieties at high temperature (Arnoldy et al, 1985; Surisetty et al., 2010).

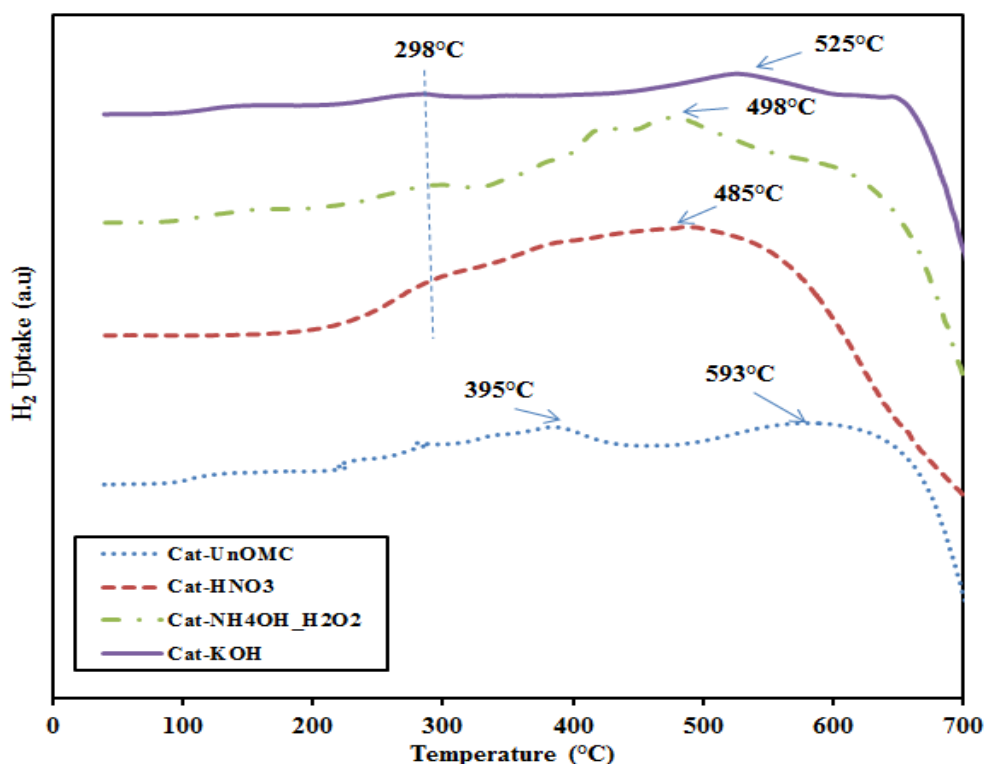


Fig. 6.7: TPR profiles of chemically treated and untreated OMC-supported catalyst

In the case of the untreated supported KCoRhMo catalyst (Cat-UnOMC), three main peaks were observed to occur at 135°C, 395°C and 593°C, respectively. The mid-range reduction

temperature peak (395°C) is as a result of bulk MoO₃ species present in the oxide catalyst undergoing reduction in the presence of hydrogen to generate its tetrahedrally coordinated forms (Mo⁴⁺), which are subsequently completely reduced to lower oxidation states. The absence of a peak occurring in the range 340-360°C could also be noted; suggesting the sufficient reduction of bulk CoO₃ species in the catalyst, giving indication of the probable formation of the Co-Mo-O phase which is active for the higher alcohol synthesis reaction. This observation is consistent with a previous study conducted by Surisetty et al., 2010 on a similar catalyst matrix supported on both activated carbon and MWCNT. One could also observe a small peak appearing around the region of 135°C from the TPR profile of Cat-UnOMC; which could be attributed to the reduction of rhodium species (Rh⁺¹) to its metallic forms (Rh⁰). A similar observation has been reported in the literature (Surisetty et al., 2010). For the treated supported catalysts, similar peaks were observed to occur in the lower (<200°C), middle (295-395°C), and higher (>400°C) temperature ranges, corresponding to the reduction of species as discussed for Cat-UnOMC above. However, the positions of these peaks varied significantly with the various chemical treatments. As compared to Cat-UnOMC, the occurrence of a reduction peaks around 135°C for the treated supported catalysts suggests the complete reduction of Rh⁺¹ to Rh⁰ species in these samples.

Similarly, it could also be seen from Fig. 6.7 that the reduction of octahedrally coordinated MoO₃ species to its tetrahedrally coordinated forms occurred around 298°C for the treated supported catalysts, which is about 100°C lower than that observed for Cat-UnOMC. That notwithstanding, it should be noted that Co₃O₄ species have the same reduction temperature so there exist the possibility that the H₂ consumption peak is an overlap contribution of multiple peaks corresponding to the reduction of MoO₃ and Co₃O₄ species. In addition, the total area under the peaks spanning the overall temperature reduction regime is greater for Cat-HNO₃ suggesting

higher H₂ uptake for this catalyst. This observation underscores the significance of chemical pretreatment of the support prior to metal precursor impregnation for the carbon-supported. In the case of reduction of Mo⁴⁺ species to lower oxidation state oxo-molybdate species, which occurred at higher reduction temperatures, the observed increasing trend for the chemically treated supported catalysts followed the order: Cat-HNO₃ (485°C) < Cat-NH₄OH/H₂O₂ (498°C) < Cat-KOH (525°C) < Cat-UnOMC (593°C). This trend can be explained by the fact that Cat-HNO₃ possesses the highest surface area as compared to its counterparts; thus, dispersed metal species can adequately interact with the support, thereby improving their reducibility and subsequent dispersion in the catalyst matrix as corroborated by XRD analysis.

6.4.8. Transmission electron microscopic analysis

The TEM images of untreated and chemically treated OMC supported catalysts were recorded and are presented in Fig. 6.8. The periodic ordering of pores with well-defined pore structure of these materials can be seen from the TEM images. The distribution of catalyst particles are quite observable in the samples as well, showing well dispersed catalysts inside the pores and also on the exterior surfaces of the carbon materials. It can also be seen that catalyst particles appear as aggregates or nanoclusters dispersed on the untreated OMC supported catalysts, most likely on the surface of the material. In addition, the existence of tubule-like features in the carbon matrix is also evident in the carbon samples of Cat-UnOMC and can probably be due to the presence of impurities in this sample, which were not removed during the chemical pretreatment step. This feature was absent in the chemically treated samples. For Cat-HNO₃ and Cat-NH₄OH/H₂O₂, despite the occurrence of well dispersed catalyst nanoparticles, the structure of the parent OMC material is also kept intact; providing evidence that treatment of the pristine OMC support with HNO₃ and NH₄OH/H₂O₂ did not have a detrimental effect on its morphology.

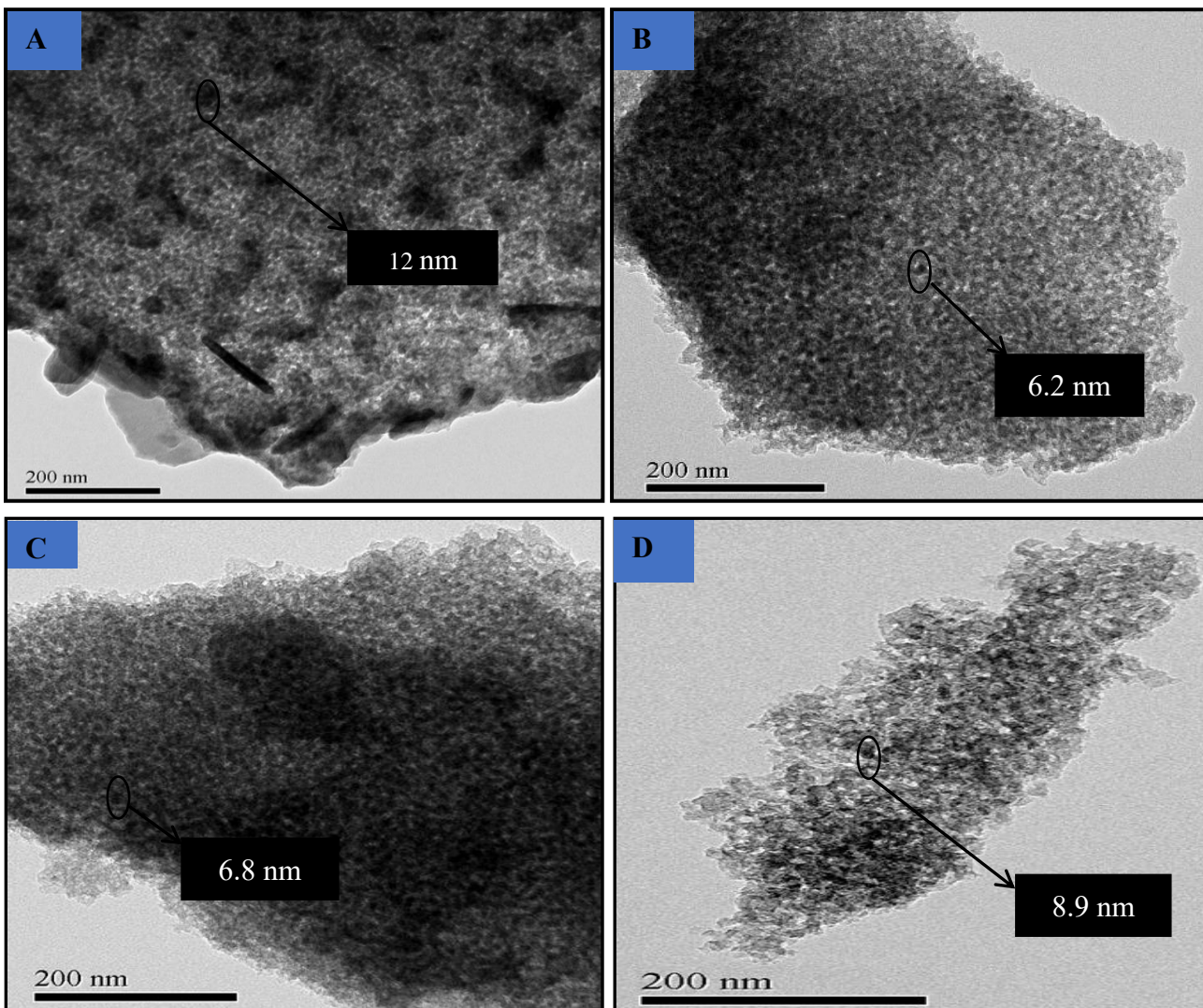


Fig. 6.8: TEM images of (A): Cat-UnOMC; (B) Cat-HNO₃; (C) Cat-NH₄OH/H₂O₂; (D) Cat-KOH

Nonetheless, a slight change in the morphology of the OMC material can be observed for the supported catalyst treated with KOH, which appears slightly distorted; suggesting the original structure of the OMC is not preserved, probably due to the oxidative attack on the carbon matrix during this chemical treatment. The particle sizes of the metal species averaged over different locations in these samples are in the range of 7-9 nm for the treated catalysts and 12 nm for the untreated supported catalyst.

6.5. Catalytic performance tests of OMC-supported KCoMoRh catalysts

The prepared catalyst samples (Cats-A to D) were screened for their performance in the HAS reaction in a high-pressure fixed-bed micro reactor using syngas as feedstock under similar conditions of pressure, temperature, H₂:CO and GHSV of 8.3 MPa, 300-340°C, 1.25, and 3.6 m³ (STP)/kgcat h, respectively. The metals loading intended for the formulation of these catalyst samples were maintained the same to help study the influence of chemical pre-treatment of the OMC support on higher alcohols productivity.

6.5.1. Effect of chemical pretreatment of OMC supports on CO Conversion

For the CO hydrogenation reaction, the catalytic activities of the MoS₂-supported catalysts are mostly at their peak performance at the onset of reaction and gradually decline as result of time-on-stream. As shown in Fig 6.9, within the last 12 h of the 24 h period, CO conversion recorded for all catalysts declined and then stabilized after 18 h on stream due to the well-known phenomenon of initial pre-coking step MoS₂-based catalysts undergo prior to attaining stable catalytic activity (Surisetty et al., 2010; Boahene et al., 2011; Boahene et al., 2014). It can be seen from Fig. 6.9 that all catalysts did not show any significant deactivation after 18 h reaction time online. Nonetheless, at the same experimental conditions, one can observe a higher CO conversion for Cat-HNO₃ as compared to its treated counterparts; probably due to its better textural properties following the chemical oxidative treatment. Thus, at the same metals loading (9%K, 4.5%Co, 15%Mo & 1.5%Rh), there exists relatively more active metal species on this catalyst as can be corroborated by the CO uptake analyses of these catalysts (Table 2). The amount of CO uptake (μmol/g) followed the trend: Cat-HNO₃ (37) > Cat-NH₄OH/H₂O₂ (30) > Cat-UnOMC (25) > Cat-KOH (16), which gives indication that more active sites were present on Cat-HNO₃ for the HAS reaction as opposed to Cat-KOH.

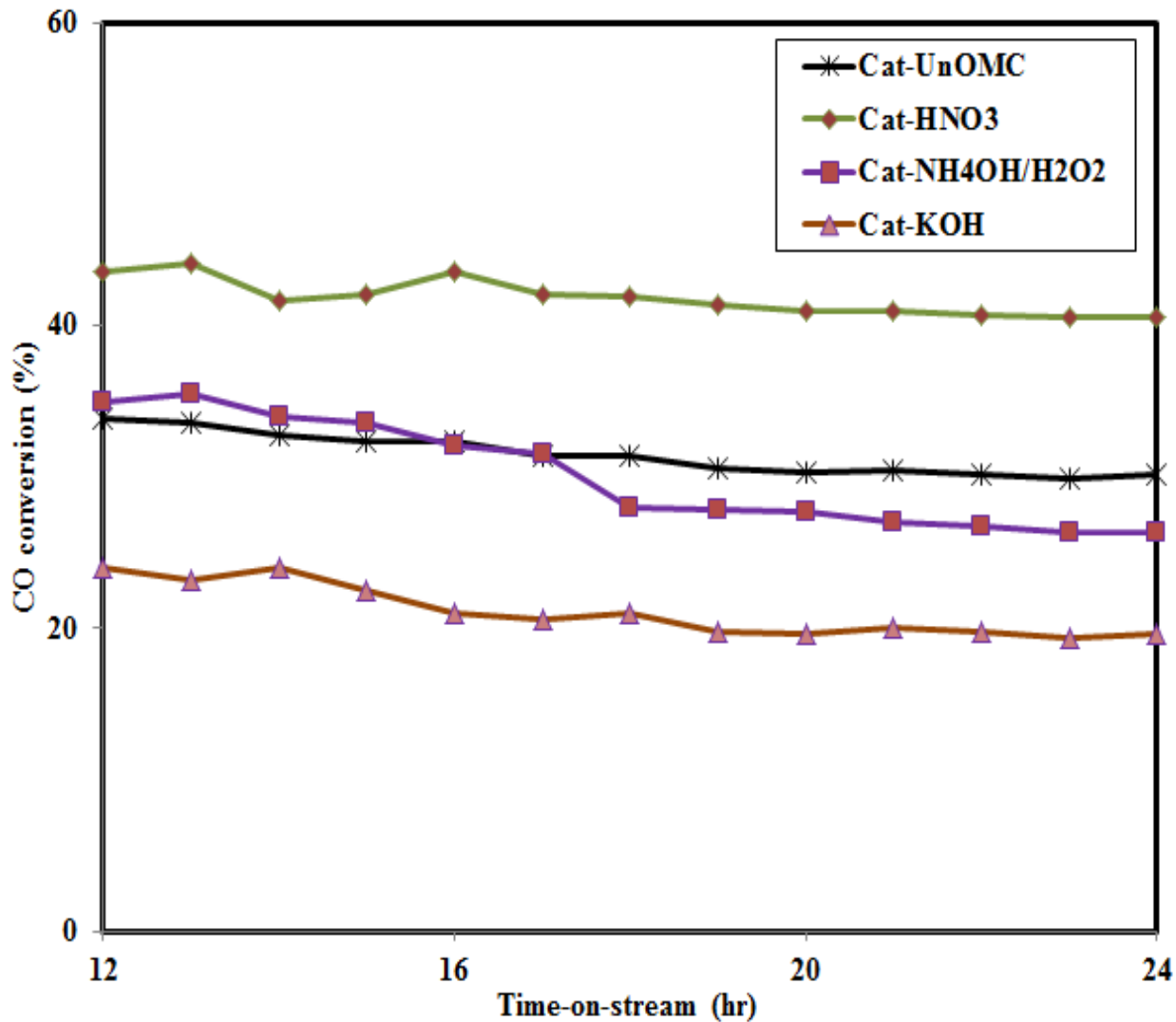


Fig. 6.9: CO conversion as a function of time-on-stream for treated and untreated supported catalysts ($P=8.3$ MPa; $T=330^{\circ}\text{C}$; Catalyst=2g; $\text{GHSV}=3.6$ m³ (STP)/h-kg_{cat}; $\text{H}_2:\text{CO}=1.25$).

Moreover, the higher surface area of Cat-HNO₃ may have greatly enhanced the uniform distribution of the dispersed metal species as confirmed by XRD analysis. Furthermore, the less desirable textural properties of Cat-KOH may be responsible for its rather reduced catalytic activity as compared to its counterparts.

6.5.2. Effects of chemical treatment on alcohol products distribution

The prepared oxide form of the KCoRhMo-supported catalysts were evaluated using a high-pressure fixed-bed downward flow reactor system for catalysts screening so as to ascertain their catalytic performance in the HAS reaction. The syngas of molar composition of 50%H₂:40%CO:10%Ar was used as the feedstock. Typical reaction conditions evaluated include pressure, temperature, and GHSV of 8.3 MPa, 300-340°C, and 3.6 m³ (STP)/kg_{cat}.h, respectively.

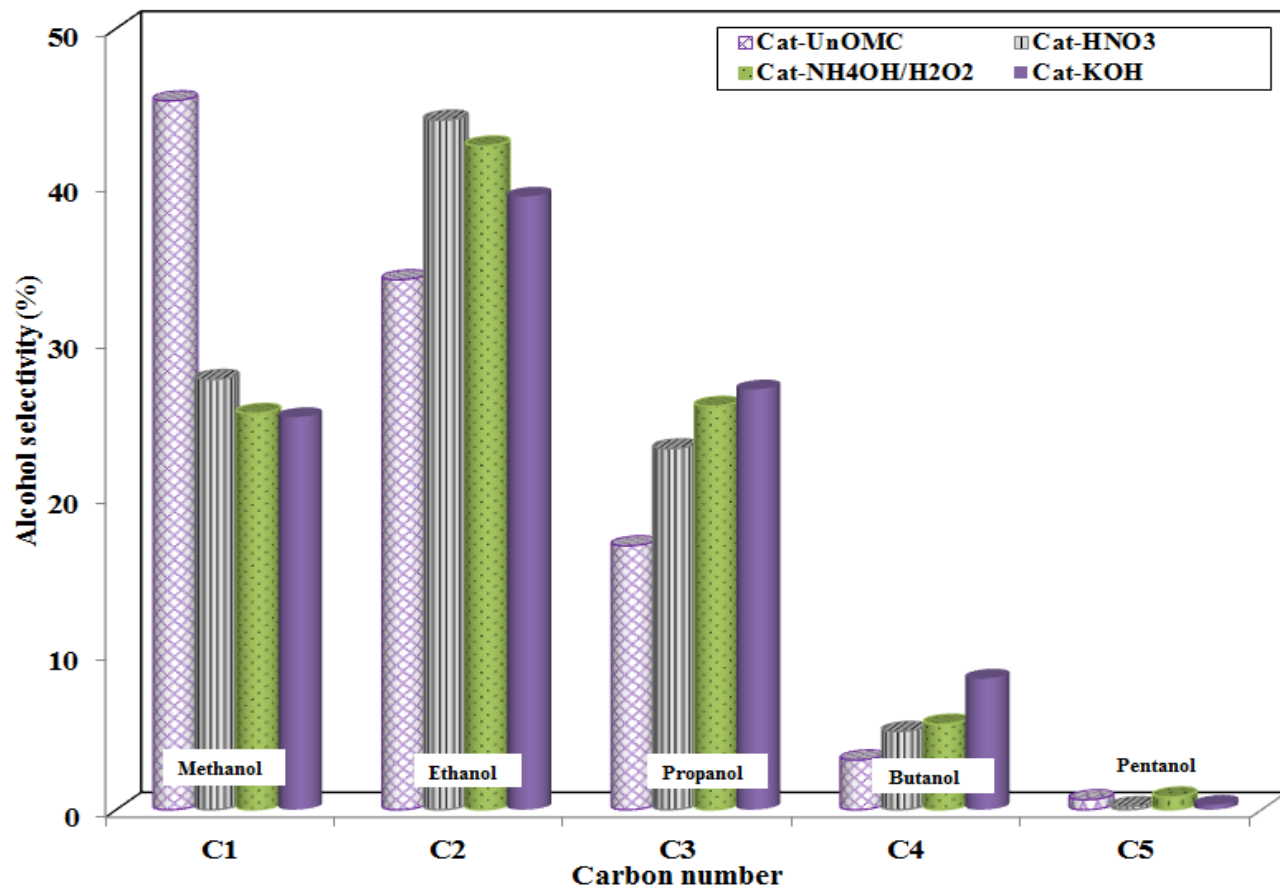


Fig. 6.10: Alcohol composition as a function of carbon number (P=8.3 MPa; T=330°C; Catalyst=2g; GHSV=3.6 m³ (STP)/h·kg_{cat}; H₂:CO =1.25).

Prior to the onset of the higher alcohol synthesis reaction, an initial catalyst activation step was necessary in order to ensure the phase conversion of the rather less active oxide catalytic

species into a more active sulfidic form. This was achieved by subjecting catalysts to an initial sulfidation/reduction step using a sulfiding gas mixture of 10% H₂S/H₂ molar compositions (Boahene et al., 2014). With the intended metals loading maintained constant for all four catalyst formulations, the influence of chemical pretreatment of the supports on the higher alcohols productivity was investigated. The extent of alcohol products distribution is crucial and depends on the nature of supports (treated or untreated) employed for the HAS reaction, since treatment of the support directly influences its surface chemistry; thus, affecting interaction of catalyst nanoparticles with the support and their capabilities of facilitating the dispersion of active metal species in the support matrix. In this regard, the influence of supports pretreatment on alcohol products distribution has been presented in Fig 6.10. It is quite obvious that alcohol products stream generated by all OMC-supported KCoRhMo catalysts constituted mostly of linear alcohols with carbon numbers in the range of C₁ to C₅. All the supported catalyst systems enhanced the production of these alcohols, mostly C₂ alcohols, with selectivities of 44.1, 42.8, & 35.1% for Cat-HNO₃, Cat-NH₄OH/H₂O₂ and Cat-KOH, respectively. However, for the untreated-supported catalyst (Cat-UnOMC), methanol was the predominant alcohol formed, with selectivity of about 49.2%.

Products selectivities for the gaseous and liquid streams of the CO hydrogenation reaction are summarized for all catalysts investigated and are presented in Table 6.3. As can be seen, Cat-UnOMC and Cat-KOH tend to produce more CO₂; suggesting their higher activity for the water-gas-shift reaction. Thus, from Fig. 6.10 and Table 6.3, it becomes quite conclusive that all the supported KCoRhMoS₂ catalysts investigated for higher alcohol productivity turned out to have high selectivity towards the production of higher alcohols, with ethanol being the most

predominant higher alcohol product in the final liquid product stream with the by-products comprising mainly CO₂ and light hydrocarbons (methane and ethane).

Table 6.3: Products selectivities for OMC-supported KCoRhMo catalysts at T=330°C

Catalyst	Product Selectivities (%)							
	Alcohol product selectivities (%)						Main by-products	
	C ₁	C ₂	C ₃	C ₄	C ₅	Total alc.	Hydrocarbons	CO ₂
Cat-UnOMC	37.0	26.3	10.0	1.9	0.3	75.5	10.9	13.4
Cat-HNO ₃	19.7	36.8	22.5	4.4	0.2	83.6	4.6	6.5
Cat-NH ₄ OH/H ₂ O ₂	17.4	15.8	17.3	2.7	0.5	66.8	7.6	9.7
Cat-KOH	15.4	14.8	15.9	2.1	0.2	52.5	12.4	22.3

6.5.3. Effects of temperature on alcohol products distribution

Temperature control is a crucial parameter that plays a significant role in all chemical reactions including CO hydrogenation reactions. Due to the exothermic nature of the HAS reaction, CO conversion and hence alcohol productivity during the reaction becomes quite temperature-dependent. That notwithstanding, it should be noted that excessively high operating temperatures may lead to rapid loss of activity and shortening of catalyst life due to an accelerated catalyst deactivation by sintering of nanocrystallite metal particles into larger less active phases (Speight, 2000) Moreover, there also exists a high tendency of enhancing side reactions such as methanation reaction, leading to coke formation, which is mostly favored at high temperatures (Subramani et al., 2008).

In Fig. 6.11, alcohol productivity as a function of temperature for the four catalysts studied is presented. As can be seen from this figure, apart from Cat-HNO₃ which showed total alcohol produced at a slightly higher temperature (330°C), all the other catalysts evidenced total alcohols produced at low temperature (300°C).

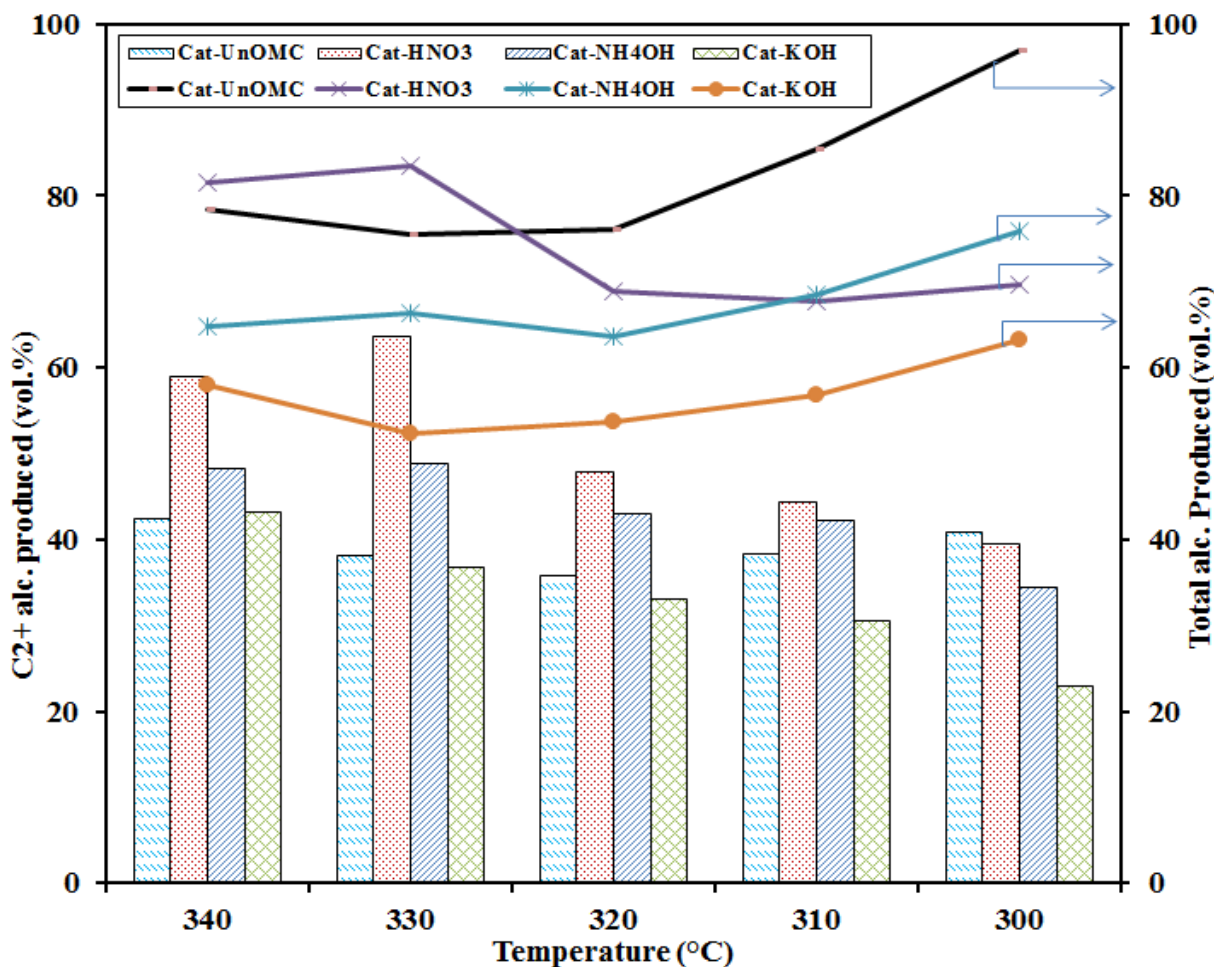


Fig. 6.11: Alcohol production as a function of temperature (P=8.3 MPa; T=300-340°C; Catalyst=2g; GHSV=3.6 m³ (STP)/h·kg_{cat}; H₂:CO = 1.25).

As temperature increased from 300 to 320°C, all catalysts showed a decline in total alcohol productivity, which then stabilized for Cat-UnOMC and Cat-NH₄OH/H₂O₂ as temperature further increased from 320 to 340°C. Alcohol productivity continued to decline for Cat-KOH with a temperature rise of 10°C in the first segment (320 to 330°C) and then increased slightly in the final

segment (330 to 340°C). On the other hand, increasing temperature slightly increased alcohol productivity for Cat-HNO₃, which eventually became stable as temperature further increased from 330 to 340°C. Furthermore, apart from Cat-UnOMC that showed a marginally higher C₂₊ alcohol productivity at 300°C, Cat-HNO₃ appears to dominate C₂₊ alcohol productivity at all temperatures, with maximum alcohol productivity recorded at 330°C.

At this temperature, the trend of C₂₊ alcohols produced followed the order: Cat-HNO₃ (63.7) > Cat-NH₄OH/H₂O₂ (48.9) > Cat-UnOMC (38.2) > Cat-KOH (36.8). Quite interestingly, the untreated pristine supported catalyst showed better alcohol productivity at all levels of temperature studied as compared to its KOH treated counterpart, suggesting that for the OMC support the kind of chemical oxidative treatment is not always advantageous and might adversely affect catalyst activity. Nonetheless, for all catalysts evaluated at the various temperatures, the main by-products observed for the CO hydrogenation reactions included carbon dioxide and hydrocarbons (mainly methane and ethane). These by-products tend to be more favorable at higher temperatures for these KCoRhMo catalysts studied.

6.5.4. Alcohol products distribution and the ASF Plots

The term higher alcohols (C₂₊OH) is used to describe alcohols with carbon numbers greater than 1; thus, total alcohols constitutes a combination of C₁, C₂ as well as all C₂₊ alcohols put together. In the formation of C₂₊ alcohols over Mo-based catalyst, a generally accepted mechanism is the CO insertion (Santiesteban et al., 1988; Subramani et al., 2008), in which syngas reactant species (CO and H₂) associatively or dissociatively adsorb onto the catalyst's active sites; yielding adsorbed formyl (HC=O) and alkyl (CH_x) species. Consequently, hydrogenation of the former species can proceed to produce methanol (CH₃OH) via reaction of adsorbed H species with the carbonyl group. Conversely, the insertion of adsorbed CO into the surface alkyl bond can also

occur to yield adsorb acetyl species (COCH_x), which can further undergo hydrogenation to form ethanol (C₂H₅OH). Furthermore, this chain propagation mechanism can continue with the insertion of CO into surface alkyl species of high carbon numbers and their subsequent hydrogenation to yield corresponding high carbon number alcohols (Schulz, 1999; Song-bai et al., 2011). During this chain surface polymerization HAS reaction, the selectivities of various alcohols can be depicted from the chain-growth probability (α) and carbon number (n) by the well-known Anderson-Shultz-Flory (ASF) model, represented as (Dry, 1982; Spivey et al., 2007).

$$\ln W_n = n \ln \alpha + \ln \frac{(1 - \alpha)^2}{\alpha} \dots \dots \dots (6.1)$$

where W_n is the weight percent of a product containing n carbon atoms and α is the chain growth probability. The higher the value of α , the longer the alcohol carbon chain length becomes (Dry, 1982).

Figure 6.12 depicts the ASF plots for the OMC-supported KCoRhMo catalysts investigated for the HAS reaction. Similarly, Fig. 6.13 compares these plots for the various treatments and their respective alcohol products distribution for all catalyst. It can be seen that alcohols products distribution for the various carbon numbers is consistent with the linear trend predicted by the ASF model; however, a deviation can be observed in the formation of methanol and pentanol for all catalysts as evidenced by the cluster of outliers as shown in Fig 6.13. Evaluation of the chain-growth probability from the slopes of the linear ASF plots (Fig. 6.12) yielded α values following the order: Cat-HNO₃ (0.26) > Cat-NH₄OH/H₂O₂ (0.22) \approx Cat-UnOMC (0.22) > Cat-KOH (0.19);

indicative of the fact that the classical CO insertion phenomenon might have governed the mechanism of HAS reaction over all the catalysts studied.

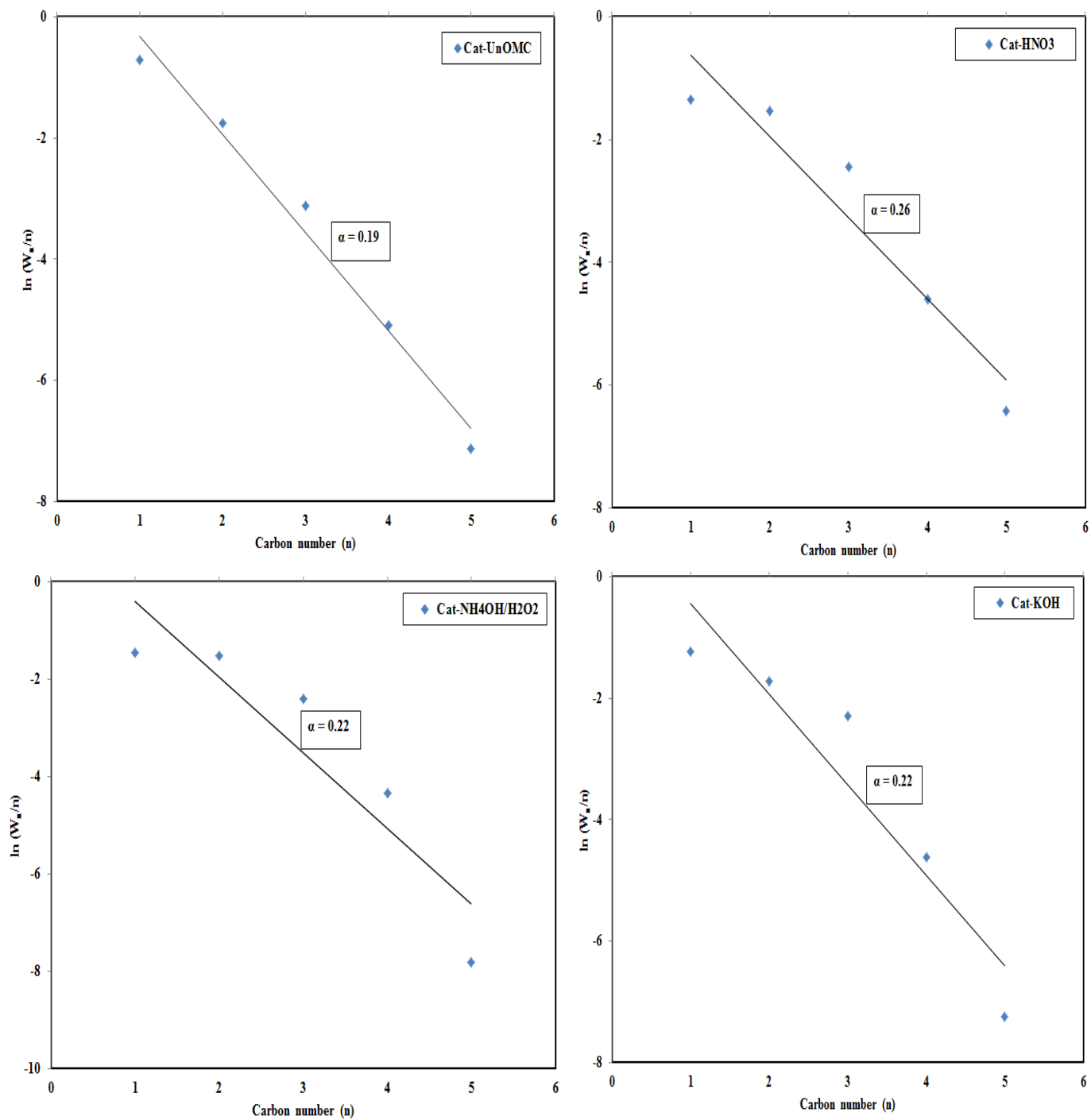


Fig. 6.12: ASF plots for OMC-supported KCoRhMo catalyst: (a) Cat-UnOMC; (b) Cat-HNO₃; (c) Cat-NH₄OH/H₂O₂; and (d) Cat-KOH

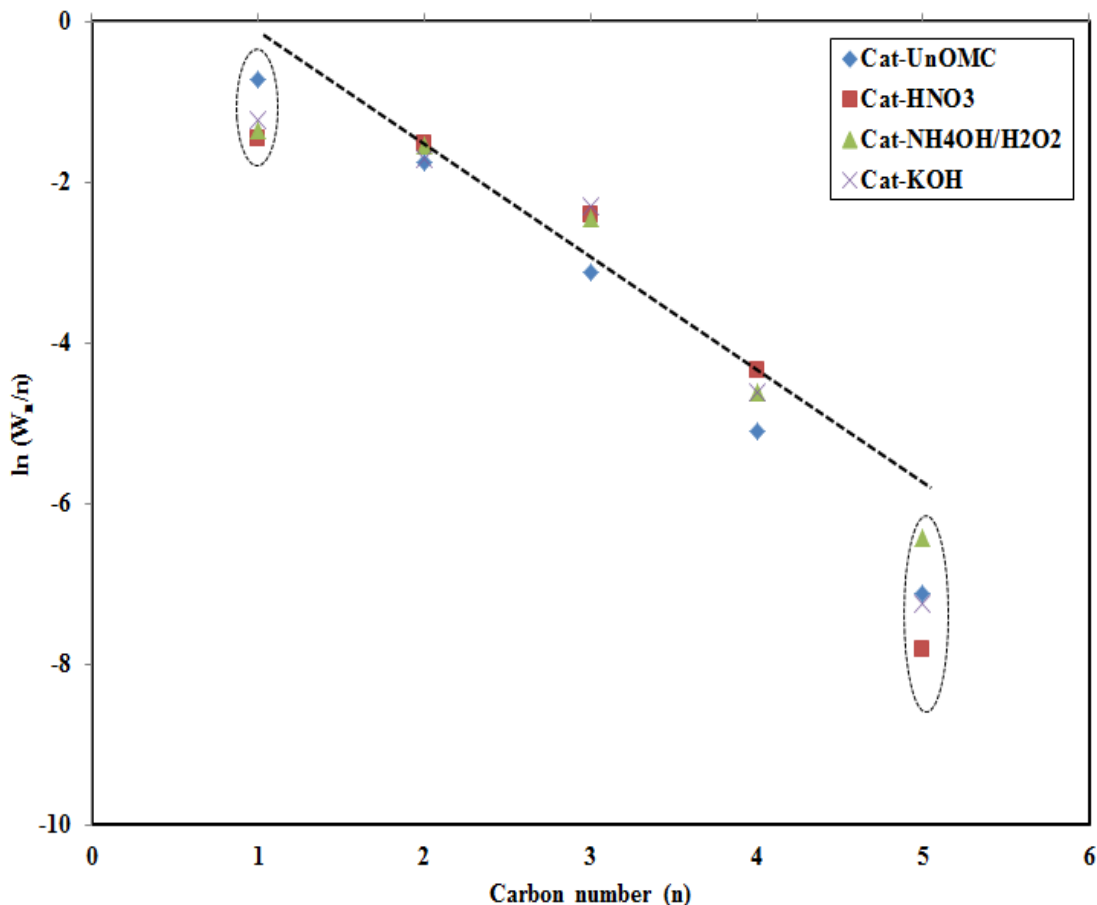


Fig. 6.13: ASF plots comparing alcohol products distribution for all catalyst (untreated and chemically treated).

Moreover, it appears the chemically treated catalysts showed a stronger CO insertion phenomenon as compared to its untreated counterpart (Cat-UnOMC) due to the higher chain-growth probability of C₂ to C₄ over former catalysts (0.22-0.26) as opposed to the latter (0.19). The α -values obtained for both alcohols and HCs were within the range of 0.2 to 0.3; which could be due to the short chain of alcohols (C₁-C₅) and hydrocarbons (C₁-C₃) obtained.

6.6. Conclusions

In summary, large pore diameter OMC supports were synthesized by the soft-templating approach, chemically treated in acidic or basic medium, and employed in the formulation of K-

doped CoRhMoS₂ catalysts for HAS applications. The wet chemical oxidation treatment modified the surface chemistry of the ordered mesoporous carbon materials and introduced oxygen-containing functional groups on the carbon frameworks, which can be used for metals anchorage via covalent bonding. At similar metals loading, BET analysis of all catalysts evidenced significant structural mesoporosity and orderliness since the physical properties of the materials were not compromised; however, a lesser pore blockage was observed in Cat-HNO₃ as confirmed by the NS_{BET} computations. Moreover, at similar metals loadings of 9%K, 4.5%Co, 15%Mo and 1.5wt.% Rh, XRD analysis evidenced a better metal nanoparticles dispersion on Cat-HNO₃ since less crystalline peaks were detected as confirmed by the TEM images. Chemical treatment of OMC support with nitric acid caused more defective sites with lower metals reducibility temperature as compared to its NH₄OH/H₂O₂ and KOH counterparts as confirmed by Raman and TPR analyses; thus, its superior catalytic performance for the HAS reaction. Nonetheless, all the chemically treated OMC-supported catalysts exhibited high activities toward the production of alcohols, especially ethanol. Quite interestingly, the untreated pristine supported catalyst showed better total alcohol productivity at all levels of temperature studied as compared to its KOH treated counterpart, suggesting that for the OMC support the kind of chemical oxidative treatment is not always advantageous and might adversely affect catalyst activity. At the optimum temperature 330°C, linear alcohols were produced and followed the ASF distribution; with the trend of C₂₊ alcohols selectivities following the order: Cat-HNO₃ (63.7) > Cat-NH₄OH/H₂O₂ (48.9) > Cat-UnOMC (38.2) > Cat-KOH (36.8). The results of this study elucidate the crucial role of chemical oxidation as a preconditioning step prior to carbon-supported catalysts preparation and their application for chemical reactions.

CHAPTER 7

Syngas conversion to higher alcohols: Application of novel K-promoted CoRhMo catalysts supported over carbon nanohorns and its by-products.

The contents of the manuscript provided in this chapter is similar to the one published in the Journal: Int. J. Petrochem. Sci. Eng.

Citation:

Boahene P.E., Sammynaiken R., Dalai A.K. (2017) Syngas Conversion to Higher Alcohols: Application of novel K-promoted CoRhMo Catalysts Supported over Carbon Nanohorns and its by-products. Int. J. Petrochem. Sci. Eng. 2(1), 2017, 00023. DOI: [10.15406/ipcse.2016.02.00023](https://doi.org/10.15406/ipcse.2016.02.00023)

Contribution of the Ph.D. Candidate

Experimental runs, development of the catalysts as well as their extensive characterizations and catalytic studies were performed by Philip Effah Boahene. Data collection, analysis and interpretations were performed by Philip Boahene with assistance from Drs. Ramaswami Sammynaiken and Ajay Kumar Dalai. All of the writing of the submitted manuscript was done by Philip Effah Boahene and discussed with Drs. Sammynaiken and Dalai. Dr. Dalai provided editorial guidance regarding the style and content of this research work.

Contribution of this chapter to overall study

Though MWCNT and OMC have proven tendencies to produce alcohols, in our present research, it was observed that carbon in the form of carbon nanohorns (CNH) can be a superior

catalyst supports for syngas conversion applications. Single-wall carbon nanohorn (SWCNH) is one of the most attractive new forms of nanocarbons as discovered by Ijima et al., 1999. Despite the fact that this novel porous carbon material (CNH) has recently attracted significant importance in the field of heterogeneous catalysis, it was gathered from our literature review that no work has yet been reported on CO hydrogenation reaction over these supports for higher alcohols synthesis, though, the CNH-supported NiMo catalysts proved successful in the hydrogenation of petroleum feedstock in hydrotreating reactions (Aryee et al., 2014). Thus, in chapter 7, the potential catalytic applications of CNH and its by-products (OCP_f and OCP) supports for higher alcohols synthesis via syngas conversion was explored.

7.1. Abstract

The submerged arc discharge in liquid nitrogen technique was used to synthesize carbon nanohorns (CNHs) using 90A and 34V; generating other carbon by-products at the high temperature (>4000°K) plasma zone, herein depicted as: “other carbon particles” (OCP) and “other fine carbon particles” (OCP_f). In the present work, a series of potassium-promoted CoRhMo catalysts with compositions 9%K, 4.5%Co, 1.5%Rh, and 15wt.% Mo, respectively, was supported over these carbon nanomaterials (CNH, OCP_f, and OCP) and characterized by BET, FTIR, RAMAN, TGA, H₂-TPR, XRD, and TEM. 30wt.% HNO₃ treatment at T=110°C under reflux conditions for 30 minutes enhanced the overall textural properties of the pristine supports and preserved their mesoporosity evidenced by the Type IV isotherms with surface area increments in the order: CNH (89 to 499) > OCP_f (34 to 82) > OCP (10 to 19 m²/g). The functionalized supports evidenced the presence of carboxylic acid (-COOH) groups with the most defective sites exhibited by CNHs as revealed by the I_D/I_G ratios ascertained by Raman spectroscopy. All three KCoRhMo-supported catalysts prepared were thermally stable up to 400°C (CNH) and 650°C (OCP_f and

OCP), and metals reducibility characterized by H₂-TPR analysis followed the trend: CNH > OCP_f > OCP. Powder XRD revealed inhomogeneous particles dispersion on the OCP-supported catalyst as compared to its CNH & OCP_f counterparts as corroborated by the TEM analyses; probably due to significant changes in textural properties. The extensive characterization of these catalysts provided insights into their characteristic catalytic performances for the conversion of syngas to higher alcohols conducted at temperatures, pressure, GHSV, and H₂/CO ratio of 300-340°C, 8.3 MPa, GHSV=3600 mL_(STP)/h.g_{cat}, and 1.25, respectively. CO conversion evaluated under stable reaction conditions at 340°C recorded a maximum of 52% for the CNH-supported KCoRhMo catalysts as opposed to 38% and 25%, respectively, for its OCP_f and OCP counterparts.

7.2. Introduction

Gasoline blends with up to 10% ethanol (E10) and higher alcohols are commercially available at gasoline pump stations in the USA, Canada, and some parts of Europe (Nylund et al., 2008; National Resources Canada, 2016). The production of these alcohols (C₂ and C₂₊) promises immense potential to replace other additives utilized as octane boosters in automotive fuels. In our previous investigation of large-pore ordered mesoporous carbon (OMC)-supported KCoRhMo catalyst and their application for the HAS reaction, it was observed that though the products selectivities was fairly comparable to its MWCNT counterpart at similar metal loadings, XRD analysis of the former catalysts evidenced better homogeneous species dispersion on former support. This observation was attributed to the enhanced textural properties of the OMC-supported catalyst, which exhibited comparative catalytic performance as its MWCNT counterpart at higher metal loadings (Boahene et al., 2016).

Though MWCNT and OMC have proven tendencies to produce alcohols, our present research has observed that carbon in the form of carbon nanohorns (CNH) can be a superior

catalyst supports for syngas conversion applications. Single-wall carbon nanohorn (SWCNH) is one of the most attractive new forms of nanocarbons. These carbon nanoparticles were discovered by Ijima and coworker in 1999 and constitutes a form of single-walled carbon nanostructures with graphitic tubes and cone-shaped caps, forming a cone angle of 20° at one end and individual SWCNH particles typically aggregating to form a spherical structure with diameters of 50-90 nm (Ijima et al., 1999). Properties, such as high surface area, high thermal stability, high purity, and conductive graphitic structures provide CNHs with specific properties that enable numerous potential applications, such as adsorbents, molecular sieves catalyst supports, among others (Bekyarova et al., 2005; Urita et al., 2006; Utsumi et al., 2006).

This family of carbon nanohorns and its byproducts synthesized by the novel submerged arc in liquid nitrogen technique were investigated as potential catalyst supports due to their diverse porous structure, resistance to acidic and basic environments, easy accessibility to their internal surface area, easy modification of their surface chemistry among other advantages. Despite the fact that this novel porous carbon material (CNH) has recently attracted significant importance in the field of heterogeneous catalysis, to the best of our knowledge, no work has yet been reported on CO hydrogenation reaction over these supports for higher alcohols synthesis. That notwithstanding, CNH-supported NiMo catalysts proved successful in the hydrogenation of petroleum feedstock in hydrotreating reactions (Aryee et al., 2014). Thus, the motivation of this phase of the work (presented in this chapter) was to explore the potential catalytic applications of CNH and its by-products (OCP_f and OCP) supports for higher alcohols synthesis via syngas conversion in a laboratory fixed bed reactor under industrial conditions and evaluate its performance with the known MWCNT counterpart at similar metals loading.

7.3. Experimental

The syntheses of pristine supports namely; CNH, OCP_f and OCP were accomplished using the submerged arc discharge in liquid nitrogen technique at a fixed current of 90A and 34V. The detailed description of the techniques employed to separate these carbon nanoparticles after syntheses, as well as their corresponding KCoRhMo catalysts formulations can be found in Chapter 3, section 3.2.2, 3.2.3 and 3.2.4 of thesis. Furthermore, characterization techniques employed as well as the CO hydrogenation experimental procedures have also been discussed in Chapter 3.

7.4. Results and discussion

7.4.1. N₂-adsorption/desorption measurement

Measurements of textural properties of the supports and catalysts were conducted by the nitrogen adsorption/desorption technique performed at liquid nitrogen temperature of -196°C. Figure 7.1A shows the isotherms of the three pristine supports (CNH, OCP_f and OCP) as well as their respective HNO₃-treated counterparts. Similar isotherms are displayed for the corresponding supported catalysts as depicted in Fig. 7.1B. The existence of textural mesoporosity is clearly observable from the profiles of the pristine and HNO₃ treated supports, as well as their respective supported KCoRhMo catalysts. The type IV isotherms with H1 hysteresis loop was confirmed and can be observed in all catalysts, corroborating the evidence of textural mesoporosity in the final catalysts, which is crucial for catalytic reactions (Murata et al., 2000; Khodakov et al., 2001). It is clear from Fig. 7.1B that the isotherms exhibited by all catalysts showed a slight change in the shape of the hysteresis loops of the supports (Fig 7.1A) as a result of metals loading.

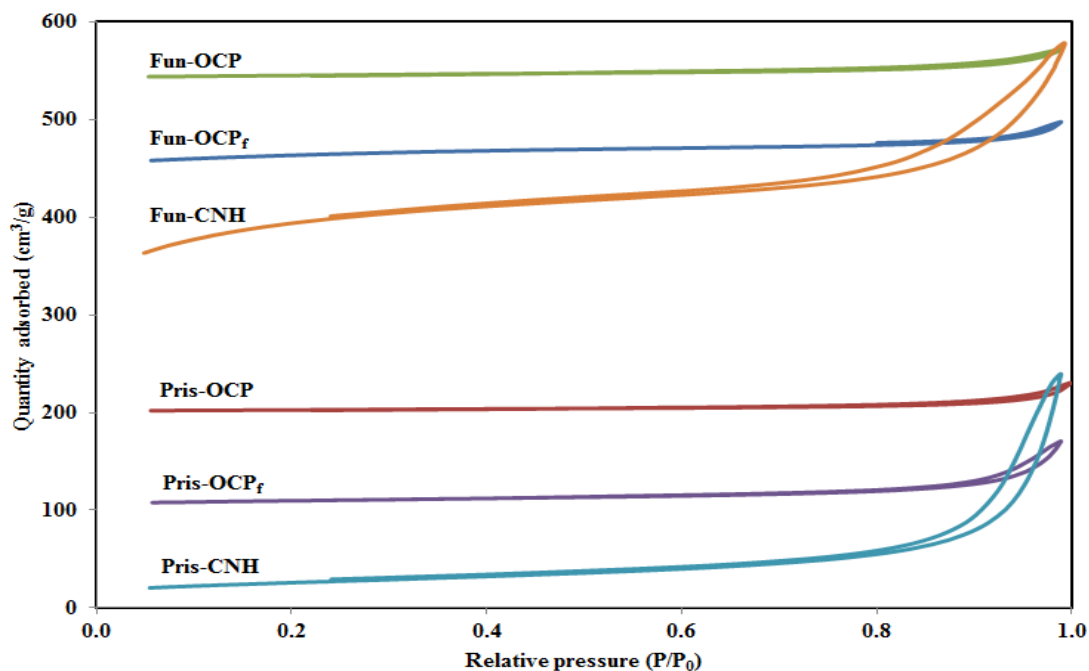


Fig. 7.1 (A): N₂-adsorption isotherms of pristine CNH, OCP_f & OCP supports as well as their functionalized forms.

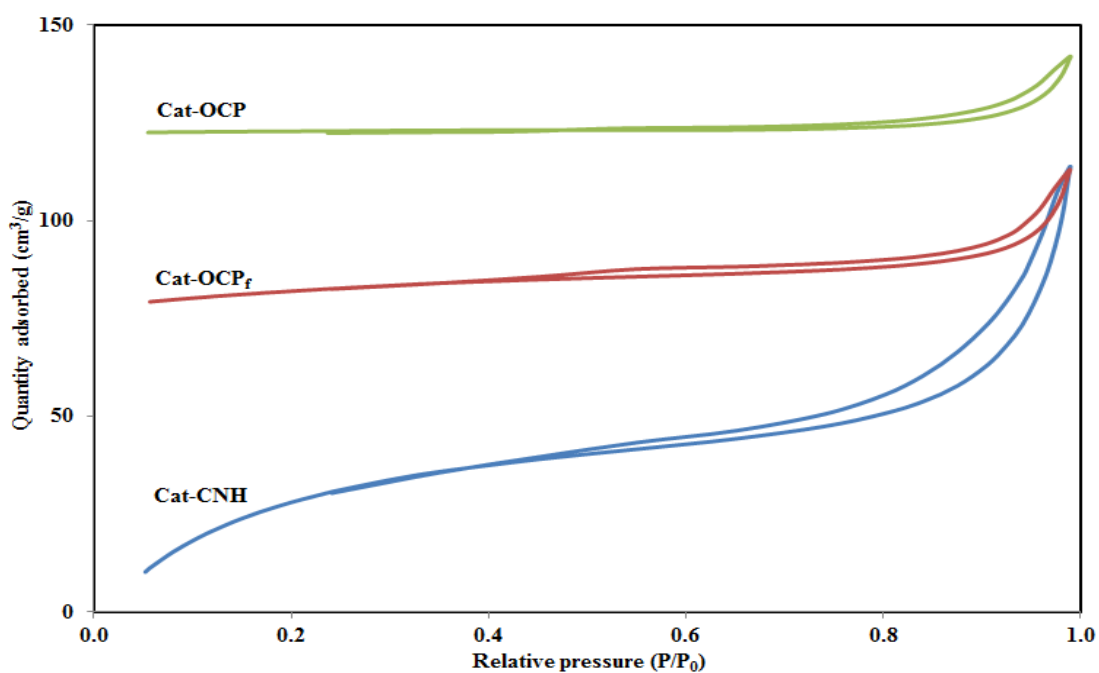


Fig. 7.1 (B): N₂-adsorption isotherms of CNH, OCP_f & OCP-supported KCoMoRh catalysts

This indicates that all supported catalysts exhibited uniform textural porosity, which is also in agreement with XRD results. It is known in heterogeneous catalytic reactions that reactants predominantly react on the surface of the catalyst; giving an indication of the important role structural porosity of the catalyst plays in controlling mass transfer processes via species diffusion in such reactions.

Table 7.1 gives a summary of the textural properties of the pristine CNH, OCP_f, OCP supports and their respective functionalized forms as well as the supported KCoRhMo catalysts.

Table 7.1: Textural properties of CNH, OCP_f, OCP supports & supported KCoRhMo catalysts

Sample ID	BET Analysis			NS _{BET}
	SSA	PV	BJH _{ads}	
	(m ² /g)	(cm ³ /g)	(nm)	
<u>SUPPORTS</u>				
Pris-CNH	89	0.34	18.5	-
Pris-OCP _f	34	0.10	14.6	-
Pris-OCP	10	0.03	13.9	-
Fun-CNH	499	0.49	9.5	-
Fun-OCP _f	82	0.11	6.7	-
Fun-OCP	19	0.05	9.2	-
<u>CATALYSTS</u>				
Cat-CNH	322	0.27	8.6	0.92
Cat-OCP _f	42	0.06	9.3	0.74
Cat-OCP	9	0.03	8.9	0.70

It is worth mentioning that HNO₃ pre-treatment of pristine carbon materials such as MWCNTs resulted in the opening of the closed ends and caps of the pristine material and also significantly improved its textural properties (Sigurdson, 2010). Similarly, for the CNH and its byproducts studied, nitric acid treatments of the pristine supports resulted in increase in surface area and pore volume. Wang et al., 2004 observed increased surface areas of their SWCNH material following an oxidization treatment by heating in air at 200°C for several hours. The observed increment in surface area was attributed to the incorporation of openings in individual nanohorns that enhance the creation of reactive adsorption sites (Wang et al., 2004). A similar phenomenon may have occurred during the HNO₃ treatments of the pristine carbon materials in our case. However, a decrease in pore diameters of the functionalized supports as observed in Table 7.1 can be attributed to the probable narrowing of the average internal pore diameter of the carbon materials due to the accumulation of various oxygen containing functional groups occupying the interior surfaces within the supports.

The CNH functionalized support (Fun-CNH) showed the highest surface area, pore volume as well as pore diameter, while the OCP functionalized support (Fun-OCP) recorded the least values of the parameters. This suggests that significant etching effect occurred in the pristine CNH material as compared to its OCP_f and OCP counterparts. The corresponding catalysts resulting from similar metals loading (9%K, 4.5%Co, 1.5%Rh, and 15%Mo) on the respective functionalized supports showed decrease in surface area and pore volumes, following the order: Cat-CNH > Cat-OCP_f > Cat-OCP; however, changes in the pore diameter of the catalysts did not follow a particular trend. The monotonic reduction in textural properties (specific surface area and pore volume) of the supports as a result of metal (Co, Rh, Mo) precursors loading was expected. Nonetheless, the decrease in specific surface area as a result of co-impregnation of Co, Mo, and

Rh metal precursors on the supports also significantly influenced the homogeneity of dispersed metal species on the surface of the supports, as corroborated by the X-ray powder diffraction analysis (Boahene et al., 2014; Boahene et al., 2016).

Furthermore, one can deduce from the computed NS_{BET} values that Cat-OCP suffered the most pore blockage as compared to Cats-CNH and OCP_f ; suggesting that while the introduction of the oxidic metal nanoparticles caused a minimal reduction in pore volume for the CNH and OCP_f catalysts (probably due to their higher surface areas), the Cat-OCP experienced quite a high reduction in pore volume. Moreover, these results also give an indication that impregnation of metal species on a catalyst support plays a vital role in the overall catalytic surface area required for a given chemical reaction and affected differently the porosity as well as the overall textural properties of the final catalysts investigated. Thus, the activity and alcohol products selectivities could be affected by the available surface areas of the respective catalysts during the surface-catalyzed HAS reaction.

7.4.2. Wide-angle X-ray diffraction

X-ray diffraction (XRD) patterns of the pristine CNH as well as the KCoRhMo catalysts samples supported on the functionalized CNH, OCP_f , and OCP supports were recorded for 2θ values in the range of $10-80^\circ$ and are shown in Fig. 7.2. The sharp peak at two theta degree of approximately 26° can be observed for Cat-CNH and is representative of a graphite (002) framework (Aryee et al., 2014). The existence of two other graphitic broad peaks were also confirmed at two theta degrees of 42° (100) and 44° (101). The presence of graphite is attributed to the single-layer graphitic wall which encompasses CNHs.

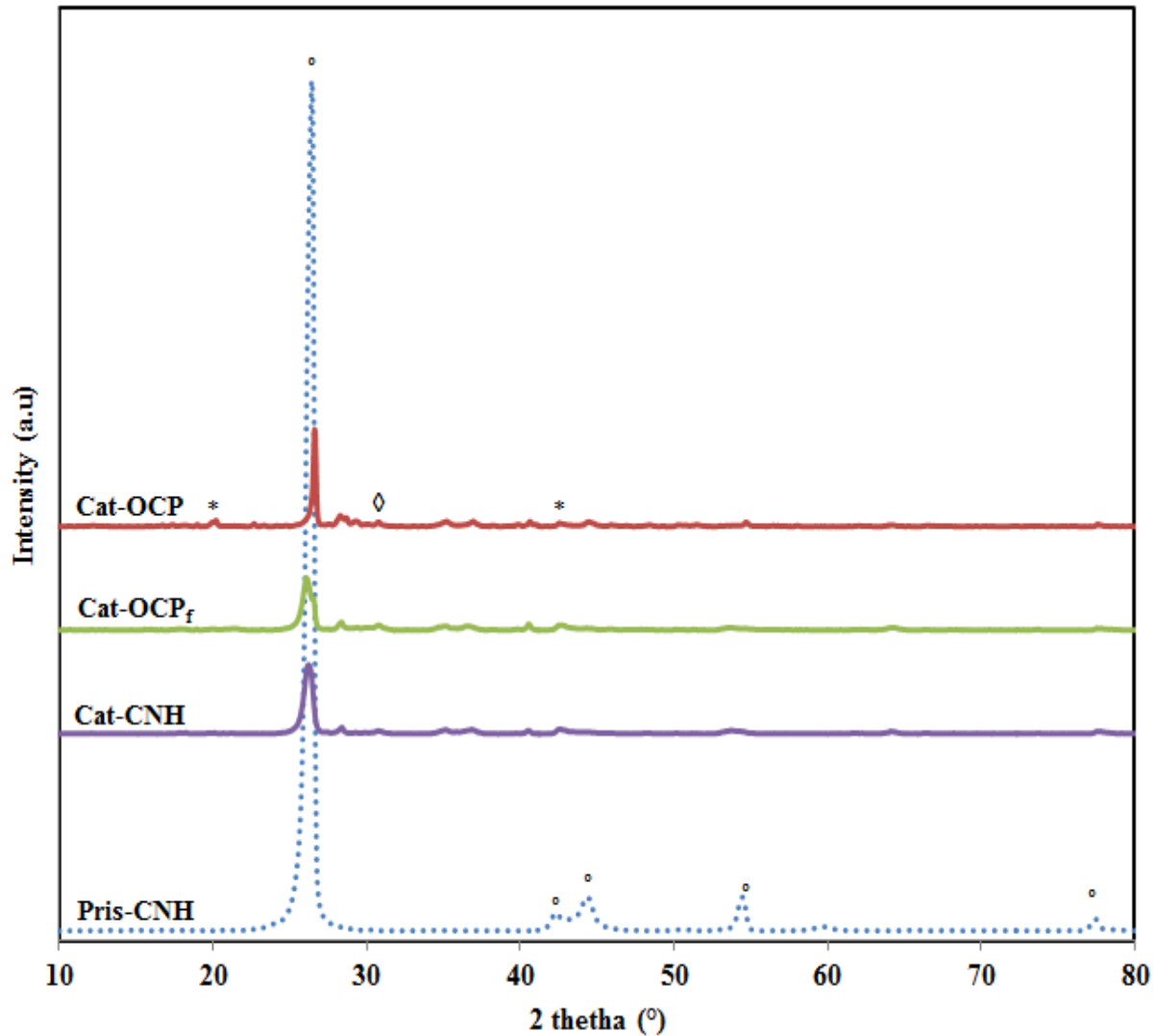


Fig. 7.2: XRD profiles for CNH, OCP_f & OCP-supported KCoRhMo catalysts

This feature was present in all samples, suggesting that all three samples have remnants of CNH present in them. Similarly, peaks occurring at 2θ of 20.5, 30.4, 36.8 and 40.6° can be attributed to the crystalline MoO₃. These crystalline phases were less on the CNH-supported catalyst, giving an indication of the uniform dispersion of nanoparticles on this support. This could be explained due to the relatively lower surface area (19 m²/g) of Cat-OCP as opposed to 499 and 82 m²/g for Cats-CNH and OCP_f, respectively. It is noteworthy that a catalyst support with more

desirable textural properties would better enhance the stabilization the active species and promoters as well as play a vital role to modify the dispersion, reducibility, and electron-donating or accepting effects of metal nanoparticles (Hindermann et al., 1983).

Consequently, the relatively higher surface area of the Fun-CNH support may have played a significant role by enhancing great dispersion of catalytic phases as confirmed by the XRD profile for its corresponding catalyst. Also, the peaks occurring at 2θ values of 26.2, 28.3 and 34.8 can be assigned to the presence of $K_2Mo_2O_7$ species in the samples (Surisetty et al., 2009; Boahene et al., 2014). The average MoO_3 crystallite size from the full width at half maximum (FWHM) diffraction profile computed by the Debye-Scherrer's equation ($L=0.9\lambda/\beta\cos\theta$) for both Cats-CNH and OCP_f , showed MoO_3 crystallite size in the range 6-10 nm as opposed to 16 nm for the Cat-OCP catalyst; giving an indication that there must have been metal species agglomeration on the latter catalyst due to its lower specific surface area. Nonetheless, all these particle sizes quite favored the higher alcohols synthesis reaction, though a much lower extent for Cat-OCP. Moreover, it should be pointed out that these nanoparticles may experience significant phase changes as a result of time-on-stream during higher alcohol synthesis reaction under prevailing operation conditions.

7.4.3. Raman spectroscopic analysis

To effectively ascertain the slight changes occurring in the orientation of the carbon-carbon bonds as a result of an interaction of light with the carbon nanomaterials analyzed, the highly sensitive vibrational spectroscopic technique, Raman spectroscopy, was used. Raman spectroscopic analysis is a nondestructive technique and particularly well suited to detect small changes in structural morphology of carbon nanomaterials (Schwan et al., 2001).

Figures 7.3 (A & B) show the Raman profiles of both the pristine and functionalized supports as well as their corresponding KCoMoRh catalysts.

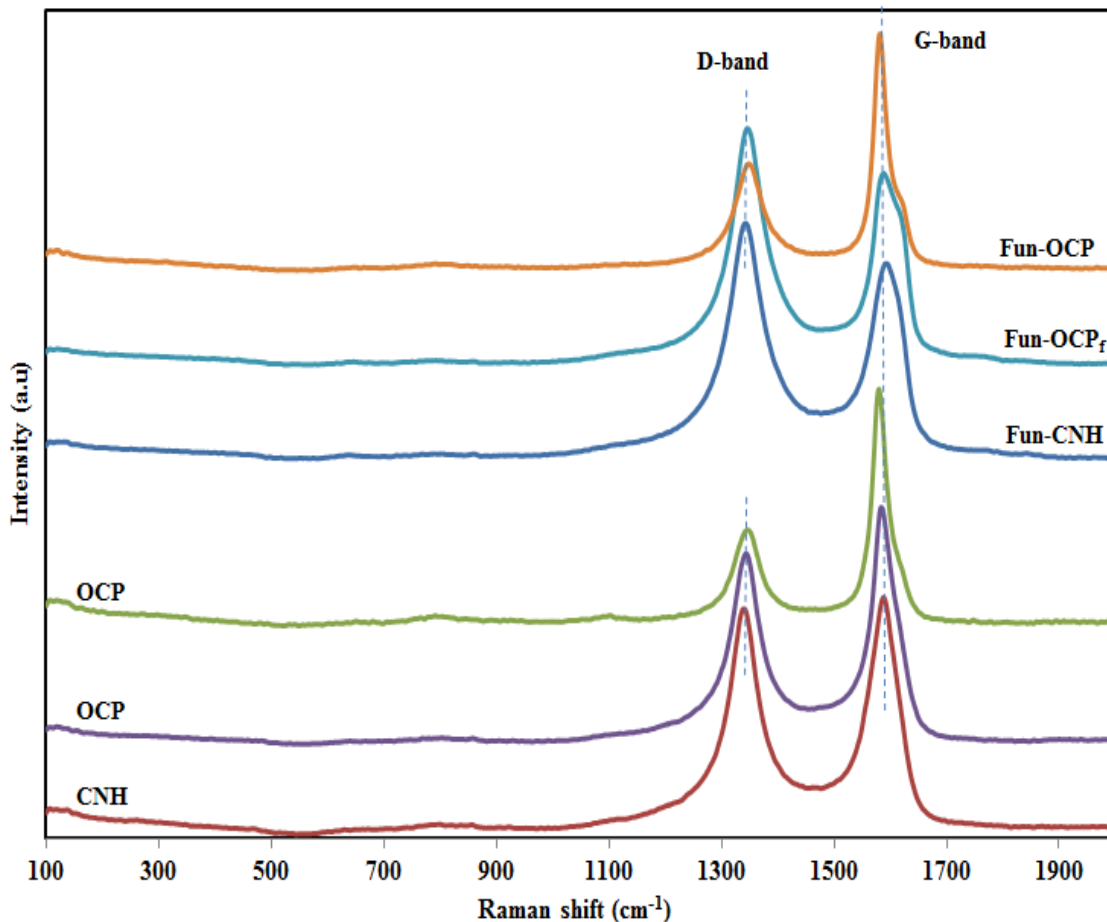


Fig. 7.3 (A): Raman spectra of pristine CNH, OCP_f & OCP as well as their functionalized supports.

From the Raman spectra, the two distinct peaks in the range of 1340-1350 cm⁻¹ and 1580-1595 cm⁻¹ observed can be attributed to the so called D- and G-bands, respectively (Wang et al., 2004; Aryee et al., 2014). The former is characteristic of the extent of disorderliness in the carbon matrix and the latter is due to the C-C stretching modes present in the material. While the G-band indicates the graphitic E_{2g} plane vibration, the D-band is due to the disordered parts such as grain boundaries, which is indicative of the A_{1g} plane (Shimodaira et al., 2002). It is known that the

intensity ratio of the D to G bands (I_D/I_G) is generally used to denote the extent of disorderliness present in the graphite layer of carbon material. The greater the value of this parameter, the more disordered the material becomes (Vinu et al., 2007).

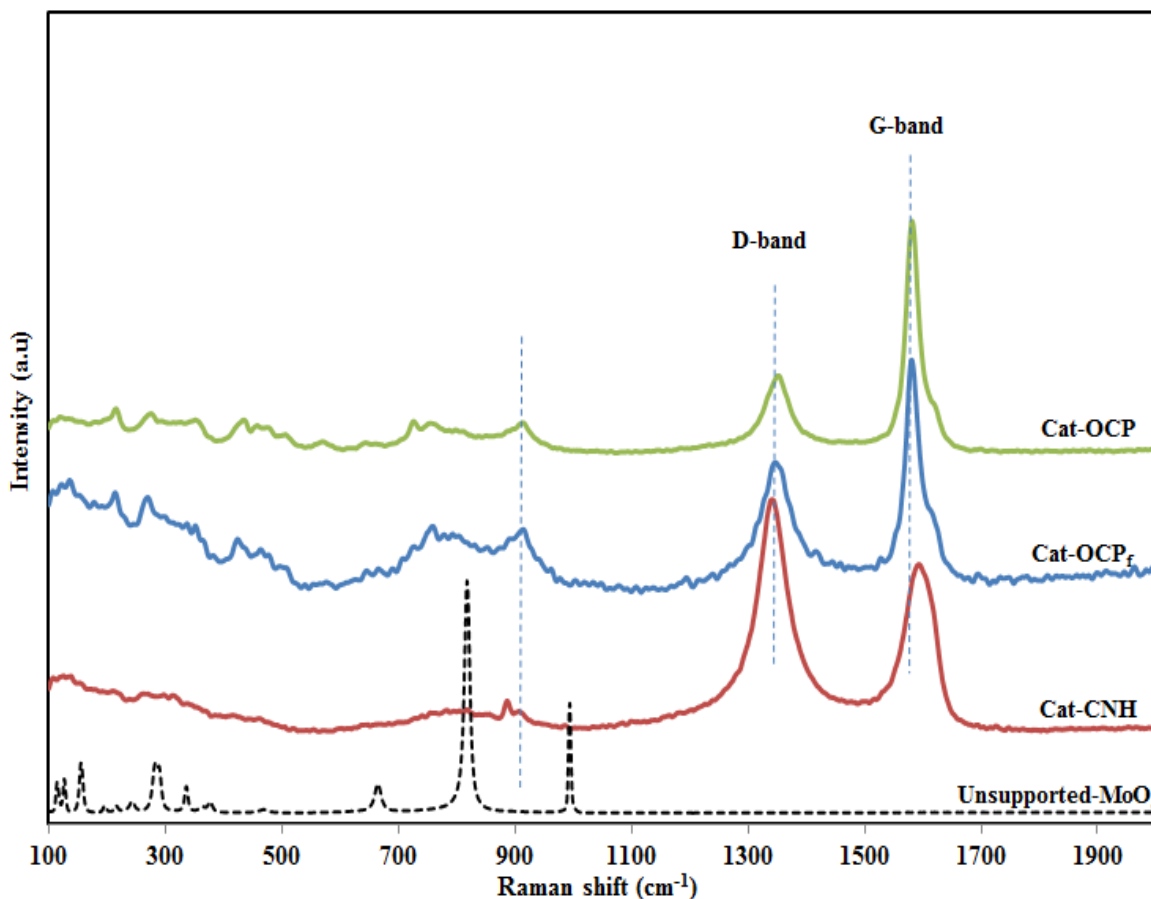


Fig. 7.3 (B): Raman spectra for CNH, OCP_f & OCP-supported KCoRhMo catalysts.

For the catalysts studied, it is clear from Fig 7.3B that the OCP-supported KCoRhMo catalyst exhibited the least I_D/I_G ratio, which is indicative of the existence of lesser defective sites for the HAS reaction as compared to the OCP and CNH-supported catalysts. The computed I_D/I_G ratios for the supported-catalysts followed the order: Cat-CNH (1.36) > Cat-OCP_f (0.74) > Cat-OCP (0.51), which corroborates the observed trend. Also, it can be noticed that for all catalysts samples studied, the linewidth of the G mode is narrower than that of the D band, confirming that

the G mode is related to the crystalline component in carbons (Haber et al., 1995). Moreover, the bandwidth of the D mode is clearly greater for the Cat-OCP as compared to Cats-CNH and OCP_f; giving an indication that of less ordering in the former samples than that of latter. It can also be noted from Fig. 7.3B that other peaks located at 261, 540, 789, 904, 967, and 1080 cm⁻¹ existed in the Raman spectra of the catalyst samples studied and can be attributed to metal-oxygen species formation, probably of the forms; O-Mo-O, K-Mo-O, and Co-Mo-O, bonds.

7.4.4. Fourier Transform Infra-red analysis

The surface functional groups present in all the carbon materials studied were analyzed by the FTIR technique and are shown in Figs. 7.4 (A & B). The spectra of functionalized samples as shown in Fig. 7.4A evidenced an additional –C=O band emerging at 1,719 cm⁻¹, which is attributed to the stretching vibration in carboxyl, ketones and aldehydes groups (Xiao et al., 2004; Teng et al., 2008). It is noteworthy to mention that these carboxylic groups can be generated due to the oxidation of some carbon atoms on the surface of the carbon supports (CNH, OCP_f & OCP) as a result of the HNO₃ pretreatment (Aryee et al., 2014; Boahene et al., 2014). The FTIR spectra also show a broad band centered at 3,450 cm⁻¹ which signifies phenolic O–H stretching vibrations (Aryee et al., 2014). The band at 1233 cm⁻¹ can be assigned to contributions from stretching C–O–C vibrations (in ether and lactone structures or other single bonded oxo-group, C–O–R). The presence of carboxylic acid groups on the surfaces of functionalized supports (CNH, OCP_f & OCP) is evidence of the introduction of oxygenated functional groups at the defect sites of the pristine materials. Furthermore, an additional prominent peak occurring at 1575 cm⁻¹ on the spectrum of Fun-CNH can be assigned to stretching vibrations (asymmetric and symmetric, respectively) of nitro group (NO₂), indicating the simultaneous occurrence of nitration reactions during the intended HNO₃ chemical oxidation treatment (Lazaro et al., 2007).

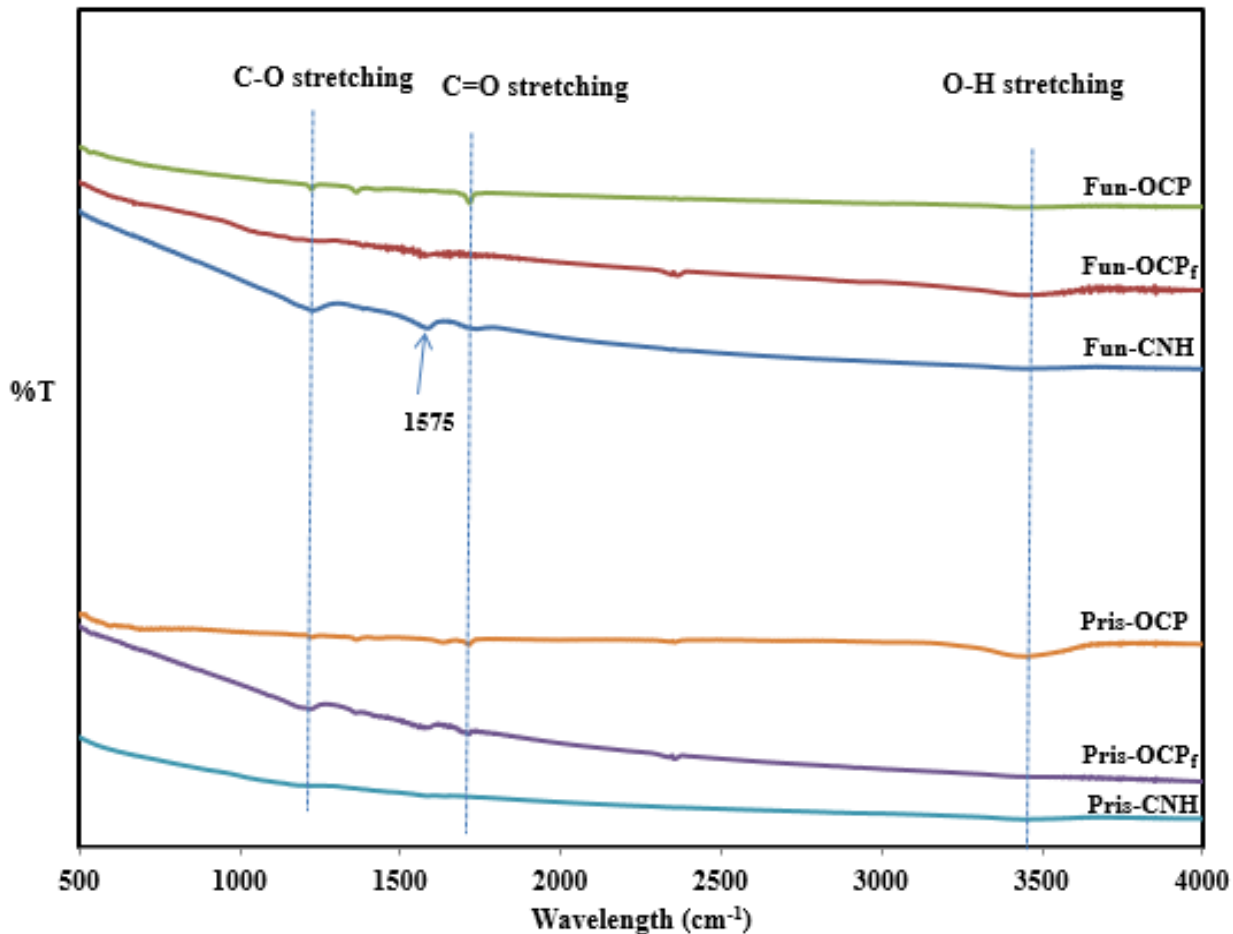


Fig. 7.4 (A): FTIR profiles of pristine CNH, OCP_f & OCP as well as their functionalized supports.

This peak was absent in the spectra of Fun-OCP_f and Fun-OCP supports; suggesting that the chemical composition of the carbon network in the CHN support undergoes a more considerable change during oxidation with nitric acid as compared to its OCP_f and OCP counterparts. This observation provides insight into the fact that for same functionalizing agent and under similar treatment conditions, the nature of carbon material will be impacted differently by the nitric acid treatment.

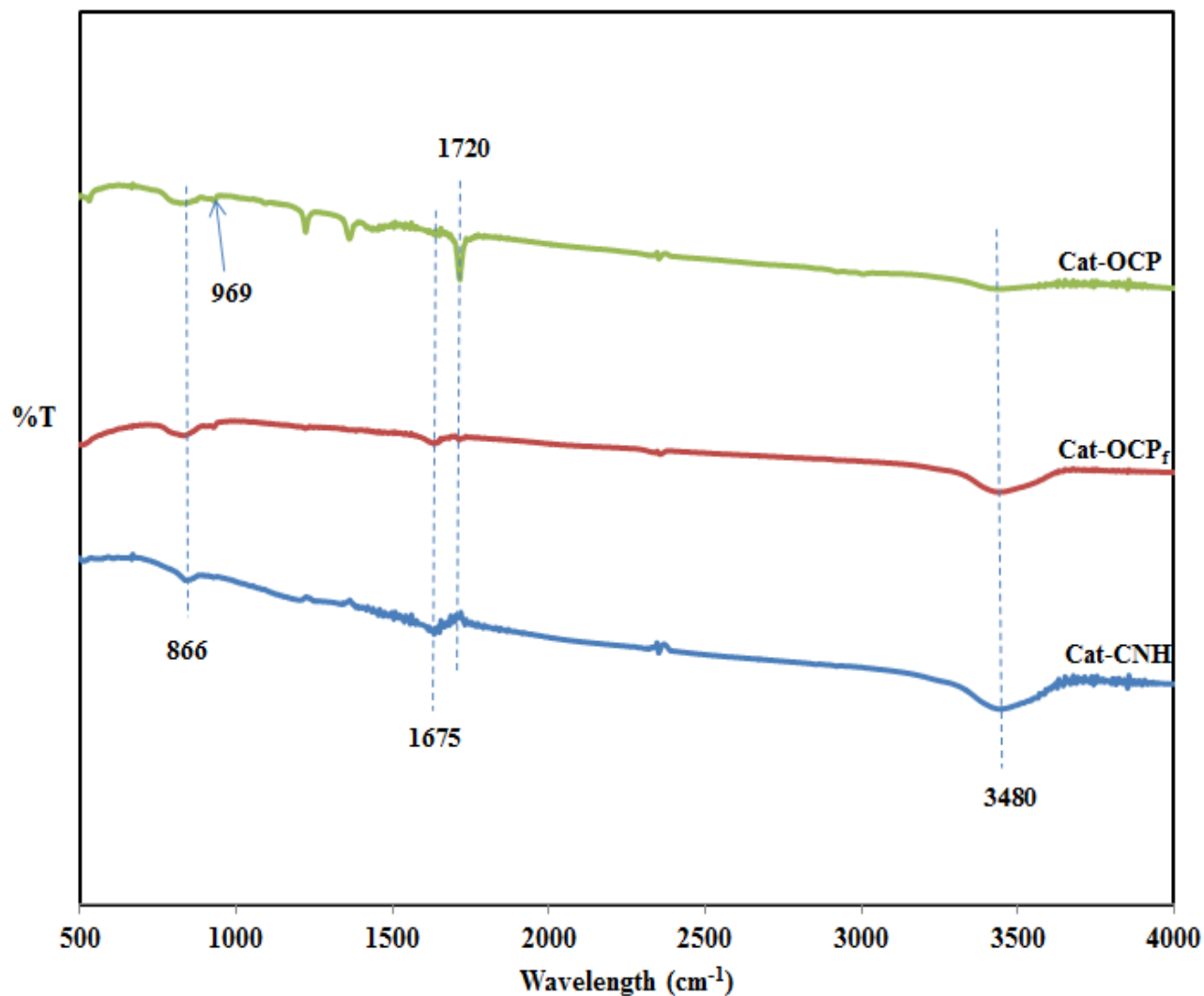


Fig. 7.4 (B): FTIR profiles for CNH, OCP_f & OCP-supported KCoRhMo catalysts.

From Figure 7.4B, it can be observed that most of the peaks disappeared due to their consumption in metal-oxygen bond formation, following metal precursor impregnation and subsequent calcination in N₂ atmosphere. All catalysts showed peaks at 866 and 969 cm⁻¹, which could be ascribed to out-of-plane deformation of C-H bonds (Lazaro et al., 2007; Bazula et al., 2008), possibly via the formation of metal species moiety. These metal-oxygen bands were absent in all pristine and functionalized supports.

7.4.5. Thermogravimetric Analysis

The thermogravimetric (TG) technique was used to determine the percent weight loss of the catalyst samples as a function of temperature so as to gain insight of the thermal stability of the carbon-supported KCoRhMo catalysts during the HAS reaction. Figure 7.5 shows the TGA profiles for the catalysts investigated. Typically, carbon-supported catalysts have the propensity to undergo significant weight loss during chemical reactions in the presence of temperature (Serp et al., 2015). This weight loss is commonly associated with the evolution of gaseous species, which can be quantifiable if the TGA setup used for analysis is equipped with mass spectrometer (MS). For instance, it has been reported that within the range of temperature for the TG analysis (150-700°C) for typical carbon materials, a significant amount of CO₂ (resulting from the decomposition of carboxyl groups) together with other compounds such as methane, butane and butanol (resulting from the decomposition of the carbon framework) have been observed in the MS traces (Bazula et al., 2008).

At low-temperature, CO₂ evolution may be the result of decomposition of carboxyl groups; however, at high-temperature, the decomposition of anhydride and lactone groups have been reported (Otake et al, 1993). Moreover, whereas CO₂ evolution mostly occurs below 500°C and CO evolution proceeding above this temperature, both physisorbed and chemisorbed water are mostly released in the range of 100–450°C (Teng et al., 1993; Cheng et al., 2003). However, in the present work, quantitative evaluation of the corresponding evolved gaseous species was not determined. Nonetheless, the corresponding % mass loss for the supported catalysts investigated in the temperature range of 200-500°C followed the trend: Cat-CNH (9.4%) > Cat-OCP_f (1.4%) > Cat-OCP (0.9%).

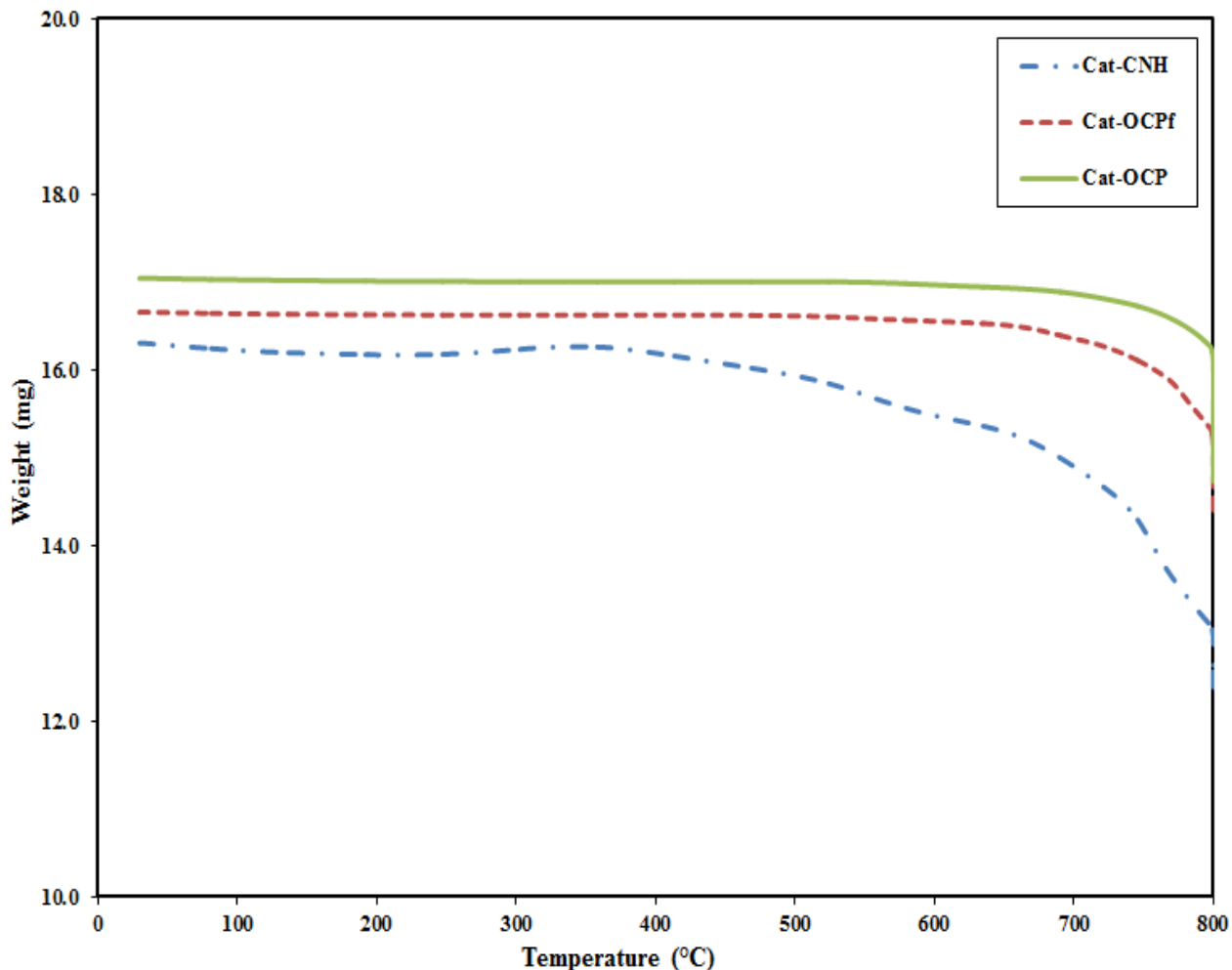


Fig. 7.5: TGA profiles for CNH, OCP_f & OCP-supported KCoRhMo catalysts

According to the observed trend, Cats-OCP_f and OCP exhibited better thermal stability properties as compared Cat-CNH; however, the latter catalyst would still survive the practical HAS reaction conditions since the actual HAS reaction does not go beyond 400°C. One could also deduce from the above trend and Figure 7.5 that significant weight loss as a function of temperature for the Cat-CNH suggests a form of decomposition of chemical species in this material as temperature gradually increased; resulting in the generation of their unique defective sites that favored the HAS reaction.

7.4.6. Temperature programmed reduction analysis

The reducibility of metal species in the catalysts was ascertained by the temperature programmed reduction (TPR) technique using hydrogen gas as the probe gas. As can be seen in the displayed H₂-TPR profiles in Fig. 7.6, all three KCoRhMo supported catalysts studied evidenced the typical two-step hydrogen consumption peaks associated with molybdenum-supported catalysts. The first step involved the reduction of octahedrally coordinated MoO₃ species (Mo⁶⁺) to its tetrahedral MoO₂ forms (Mo⁴⁺), which undergoes further reduction to lower oxidation state molybdate moieties in the second step at higher temperatures (Arnoldy et al., 1985; Surisetty et al., 2010).

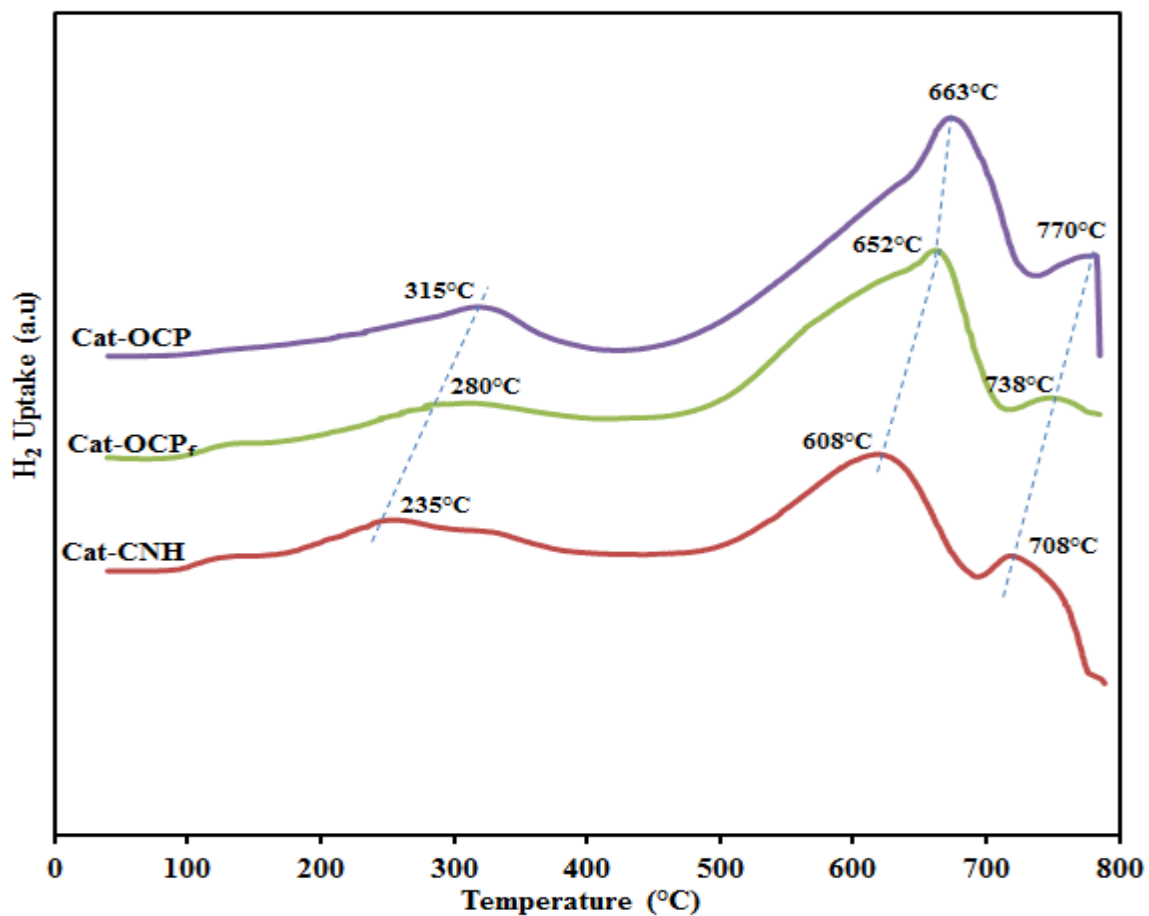


Fig. 7.6: TPR profiles for CNH, OCP_f & OCP-supported KCoRhMo catalysts

From the TPR profiles, four main peaks were observed to occur at 135°C, 235°C, 608°C and 708°C, respectively for Cat-CNH. The mid-range reduction temperature peak (235°C) is as a result of bulk MoO₃ species present in the oxidic catalyst undergoing reduction in the presence of hydrogen to generate its tetrahedrally coordinated forms (Mo⁴⁺), which are subsequently completely reduced to lower oxidation states. The absence of a peak occurring in the 340-360°C temperature range could also be noted; suggesting the sufficient reduction of bulk CoO₃ species in the catalyst, giving indication of the probable formation of the Co-Mo-O phase, which forms the active phase for the HAS reaction. This observation is consistent with a previous study conducted by Surisetty and coworkers on a similar catalyst matrix supported on both activated carbon and MWCNT (Surisetty et al., 2010). One could also observe a small peak appearing around the region of 135°C from the TPR profile of Cat-CNH; which could be attributed to the reduction of rhodium species (Rh⁺¹) to its metallic forms (Rh⁰). A similar observation has been reported in the literature (Murata et al., 2000). For the treated supported catalysts, similar peaks were observed to occur in the lower (<200°C), middle (200-400°C), and higher (>400°C) temperature ranges, corresponding to the stepwise reduction of various molybdate species present in the catalysts. However, the positions of these peaks varied significantly with the different carbon material used for the catalyst formulation. As compared to Cat-OCP, the occurrence of a reduction peaks around 135°C for the Cats-CNH and OCP_f suggests the complete reduction of Rh⁺¹ to Rh⁰ species in these samples (Surisetty et al., 2010).

Similarly, it could also be seen from Fig. 7.6 that the first step reduction: Mo⁶⁺ to Mo⁴⁺ occurred at 280 and 315°C for Cats-OCP_f and OCP, respectively, which is higher than that observed for Cat-CNH. That notwithstanding, it should be noted that Co₃O₄ species have the same reduction temperature so there exists the possibility that the H₂ consumption peak is an overlap

contribution of multiple peaks corresponding to the reduction of MoO_3 and Co_3O_4 species (Surisetty et al., 2010). Furthermore, in the case of reduction of Mo^{4+} species to lower oxidation state oxo-molybdate species occurring at higher reduction temperatures, the observed trend followed the order: Cat-CNH (608°C) < Cat-OCP_f (652°C) < Cat-OCP (663°C). This trend can be explained by the fact that Cat-CNH possesses the highest surface area as compared to its counterparts; thus, dispersed metal species can adequately interact with the support; thus improving their reducibility and subsequent dispersion in the catalyst matrix as corroborated by XRD analysis.

7.4.7. Transmission Electron Microscopic analysis

The TEM images of the pristine supports as well as the KCoRhMo catalysts were recorded and are presented in Fig. 7.7.

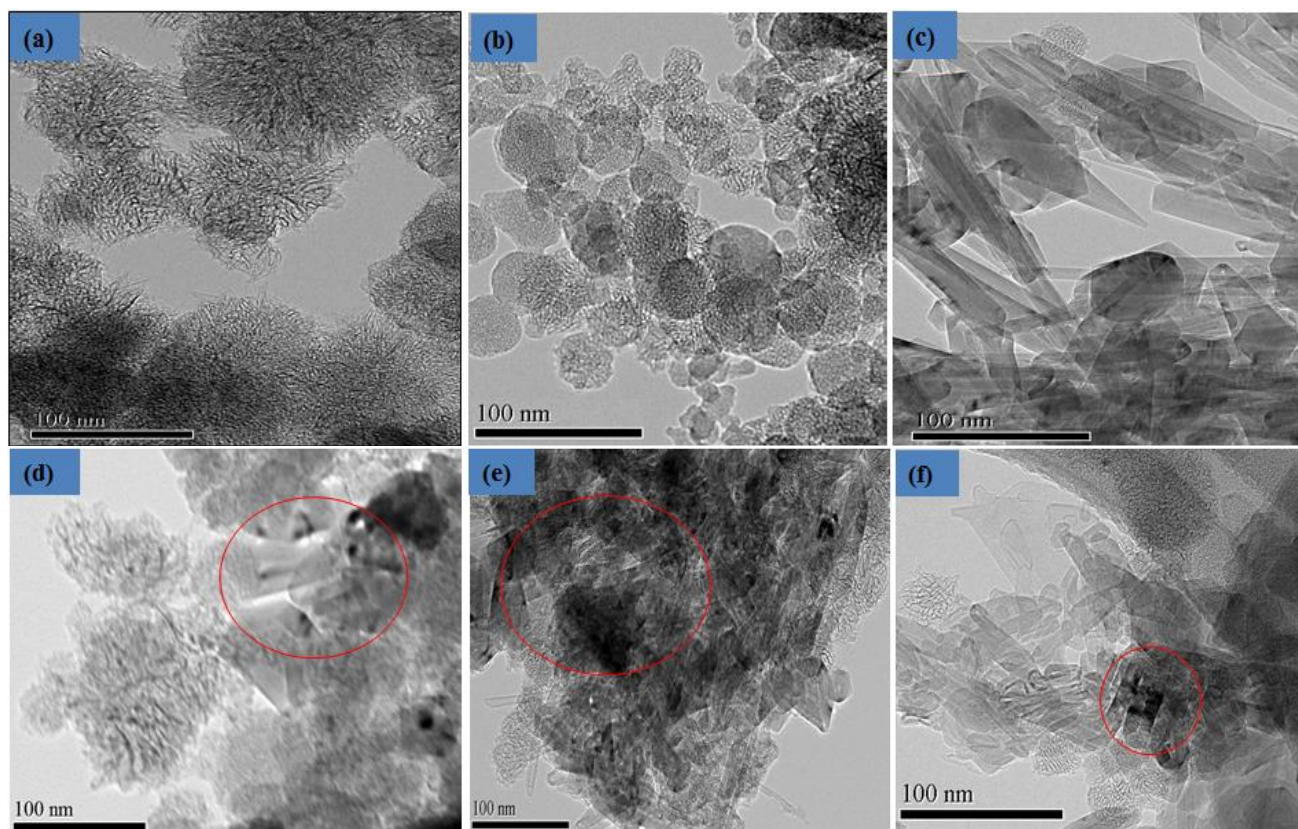


Fig. 7.7: TEM images of KCoRhMo catalysts supported on: d) CNH; e) OCP_f; and f) OCP

Common CNHs assemblies such as bud-like and dahlia-like CNHs were seen in the TEM images as shown in Figs. 7.7 (a-f). Aggregated CNHs sizes were within the range of 50-115 nm, which is consistent with published literature. It can also be observed from the TEM images of the pristine OCP and its supported catalyst (see Fig. 7.7 c & f) show a blend of CNH and other tube-like carbon morphologies. These were not observable in the CNH and OCP_f counterparts; thus, suggesting that the OCP material could be a mixture of CNH and CNT which are known to have similar morphologies. Though the presence of nano-windows generated on the CNHs as a result of acid treatment was not clearly visible from the TEM images due to weak resolutions, the enhancement of surface area and pore volume of these samples as well as the nature of their isotherms is enough evidence of the occurrence of nano-windows in these samples.

For the supported catalysts (Figs. 7.7d-f), the presence of dark particle spots (which were absent in the pristine samples) suggests the incorporation of catalyst metal precursors into the various carbon matrix. As can be seen in Fig. 7.7d, metal species were fairly dispersed following the co-impregnation step. However, not much homogeneous dispersion was observed for the OCP_f and OCP-supported catalysts, probably due to their reduced surface areas as compared to its CNH counterpart.

7.5. Catalytic Performance Tests of OMC-supported KCoMoRh Catalysts

The prepared catalyst samples were screened for their performance in the HAS reaction in a high-pressure fixed-bed micro reactor using syngas as feedstock under similar conditions of pressure, temperature, H₂:CO, and GHSV of 8.3 MPa, 300-340°C, 1.25, and 3.6 m³ (STP)/kg_{cat} h, respectively. The metals loading intended for the formulation of these catalyst samples were maintained the same to help study the influence of carbon (CNH, OCP_f and OCP)-supported KCoRhMo catalysts on higher alcohols productivity.

7.5.1. Effect of temperature on CO Conversion

Catalytic activities involving MoS₂-supported catalysts are mostly at their peak performance at the onset of reaction and gradually decline as a result of time-on-stream due to the well-known phenomenon of initial pre-coking (Sigurdson, 2010). Computation of the CO conversion was done for the catalysts following the attainment of stable catalytic activity, typically, after 18 h time-on-stream (Surisetty, 2010; Boahene et al., 2014; Boahene et al., 20016). As shown in Fig 7.8, CO conversion recorded for all the carbon-supported KCoRhMo catalysts increased as a function of temperature.

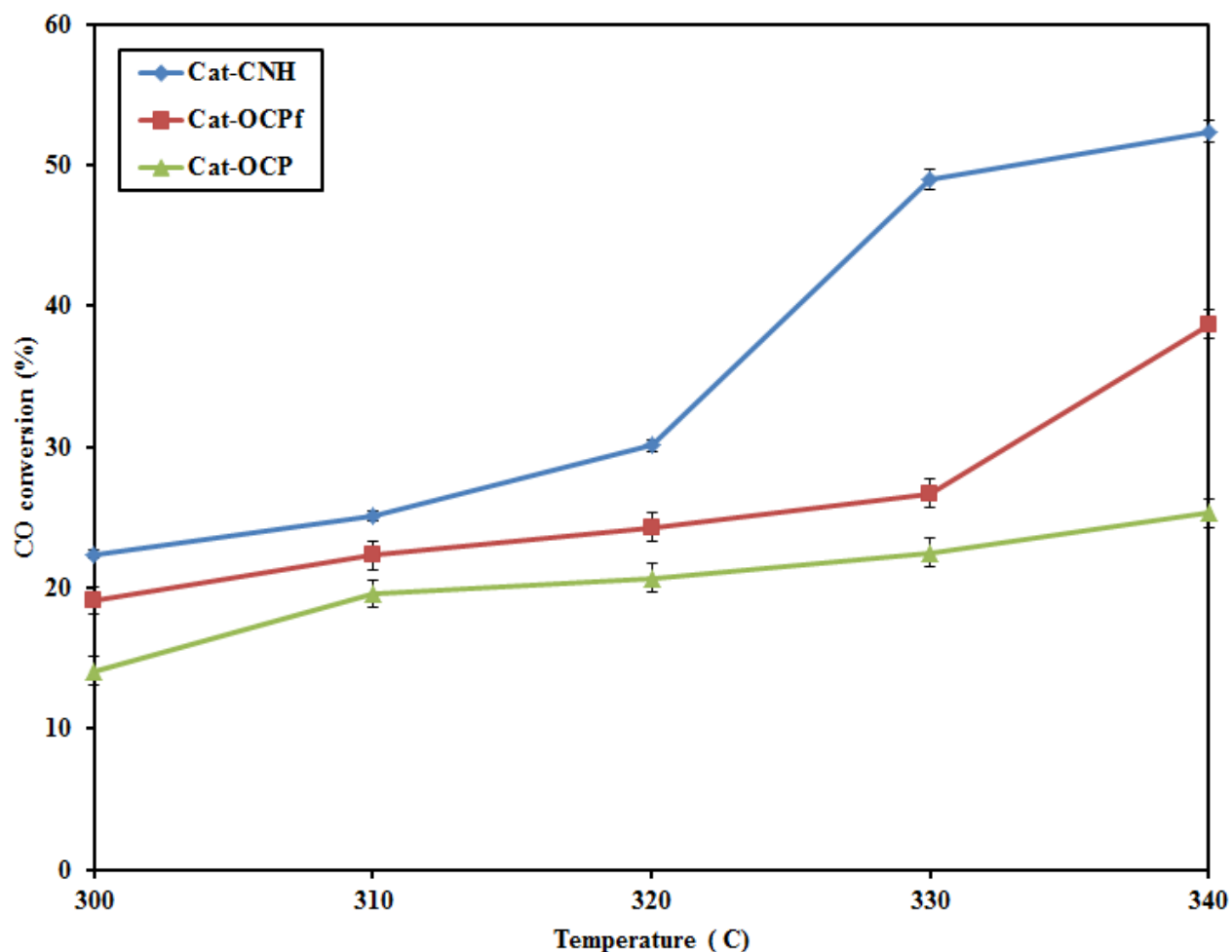


Fig. 7.8: CO conversion as a function of temperature for KCoMoRh-supported catalysts (P=8.3 MPa; T=300-340°C; Catalyst=2g; GHSV=3.6 m³ (STP)/h·kg_{cat}; H₂:CO=1.25).

It can be seen that increasing temperature from 330 to 340°C resulted in marginal increments in CO conversion. For the OCP-supported catalyst, CO conversion did not significantly increase with temperature from 310-340°C; however, the converse is this case for Cat-CNH. For the latter catalyst, increasing temperature from 320 to 330°C resulted in ~63% increment in CO conversion; giving an indication of the critical role temperature plays in the CO hydrogenation reaction. The recorded CO conversion at the highest temperature 340°C followed the trend: Cat-CNH (52.4%) > Cat-OCP_f (38.1%) > Cat-OCP (25.4%). The observed trend can be attributed to the superior textural properties of the CNH-supported catalyst as compared to its OCP_f and OCP counterparts. Moreover, the higher surface area of Cat-CNH may have greatly enhanced the uniform distribution of the dispersed metal species as confirmed by XRD analysis. Furthermore, the less desirable textural properties of Cat-OCP may be responsible for its rather reduced catalytic activity as compared to its counterparts.

7.5.2. Alcohol products distribution for CNH, OCP_f & OCP-supported catalysts

Catalytic performance of the oxidic form of the catalysts were evaluated in a high-pressure fixed-bed downward flow reactor system using syngas (molar composition: 50% H₂:40% CO:10% Ar) as the feedstock. Typical reaction conditions evaluated include pressure, temperature, and GHSV of 8.3 MPa, 300-340°C, and 3.6 m³ (STP)/kg_{cat}.h, respectively. An initial catalyst activation step was necessary prior to the onset of the HAS reaction to attain a more active sulfidic form of the catalyst. This was achieved by subjecting catalysts to an initial sulfidation/reduction step using a sulfiding gas mixture of 10% H₂S/H₂ molar compositions (Surisetty, 2010; Boahene et al., 2014; Boahene et al., 20016). With the intended metals loading maintained constant for all four catalyst formulations, the influence of the different carbon (CNH, OCP_f, and OCP) catalyst supports on the higher alcohols productivity was investigated.

The extent of alcohol products distribution is crucial and depends on the nature of supports employed for the HAS reaction, since the structure and morphology of the support would directly influence its porosity and the ease of modifying its surface chemistry via functionalization. This property of the supports can also affect its interaction with catalyst nanoparticles; thus, their capabilities of facilitating the dispersion of active metal species in the support matrix.

The alcohol composition as a function of carbon numbers for the supported catalysts has been presented in Fig. 7.9.

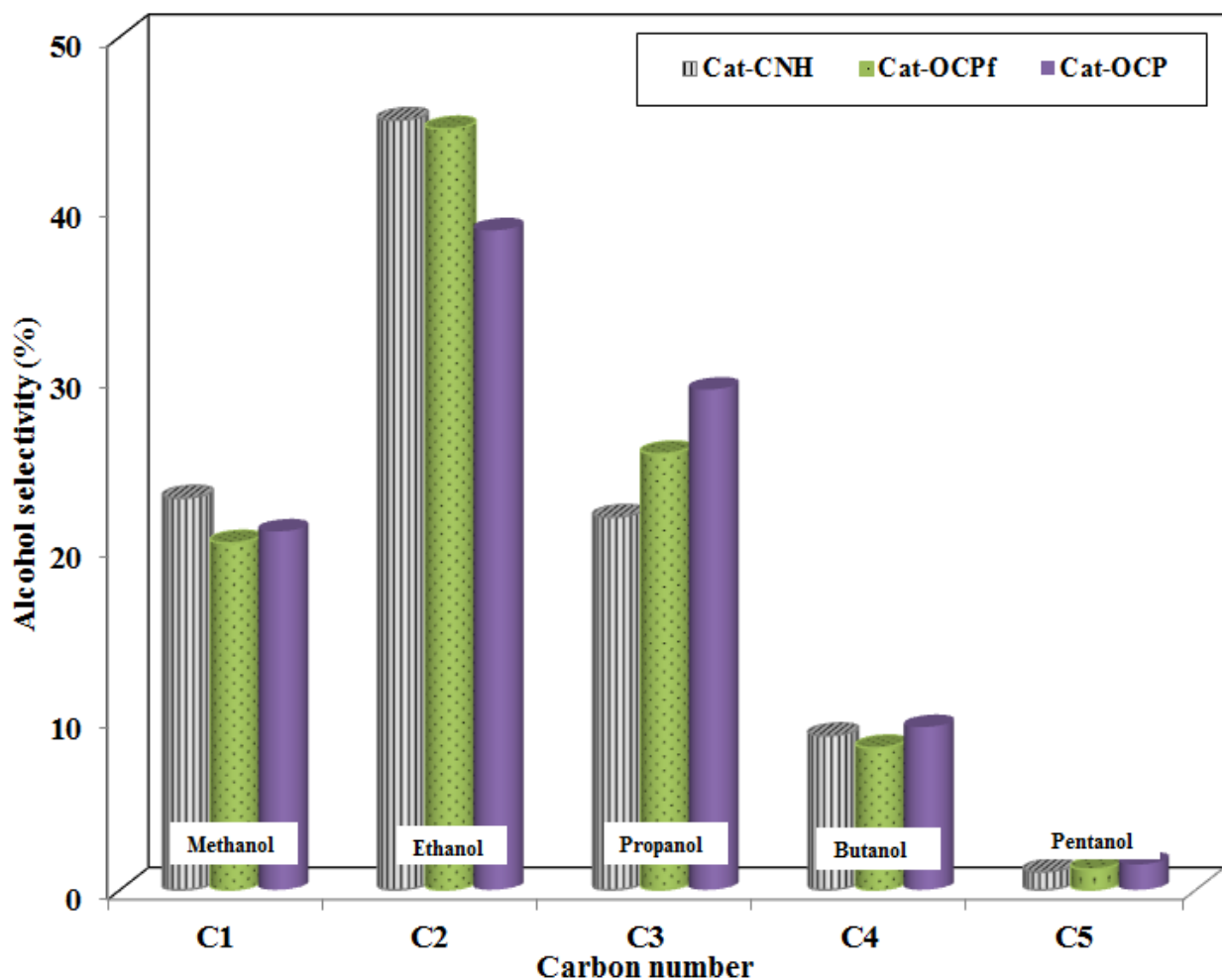


Fig. 7.9: Alcohol composition as a function of carbon number (P=8.3 MPa; T=330°C; Catalyst=2g; GHSV=3.6 m³ (STP)/h·kg_{cat}; H₂:CO=1.25)

It is quite obvious that alcohol products stream generated by CNH, OCP_f, and OCP-supported KCoRhMo catalysts investigated consisted mostly of linear alcohols with carbon numbers in the range of C₁ to C₅. All the supported catalyst systems enhanced the production of these alcohols, mostly C₂ alcohols, with selectivities of 45.1, 43.8, & 36.8% for Cat-CNH, Cat-OCP_f and Cat-OCP, respectively. Products selectivities for the gaseous and liquid streams of the CO hydrogenation reaction are summarized for all catalysts investigated and are presented in Table 7.2. As can be seen, Cats-OCP_f and OCP tend to produce more CO₂; suggesting their higher activity for the water-gas-shift reaction. Thus, from Fig. 7.9 and Table 7.2, it becomes quite conclusive that all the supported KCoRhMoS₂ catalysts investigated for higher alcohol productivity turned out to have high selectivity towards the production of higher alcohols, with ethanol being the most predominant higher alcohol product in the final liquid product stream with the by-products comprising mainly CO₂ and light hydrocarbons (methane and ethane).

Table 7.2: Products selectivities for CNH, OCP_f and OCP-supported KCoRhMo catalysts at T=330°C.

Catalyst	Product Selectivities (%)							
	Alcohol product selectivities (%)						Main by-products	
	C ₁	C ₂	C ₃	C ₄	C ₅	Total alc.	Hydrocarbons	CO ₂
Cat-CNH	21.1	40.6	23.2	7.1	0.9	92.9	3.2	2.4
Cat-OCP_f	16.5	30.2	18.3	4.3	0.8	70.1	10.2	16.8
Cat-OCP	14.5	20.1	16.5	2.7	0.7	54.6	16.1	26.5

7.5.3. Arrhenius plot and activation energy calculations by the power law model

The energetics of three catalysts studied for the HAS reaction were evaluated and their respective apparent activation energies (E_a) were computed by assuming a pseudo-first order for the higher alcohol reactions. To determine the activation energies and pre-exponential factors, a plot of $\ln k$ against $1/T$ was computed and displayed in Figure 7.10. These parameters were determined from the Arrhenius plot for the rate constants and are summarized in Table 7.3.

As can be seen by the profiles of the Arrhenius plots, increasing temperature resulted in increases in the rate constants, confirming the strong dependency of temperature in the HAS reaction. The apparent activation energies (E_a , kJ/mol) computed within the range of temperatures studied (300-340°C) followed the order: Cat-OCP (157.9) > Cat-OCP_f (99.8) > Cat-CNH (54.4). This trend can be explained by the fact that the CNH had superior textural properties as compared to its OCP_f and OCP counterparts; however, the enhanced textural properties of CNH-supported catalysts did not only enhance its catalytic performance but also influenced the energetics as confirmed by the differences observed in apparent activation energies of the supports studied. By comparing the energetics of the catalysts investigated in the present study to that in the literature as depicted in Table 7.3, the observed trend for activation energies followed the trend: Cat-CNH > Cat-CNT > Cat-OMC > Cat-OCP_f > Cat-OCP. It can be concluded that at similar metals loading, the CNH and OCP_f-supported KCoRhMo catalysts can be promising for the conversion of syngas to higher alcohols.

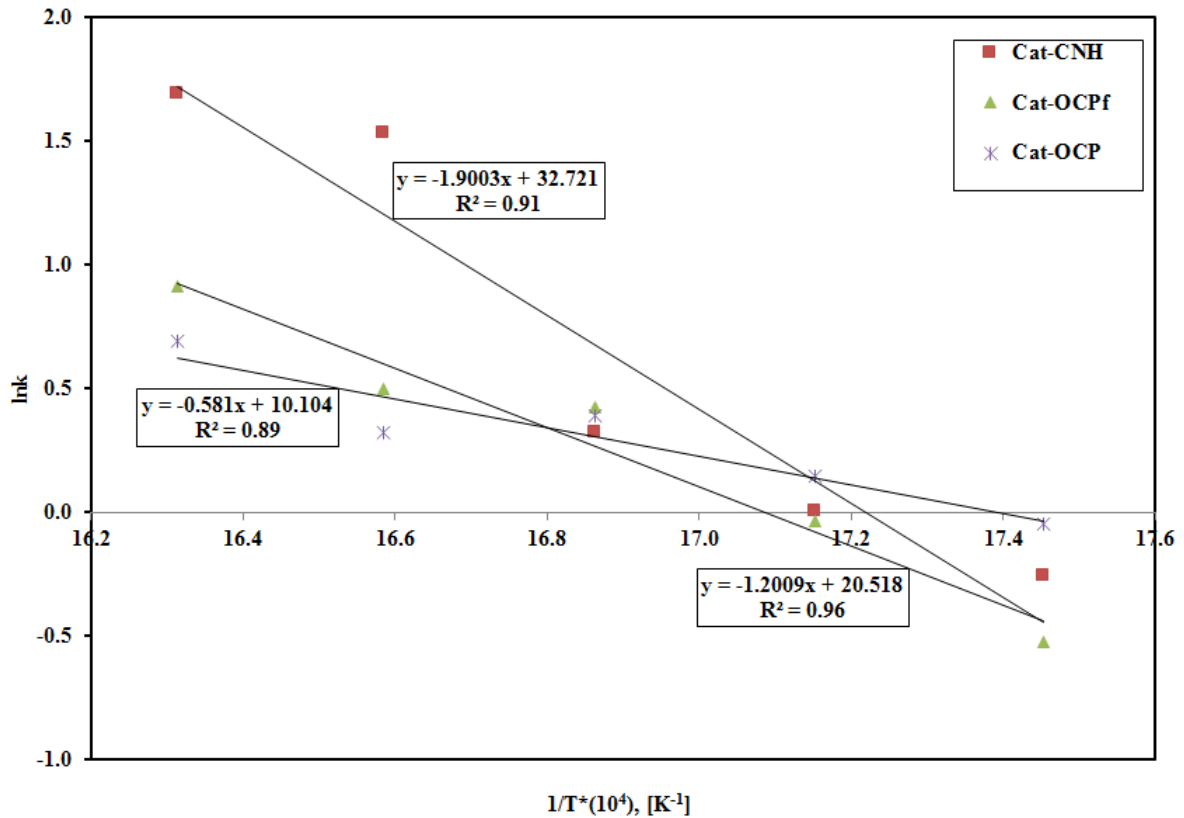


Fig. 7.10: Arrhenius plot & activation energy for CNH, OCP_f and OCP-supported catalysts

Table 7.3: Activation energies comparison for carbon-supported KCoRhMo catalysts for the HAS reaction.

Catalyst	Activation energy, E _a (kJ/mol)	Reference
Cat-CNH	54.4	Present work
Cat-OCP _f	99.8	Present work
Cat-OCP	157.9	Present work
KCoRhMo/OMC	86.4	Boahene et al., 2014
KCoRhMo/MWCNT	72.4	Boahene et al., 2014
*CoMoK-10%CNT	74.3	Ma et al., 2006

7.6. Conclusions

In summary, CNH support and its by-products (OCP_f and OCP) were synthesized by the submerged arc discharge in liquid nitrogen technique, functionalized with 30wt.% nitric acid under reflux conditions, and employed in the formulation of K-doped CoRhMoS₂ catalysts for HAS applications. All catalysts prepared using these novel supports showed activity towards higher alcohols via the CO hydrogenation route. At similar metals loading, BET analysis of all catalysts evidenced significant structural mesoporosity and orderliness since the physical properties of the materials were not compromised; however, a significant blockage was observed in Cat-OCP as confirmed by the NS_{BET} computations. Moreover, at similar metals loadings of 9%K, 4.5%Co, 15%Mo and 1.5wt.% Rh, XRD analysis evidenced a better metal nanoparticles dispersion on Cat-CNH since less crystalline peaks were detected as confirmed by the TEM images. At the optimum temperature 330°C, linear alcohols were produced with the trend of C₂₊ alcohols selectivities following the order: Cat-CNH (63.7) > Cat-OCP_f (48.9) > Cat-OCP (38.2). Finally, within the range of temperatures studied (300-340°C), the calculated apparent activation energy, (E_a, kJ/mol), for the catalysts followed the order: Cat-OCP (157.9) > Cat-OCP_f (99.8) > Cat-CNH (54.4), corroborating the superior catalytic performance of the CNH-supported catalysts as compared to its OCP_f and OCP counterparts. The results of this study provide insight to elucidate the crucial role different carbon materials play as catalyst support in their application for higher alcohol synthesis.

CHAPTER 8

Higher Alcohols Synthesis: Experimental and process parameters study over CNH-supported KCoRhMo catalyst

The content of this chapter has been prepared and submitted for Journal publication.

Citation:

Boahene P.E., Dalai A.K. Higher Alcohols Synthesis: Experimental and process parameters study over CNH-supported KCoRhMo catalyst, Ind. Eng. Chem. Res., 2017, 56 (46), 13552–13565.

Contribution of the Ph.D. Candidate

Experimental runs, development of the catalysts as well as their extensive characterizations and catalytic studies were performed by Philip Effah Boahene. Data collection, analysis and interpretations were performed by Philip Boahene with assistance from Dr. Ajay Kumar Dalai. All of the writing of the manuscript submitted for publication was done by Philip Effah Boahene and discussed with Dr. Ajay K. Dalai. Dr. Dalai provided editorial guidance regarding the style and content of this chapter.

Contribution of this chapter to overall study

This chapter investigated process parameters (temperature, pressure, and gas hourly space velocity) and their interaction effects on the higher alcohol synthesis reaction. Design Expert Software (version 9.0) was used to design the experimental runs spanning the range of process

parameters studied. Also, optimization of the operating conditions was performed to obtain the maximum ethanol and higher alcohols selectivities and space time yields. The CNH-supported KCoRhMo catalyst was used for this study due to its superior catalytic performance for higher alcohols as concluded from Chapters 8.

8.1. Abstract

The present work investigated the effects of operating conditions (T, P, and GHSV) on the higher alcohols synthesis reaction using a downward-flow fixed-bed reactor. The CNH-supported KCoRhMo catalysts with compositions 9%K, 4.5%Co, 1.5%Rh, and 15wt.% Mo, respectively, was used for this study. The Design-Expert software was used to analyze the interaction effects of temperature (290-370°C), pressure (5.52-9.65 MPa), and gas hourly space velocity (2.4-4.8 m³ (STP)/(kg of cat.)/h) on CO conversion, alcohols and hydrocarbons products selectivities as well as their respective yields. The validity of the models was assessed by statistical tests: test of significance and coefficient of determination values. The recorded R²-values suggested that the quadratic models generated could sufficiently depict the experimental data. Increasing temperature and pressure in the ranges 290-370°C and 5.52-9.65 MPa, respectively, resulted in corresponding increases in CO conversions; however, with increasing GHSV, the CO conversion decreased monotonically. Numerical optimization assessments of the models selected the optimum operating conditions to be 325°C, 9.1 MPa, and 2.4 m³ (STP)/(kg of cat.)/h to give the maximum ethanol and higher alcohols space time yields of 0.126 and 0.138 g/g of cat-h, respectively.

8.2. Introduction

Mixed alcohols including C₂₊ alcohols are important compounds with widespread applications in the chemical, pharmaceutical and energy sectors (Luk et al., 2017). In North America (USA and Canada) and some parts of Europe, gasoline blends with up to 10% ethanol (E10) and higher alcohols

are commercially available at gasoline pump stations (Nylund et al., 2008; National Resources Canada, 2016). These alcohols (C_2 and C_{2+}) can be used as additives to boost octane levels in gasoline fuels. Higher alcohols synthesis from syngas conversion provides an alternative direct catalytic synthesis route for the production of fuels and industrial chemicals (Fei et al., 2014). Though much research works have appeared in the literature on this topic, there is the need to further enhance the higher alcohol yields and selectivities to make it commercially attractive.

Heterogeneous catalytic systems for the HAS reaction is commonly based on MoS_2 due to its high sulfur tolerance and high activity for the water-gas-shift reaction (Woo et al., 1991). The reaction mechanism for the generation of higher alcohols on this MoS_2 catalyst matrix was proposed to follow the classical CO insertion into the corresponding precursor alcohol (Santiesteban et al., 1988). The product distribution and carbon chain growth scheme over these catalysts follows the Anderson-Schulz-Flory (ASF) polymerisation pathway (Smith et al., 1984). The incorporation alkali promoters suppressed the hydrogenation ability of surface alkyl species to form alkanes; thus, increasing the active sites needed for higher alcohols formation (Gandia et al., 1994).

The alcohol products selectivities are affected by the catalyst support materials as well as the reaction conditions (Forzatti et al., 1981; Herman, 2000; Subramani et al., 2008). For instance, $KCoRhMo$ catalysts supported on multi-walled carbon nanotubes (MWCNTs) outperformed its counterparts for higher alcohol synthesis (Surisetty, 2010; Haifeng et al., 2015). Furthermore, despite the successful application of the MWCNTs for the HAS reaction, their potential could be restrained by the limited surface area (Surisetty et al., 2011). Also, with their enhanced textural properties and at similar metal loadings (9%K, 4.5%Co, 15%Mo and 1.5%Rh), ordered mesoporous carbon (OMC) recorded about 5% less in total alcohol selectivity as compared to its

MWCNT counterpart (Boahene et al., 2016). Though MWCNT and OMC have proven tendencies to produce alcohols, it was concluded from our previous study that carbon in the form of carbon nanohorns (CNH) can be a superior catalyst supports for syngas conversion applications and compared to its byproducts (Boahene et al., 2017).

In the CO hydrogenation reaction, varying the operating conditions (T, P, and GHSV) have direct impact on the products selectivity and yields. For such reactions, typical process parameters monitored for temperature and pressure spans the ranges of 250-350°C and 5-10 MPa, respectively (Spivey et al., 2007, Subramani et al., 2008). Though, the effects of independent process variables (T, P, and GHSV) on CO conversion, alcohol products yield, hydrocarbons and CO₂ have been studied by various researcher (Su et al., 2014; Christensen et al., 2009), their combined interaction effects is limited in the literature. In our study of CNH-supported KCoRhMo catalyst, it was observed that the catalyst displayed improved catalytic properties for the HAS reaction as compared to its OCP_f and OCP counterparts. The space time yields of total alcohols as well as higher alcohols were recorded at 340°C, 8.28 MPa, and 3.6 m³ (STP)/(kg of cat.)/h to be 0.5026 and 0.4104 g/(g of cat.)/h, respectively (Boahene et al., 2017).

The motivation of the present study was to develop models to correlate the interaction effects of independent process variables (T, P and GHSV) to dependent variables (%CO conversion, alcohol products yields, hydrocarbons and CO₂ selectivities) during the HAS reaction over the optimum CNH-supported KCoRhMo catalyst. Finally, the optimized conditions required to obtain maximum ethanol and higher alcohol selectivities was also to be determined.

8.3. Experimental

The syntheses of pristine supports namely; CNH, OCP_f and OCP were accomplished using the submerged arc discharge in liquid nitrogen technique at a fixed current of 90A and 34V. The

detailed description of the techniques employed to separate these carbon nanoparticles after syntheses, as well as their corresponding KCoRhMo catalysts formulations can be found in Chapter 3, section 3.2.2, 3.2.3 and 3.2.4 of thesis. Furthermore, characterization techniques employed as well as the CO hydrogenation experimental procedures have also been discussed in Chapter 3.

8.3.1. Experimental design for process parameters study

The experimental design for process parameters study was achieved using the Design Expert (version 9.0) statistical software. The parameters T, P, and GHSV were varied in the ranges of 290-350°C, 5.52–9.65 MPa, and 2.4 to 4.8 m³ (STP)/(kg of cat.)/h, respectively. To analyze the interaction effects of process parameters as well as their optimized conditions for the HAS reaction, the central composite design (CCD) method was used to develop the experimental plan. This design approach is one of the commonly used response surface methods (RSM) for designed experiment; and it employs factorial or fractional factorial design with center points, augmented with a group of axial points to help estimate curvature (Box et al., 2007). The main idea of RSM is to use a sequence of designed experiments to obtain an optimal response using a second-degree polynomial model. It should also be mentioned that statistical approaches such as RSM can be employed to maximize the production of a special substance by optimization of operational factors. In contrast to conventional methods, the interaction among process variables can be determined by statistical techniques (Asadi et al., 2017).

The experiments were performed using a syngas mixture with molar composition of 40% CO, 50% H₂, and 10% Ar. Reproducibility of the results was ensured by repeating some of the experimental conditions a few more times to ascertain the degree of inherent errors. Perturbation plots were used to show the one-variable effect on the dependent variable as the others independent

variables remained constant. These plots were used along with the 3-D surface responses plots to help compare the relative influences of the factors studied through a multifactor surface (Surisetty et al., 2011).

8.4. Results and discussion

8.4.1. Effects of operating variables on higher alcohol synthesis

Syngas conversion to higher alcohols among others is markedly influenced by various operating conditions such as temperature, pressure, gas hourly space velocity (GHSV), and H₂-to-CO ratio. The effects of the individual process variables on the higher alcohols productivities are discussed.

8.4.2. Effects of temperature on higher alcohol synthesis

The range of temperatures mostly suited for the conversion of syngas to higher alcohols is usually favorable in a narrow window (270-330°C), and in most cases greatly dependent on the catalyst used (Forzatti et al., 1991; Mills et al., 1994; Gupta et al., 2011). For instance, the best temperature range for higher alcohol synthesis on most of the Cu-based catalysts is 250-300°C and that for alkali-doped MoS₂-based catalyst is 270-330°C (Subramani et al., 2008; Gupta et al., 2011). However, the main problems associated with higher temperatures are: (1) instability of some oxygenates at higher temperatures; (2) excessive formation of CO₂ and methane; and (3) deactivation of the catalyst due to sintering (Gupta et al., 2011). Generally, higher temperatures are required for enhanced selectivity toward higher alcohols than toward methanol (Boz et al., 1994; Majocchi et al., 1998). Majocchi et al., 1998, reported that the selectivity to all alcohols goes through a maximum with temperature due to the dominance of CO₂ pathway at higher temperatures. Furthermore, in the range 260-330°C, Apesteguia et al., 1997, found that methanol selectivity decreased, isobutyl alcohol selectivity increased, and C₂₊ linear alcohol selectivity

passed through a maximum. They explained these findings by assuming that methanol synthesis was close to equilibrium, isobutyl alcohol synthesis was under kinetic control, and linear alcohols were intermediates in isobutyl alcohol synthesis.

8.4.3. Effects of pressure on higher alcohol synthesis

At constant temperatures, the formation of higher alcohols is thermodynamically favored with increasing pressures (Iranmaboob et al., 2002; Gupta et al., 2011). The general observed trend is that as pressure increases the productivity of higher alcohols increases; however, the effect of pressure on reaction kinetics is also catalyst specific to some extent (Xu et al., 1987). On a SiO₂-supported Rh-Mn catalyst for the study of C₂ oxygenates production, Yin et al., 2003, observed that increasing the pressure was favorable for the synthesis of C₂ oxygenates. Approximately 2.7 times increment in STY of C₂ oxygenates was observed when pressure was increased from 2.0 to 5.0 MPa with selectivity toward C₂ oxygenates increasing from 50.5 to 66.5%. On a MWCNT-supported K-Co-Rh-MoS₂ catalyst system for higher alcohol synthesis, Surisetty et al., 2009, observed a monotonic increase in the rate of %CO conversion, total alcohol production, and hydrocarbon formation.

8.4.4. Effects of gas hourly space velocity

Generally, increasing the syngas flow rate (GHSV) has an opposing effect on the CO conversion as well as the selectivity towards higher alcohols (Mahdavi et al., 2005). Low space velocities (higher contact times) are mostly favorable for higher-alcohol synthesis which indicates that higher alcohols are formed at a slower rate than methanol (Boz et al., 1994; Storm et al., 1995). Low space velocities are also favorable for high CO conversion. With an increase in GHSV, Iranmahboob et al., 2002, observed an increase in the total alcohol productivity; conversely, CO conversion decreased probably due to insufficient contact time of reactants with the active catalyst

surface species. Furthermore, Boz et al., 1994, observed that a decrease in space velocity increased higher alcohol, methane, and CO₂ selectivities and decreased methanol selectivity.

8.4.5. Effects of H₂-to-CO ratio

The ratio of H₂/CO constituting the syngas feedstock has a significant effect on higher alcohol selectivity (Smith et al., 1984). Typical H₂/CO ratios reported in the literature for higher alcohol formation range 1 to 2 (Smith et al., 1984; Forzatti et al., 1991; Spivey et al., 2007; Gupta et al., 2011). Whereas H₂/CO ratio of 2 favors methanol formation, an optimum ratio of 1 is mostly favorable for the formation of higher alcohols (Forzatti et al., 1991). However, the general trend to be noted is that the overall activity decreases with decreasing H₂/CO ratio (Mahdavi et al., 2005). In general, low H₂/CO ratios favors coke formation and C-C chain growth; and therefore the selectivity toward higher alcohols. Higher H₂/CO ratios favor methanol synthesis and may either increase or decrease selectivity to methane (Subramani et al., 2008; Gupta et al., 2011). In an effort to understand the effect of feed composition on higher-alcohol synthesis, Surisetty et al., 2010, used results obtained from Design Expert Software 6.0.1 in their kinetics study of higher alcohol synthesis from syngas over a sulfided K-Co-Rh-Mo/MWCNT catalyst by varying the H₂/CO ratio at four different levels in the range of 0.5-2. The major products obtained at an optimum H₂/CO ratio of 1.25 (i.e. H₂:CO = 50:40) were mainly methane, carbon dioxide, methanol, ethanol, n-propanol, and n-butanol.

8.4.6. Quadratic models development by Design Expert for higher alcohol synthesis

Higher alcohols have their carbon numbers (C > 1), whereas, total alcohols represent alcohols with carbon number equal to 1 and higher. After the HAS reaction, analysis of tail gas exiting the reactor indicated that methane is the major hydrocarbon component apart from CO₂, unconverted CO, and H₂. The liquid products analyzed by gas chromatography (GC) equipped

with Stabil Wax column evidenced linear alcohols including C₁ to C₅ alcohols as the main products along with other higher alcohols.

A series of data collected from experimental runs were used in Design Expert to develop quadratic modules spanning selected operating conditions. Evaluation of the models was done by employing two main statistical tests namely; the test of significance of factors or interactions and the coefficient of determination (Azargohar et al., 2008; Surisetty, 2010). The probability values (*p*-values) were used to test for significance of factors of the models generated. The models were further simplified by eliminating the insignificant factors to ease the interpretation (Lazic, 2004). In this regard, the factor or interaction was deemed insignificant at a 95% confidence level, when a *p* > 0.05. The value of the coefficient of determination (*R*²) indicates the proportion of the variance in the dependent variable that is predictable from the independent variables (Devore, 2011). This value is used to test for the goodness of fit, with values of *R*² approaching one depicting a good fit and that approaching zero depicting no fit. Adjusted *R*² value (also called 2*R* value) is a modification of *R*², which improves its value only if the newly added factors or interactions are significant (Montgomery, 1997).

8.4.7. Effects of temperature, pressure, and GHSV on CO conversion

The interaction effects of temperature, pressure and gas hourly space velocity on CO conversion as generated by the regression analysis (ANOVA) of experimental data is given in the response surface model below:

%CO conversion

$$= 103.02489 - 0.26035 * T - 0.16118 * P - 4.70342 * GHSV + 5.72222 * 10^{-4} * T * P \dots \dots \dots (8.1)$$

where units of T, P and GHSV are in °C, psi and m³ (STP)/(kg of cat./h), respectively.

The independent operating conditions used for the experimental data collection as well as model development were in the ranges: T = 290-350°C; P = 5.52-9.65 MPa; and GHSV = 2.4-4.8 m³ (STP)/(kg of cat./h). Syngas feedstock of H₂/CO molar ratio of 1.25 was used throughout the experiments.

The results showing the test of significance of the independent variables studied or their interaction effects on CO conversion can be found in Tables 8.1 along with their respective R² values. In this table, the independent variables were represented as A, B, and C to denote T, P, and GHSV, respectively.

Table 8.1: Test of significance results for independent variables or interactions for the model derived for CO conversion.

Variable/interactions	p-value of %CO conversion	
	All variables included	Insignificant variables rejected
A-Temp	0.0001	< 0.0001
B-Pressure	0.0066	0.0037
C-GHSV	0.0206	0.0086
AB	0.0674	0.0463
AC	0.7441	-
BC	0.916	-
A ²	0.8373	-
B ²	0.1077	-
C ²	0.6600	-
Model	0.0013	< 0.0001
R ²	0.9533	0.9755
R ² -adjusted	0.9212	0.9355

By discarding the insignificant variables using their p-values as a check helped improve the final model developed. As can be seen from Table 8.1, rejecting the interacting parameters (AC, BC, A^2 B^2 and C^2) with their corresponding p-values greater than 0.05 resulted in the development of a final model with improved R^2 value of 0.9755.

The response surface plots representing the interaction effects of T, P, and GHSV on % CO conversion are shown in Figures 8.1 (a and b).

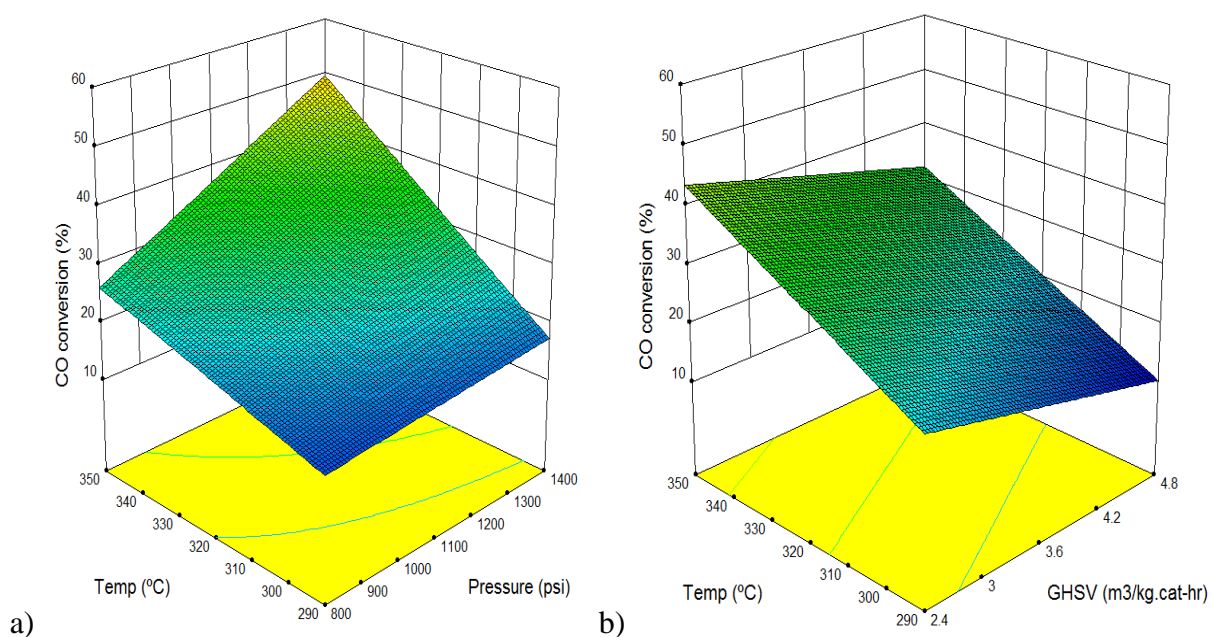


Fig. 8.1 (a & b): 3-D surface response plots showing the interaction effects of temperature, pressure, and GHSV on CO conversion over KCoRhMo/CNH catalyst.

A strong correlation between T, P, GHSV and %CO conversion can be depicted from the surface plots. Increasing T and P resulted in a corresponding increase in CO conversion; suggesting that CO hydrogenation over the KCoRhMo/CNH catalyst was enhanced at high temperature and pressure. It could be inferred from the reaction stoichiometry and the Le-Chatelier's principle that increasing pressure favored the direction that proceeds with decreasing number of moles; thus,

leading to the formation of methanol as well as higher alcohols. Also, a consistent decrease in CO conversion can be observed when GHSV was increased from 2.4 to 4.8 m³ (STP)/(kg of cat.)/h. This could be due to the short contact time between the reactants (CO+H₂) and catalytic active sites at high GHSV.

The perturbation plot showing the individual effects of T, P, and GHSV on % CO conversion as well as the parity plot (predicted vs. actual) are shown in Figures 8.2 (a and b).

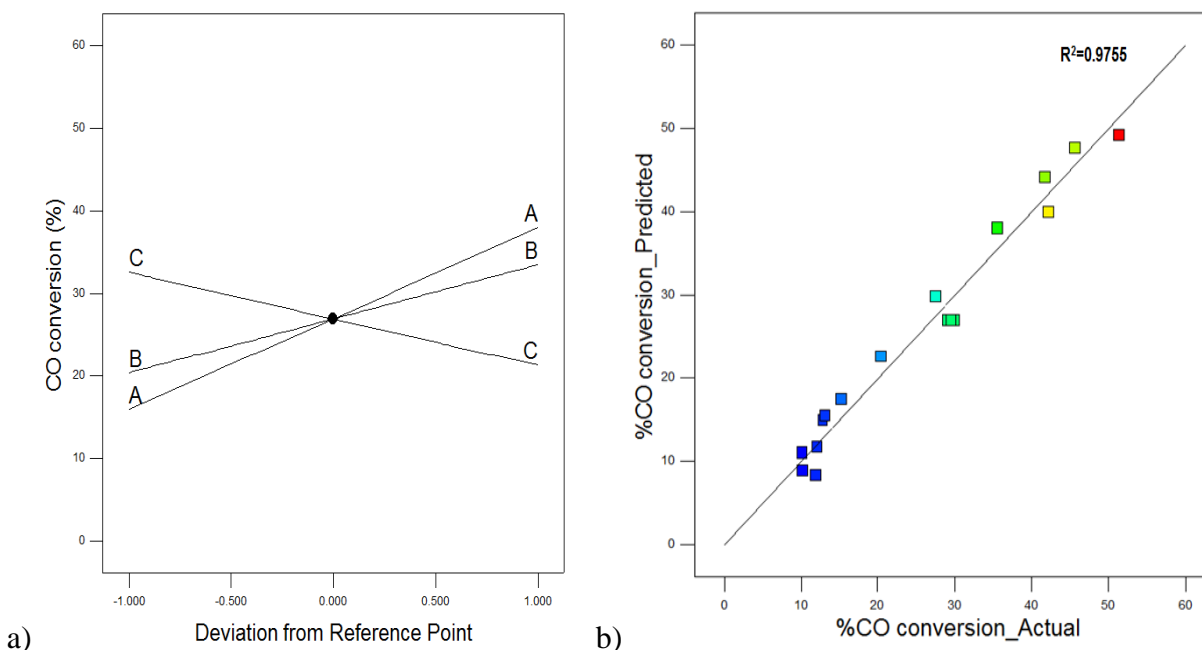


Fig. 8.2: Effects of temperature, pressure, and GHSV on CO conversion over KCoRhMo/CNH catalyst. a) Perturbation plot; b) Parity plot.

From the perturbation plot provided in Fig. 8.2a, the individual effects of the independent variables T, P, and GHSV on %CO conversion were found to be significant as can be seen from Table 8.1. The parity plot shown in Fig. 8.2b compares values of CO conversion obtained from experiments to that predicted by the model equation. It can be concluded that within the operating conditions evaluated, the derived quadratic model for %CO conversion could sufficiently predict the corresponding experimented values to a greater degree. The obtained R² value of 0.9755

corroborates a quite strong correlation between the model predicted values and the actual CO conversions recorded.

8.4.8. Effects of temperature, pressure, and GHSV on STY of alcohols, hydrocarbons, and CO₂

The surface response models shown below were generated by the regression analysis (ANOVA) of experimental data to depict the interaction effects of operating variable: T, P and GHSV on the STY of alcohols produced, hydrocarbons, and CO₂ after rejecting insignificant factors:

$$STY_{MeOH} = -4.52659 + 0.026924 * T + 6.91051 * 10^{-4} * P - 0.026856 * GHSV - 4.16609 * 10^{-5} * T^2 - 2.62818 * 10^{-7} * P^2 \dots \dots \dots (8.2)$$

$$STY_{EtOH} = -2.27723 + 0.013889 * T + 4.11422 * 10^{-4} * P - 7.84578 * GHSV - 2.23521 * 10^{-5} * T^2 - 1.66830 * 10^{-7} * P^2 \dots \dots \dots (8.3)$$

$$STY_{Tot. Alc.} = -8.86615 + 0.046987 * T + 1.39375 * 10^{-3} * P - 0.0403 * GHSV - 7.31096 * 10^{-5} * T^2 - 5.39046 * 10^{-7} * P^2 \dots \dots \dots (8.4)$$

$$STY_{HA} = -3.2301546 + 0.019528 * T + 8.18377 * 10^{-5} * P - 0.014978 * GHSV - 3.06113 * 10^{-5} * T^2 \dots \dots \dots (8.5)$$

$$STY_{HC} = 1.87983 - 0.010065 * T - 5.29747 * 10^{-4} * P - 0.067919 * GHSV + 1.79653 * 10^{-6} * T * P + 1.4145 * 10^{-5} * T^2 + 7.83798 * 10^{-7} * GHSV^2 \dots \dots \dots (8.6)$$

$$STY_{CO2} = 23.14245 - 0.024731 * T + 5.76546 * 10^{-5} * P - 8.75586 * GHSV + 4.17203 * 10^{-5} * T^2 \dots \dots \dots (8.7)$$

where units of T, P and GHSV are in °C, psi and m³ (STP)/(kg of cat./h), respectively.

Results of the test of significance of independent factors (T, P, and GHSV) or their interactions for the STY of C₁-C₅ alcohols, total alcohols, hydrocarbons, and CO₂ after discarding insignificant factors is shown in Table 8.2. The p-value of each model observed from Table 8.2 was less than 0.05; suggesting that the individual factors used for the model development were significant. Thus, the computed p-values for the developed models make them significant to be considered for parameters prediction within the range of operating conditions evaluated.

Table 8.2: Test of significance results for independent factors or interactions for the model derived for the STY of different products.

Variable/interaction	p-value of models after rejecting insignificant variables					
	STY _{MeOH}	STY _{EtOH}	STY _{Tot. Alc.}	STY _{HA}	STY _{HC}	STY _{CO₂}
A-Temp	0.06172	0.01061	0.04993	0.08503	0.0001	< 0.0001
B-Pressure	0.0449	0.0886	0.0167	0.026	0.0257	0.01151
C-GHSV	0.0513	0.02095	0.05003	0.0836	0.0205	0.03141
AB	-	-	-	-	0.0371	-
AC	-	-	-	-	-	-
BC	-	-	-	-	-	-
A ²	0.0024	0.0124	0.0101	0.0113	0.029	0.0018
B ²	0.00135	0.0519	0.0471	-	-	-
C ²	-	-	-	-	0.0526	-
Model	0.00198	0.00156	0.0059	0.00123	0.0003	< 0.0001
R ²	0.9553	0.9887	0.9566	0.9553	0.9689	0.9736
R ² adjusted	0.9342	0.9452	0.9336	0.9438	0.9353	0.9675

The R² statistics for the models depicting the STY of different products can also be found in Table 8.2. The predicted R² values of all models are in reasonable agreement with the adjusted R² values; suggesting that these models can be quite useful to predict the STY of products (liquid and gaseous) during the higher alcohol synthesis.

The effects of T, P, and GHSV on the STY of methanol using H₂ to CO molar ratio equal to 1.25 are presented in Figures 8.3 (a, b & c) as 3-D response surface plots and perturbation plot, respectively.

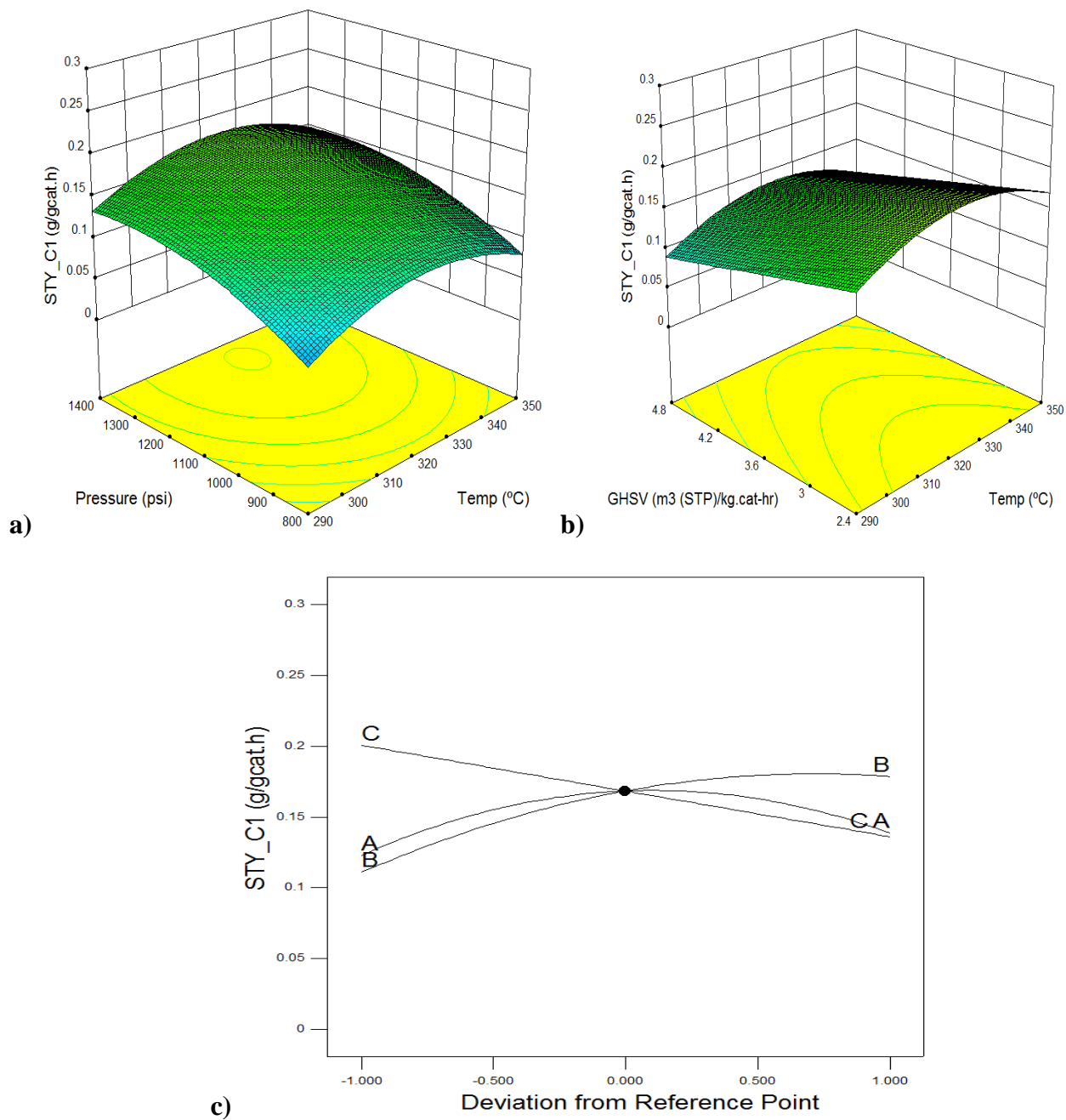


Fig. 8.3: The effects of the temperature, pressure, and GHSV on methanol STY over KCoRhMo/CNH catalyst. (a & b) 3-D surface responses; and (c) Perturbation plot

The methanol STY increased monotonically to a point and decreased with increasing temperature; suggesting that for the catalyst studied, an optimum temperature exists where conversion of produced methanol to higher alcohols occurs. Increasing pressure resulted in a corresponding increase in the formation of methanol; however, GHSV had an opposite effect on methanol formation. The effect of pressure on methanol STY can be explained by Le-Chatelier's principle. With pressure increments imposed on the system, the equilibrium nullifies this change by shifting the reaction to the product side; thus, increasing methanol formation. At high GHSVs, the methanol formation is low due to short contact time between gas reactants and catalyst, which explains the low methanol yields recorded under this condition. The R^2 value of 0.9553 (Table 8.2) obtained from the parity plot of the experimental methanol STY values with that of the predicted values, confirmed a good correlation between these parameters within the experimental conditions.

The effects of T, P, and GHSV reactions on the STY of ethanol at H_2 to CO molar ratio of 1.25 are represented as 3-D plots in Figs. 8.4 (a and b) and the perturbation plot in Fig. 8.4c. Compared to P and GHSV, temperature had great effect on ethanol STY, with the rate of ethanol formation reaching a maximum value and then decreasing at higher temperatures. Depending on the temperature, the ethanol formation increased up to certain pressures and then levelled off at higher pressures. With respect to GHSV, a slightly decreasing trend in the ethanol STY was observed. The model fits the experimental results with an R^2 value of 0.9452 as seen from Table 8.2. Higher alcohols STY exhibit similar trends of operating conditions dependency as that of ethanol STY, with the maximum amount of higher alcohols formation observed with respect to temperature and GHSV (figure not given). With increased pressure, the higher alcohols STY increased to a certain value and then remained constant at higher pressures. An R^2 value of 0.9553

was recorded from the fitting of the model depicting STY for higher alcohols as shown in Table 8.2.

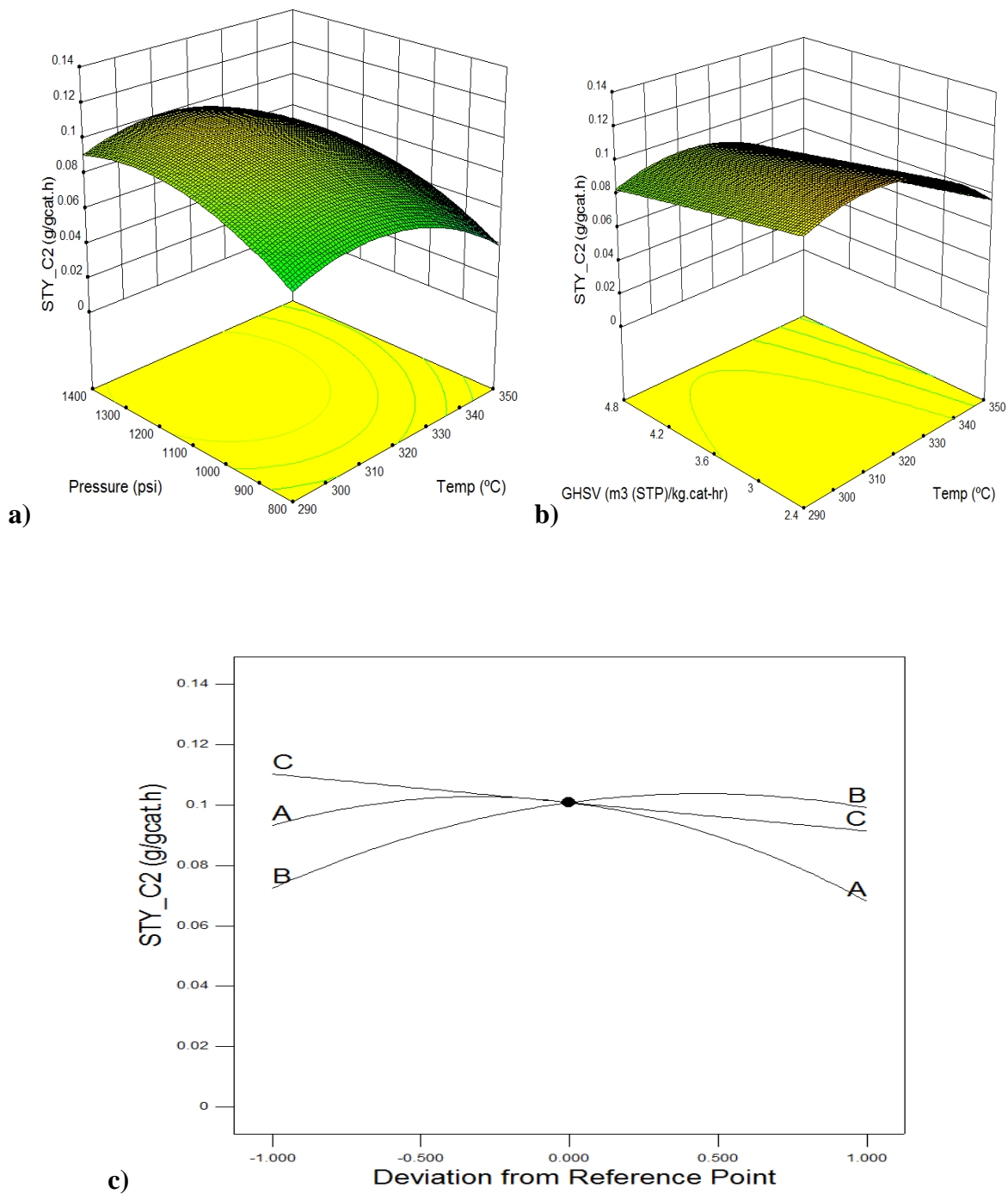


Fig. 8.4: The effects of the temperature, pressure, and GHSV on ethanol STY over KCoRhMo/CNH catalyst. (a & b) 3-D surface responses; (c) Perturbation plot

The effects of T, P, and GHSV on the total alcohol formation for the HAS reactions are shown by the surface plots in Fig. 8.5 (a and b) and the perturbation plot in Fig. 8.5c. Table 8.2 displays the quality of the model's fit with an R^2 value of 0.9566.

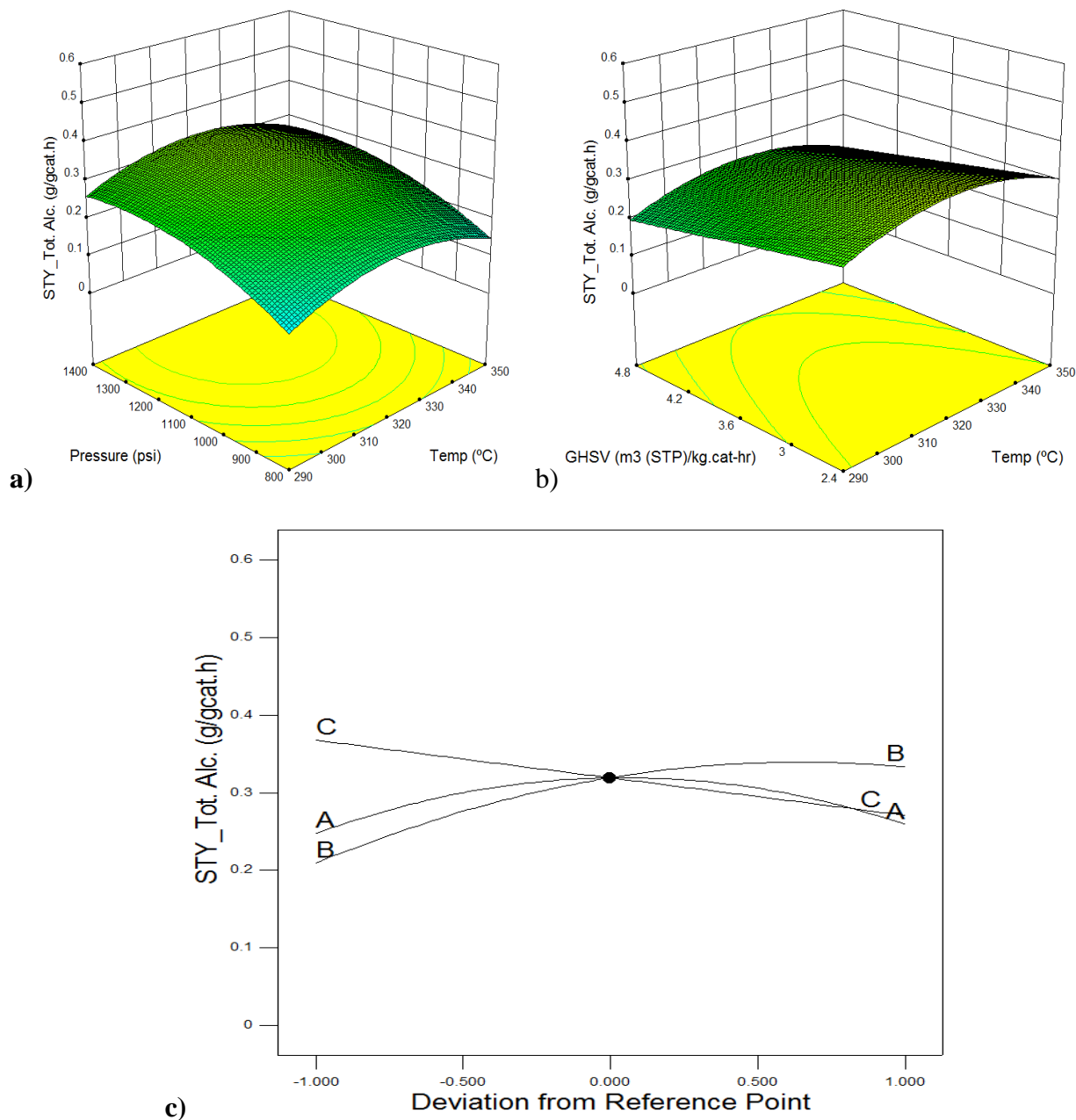


Fig. 8.5: The effects of temperature, pressure, and GHSV on total alcohols STY over KCoRhMo/CNH catalyst. (a & b) 3-D surface responses; (c) Perturbation plot

Increasing temperature passed through a maximum for the total alcohols STY; suggesting the existence of an optimum temperature for total alcohols production. Similarly, increasing pressure enhanced the formation of total alcohols, with the STY of total alcohols increasing to a maximum and then levelling off at higher pressures. It can be seen in Fig. 8.5c that GHSV had a marginal decreasing effect on the total alcohols space time yield, probably due to short contact time at high GHSVs. As compared to temperature and pressure, the influence of GHSV was quite subtle for the catalyst investigated for the HAS reaction. In the kinetic analysis of K-MoS₂ catalyst for syngas conversion to mixed alcohols, Park et al. 1997 observed a maximum value of 320°C to be the temperature for maximum mixed alcohols formation.

Surisetty et al. 2010 found an optimum temperature of 330°C from their intrinsic kinetic analysis of MWCNT-supported trimetallic Co-Rh-Mo-K catalyst for a similar reaction. In the present study, an optimum temperature for total alcohol STY was found to be 325°C. Thus, it can be inferred that though temperature plays a critical role in this kind of reactions, the total alcohols formation is dependent on the nature of catalyst used as well.

The dependency of operating conditions on hydrocarbons STY is shown in Figures 8.6 (a-c). A strong temperature dependency was observed for hydrocarbons formation. At constant pressure and GHSV, increasing temperature resulted in an increase in hydrocarbons formation. Though the results of this study suggests that the produced light alcohols are consumed at some point to generate higher alcohols as temperature increases, the detrimental effects on hydrocarbons formations at high temperatures should be adequately considered during the HAS reaction. With increasing pressure, slight increments were observed in the hydrocarbons space time yields; however, an opposing effect was observed with increasing GHSV. This can be explained by the fact that at high temperature and low GHSVs, the long contact time between reacting species and

catalyst can enhance gaseous byproducts (hydrocarbons and CO₂) formation. As seen in Table 8.2, the model fits well with the experimental results with R² value of 0.9689.

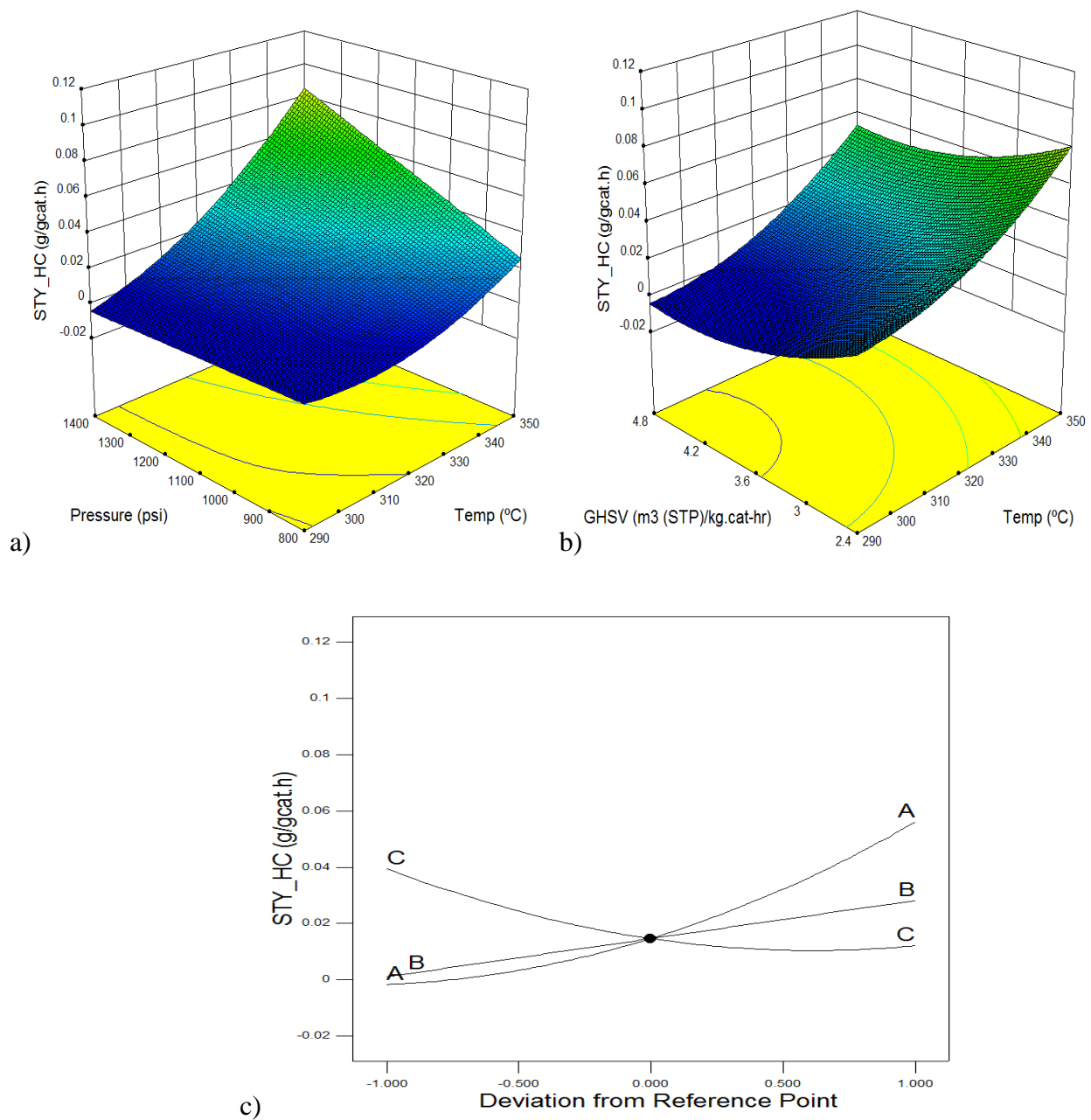


Fig. 8.6: The effects of temperature, pressure, and GHSV on hydrocarbon STY over KCoRhMo/CNH catalyst. (a & b) 3-D surface responses; (c) Perturbation plot

The dependence of STY of CO₂ follows a similar trend as that of the hydrocarbon formation. As can be seen in Figures 8.7 (a-c), by comparing STYs of byproducts, it was observed that slightly higher STY of CO₂ was recorded at all experimental conditions than that of hydrocarbons. This suggests that the KCoRhMo/CNH catalyst appreciably enhanced the water gas shift reaction as well. An R² value of 0.9736 was recorded from its model fitting (Table 8.2).

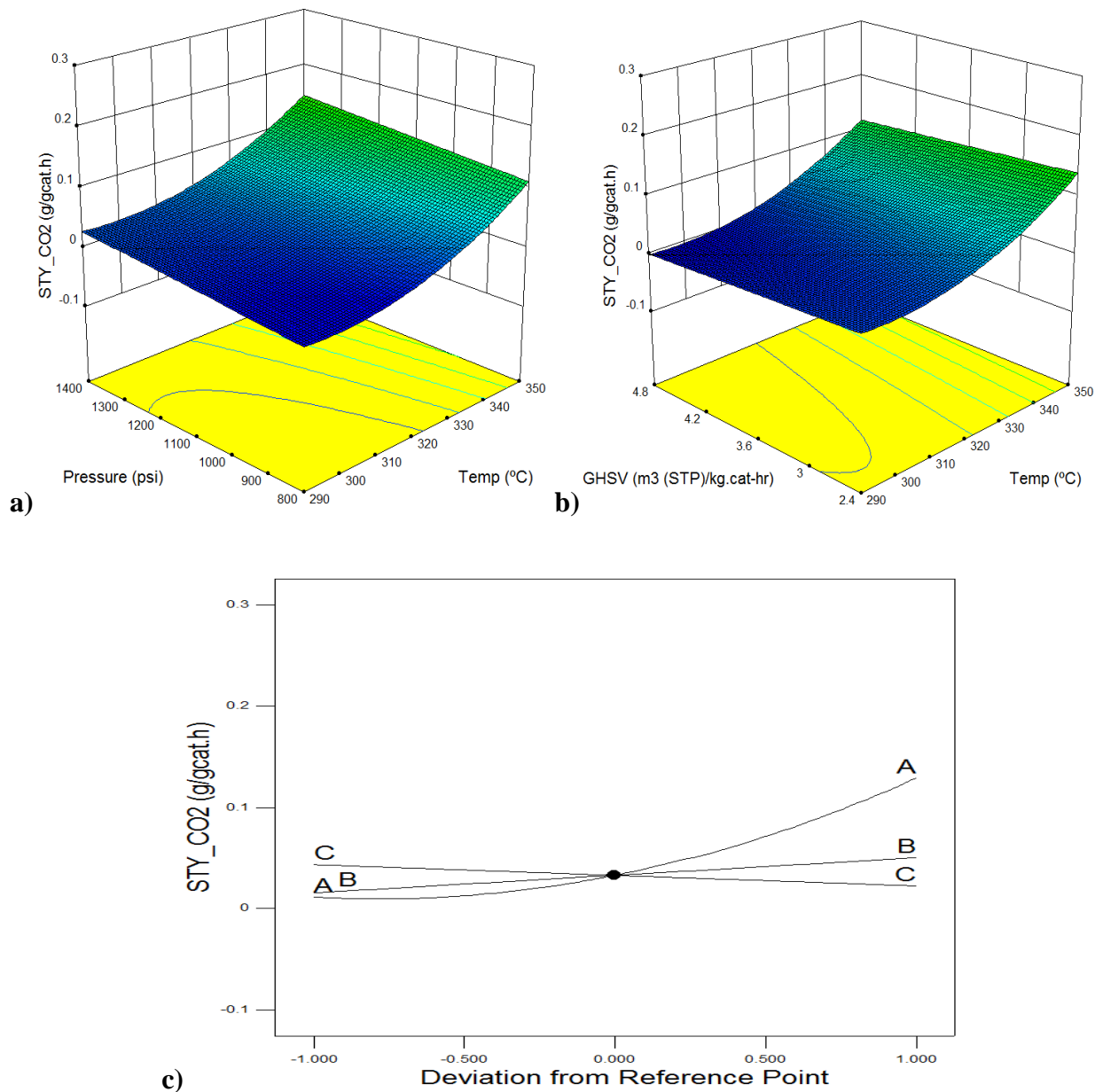


Fig. 8.7: The effects of temperature, pressure, and GHSV on CO₂ STY over KCoRhMo/CNH catalyst. (a & b) 3-D surface responses; (c) Perturbation plot

8.4.9. Effects of temperature, pressure, and gas hourly space velocity on selectivity of alcohols

The model equations generated for the selectivities (wt.%) of methanol, ethanol, higher alcohols, and total alcohols spanning the operating conditions investigated are presented as follows:

$$S_{MeOH} = -93.21325 + 0.67943 * T + 2.61126 * P + 8.28943 * GHSV - 1.24451 * 10^{-3} * T^2 - 1.21846 * GHSV^2 \dots \dots \dots (8.8)$$

$$S_{EtOH} = -242.01008 + 1.36203 * T + 0.062527 * P - 1.195 * GHSV - 2.04918 * 10^{-3} * T^2 - 2.50307 * 10^{-5} * P^2 \dots \dots \dots (8.9)$$

$$S_{HA} = -265.96 + 1.52 * T + 0.08 * P - 11.12 * GHSV - 2.21 * 10^{-3} * T^2 - 2.97 * 10^{-5} * P^2 + 1.33 * GHSV^2 \dots \dots \dots (8.10)$$

$$S_{Tot. Alc.} = -41.10071 - 8.70623 * 10^{-3} * T + 0.13953 * P - 1.90515 * GHSV - 5.44405 * 10^{-5} * P^2 \dots \dots \dots (8.11)$$

$$S_{HC} = 228.83398 - 1.59128 * T + 8.0006 * P - 1.05876 * GHSV + 2.75532 * 10^{-3} * T^2 \dots \dots \dots (8.12)$$

$$S_{CO_2} = 301.6488 - 1.9808 * T + 0.011292 * P - 11.16191 * GHSV - 3.41661 * 10^{-3} * T^2 + 1.35518 * GHSV^2 \dots \dots \dots (8.13)$$

Table 8.3 shows the results of the test of significance of factors or interactions for the selectivities of methanol, ethanol, higher alcohols, total alcohols, hydrocarbons, and CO₂ after power transformation and discarding insignificant terms. It also presents R² statistics for all models depicting the products selectivities. The predicted R² and adjusted R² values were quite

comparable. For generating these models, the power transform analysis was carried out on the various responses. The range of the response under study was first found and the ratio of the maximum value to the minimum was then computed. A ratio greater than 10 usually indicates that power transform is required. In cases where the ratio was less than 3, power transforms had little effects on the response parameter.

Table 8.3: Test of significance results for independent factors or interactions for the model derived for the selectivities of different products.

Variable/interactions	p-value of models after rejecting insignificant variables					
	S _{MeOH}	S _{EtOH}	S _{Tot. Alc.}	S _{HA}	S _{HC}	S _{CO2}
A-Temp	0.0024	0.0987	0.8849	0.0008	0.0001	< 0.0001
B-Pressure	0.4276	0.0212	0.0046	< 0.0001	0.0317	0.0034
C-GHSV	0.5435	0.1129	0.2118	0.029	0.2181	0.0927
AB	-	-	-	-	-	-
AC	-	-	-	-	-	-
BC	-	-	-	-	-	-
A ²	0.2458	0.0435	-	0.0177	0.0222	0.0051
B ²	-	0.0176	0.0124	0.003	-	-
C ²	0.0841	-	-	0.0229	-	0.0582
Model	0.00199	0.0066	0.0052	< 0.0001	0.0003	< 0.0001
R ²	0.9325	0.9499	0.9605	0.9714	0.9323	0.9534
R ² adjusted	0.9234	0.9249	0.9506	0.9611	0.91254	0.9356

The developed models were significant, with their p-values less than 0.0001. A good agreement between the simulated results and the experimental observed data suggested that the

models can be applied reliably within the design space of the independent factors. The methanol selectivity decreased monotonically with increasing temperature, but increased with increasing pressure and GHSV.

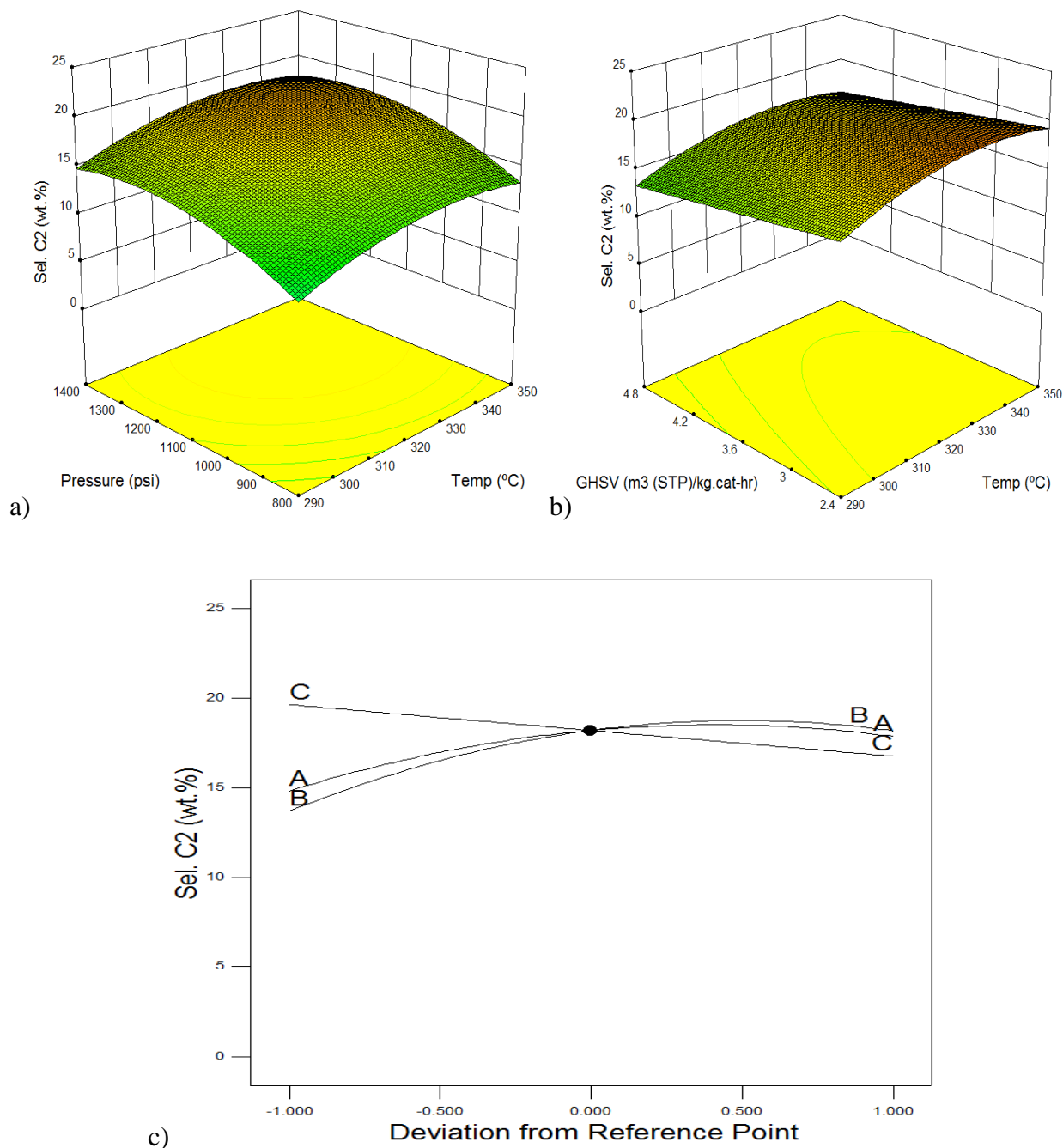


Fig. 8.8: The effects of temperature, pressure, and GHSV on ethanol selectivity over KCoRhMo/CNH catalyst. (a & b) 3-D surface responses; (c) Perturbation plot

The ethanol, higher alcohols, and total alcohols selectivities displayed pronounced increases with increasing temperature and reached a maximum value. Higher reaction temperature can promote the dehydration of higher alcohols formed to produce corresponding alkenes and water. With increasing pressure, ethanol selectivity increased to a certain value and remained constant, whereas, ethanol selectivity slightly decreased with increased GHSV (Fig. 8.8b).

The higher alcohols and total alcohols selectivity monotonically increased with increasing pressure and GHSV (figures are shown). This discrepancy between the ethanol and higher alcohols selectivities at higher pressures and GHSVs is due to the increasing ability of chain growth from ethanol to higher alcohols.

8.5. Process parameters optimization and reproducibility study

The optimum operating conditions using H₂ to CO molar ratio of 1.25 were defined using the numerical optimization procedure in Design Expert software according to the following constraints: (1) Ethanol and higher alcohol selectivities and STYs to be maximized; and (2) hydrocarbons and CO₂ selectivities and STYs to be minimized. The best solution was chosen from 22 solutions generated based on the desirability factor, which assigns a score to the set of multiple responses (products selectivities and STYs) evaluated and suggests a group of parameter combinations that maximizes the overall score. The optimum operating conditions selected was T = 325°C, P = 9.1 MPa, and GHSV = 2.4 m³ (STP)/(kg of cat.)/h., with a desirability factor of 0.73 as can be seen in the Table 8.4.

Table 8.4: The results of optimization studies (T=290-350°C; P=800-1400 psig (5.52-9.65 MPa); GHSV=2.4-4.8 m³ (STP)/kg of cat-h, catalyst = 1g)

#	T	P	GHSV	CO conversion, %	Selectivity (wt.%)		STY (g/g of cat-h)				Desirability	
					S _{Tot. Alc.}	S _{HA}	STY _{Tot. Alc.}	STY _{HA}	STY _{HC}	STY _{CO₂}		
1	324.8	1320.0	2.40	41.70	40.14	29.85	0.38	0.18	0.06	0.07	0.728	<i>Selected</i>
2	324.4	1320.0	2.40	41.53	40.14	29.82	0.38	0.18	0.06	0.07	0.728	
3	325.1	1310.0	2.40	41.90	40.14	29.88	0.38	0.18	0.06	0.07	0.728	
4	325.5	1320.0	2.40	42.07	40.13	29.91	0.38	0.18	0.06	0.07	0.728	
5	323.9	1320.0	2.41	41.21	40.14	29.75	0.38	0.18	0.06	0.07	0.728	
6	322.4	1310.0	2.40	40.43	40.16	29.63	0.38	0.18	0.06	0.07	0.727	
7	324.7	1310.0	2.43	41.52	40.09	29.72	0.38	0.18	0.06	0.07	0.727	
8	321.9	1308.0	2.40	40.09	40.19	29.59	0.38	0.18	0.06	0.06	0.725	
9	316.8	800.0	3.35	20.88	26.55	17.11	0.22	0.11	0.00	0.01	0.715	
10	316.8	800.0	3.34	20.92	26.56	17.13	0.22	0.11	0.00	0.01	0.715	

In this regard, a few experiments were performed at these optimized operating conditions to test the validity of the developed models for the prediction of both STY and selectivity of ethanol as well as data reproducibility. A marginal error of $\pm 5\%$ in both the ethanol STY and selectivity suggests that the models can be reliable for products selectivities and STYs predictions during the HAS reaction.

Table 8.5: The results of reproducibility studies

Repetitions #	CO conversion (%)	Selectivity (wt.%)		STY (g/g of cat-h)			
		Tot. Alc.	HA	Tot. Alc.	HA	HC	CO ₂
1*	41.70	40.14	29.85	0.38	0.177 \pm 0.01	0.06	0.07
2*	41.53	40.14	29.82	0.38	0.177 \pm 0.01	0.06	0.07
3*	41.90	40.14	29.88	0.38	0.176 \pm 0.01	0.06	0.07
4‡	42.07	40.13	29.91	0.38	0.18 \pm 0.01	0.06	0.07
5‡	41.21	40.14	29.75	0.38	0.18 \pm 0.01	0.06	0.07
6‡	40.43	40.16	29.63	0.38	0.18 \pm 0.01	0.06	0.07

*Same catalyst was used for experiment; ‡Freshly loaded catalysts used for experiments

Reproducibility of the experimental data was tested at the optimized operating T, P, and GHSV using the same syngas feedstock. A set of three experimental runs were repeated at these conditions using the spent KCoRhMo/CNT catalyst to determine the error margins in selectivity and space time yields of products as reported in Table 8.5. Also, in order to determine the effect of packing on the experimental results, the reactor was reloaded with a fresh batch of catalyst and another set of three experimental runs were repeated at the optimized conditions. The unequal sample sizes equal variance Student's *t* test method was used to determine reproducibility of the results. The results indicated that the standard deviation associated with the measurement of the sample was minimal, providing evidence that the means are representative of the data collected. This proves that the data were reproducible with small (≤ 5) experimental errors as shown in Table 8.6.

Table 8.6: Means and standard errors of data sets for reproducibility studies (T=325°C; P=9.1 MPa; GHSV=2.4 m³ (STP)/kg of cat-h, catalyst = 1g)

Expt. Set	CO conversion (%)	Selectivity (wt.%)		STY (g/g of cat-h)			
		Tot. Alc.	HA	Tot. Alc.	HA	HC	CO ₂
A	39.93 ±	39.81 ±	24.01 ±	0.42 ±	0.16 ±	0.01 ±	0.11 ±
	0.73	1.02	0.21	0.01	0.003	0.002	0.002
B	50.63 ±	48.13 ±	34.81 ±	0.54 ±	0.25 ±	0.12 ±	0.14 ±
	0.93	1.13	0.41	0.01	0.001	0.013	0.013

8.6. Conclusions

A CNH-supported K-promoted trimetallic sulfided Co-Rh-Mo catalyst was used to study the effects of operating conditions on the higher alcohols synthesis reaction from synthesis gas. Quadratic models were developed using the central composite design (CCD) method for % CO conversion, products STY, and alcohol selectivities as functions of T, P and GHSV using an H₂ to

CO molar ratio of 1.25. The statistical tests, test of significance, and R^2 value statistics proved that the models could adequately represent the experimental data. The %CO conversion increased monotonically with increasing reaction temperature (from 290 to 350°C) and pressure (from 5.52-9.65 MPa), while decreasing monotonically with increasing GHSV (from 2.4 to 4.8 m³ (STP)/(kg of cat.)/h). The ethanol STY and selectivity reached a maximum value with respect to temperature and GHSV, while increasing to a constant value with increasing pressure. The ethanol STY and selectivity obtained at optimum T, P, and GHSV were in good agreement with model predictions. A Student's t-test confirmed that the data are reproducible with small ($\leq \pm 5$) experimental errors. = 325°C, P = 9.1 MPa, and GHSV = 2.4 m³ (STP)/(kg of cat./h)).

CHAPTER 9

Higher alcohols synthesis over carbon nanohorn-supported KCoRhMo catalyst: Influence of bentonite clay incorporation, mass transfer considerations, and kinetic modelling.

The content of this chapter has been prepared and submitted for Journal publication.

Citation:

Boahene P.E., Dalai A.K. (2017) Higher alcohols synthesis over CNH-supported KCoRhMo catalyst: Influence of bentonite clay incorporation, mass transfer considerations and kinetic modelling (Submitted to Industrial & Engineering Chemistry Research – Under review).

Contribution of the Ph.D. Candidate

Preparation of the KCoRhMo/CNH and KCoRhMo/5%BC-CNH catalysts as well as their screening tests were performed by Philip Effah Boahene. Data collection, analysis and interpretations were performed by Philip Boahene with assistance from Dr. Ajay Kumar Dalai. The Polymath program for data model development and experimental data fitting was done by Philip Effah Boahene. All of the writing of the manuscript to be submitted for publication was done by Philip Effah Boahene and discussed with Dr. Ajay Dalai. Dr. Dalai provided editorial guidance regarding the style and content of this work.

Contribution of this chapter to overall study

In chapter 4, the influence of three binders (bentonite clay, coal tar, and humic acid) incorporation, pelletization and particle size effects was investigated for the HAS reaction using

KCoRhMo/MWCNT catalyst system. A performance trend was observed with the bentonite clay-incorporated catalyst exhibiting the best mechanical strength (~340 N). In this chapter, 5 wt.% bentonite clay was incorporated into the formulation of KCoRhMo/CNH catalyst developed from chapters 7 and 8. Furthermore, the effects of mass transfer (internal and external) were evaluated by running experiments with this catalyst of different particle sizes (i.e. finely ground powder (88 μm) and two pelletized forms – with and without bentonite clay added). It should be noted that the mesh size of 210-297 μm (i.e. particle size 254 μm or 0.254 mm) was chosen for the pelletized catalysts from a previous study by Surisetty et al., 2010 since it exhibited the optimum particle size range beyond which external mass transfer diffusion affected the intrinsic kinetics of the HAS reaction. The power law model was then used to fit the experimental data collected using the catalyst exhibiting no external mass transfer limitations. Finally, the activation energies, reaction orders and rate constants for the alcohol products have been compared with similar studies reported in the literature.

9.1. Abstract

In this study, two catalyst grain sizes (fine powders and pellets) have been investigated to elucidate the effects of particle size on both external and internal mass transfer diffusion during the higher alcohol synthesis reaction. The catalyst grain sizes (88 μm and 254 μm) were advisedly chosen based on our previous investigations with a similar catalyst matrix for the CO hydrogenation reaction. The influence of bentonite clay as a binder was also investigated by incorporating 5wt.% of this binder into the formulation of the KCoRhMo/CNH catalyst. A series of experiments were performed in a downward flow fixed-bed reactor to evaluate the intrinsic kinetics of the formation of the liquid alcohol products (methanol, ethanol, higher alcohols) as well as the gaseous products generated by the reaction. Syngas of H_2/CO ratio of 1.25 was used as

feedstock under the reaction conditions: $T=290-350^{\circ}\text{C}$; $P=5.52-9.65\text{ MPa}$ and $\text{GHSV}=2.4-4.8\text{ m}^3$ (STP)/(kg of cat.)/h. For mass transfer considerations, the finely ground powdered form of the catalyst (with particle size of $88\text{ }\mu\text{m}$) was used so as to eradicate mass transfer resistance. Experimental data were fitted with the power law model and the kinetic parameters for higher alcohols synthesis on the catalyst surface were determined. Fitting of the experimental data with the developed power law models showed good fits with high R^2 values for the components evaluated. The activation energies computed for ethanol and propanol in the HAS reaction over CNH-supported KCoRhMo catalyst were 54.4 and 92.2 kJ/mol , which are low compared to values obtained by other researchers in a similar study.

9.2. Introduction

Mixed alcohols including C_{2+} alcohols are considered worldwide as additives to boost octane levels in gasoline fuels (National Resources Canada, 2016; Luk et al., 2017). Higher alcohols synthesis from syngas conversion provides an alternative direct catalytic synthesis route to produce fuels and industrial chemicals (Fei et al., 2014). Though much research works have appeared in the literature on this topic, there is still the need to further enhance the yields and selectivities of these alcohols to make them commercially attractive.

Heterogeneous catalytic systems for the higher alcohol synthesis (HAS) reaction based on MoS_2 matrix is as a result of its high sulfur tolerance and high activity for the water-gas-shift reaction (Woo et al., 1991). The reaction mechanisms for the generation of higher alcohols on this MoS_2 catalyst matrix was proposed to follow the classical CO insertion into the corresponding precursor alcohol (Santesteban et al., 1988). The product distribution and carbon chain growth scheme over these catalysts follows the Anderson-Schulz-Flory (ASF) polymerisation pathway (Smith et al., 1984). The incorporation alkali promoters suppress the hydrogenation ability of

surface alkyl species to form alkanes; thus, increasing the active sites needed for higher alcohols formation (Gandia et al., 1994).

The alcohol products selectivities can be affected by the formulation of the catalyst (i.e active metals, support materials, binders, etc.) as well as the reaction kinetics (Forzatti et al., 1981; Herman, 2000; Subramani et al., 2008). For instance, KCoRhMo catalysts supported on multi-walled carbon nanotubes (MWCNTs) outperformed its counterparts for higher alcohol synthesis (Surisetty, 2010; Haifeng et al., 2015). Furthermore, in our previous work, we investigated the influence of selected binders (bentonite clay, coal tar and humic acid) incorporation into the formulation of MWCNT-supported KCoRhMo catalyst and their subsequent pelletization for the HAS reaction (Boahene et al., 2014). It was concluded that though the crushing strength of the binder-incorporated catalysts followed the order: bentonite clay > coal tar > humic acid, the pelletized catalyst formulated with bentonite clays as a binder exhibited the best mechanical strength (~340N) prior to crushing into fines as compared to the pelletized binder-free catalyst (1.4N). That notwithstanding, though MWCNT and OMC-supported KCoRhMo catalysts have also proven tendencies to produce mixed alcohols, it was concluded from our previous study that carbon in the form of carbon nanohorns (CNH) can be a superior catalyst support for syngas conversion applications as compared to its other carbon byproducts generated during the submerged arc in liquid nitrogen experiment (Boahene et al., 2017).

In a typical CO hydrogenation reaction where diffusion of reactants or products between the bulk fluid and the external catalyst surface precedes surface reaction, mass transfer considerations becomes relevant if reliable experimental data collection is to be obtained. In cases where diffusion of the reactants from the external surface (pore mouth) to the interior (active site) of the particles and the subsequent diffusion of products from the interior of the particles to the

external surface becomes prevalent, internal resistances can influence experimental data collected. For a true representative experimental data collection for kinetic studies and modelling, the data collection for kinetic parameters determination as well as rate expressions generations needs to be acquired in the absence of both external and internal diffusion resistances (Fogler, 1999). For kinetic parameters evaluations during the HAS reaction, the two commonly used models for data fitting and rate expressions generations are the Langmuir-Hinshelwood and Power Law models (Gunturu et al., 1998; Beretta et al., 1998, Surisetty, 2010). Though the former model can be complicated, the power law model has commonly been used for data fitting of the HAS reaction due to its simplicity (Surisetty, 2010, Portillo et al., 2016).

The motivation of the present study was to investigate the intrinsic kinetic data for higher alcohols synthesis from synthesis gas over KCoRhMo/CNH catalyst using a central composite designed (CCD) experimental plan. This statistical design approach minimizes the overall variance of the estimated parameters and reduces the number of trials required without restricting the confidence region for the estimated parameter. This work also evaluated the influence of bentonite clay as a binder for the KCoRhMo/CNH catalyst formulation as well as relevant mass-transfer diffusion considerations prior to data acquisition for intrinsic kinetic parameters computations during the HAS reactions.

9.3. Experimental

The syntheses of pristine carbon nanohorn support was accomplished using the submerged arc discharge in liquid nitrogen technique at a fixed current of 90A and 34V. The detailed description of the techniques employed to separate these carbon nanoparticles after syntheses, as well as their corresponding KCoRhMo catalysts formulations can be found in Chapter 3, sections

3.2.2 to 3.2.5 of thesis. Furthermore, characterization techniques employed as well as the CO hydrogenation experimental procedures have also been discussed in Chapter 3.

9.4. Results and discussion

9.4.1. Influence of bentonite clay and external mass-transfer diffusion evaluations

In heterogeneous catalytic reaction where reaction of reactants and generation of products occur on the surface of the catalyst particle, the species diffusion through the imaginary boundary layer surrounding the catalyst pellet is important (Fogler, 1999). The boundary layer is a region of laminar flow directly adjacent to the catalyst pellet whereby diffusion can only take place by molecular means (Fogler, 1999; Kent, 2013). In reaction kinetics, the influence of external mass-transfer resistances can affect the overall rate of reaction. However, depending on the boundary layer thickness, diffusion of reactant species from the bulk fluid to the catalytic active site in the pores can be hindered. The boundary layer thickness is represented by the distance from the solid catalyst particle to the region where the concentration of the diffusing species reaches 99% of the bulk concentration (Fogler, 1999). Also, the mass transfer coefficient (k_c) is related inversely to the boundary layer thickness (δ) and directly to the diffusion coefficient (D_e) by the correlation:

$$\delta = \frac{D_e}{k_c} \dots \dots \dots (9.1)$$

where k_c is the mass transfer coefficient (m/s), which accounts for the resistance to mass transfer resulting from the boundary layer and D_e is the diffusion coefficient (m^2/s), which determines the extent of diffusion of reactants through the mixture. The impact of boundary later thickness can be eliminated either by using very small catalyst particle sizes or increasing the fluid velocity in the region of the particles (Fogler, 1999).

The influence of external mass transfer was investigated using one gram of KCoRhMo/CNH catalyst for the HAS reaction. Catalyst samples of two mesh sizes 75-100 and

210-297 μm , with average particle size ranges of 0.088 and 0.254 mm, were used. In addition, two catalyst of the latter particle sizes were made with 0 and 5% bentonite loadings, respectively, to help study the influence of binder incorporation in the catalyst formulation. Feed gas of molar compositions: 50 % H_2 , 40 % CO , and 10 % Ar was used. The HAS reactions were carried out under conditions: $T = 290\text{-}350^\circ\text{C}$, $P = 9.1 \text{ MPa}$, and $\text{GHSV} = 2.4 \text{ m}^3 \text{ (STP)}/(\text{kg of cat.})/\text{h}$.

As can be seen in Figure 9.1, increasing the particle size resulted in a slight decrease in CO conversion and total alcohols selectivities at all temperatures studied. A similar trend can be observed with the incorporation of bentonite clay as a binder. This decrease in higher alcohols productivity could be explained by the reduction of textural properties of the binder-incorporated catalyst as opposed to its binder-free counterpart. Incorporation of binders decreased the surface area from 373 to 336 m^2/g (i.e. 9.9 % reduction); resulting in a limited active surface area for the interaction of reactant species during the HAS reaction. One can expect that the catalyst with smaller particle size (0.088 mm) performed better than its counterpart due to the relatively shorter distance reactants must travel to reach the active sites in the catalyst pores. Moreover, with smaller particle size, the internal diffusion limitations will be reduced as a result of reactants taking lesser time to diffuse into and out of the interior of the particle.

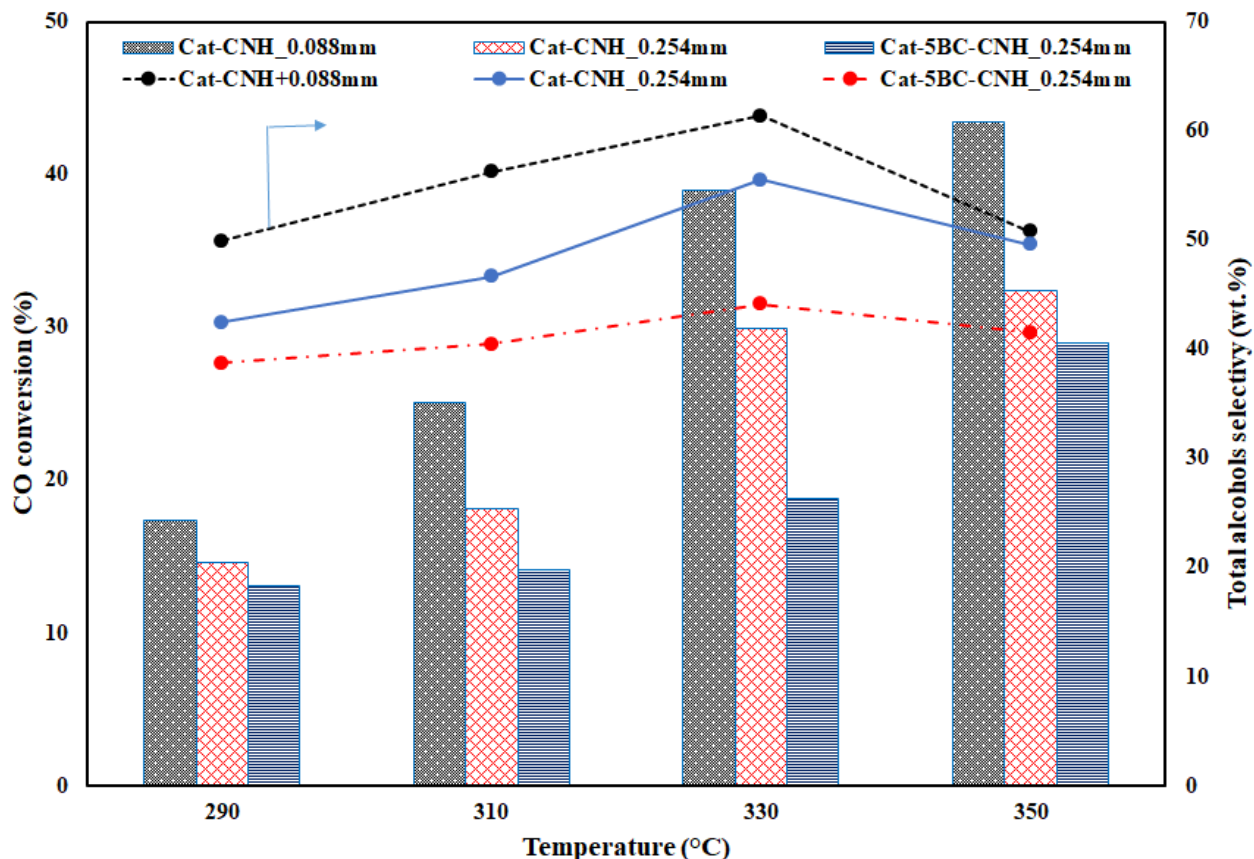


Fig. 9.1: Effects of different catalyst particle sizes and temperature on CO conversion and total alcohols selectivities over KCoRhMo/CNH catalysts.

It can also be seen from Figure 9.2 that increasing the average catalyst particle size from 0.088 to 0.254 mm resulted in corresponding decrease in higher alcohols STY at all reaction temperatures evaluated; suggesting that catalyst particle size influenced the higher alcohols synthesis reaction. It should be noted that in a similar work reported by Surisetty et al., 2010, it was concluded that mass transfer across the boundary layer limited the rate of reaction when catalyst with particle size (d_p) greater than 0.254 mm was used for the HAS reaction (Surisetty et al., 2010). In this regard, the catalyst with $d_p < 0.254$ mm (i.e. the fine powder) was used in the experiment for the kinetic parameters evaluation so as to ensure negligible resistances to external mass transfer.

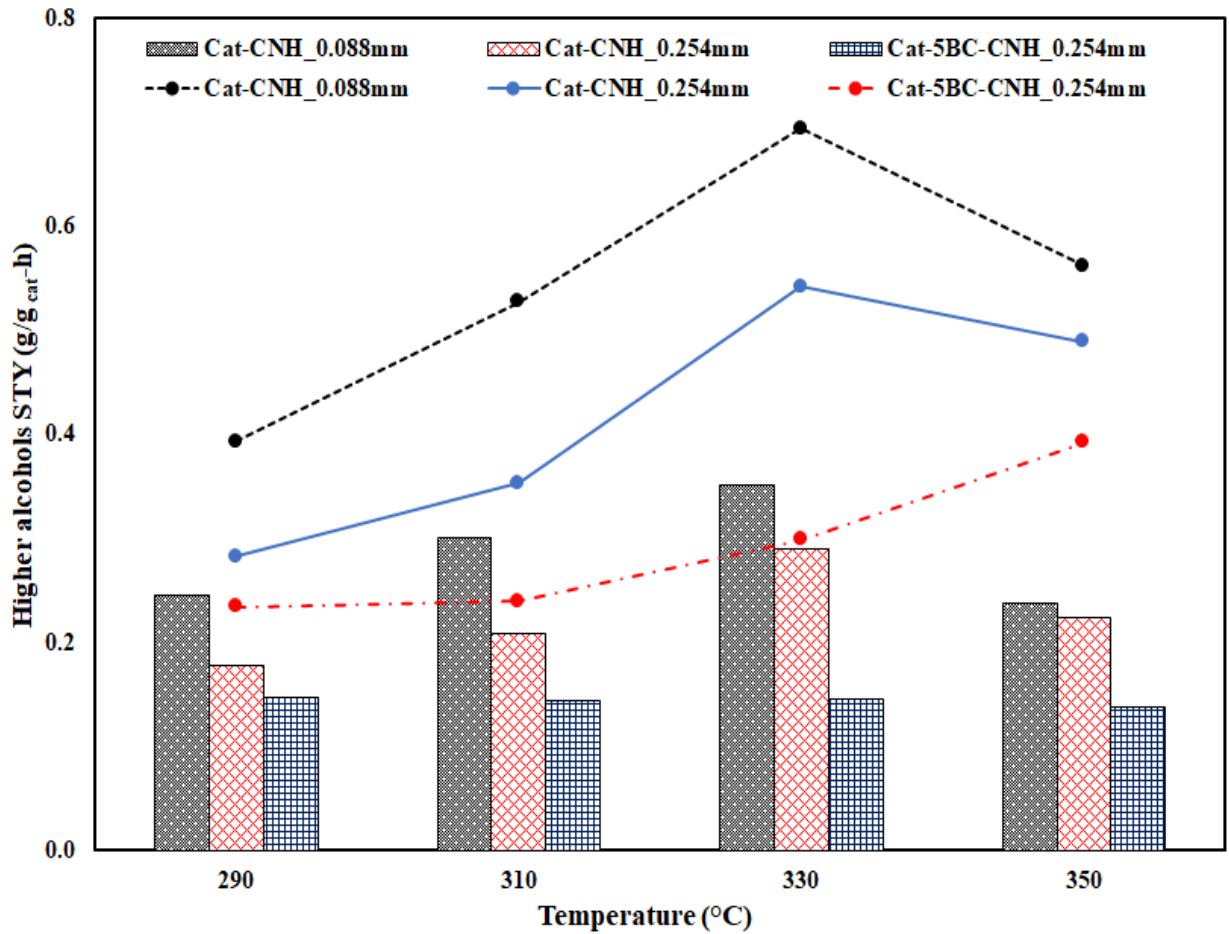


Fig. 9.2: Effects of different catalyst particle sizes and temperature on higher alcohols space-time-yield (STY) over KCoRhMo/CNH catalysts.

The Frössling correlation (Frössling, 1938) is applied to flow of fluid around spherical particles to obtain the relation between the particle size (d_p) of the catalyst, mass-transfer coefficient (k_c), and boundary layer thickness (δ). The required parameters and constants for the estimation of Frössling correlation were calculated and are presented in Table 9.1 using the following correlations (Surisetty et al., 2010):

$$Sh = 2 + 0.6 (Re)^{1/2} (Sc)^{1/3} \dots\dots\dots (9.2)$$

where Sh , Re , and Sc are the Sherwood, Reynold's and Schmidt's numbers, respectively, and are given by:

$$Sh = \frac{k_c d_p}{D_e} \dots \dots \dots (9.3)$$

$$Sc = \frac{\mu}{\rho D_e} \dots \dots \dots (9.4)$$

$$Re = \frac{\rho u d_p}{\mu} \dots \dots \dots (9.5)$$

where d_p is the average diameter of the catalyst particle (m), u is the free stream velocity of fluid (m/s), ρ is the gas density (kg/m^3), and μ is the gas dynamic viscosity (kg/(m-s)).

It is quite clear from the calculated values presented in Table 9.1 that variation of catalyst particle size affected the rate of reactants diffusion during the HAS reaction. As the particle size of Cat-CNH was decreased from 0.254 to 0.088 mm, a corresponding increase in the value of mass transfer coefficient was observed at all temperatures studied. For the binder-free catalysts of different particle sizes, k_c values of about 2.4 times more were recorded at all temperatures as particle size decreased from 0.254 to 0.088 mm. Similarly, it can be noted that k_c values of about 2.6 times more were recorded for the binder-incorporated catalyst within the same particle size range; suggesting that the incorporation of binder did not significantly hinder the external mass transfer diffusion of reactants from bulk flow to the catalyst particles. This observation could be corroborated with the marginal decreases in k_c and δ values for Cat-CNH and Cat-5BC-CNH of the same average particle sizes. Finally, within the range of temperature studied (290-350°C), the k_c and δ values were not significantly affected; suggesting a negligible influence of temperature on the external mass-transfer diffusion.

To investigate the influence of gas flow rate on external mass transfer diffusion, 1 g of Cat-CNH (average particle size = 0.088 mm) was used in the HAS experiment with the same syngas composition and under the specified conditions: T = 325°C, P = 9.1 MPa, and GHSV = 1.6 - 5.6 m³/kg_{cat}-h.

Table 9.1: Influence of particle size and binders on the external mass transfer diffusion

T (°C)	Parameters	Sample ID		
		Cat-CNH	Cat-CNH	Cat-5BC-CNH
290	<i>Av. particle size (mm)</i>	0.088	0.254	0.254
	k _c (m/s)	1.65*10 ⁻³	6.87*10 ⁻⁴	6.28*10 ⁻⁴
	δ (mm)	3.12*10 ⁻²	7.49*10 ⁻²	7.38*10 ⁻²
310	<i>Av. particle size (mm)</i>	0.088	0.254	0.254
	k _c (m/s)	1.72*10 ⁻³	7.17*10 ⁻⁴	6.59*10 ⁻⁴
	δ (mm)	3.16*10 ⁻²	7.56*10 ⁻²	7.46*10 ⁻²
330	<i>Av. particle size (mm)</i>	0.088	0.254	0.254
	k _c (m/s)	1.80*10 ⁻³	7.47*10 ⁻⁴	6.82*10 ⁻⁴
	δ (mm)	3.16*10 ⁻²	7.63*10 ⁻²	7.52*10 ⁻²
350	<i>Av. particle size (mm)</i>	0.088	0.254	0.254
	k _c (m/s)	1.89*10 ⁻³	7.79*10 ⁻⁴	7.10*10 ⁻⁴
	δ (mm)	3.18*10 ⁻²	7.69*10 ⁻²	7.59*10 ⁻²

Table 9.2 shows the variation of feed gas flow rate on CO conversion as well as external mass transfer parameters (k_c and δ). Increasing the feed gas flow rate resulted in a slightly increased corresponding k_c values; however, the δ values decreased accordingly. This means that at high gas flow rates, the boundary layer thickness around the catalyst particle reduces; thus, enhancing the faster diffusion of reactants species. However, the resulting shorter contact times at

higher flow rates resulted in the lower CO conversions recorded as gas flow rate was increased from 26.3 to 93.7 mL/min. In addition, under the operating conditions investigated for Cat-CNH sample (average particle size of 0.088 mm) and from the corresponding k_c and δ values computed at different flow rates, one can deduce that feed gas flow rate only had a negligible effect on external mass-transfer diffusion during the HAS reaction.

Table 9.2: Effects of gas flow rate on CO conversion and external mass transfer diffusion

GHSV (m³/kg_{cat}-h)	Flow rate (mL/min)	CO conversion (%)	k_c (m/s)	δ (mm)
1.6	26.3	47.9	1.61*10 ⁻³	3.49*10 ⁻²
2.4	40.0	41.5	1.69*10 ⁻³	3.33*10 ⁻²
3.6	60.0	29.6	1.78*10 ⁻³	3.16*10 ⁻²
4.8	80.0	20.4	1.86*10 ⁻³	3.02*10 ⁻²
5.6	93.7	15.3	1.91*10 ⁻³	2.95*10 ⁻²

(Conditions: T = 325°C; P = 9.1 MPa; average particle size = 0.088 mm; catalyst weight = 1g)

9.4.2. Internal mass-transfer diffusion evaluation

For the HAS reaction, the Weisz–Prater criterion (C_{WP}) was used to ascertain the possibility of internal mass transfer resistance during the catalytic reactions. To validate this criterion, C_{WP} should either be far less than 1 or greater than 1 to suggest a conclusion (Fogler, 1999). In cases where internal diffusion of reactant species has insignificant effect on the reaction rate, the calculated C_{WP} value becomes very small (i.e., $C_{WP} \ll 1$); and if internal diffusion severely limits the reaction rate, then $C_{WP} \gg 1$ (Weisz, 1954; Fogler, 1999). The Weisz–Prater criterion (C_{WP}) can be given as follows:

$$C_{WP} = \frac{-(r_A)_{obs} * \rho_c * r^2}{C_{As} * D_e} \dots \dots \dots (9.6)$$

where $(r_A)_{\text{obs}}$ is the reaction rate per unit mass of catalyst; ρ_c is the catalyst density, r is the particle radius, C_{As} is the surface concentration of reactant A, and D_e is the effective diffusivity. The calculated value for Cat-CNH with average particle diameter of 0.088 mm at 325°C was obtained as 1.49×10^{-3} , which is far less than 1. This confirms that internal diffusion limitation is negligible on the catalyst with the average particle diameter of 0.088 mm.

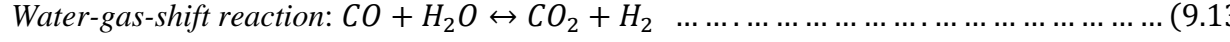
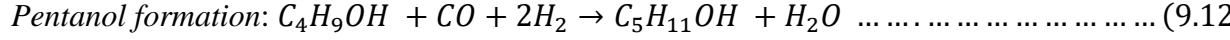
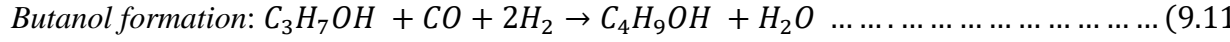
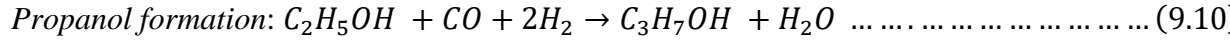
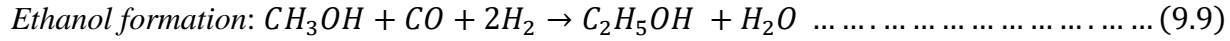
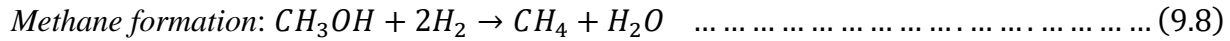
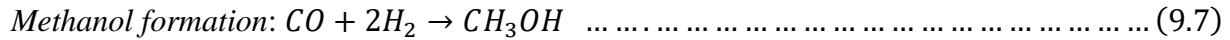
9.4.3. Intrinsic kinetic parameters analyses

In heterogeneous catalytic reaction, reliable kinetic experiments and data collection are critical for intrinsic kinetic parameters determination and analysis as well as the development of consistent rate expressions for industrial reactor design purposes. As opposed to apparent kinetics, which minimizes mass transport effects, the possibilities of diffusion transport limitations is key in intrinsic chemical kinetics. During the HAS reaction, liquid products analysis showed predominantly linear alcohols namely; methanol, ethanol, n-propanol, n-butanol, and pentanol. The amount of water in the liquid product was minimal (i.e. less than 1 wt. %); thus, its concentration was neglected. The gas product analysis confirmed methane as the major hydrocarbon component along with CO_2 and unreacted syngas species ($\text{CO} + \text{H}_2$).

9.4.3.1. Reaction scheme for higher alcohols synthesis

In the HAS reaction over the sulfided KCoRhMo/CNH catalysts, the reaction scheme proposed by Santiesteban and coworkers (Santiesteban et al., 1988) was used to evaluate the intrinsic reaction kinetics. Due to the complex nature of the series of chemical reactions taking place, it is quite challenging for a statistically valid model to be developed to account for all the products and their complexities. In this regard, the simplified reaction scheme based on the kinetic model of five main alcohol products and two main gaseous products was considered (Portillo et

al., 2016). In this approach, components in the product streams selected includes MeOH, EtOH, PrOH, BuOH, PeOH, CO₂, and CH₄. The CO insertion mechanism as proposed by Santiesteban and Park was used due to its successful application to describe the kinetics of the HAS reaction over MoS₂ catalyst matrix (Santiesteban, 1988; Gunturu et al., 1998). In this study, all the alcohols formed were assumed to be linear (C₁ to C₅) and the reactions were assumed to be stoichiometric with their respective simplified reaction schemes for products formation. The reaction equations for the products formation are provided as:



Finally, aside from the water-gas-shift reaction (eqn. 9.13) which is assumed to be reversible, all the other reactions were assumed to be irreversible (Portillo et al., 2016).

9.4.3.2. Assumptions for kinetic models development

Assumption made in the development of kinetic models include: 1) formation of the starting methanol precursor is to be obtained directly from CO and H₂; 2) methane is predominantly the major product in the hydrocarbon stream; 3) apart from the water-gas-shift (WGS) which is assumed to be in thermodynamic equilibrium, all the other reactions are supposed to be irreversible; and 4) ethanol and higher alcohols (C₂₊) formation proceeded by stepwise chain

growth of alcohols by CO insertion into the lower molecular weight alcohol as the recurrent precursor for CO hydrogenation. (Santiesteban, 1988; Portillo et al., 2016).

9.4.3.3. Considerations for rate expressions development for the HAS reaction

The power law model was used for the surface catalytic reaction occurring in the CO hydrogenation reaction. Due to the simplicity of this model for the prediction of kinetic parameters, it has been widely used in applications for the higher alcohols synthesis reaction (Gunturu et al., 1998; Christensen et al., 2009; Surisetty et al., 2010). The approach used by Portillo and coworkers (Portillo et al., 2016) was adopted in this work. In this regard, whereas reversible kinetic expressions were used for the WGS reactions, irreversible kinetic expressions were applied to the remaining products formed (eqns. 9.6-9.13). Also, the non-ideal behavior of gases under operating conditions (high temperature and pressures) was also considered in the model development (Portillo et al., 2016). The following rate equations can be written for the components in the HAS reaction as:

$$r_{MeOH} = A_1 * \exp\left(-\frac{E_{a,M}}{R.T}\right) * (P_{CO}^a * P_{H_2}^b) \dots \dots \dots (9.14)$$

$$r_{CH_4} = A_2 * \exp\left(-\frac{E_{a,CH_4}}{R.T}\right) * (P_{MeOH}^c * P_{H_2}^d) \dots \dots \dots (9.15)$$

$$r_{EtOH} = A_3 * \exp\left(-\frac{E_{a,E}}{R.T}\right) * (P_{MeOH}^e * P_{CO}^f * P_{H_2}^g) \dots \dots \dots (9.16)$$

$$r_{PrOH} = A_4 * \exp\left(-\frac{E_{a,Pr}}{R.T}\right) * (P_{EtOH}^h * P_{CO}^i * P_{H_2}^j) \dots \dots \dots (9.17)$$

$$r_{BuOH} = A_5 * \exp\left(-\frac{E_{a,Bu}}{R.T}\right) * (P_{PrOH}^k * P_{CO}^l * P_{H_2}^m) \dots \dots \dots (9.18)$$

$$r_{PeOH} = A_6 * \exp\left(-\frac{E_{a,Pe}}{R.T}\right) * (P_{BuOH}^n * P_{CO}^o * P_{H_2}^p) \dots \dots \dots (9.19)$$

$$r_{CO_2} = A_7 * \exp\left(-\frac{E_{a,CO_2}}{R.T}\right) * \left[P_{CO}P_{H_2O} - \left(\frac{k_x}{K_{WGS}}\right) * P_{CO_2}P_{H_2}\right] \dots \dots \dots (9.20)$$

where:

$$K_{WGS} = \exp\left(\frac{-\Delta G_{WGS}^\circ}{R.T}\right) \dots \dots \dots (9.20a)$$

$$\Delta G_{WGS}^\circ = -8514 + 7.71 * T \left(\frac{cal}{mol}\right) \dots \dots \dots (9.20b)$$

where A_i and $E_{a,i}$ are the pre-exponential factors and activation energy of species. K_{WGS} is the equilibrium constant of the WGS reaction (Beretta et al., 1998; Surisetty et al., 2010) and k_x is a parameter that takes into account the non-ideality of gases due to high operating pressures. Reaction orders for species i have been denoted with the exponent terms a to p ; however, it was assumed to be equal to 1 in the WGS reaction for simplicity (Portillo et al., 2016). The independent variables are the temperature and the partial pressures of reactants, while A_i , $E_{a,i}$, a to p and k_x are the parameters of the kinetic model to be determined.

9.4.4. Reactor modelling

The downward flow micro reactor was used in the HAS reaction for the kinetic study. The CNH-supported KCoRhMo catalyst sample of average particle size 0.088 mm was selected for the kinetic study to eliminate the influence of external and internal mass-transfer resistances. By assuming an isothermal and ideal plug-flow reactor, the following can be written to represent the differential mole balance equations for the components:

$$\frac{dF_{CO}}{d(W)} = -(r_{MeOH} + r_{EtOH} + r_{PrOH} + r_{BuOH} + r_{PeOH} + r_{CO_2}) \dots \dots \dots (9.21)$$

$$\frac{dF_{H_2}}{d(W)} = -(2r_{MeOH} + 2r_{EtOH} + 2r_{PrOH} + 2r_{BuOH} + 2r_{PeOH} + r_{CH_4}) + r_{CO_2} \dots \dots \dots (9.22)$$

$$\frac{dF_{H_2O}}{d(W)} = r_{EtOH} + r_{PrOH} + r_{BuOH} + r_{PeOH} + r_{CH_4} - r_{CO_2} \dots \dots \dots (9.23)$$

$$\frac{dF_{MeOH}}{d(W)} = r_{MeOH} - r_{EtOH} - r_{CH_4} \dots \dots \dots (9.24)$$

$$\frac{dF_{EtOH}}{d(W)} = r_{EtOH} - r_{PrOH} \dots \dots \dots (9.25)$$

$$\frac{dF_{PrOH}}{d(W)} = r_{PrOH} - r_{BuOH} \dots \dots \dots (9.26)$$

$$\frac{dF_{BuOH}}{d(W)} = r_{BuOH} - r_{PeOH} \dots \dots \dots (9.27)$$

$$\frac{dF_{PeOH}}{d(W)} = r_{PeOH} \dots \dots \dots (9.28)$$

$$\frac{dF_{CH_4}}{d(W)} = r_{CH_4} \dots \dots \dots (9.29)$$

$$\frac{dF_{CO_2}}{d(W)} = r_{CO_2} \dots \dots \dots (9.30)$$

where W is the mass of catalyst and F_i is the mole flow of component i. The differential mole balances are expressed as a function of the seven independent gross reaction rates (Eqs. 9.14–9.20). Polymath software (version 6.1) was used in the kinetic parameters determination. Solving these equations required initial guesses of the kinetic parameters. This has been obtained using a simplified method whereby the integration of the differential equations along the reactor is avoided (Portillo et al. 2016). The method assumes that the total molar flow rate (F) remains constant along the reactor. Thus, the left-hand term of the differential equations, i.e. the net reaction rate, can be expressed as follows: (Eq. 9.31):

$$\frac{dF_i}{dW} = \frac{d(Fy_i)}{dW} \approx \frac{Fd(y_i)}{dW} = \frac{d(y_i)}{d\left(\frac{W}{F}\right)} = r_i \dots \dots \dots (9.31)$$

where y_i denotes the outlet molar composition of species i and F is the total inlet molar flow. To calculate the net reaction rate, a series of experiments were carried out at different inlet molar flow rates (i.e. varied GHSVs) and constant T , P and inlet H_2/CO ratio to generate a range of W/F as shown in Table 9.3.

Table 9.3: Experimental design for the estimation of the net reaction rates of components in the HAS reaction ($P = 9.1\text{MPa}$ and inlet $H_2/CO = 1.25$).

T (°C)	Expt. #	W/F (kg_{cat}-h/kmol)
290	1	9514
	2	11100
	3	14799
	4	22199
	5	34153
310	6	9514
	7	11100
	8	14799
	9	22199
	10	34153
330	11	9514
	12	11100
	13	14799
	14	22199
	15	34153

For each series of experiments designed, plots of y_i versus W/F at fixed temperatures yielded curves with slopes representing the net reaction rate of species i at the outlet of the reactor. For instance, Figure 9.3 shows plots of outlet ethanol mole fractions versus W/F at various temperatures ($T=290\text{-}330^\circ\text{C}$) to obtain the r_{EtOH} at these temperatures. Similarly, the net reaction

rates of all the seven components namely; methanol, ethanol, propanol, butanol, pentanol, carbon dioxide and methane were calculated from the slope of the curves.

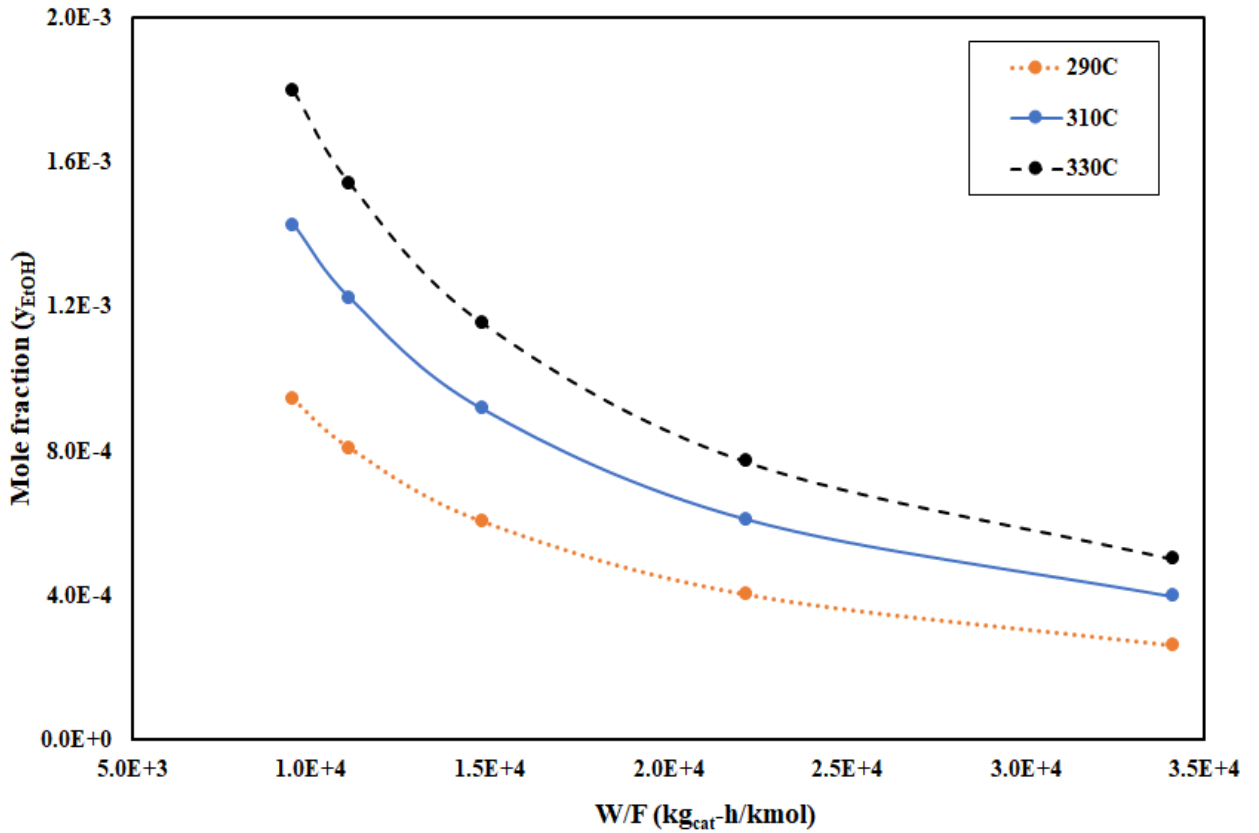


Fig. 9.3: Plot of outlet ethanol mole fraction versus W/F at various temperatures for obtaining reaction rates (T=290-330°C).

Next, the initial guess of the kinetic parameters was determined with non-linear regression by minimizing the sum of the squares of the differences between experimental and predicted reaction rates for each compound (Eq. 9.32).

$$S_i = \sum_{j=1}^N (r_{ij} - \hat{r}_{ij})^2; \quad i = 1 \dots 5; \quad \dots \dots \dots (9.32)$$

For Eq. 9.32, the partial pressures in the kinetic equations were evaluated at the outlet of the reactor. It should be mentioned that in the evaluation of kinetic parameters by the Polymath

software (using the STIFF method), the kinetic equation for the WGS reaction was simplified (Eq. 9.33). The reason is that by using Eq. 9.20 for the WGS reaction, or the irreversible version, a good fit was not possible and negative values for the frequency factor were obtained. Therefore, Eq. 9.33 was used in the determination of the values of both A_7 and E_{a, CO_2} .

$$r_{CO_2} = A_7 * \exp\left(-\frac{E_{a,CO_2}}{R.T}\right) * [P_{CO}P_{H_2O}] \dots \dots \dots (9.33)$$

The kinetic parameters were estimated by fitting the experimental data in the sum of the squares function and minimizing the errors. The residual error values obtained at 290, 310, and 330°C are 0.0832, 0.0435 and 0.0654, respectively. Table 9.4 shows parameters of the kinetic model computed using the simplified power law model. The kinetic parameters from Table 6 were used as initial values for the rigorous method. The initial value of k_x in Eq. 9.20 was assumed 0.85 (Protillo et al., 2016). The parameters of the kinetic model calculated are comparable to values reported in the open literature.

Table 9.4: Computed values of kinetic parameters by the Power Law Models.

Species	Species order of reaction						E_a (kJ/mol)	A^\ddagger
	MeOH	EtOH	PrOH	BuOH	CO	H ₂		
Methanol	-	-	-	-	1.89	0.49	36.1	7.36*10 ⁴
Ethanol	1.00	-	-	-	1.32	0.27	54.4	2.22*10 ²
Propanol	-	0.78	-	-	1.31	1.28	92.2	8.19*10 ²
Butanol	-	-	1.00	-	0.28	1.00	148.6	1.32*10 ³
Pentanol	-	-	-	1.00	1.00	1.00	178.7	2.82*10 ³
Methane	0.63	-	-	-	-	0.08	126.4	4.81*10 ³
Carbon dioxide	-	-	-	-	1.00	1.00	90.7	7.81*10 ¹
k_x								0.85

[‡]Units depend on the kinetic expression: kmol/kg·s·bar^{Σreaction orders}

Figure 9.4 shows the Arrhenius plots for the main alcohol products (C₁ to C₃-OH) and by products (CH₄ and CO₂) during the HAS reactions. A linear dependency of rate constant on temperature could be observed for all the components evaluated.

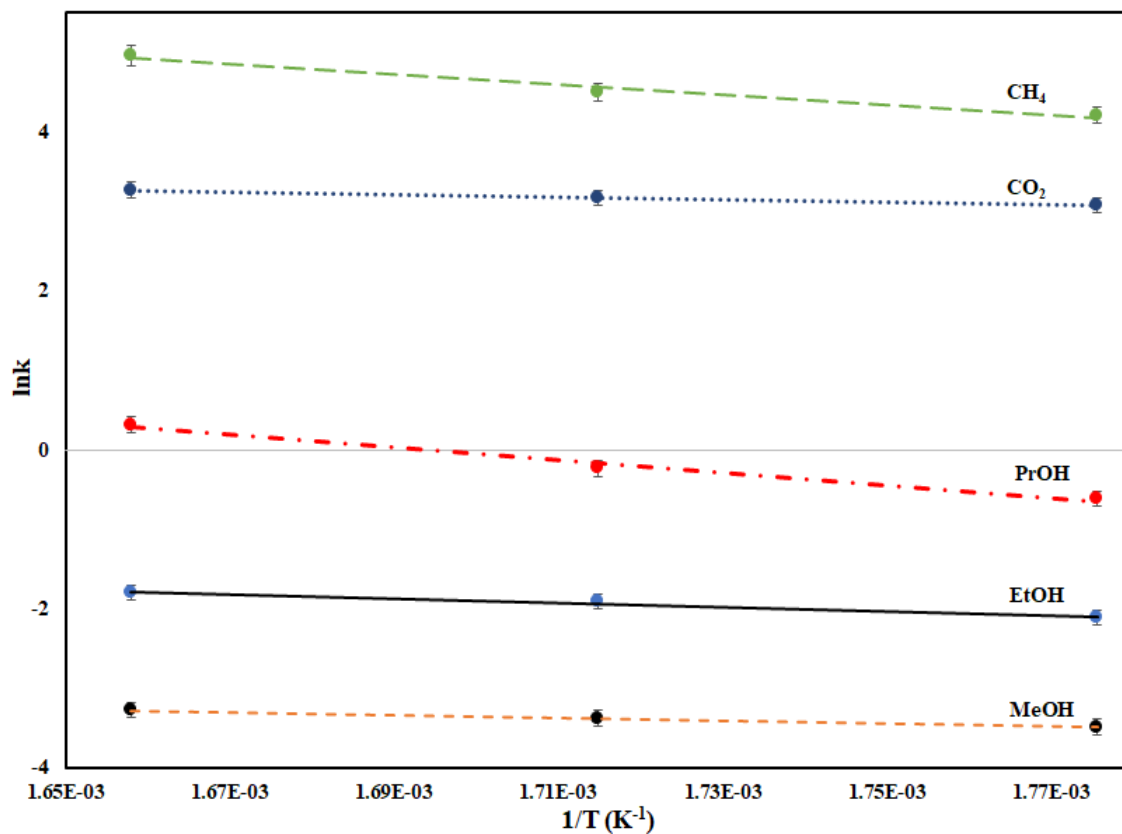


Fig. 9.4: Arrhenius plots of alcohol products (C₁ to C₃-OH) and by-products (CH₄ and CO₂).

Figs. 9.5 (A and B) give the parity plots showing the fit between experimental molar rates and the predicted model values of methanol, ethanol, propanol, methane, and carbon dioxide, respectively. The R² values by the models show a good fit with the experimental results.

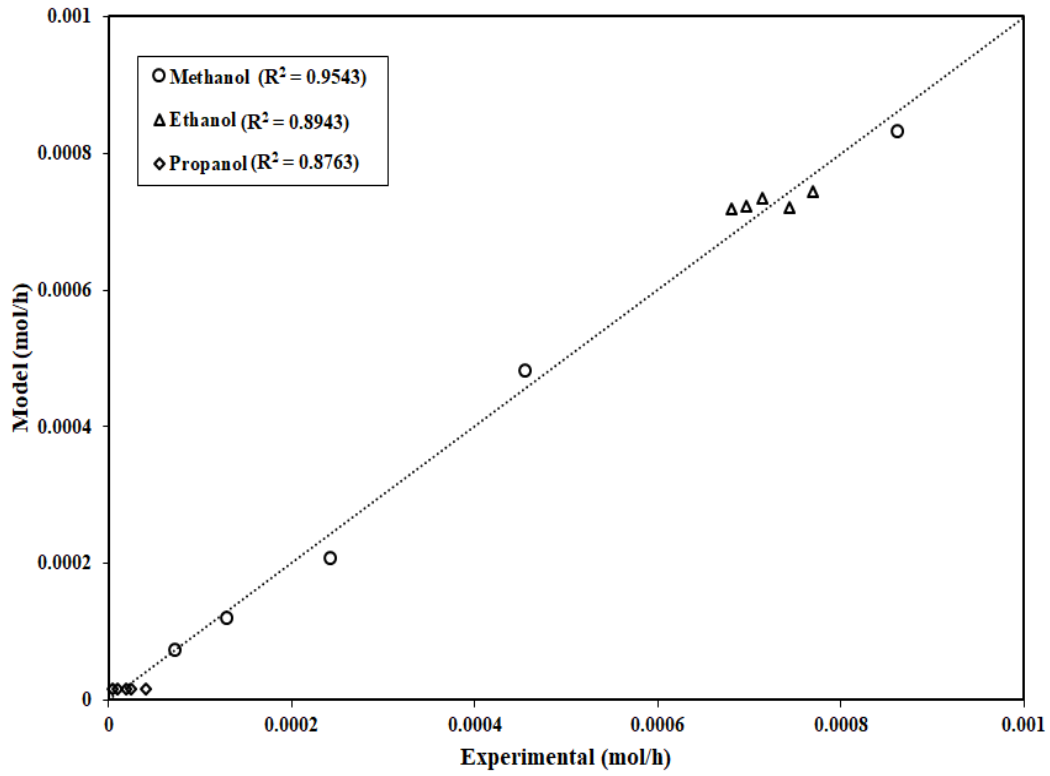


Fig. 9.5 (A): Parity plot of the experimental and model flow rates for the different alcohols.

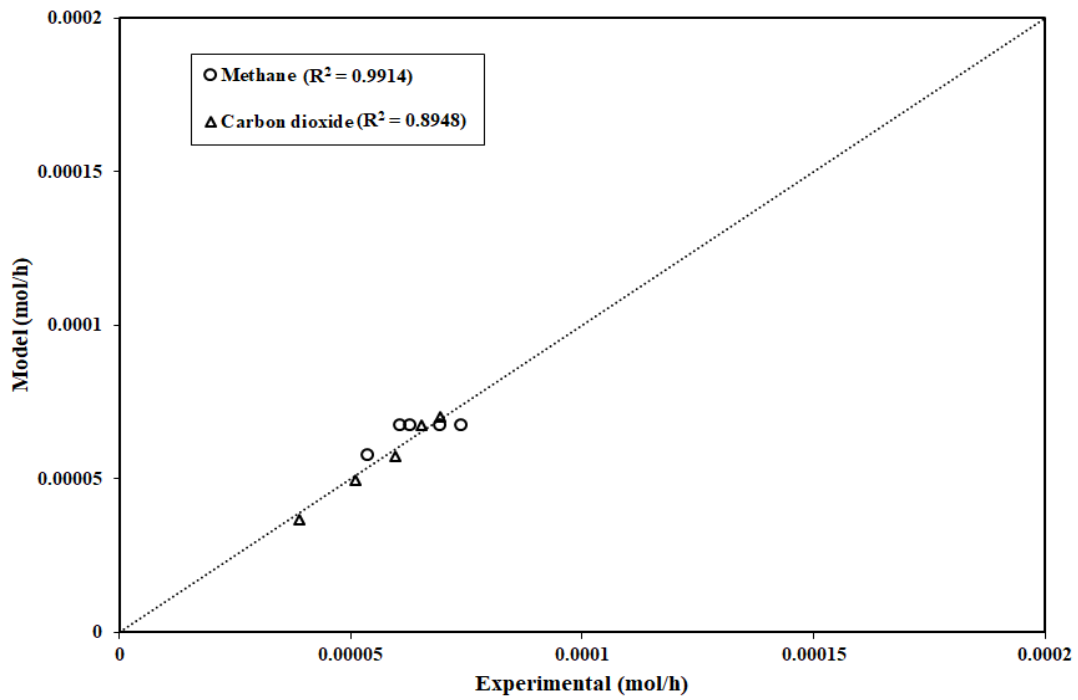


Fig. 9.5 (B): Parity plot of the experimental and model flow rates for the gaseous products.

9.4.5. Long-term stability studies over CNH-supported KCoRhMo catalyst

The sulfided CNH-supported KCoRhMo catalyst was tested for its long-term durability in the HAS reaction using the conditions: $T=325^{\circ}\text{C}$, $P=9.1\text{ MPa}$, $\text{H}_2/\text{CO}=1.25$, and $2.4\text{ m}^3\text{ (STP)}/(\text{kg of cat.})/\text{h}$. The CO conversion profile as function of time-on-stream for a continuous 504 hours of catalyst screening test is shown in Figure 9.6. Liquid condensation in the system could be neglected since steady-state reaction conditions was assumed. As can be seen, two different deactivation steps are observable. An initial drop of 17.7% in CO conversion occurred within 18 h time on stream (i.e. from 50.8 to 41.8%). As a result, an initial induction period of 18 h was allowed during the experiment prior to product sampling and analyses. CO conversion remained almost constant afterwards with only $\sim 2.3\%$ drop for the remaining time-on-stream.

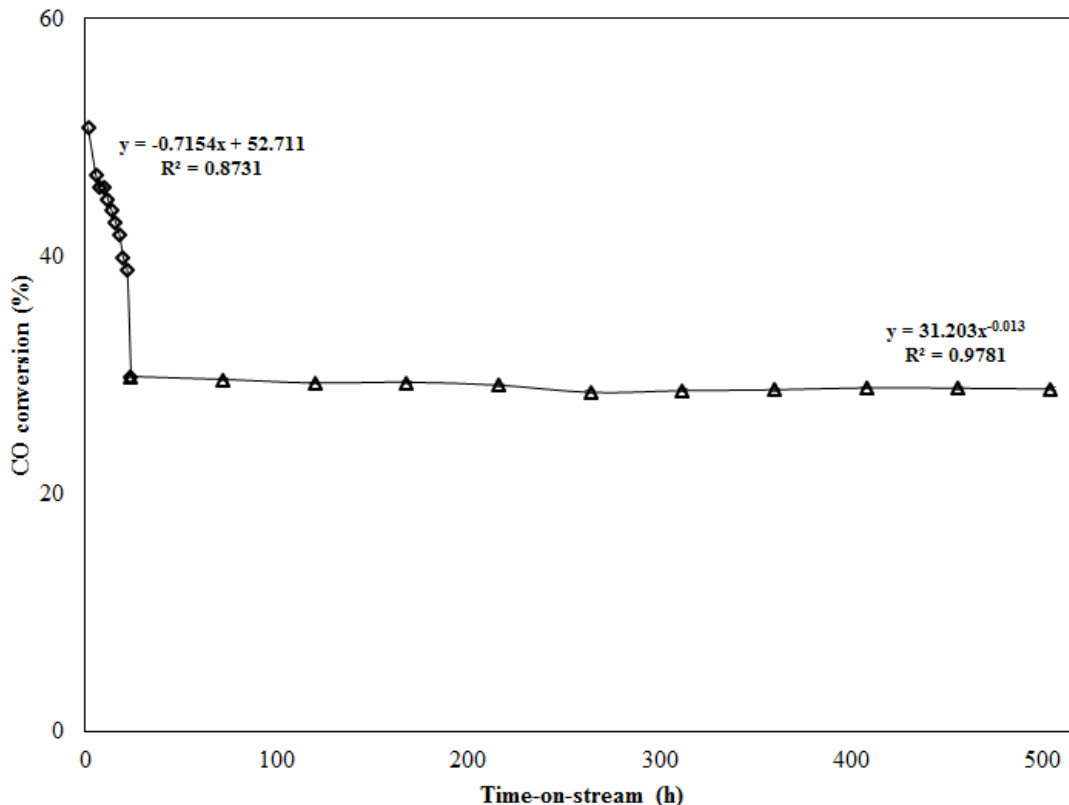


Fig. 9.6: Profile of CO conversion as a function of time-on-stream for CNH-supported KCoRhMo catalyst ($P = 9.1\text{ MPa}$, $T = 325^{\circ}\text{C}$, $\text{GHSV} = 2.4\text{ m}^3\text{ (STP)}/\text{h}/(\text{kg of cat.})/\text{h}$, H_2 to CO molar ratio = 1.25, wt. of cat. = 1 g).

The loss of catalytic activity spanning the two deactivation steps can be simulated with the following linear correlation:

$$X_{CO} = -0.715 * t + 52.711; \quad t < 18h \quad \dots \dots \dots (9.34)$$

$$X_{CO} = 31.203 * t^{-0.013}; \quad 18h < t < 504h \quad \dots \dots \dots (9.35)$$

where X_{CO} and t represent CO conversion (mol %) and time-on-stream (h), respectively.

A steep decline in catalytic activity of trimetallic MWCNT-supported Co-Rh-Mo-K catalyst investigated for the conversion of syngas to higher alcohols was observed during the first 12 h time-on-stream by Surisetty and coworkers (Surisetty et al., 2011). They attributed the observation to two possible factors namely; the tendency of temperature of the catalyst bed increasing as a result of its contact with the feed syngas. As a result of the exothermicity of the HAS reaction, an initial higher CO conversion can be expected, which then reached to a steady state. Also, the reduction of CO conversion during the HAS reaction has been attributed to the significant loss of sulfur from the catalyst surface. For the MoS₂-based catalyst, Ratnasamy and coworkers attributed the loss of sulfur to the formation of unstable negative charge sulfur ions located at the edge of MoS₂ crystallites (Ratnasamy et al., 1980).

Figure 9.7 shows the profile of products (liquid and gaseous) STYs as a function of time-on-stream over the CNH-supported KCoRhMo catalyst during the HAS reaction. For the period of 504 h of the catalyst on stream, it was observed that the STYs of higher alcohols and total alcohols increased from 0.246 to 0.304 g/(g of cat.)/h and 0.413 to 0.433 g/(g of cat.)/h, respectively. Subsequently, the STYs of the alcohols stabilized over the remaining reaction time following the initial changes during the 18 h induction period with only ~1.2 % variations in STY afterwards. The enhance formation of total alcohols after the induction period was also observed

by Christensen and coworkers (Christensen et al., 2009), and they attributed this phenomenon to the gradual spreading of the alkali promoter across the surface of the catalyst (Christensen et al., 2009; Surisetty et al., 2010).

In addition, during the 18 h induction period, it can also be seen from Figure 9.7 that the total hydrocarbon STY decreased from 0.297 to 0.222 g/(g of cat.)/h and remained almost constant during the remaining time-on-stream. Similarly, CO₂ productivity also decreased from 0.136 to 0.121 g/(g of cat.)/h and then levelled off during the remaining reaction period. In the CO hydrogenation over MoS₂ catalysts, it is known that the generated metal sulfide sites formed during H₂S/H₂ activation can favor the adsorption of hydrogen, which can then promotes the methanation reaction; leading to the formation of hydrocarbons (Santiesteban et al., 1988).

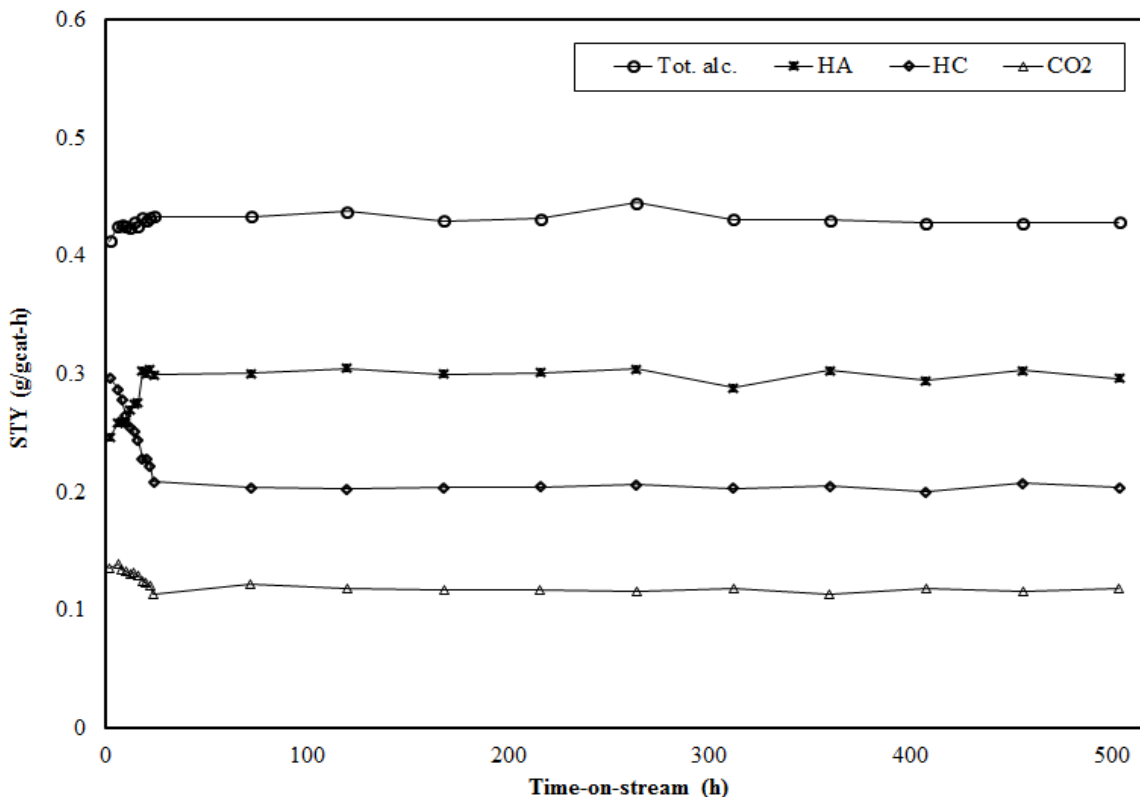


Fig. 9.7: Profile of STYs of products as a function of time-on-stream for CNH-supported KCoRhMo catalyst ($P = 9.1$ MPa, $T = 325^{\circ}\text{C}$, $\text{GHSV} = 2.4 \text{ m}^3 \text{ (STP)/h/(kg of cat.)/h}$, H_2 to CO molar ratio = 1.25, wt. of cat. = 1 g).

Moreover, in their study of MWCNT-supported Co-Rh-Mo catalyst for the HAS reaction, Surisetty and coworkers attributed the initial decrease in total hydrocarbons STY to the loss of sulfur from unstable metal sulfide crystallites on the surface of the catalyst to the products (Surisetty, 2010). These factors explain the decrease in STY of HC and CO₂ as observed over the CNH-supported KCoRhMo catalyst investigated.

9.4.6. Comparison of activation energies of alcohols over MoS₂-based catalysts

Table 9.5 presents a comparison of the activation energies of alcohol products as well as main hydrocarbons obtained in the present work to those reported in the open literature over MoS₂-based catalysts for the HAS reaction.

Table 9.5: Comparison of activation energies of alcohols over MoS₂-based catalysts for the HAS reaction.

Reference	Gunturu et al., 1998	Santiesteban et al., 1989	Surisetty et al., 2010	Christensen et al. 2011	Portillo et al., 2016	Present work
Catalyst	K/Co/MoS ₂ /C	Cs/MoS ₂	Co-Rh-Mo-K/MWCNT	K/Co/MoS ₂ /C	K/Co/MoS ₂	KCoRhMo/CNH
<i>Operating conditions</i>						
T (°C)	300-350	235-275	275-340	300-350	280-320	290-350
P (bar)	40-70	82.7	55.2-96.5	100	70-110	55.2-96.5
H ₂ /CO	0.5-2.0	0.96	0.5-2.0	1.0	0.75-1.75	1.25
MeOH co-feeding	Yes	No	No	No	Yes	No
<i>Activation energies (kJ/mol)</i>						
MeOH	-	68	35	49	83.1	36.1
EtOH	38	95	57	76	83.3	54.4
PrOH	98	98	94*	109	159.1	92.2
BuOH	107	-	-	-	-	148.6
PeOH	-	-	-	-	-	178.7
CH ₄	-	-	112**	118	115	116.5

*Higher alcohols were lumped together as alcohols with carbon number greater than 2.

**Hydrocarbons were lumped together with CH₄ being the predominant species.

As can be seen in Table 9.5, there was no consistent agreement between values obtained in the various kinetic studies; probably due to the varied operating conditions, catalyst compositions, support matrixes, structure of active phases, among others, investigated. That notwithstanding, the results show a general agreement in the activation energies, which tend to increase with the chain length of alcohol carbon numbers (Christensen et al., 2011). The activation energies of ethanol and propanol recorded over the CNH-supported KCoRhMo catalyst were low compared to those values reported in the literature. This observation could be attributed to the enhanced textural properties of CNH support used in the catalyst formulation. The support plays a crucial role in the dispersion and subsequent modification of catalytic metal species of the surface of the catalyst. Finally, the activation energies of methane (main hydrocarbon) was quite comparable to those reported by different researchers. Therefore, an increase in temperature favors the formation of hydrocarbons but also higher alcohols.

9.5. Conclusions

In this study, sulfided CNH-supported KCoRhMo catalyst was investigated for the intrinsic kinetics of higher alcohols synthesis reaction from syngas. The influence of bentonite incorporation to the formulation of CNH-supported KCoRhMo catalyst was also explored. Of the two catalyst particle sizes (88 and 254 μm) examined, the catalyst with particle size of 88 μm was selected for the kinetic screening experiments so as to eliminate the possibility of external mass transfer resistance. The very small value of 1.49×10^{-3} obtained by the Weisz-Prater criterion confirmed that internal diffusion limitation was negligible in the catalyst. A proposed reaction scheme from the literature based on the CO insertion mechanism was used to describe the kinetics of the higher alcohols synthesis over the sulfided KCoRhMo/CNH catalyst. The simple power-law model was chosen for the reaction rate of compounds. A CCD method in Design Expert 6.0 was

used to develop the experimental plan by varying reaction temperature, pressure, and gas hourly space velocity in the ranges of 270-350°C, 5.52-9.65 MPa, and 2.4-4.8 m³ (STP)/(kg of cat-h), respectively. The reaction products constituted linear alcohols namely; methanol, ethanol, n-propanol, butanol and pentanol as well as methane and carbon dioxide as the major products. The fitting of the experimental data with the developed power law models showed good fits with high R² values for the components evaluated. The activation energies computed for ethanol and propanol in the HAS reaction over CNH-supported KCoRhMo catalyst were 54.4 and 92.2 kJ/mol, which are low compared to values obtained by other researchers in a similar study.

CHAPTER 10

Conclusions and Recommendations

10.1. Overall project discussion and conclusions

The overall research was focused on the development of novel potassium-promoted CoRhMo catalyst systems supported on three main carbon nanomaterials; namely multi-walled carbon nanotubes (MWCNTs), ordered mesoporous carbon (OMC) and carbon nanohorns (CNH), and their application for higher alcohols synthesis from syngas conversion. This work also explored the possibilities of binders incorporation into the formulation of the powdered form of the carbon-supported KCoRhMo catalysts for the HAS reaction. Furthermore, the catalytic screening of two other carbon supports (OCP_f and OCP) generated as by-products during the synthesis of pristine CNH support by the submerged arc discharge in liquid nitrogen method was also investigated. Extensive characterization studies of the physico-chemical properties of these catalysts as well as their respective HAS activity results have also been presented. Finally, the optimization of process parameters (T, P, and GHSV), kinetic modelling as well as the long-term catalyst stability studies have also been presented in the kinetic evaluation of the optimum catalyst developed from this study.

In Chapter 2, extensive literature review conducted helped to identify pertinent knowledge gaps in this area of research. This was necessary since it provided insights on the

research topic and unexplored areas as well; thus, providing the essential tools to bridge some gaps in the literature. In chapter 3, the required experimental procedures were adopted/developed to help meet the research needs. The various characterization techniques employed throughout the study have also been discussed in this chapter.

In chapter 4, the influence of pelletization and particle size as well as the incorporation of selected binders in the formulation of potassium promoted $\text{CoRhMoS}_2/\text{MWCNT}$ catalysts was investigated. An equal binder loading of 30 wt% was used in the preparation of all the binder-incorporated catalysts. Though the crushing strength of the binder-incorporated catalysts followed the order: bentonite clay > Coal Tar > Humic acid, the pelletized catalyst formulated with bentonite clays as a binder (Cat-2) exhibited the best mechanical strength, which could withstand a maximum load of ~340 N before crushing into fines as compared to the pelletized binder-free catalyst (Cat-1). Also, CO conversion for the binder-free catalysts evaluated at the same temperature for two particles sizes (88 and 1,700 μm) showed that the catalyst with fine particle sizes (88 μm) performed better than that in the pelletized form (binder-free, 1,700 μm).

In chapter 5, large pore diameter ordered mesoporous carbon (OMC)-supported KCoRhMo catalyst was compared with MWCNT-supported catalyst of similar pore diameter for the HAS reaction. At similar metals loadings of 9%K, 4.5%Co, 15%Mo and 1.5wt.% Rh, XRD analysis evidenced a better metal nanoparticles dispersion on OMC-supported catalyst since less crystalline peaks were detected as confirmed by the TEM images. Both the OMC & MWCNT-supported catalysts exhibited high activities toward the production of alcohols, especially ethanol. Though the OMC-supported KCoMoRh catalyst showed overall better textural properties, the MWCNT-supported catalyst showed the maximum (38.5%) total amount of higher alcohol produced as compared to its OMC counterpart (36.5%).

In chapter 6, large pore diameter OMC supports used in the K-doped CoRhMoS₂ catalysts formulation were subjected to wet chemical oxidation treatments (acidic or basic) to modify the surface chemistry prior to the HAS application. Chemical treatment of OMC support with nitric acid caused more defective sites with lower metals reducibility temperature as compared to its NH₄OH/H₂O₂ and KOH counterparts as confirmed by Raman and TPR analyses; thus, its superior catalytic performance for the HAS reaction. Nonetheless, all the chemically treated OMC-supported catalysts exhibited high activities toward the production of alcohols, especially ethanol.

Chapter 7 focused on investigating carbon nanohorns (CNH) support and its by-products (OCP_f and OCP) for the HAS reaction. These supports were synthesized by the submerged arc discharge in liquid nitrogen technique and treated with 30wt.% nitric acid prior to K-doped CoRhMoS₂ catalyst formulations. At the optimum temperature of 330°C, pressure of 8.3 MPa, and GHSV of 3.6 m³ (STP)/kg_{cat}-h, linear alcohols were produced with the trend of C₂₊ alcohols selectivities following the order: Cat-CNH (63.7) > Cat-OCP_f (48.9) > Cat-OCP (38.2). The results of this study provided insight to elucidate the crucial role different carbon materials play as catalyst support in their application for higher alcohol synthesis.

The effects of process parameters (T, P, and GHSV) on higher alcohols synthesis reaction from synthesis gas was investigated using sulfided CNH-supported KCoRhMo catalyst as discussed in Chapter 8. Quadratic models were developed using the central composite design (CCD) method for % CO conversion, products STY, and alcohol selectivities as functions of T, P and GHSV using an H₂ to CO molar ratio of 1.25. The statistical tests, test of significance, and R² value statistics proved that the models could adequately represent the experimental data. Increasing temperature and pressure resulted in increases in the ethanol selectivity and space

time yield up to a maximum value, while slightly decreasing with increasing GHSV. The developed quadratic models used to predict the selectivity and space time yield of ethanol were in good agreement with experimental results obtained at the optimized conditions. Numerical optimization assessments of the models selected the optimum operating conditions to be 325°C, 9.1 MPa, and 2.4 m³ (STP)/(kg of cat.)/h to give the maximum ethanol and higher alcohols space time yields of 0.126 and 0.177 g/g of cat-h, respectively.

Chapter 9 focused on investigating the intrinsic kinetics of sulfided CNH-supported KCoRhMo catalyst for the HAS reaction. The influence of bentonite incorporation to the formulation of CNH-supported KCoRhMo catalyst was also explored. Catalyst samples of two mesh sizes of 75-100 and 210-297 μm (average particle size ranges of 88 and 254 μm) were examined; with the catalyst of particle size of 88 μm being selected for the kinetic screening experiments. The very small value obtained by the Weisz-Prater criterion confirmed that internal diffusion limitation was negligible in the catalyst. A proposed reaction scheme from the literature based on the CO insertion mechanism was used to describe the kinetics of the higher alcohols synthesis over the sulfided KCoRhMo/CNH catalyst. The fitting of the experimental data with the developed power law models showed good fits with high R^2 values for the components evaluated. The activation energies computed for ethanol and propanol in the HAS reaction over CNH-supported KCoRhMo catalyst were 54.4 and 92.2 kJ/mol, which are low compared to values obtained by other researchers in a similar study. Finally, the sulfided CNH-supported KCoRhMo catalyst showed excellent reaction stability for the synthesis of higher alcohols from synthesis gas. This study revealed that carbon nanohorns can be an innovative catalyst support to enhance the productivity of the higher alcohol synthesis reaction by enhancing metal species

dispersion and reducing coke formation during the CO hydrogenation reaction over the sulfided MoS₂-based catalyst.

10.2. Recommendations

In this study, attempt was made to develop a highly efficient Co and Rh-promoted alkali-modified MoS₂ catalyst supported on carbon materials. The research provided insights in the operating conditions needed for optimum performances of the catalyst during the HAS reaction. The novel catalyst developed exhibited stable performance during the production period of higher alcohols from synthesis gas. That notwithstanding, the following recommendations can be advanced to provide guideline for future research work in this area:

1. Catalyst preparation methods

It is well known that the catalytic activity and products selectivities depend on method of catalyst preparation as well the metal precursors employed for catalysts formulation. This work only investigated the sequential pore volume impregnation technique. Future work can investigate the influence of preparation methods such as the sol gel technique and micro-emulsion methods as well the incorporation of additives like chelating agents EDTA, NTA, etc. to enhance catalytic performance of carbon supported MoS₂-based catalysts.

2. Sulfidation/reduction of oxidic catalyst

Prior to the CO hydrogenation reaction, the oxidic form of the catalyst needs to be sulfided to obtain the active sulfide phases. This sulfidation/reduction step will play a critical role in the phases generated on the catalyst; hence, impacting the catalytic performance. That notwithstanding, the influence of gas composition as well as duration of the catalyst activation process were not investigated in this study. Thus, for the developed sulfided carbon-supported

KCoRhMo catalysts to be considered for future industrial/commercial applications, these parameters would have to be further investigated.

3. Incorporation of binder and catalyst pelletizing

For the developed catalysts to be applied for the HAS reaction in industrial reactors, it is important to consolidate the fine powdered form of the carbon-supported KCoRhMo catalysts into pellets using various binders. Though, of the three selected binders investigated (i.e. bentonite clay, coal tar, and humic acid), the bentonite clay exhibited the superior characteristics for the carbon-supported catalyst formulation, other binders could also be explored in future works.

4. In-situ catalyst characterization of sulfided catalysts

Due to the constant changes occurring on the surface of a working catalyst, it is important to conduct in-situ characterization technique to obtain information to better describe the catalyst. It will be interesting to obtain an in-situ cell to help conduct the HAS reaction as a time resolved experiment to gain a clearer understanding of the catalysts during the reaction. Characterizations of the sulfided forms of the CNH-supported catalysts were not completed in this study. Thus, future work should consider a thorough characterization of the sulfided OMC and CNH-supported KCoRhMo catalysts using techniques such as X-ray diffraction, X-ray absorption near edge structure (XANES), and extended X-ray absorption fine structure (EXAFS). These techniques can identify the different metal species present on the catalyst surface, provide information on the catalyst structure such as bond lengths, coordination numbers, and slab lengths of the different catalytic species to gain proper understanding of the catalyst structure-activity relationship during the HAS reaction.

5. Coking/catalyst deactivation

Carbon deposition on the surface of the catalyst can contribute to the deactivation of the catalyst. Though, a long-term catalyst stability evaluation was conducted for the CNH-supported KCoRhMo catalyst to ascertain the deactivation propensity of the catalyst, no quantitative measurement of the amount of carbon deposits was assessed in this study. However, it will be interesting to use CHNSO technique to evaluate the fresh and spent catalyst in order to ascertain the level of coking suffered by the catalyst as result of time-on-stream.

6. Catalyst activity studies using industrial synthesis gas

In this research, a premixed syngas of specified molar composition was used throughout the experiments. The synthesis gas obtained from biomass or coal gasification is associated with impurities such as H₂S, CO₂, N₂, etc. The presence of these undesirable component in the syngas may affect the catalytic activity and selectivity. Thus, to be considered for industrial applications, a model industrial syngas containing the above impurities need to be tested under similar conditions and compare the performance of the developed catalysts under such conditions.

7. H₂S in feed syngas and methanol cofeeding

The influence of H₂-to-CO ratio as well as the incorporation of H₂S in the feedstock should be investigated with the optimum CNH-supported KCoRhMo catalysts to help regenerate the active sulfidic sites during the HAS reaction. The addition of 10-50 ppm sulfiding agent (e.g. H₂S) in the feedstock should be investigated to help maintain the catalytic activity levels during the HAS reaction. It is important to develop a system to co-feed methanol along with syngas to help improve the production of higher alcohols.

8. Catalysts evaluation for commercial application

Before using the catalyst in industry, a detailed pilot plant study under optimum operating conditions may be performed to evaluate heat transfer and mass transfer resistances associated with the higher alcohols synthesis reaction. Experiments should be designed and run in a large reactor with increased amount of catalyst to investigate the influence of catalyst weight on the products selectivities and distribution as well as kinetic parameters comparisons using similar experimental designs and reaction conditions. Also, a thorough techno-economic analysis should be conducted to assess the economic viability of the process prior to scaling-up.

10.3. Acknowledgment

Financial supports from BioFuelNet Canada, MITACS and the Natural Science and Engineering Research Council of Canada for this research are duly acknowledged.

REFERENCES

- Aasberg-Petersen, K.; Christensen, T. S.; Dybkjær, I.; Sehested, J.; Østberg, M.; Coertzen, R. M.; Keyser, M. J.; Steynberg, A. P. Synthesis Gas Production for FT Synthesis. *Stud. Surf. Sci. Catal.*, 152, **2004**, 258-405.
- Abbaslou, R.M.; Soltan, J. Dalai A.K. Iron Catalyst Supported on Carbon Nanotubes for Fischer–Tropsch Synthesis: Effects of Mo Promotion. *J. Fuel*, 90, **2011**, 1139-1144.
- Anderson, R.B. *The Fischer-Tropsch Synthesis*, Academic Press Inc., Orlando, **1984**.
- Andersson, R. Catalytic Conversion of Syngas to Higher Alcohols over MoS₂-based Catalysts, Ph.D. Thesis, KTH Royal Institute of Technology, Stockholm, Sweden, **2015**.
- Ansari, M.B.; Min, B.H.; Mo, Y.H.; Park, S.E. CO₂ Activation and Promotional Effect in the Oxidation of Cyclic Olefins over Mesoporous Carbon Nitrides. *Green Chem.*, 13, **2011**, 1416-1421.
- Antolini, E. Carbon Supports for Low-Temperature Fuel Cell Catalysts. *Applied Catal. B: Env.*, 88, **2009**, 1-24.
- Apestequia, C.R.; De Rites, B.; Miseo, S.; Soled, S. Catalysts for Producing Methanol and Isobutanol Mixtures from Synthesis Gas. *Catal. Lett.*, 44, **1997**, 1-5.
- Arnoldy, P.; Moulijn, J.A. Temperature-Programmed Reduction of CoO/Al₂O₃ Catalysts. *J. Catal.*, 93, **1985**, 38-54.
- Arsalanfar, M.; Mirzaei, A.A.; Bozorgzadeh, H.R. Effect of Calcination Conditions on the Structure and Catalytic Performance of MgO-supported Fe-Co-Mn Catalyst for CO Hydrogenation. *J. Nat. Gas Sci. Eng.*, 6, **2012**, 1-13.
- Aryee, E.; Dalai, A.K.; Adjaye, J. Functionalization and Characterization of Carbon Nanohorns (CNHs) for Hydrotreating of Gas Oils. *Top. Catal.*, 57, 6, **2014**, 796-805.

- Asadi, N.; Zilouei, H. "Optimization of Organosolv Pretreatment of Rice Straw for Enhanced Biohydrogen Production Using *Enterobacter Aerogenes*". *Biores. Tech.*, 227, **2017**, 335-344.
- Azargohar, R.; Dalai, A. K. Steam and KOH activation of Biochar: Experimental and modeling Studies. *Microporous Mesoporous Mater.*, 110, **2008**, 413-421.
- Badische Anilin- & Soda-Fabrik (BASF), German Patent 293787, **1913**.
- Bahome, M. C.; Jewell, L. L.; Hildebrandt, D.; Glasser, D.; Coville, N. J. Fischer-Tropsch Synthesis over Iron Catalysts Supported on Carbon Nanotubes. *Appl. Catal., A*, 287, **2005**, 60-67.
- Balakos, M.W.; Chaung, S.S.C., The Conversion of Synthesis Gas to Higher Oxygenated Fuel on Rh-based Catalysts: Effects of Chemical Additives, *Fuel Sci. & Tech Int.*, 9, **1991**, 793-810.
- Bazula, P.A.; Lu, A.H.; Nitz, J.J.; Schuth, F. Surface and pore structure modification of ordered mesoporous carbons via a chemical oxidation approach. *Micro. & Meso. Mater.*, 108, **2008**, 266-275.
- Bekyarova, E.; Hashimoto, A.; Yudasaka, M.; Hattori, Y.; Murata, K.; Kanoh, H.; Kasuya, D.; Iijima, S.; Kaneko, K. Palladium Nanoclusters Deposited on Single-Walled Carbon Nanohorns. *J. Phys. Chem. B*, 109, **2005**, 3711-3714.
- Beretta, A.; Micheli, E.; Tagliabue, L.; Tronconi, E. Development of a Process for Higher Alcohol Production via Synthesis Gas. *Ind. Eng. Chem. Res.*, 37, **1998**, 3896-3908.
- Bo L.; Klaus-Joachim, J.; Low-Temperature and Low-Pressure Methanol Synthesis in the Liquid Phase Catalyzed by Copper Alkoxide Systems. *Ind. Eng. Chem. Res.*, 53, **2014**, 1735-1740.
- Boahene, P.E.; Soni, K.K.; Dalai, A.K.; Adjaye J. Application of Different Pore Diameter SBA-15 Supports for Heavy Gas Oil Hydrotreatment Using Few Catalysts. *Appl. Catal. A: Gen.*, 402, **2011**, 31-40.

- Boahene, P.E.; Surisetty, V.R.; Sammynaiken, R.; Dalai, A.K. Higher Alcohol Synthesis Using K-Doped CoRhMoS₂/MWCNT Catalysts: Influence of Pelletization, Particle Size and Incorporation of Binders. *Top. Catal.* **57**, **2014**, 538-549.
- Boahene, P.E.; Sammynaiken, R.; Dalai, A.K. Syngas Conversion to Higher Alcohols: A Comparative Study of Large-Pore OMC- and MWCNT-Supported KCoRhMoS₂ Catalysts. *Fischer-Tropsch Synthesis, Catalysts, and Catalysis*. **15**, **2016**, 275-294.
- Boahene, P.E.; Sammynaiken, R.; Dalai, A.K. Syngas Conversion to Higher Alcohols: A Comparative Study of Acid & Base-Treated Mesoporous Carbon-Supported KCoRhMoS₂ Catalysts. *Catal. Tod.*, **291**, **2017**, 106-123.
- Boahene P.E., Sammynaiken R., Dalai A.K. Syngas Conversion to Higher Alcohols: Application of Novel K-promoted CoRhMo Catalysts Supported over Carbon Nanohorns and its by-products. *Int. J. Petrochem. Sci. Eng.* **2**, **1**, **2017**, 1-14.
- Boehm, H.P., in D.D Eley (edition). *Adv. Catal.*, 16th ed. Academic Press, New York. **1966**, 179-274.
- Bonard, J.M.; Gaal, R.; Garaj, S.; Thien-Nga, L.; Forro, L. Field Emission Properties of Carbon Nanohorn Films, *J. Appl. Phys.*, **2002**, **91**, 10107-10109.
- Box, G.E.P.; Draper, N. *Response Surfaces, Mixtures, and Ridge Analyses*, 2nd ed., Wiley, **2007**.
- Boz, I.; Sahibzada, M.; Metcalfe, I.S. Kinetics of the Higher Alcohol Synthesis over a K-promoted CuO/ZnO/Al₂O₃ Catalyst. *Ind. Eng. Chem. Res.*, **33**, **1994**, 2021-2028.
- Butt, J. B. *Reaction Kinetics and Reactor Design*, 2nd ed., Marcel Dekker Inc., New York, **2000**.
- Calafata, A.; Vivas, F.; Brito, J.L. Effects of Phase Composition and Potassium Promotion on Cobalt Molybdate Catalysts for the Synthesis of Alcohols from CO₂ and H₂. *Appl. Catal. A Gen* **172**, **1998**, 217-224.
- Calvo, L.; Gilarranz, M.A.; Casas, J.A.; Mohedano, A.F.; Rodriguez, J.J. Effects of Support Surface Composition on the Activity and Selectivity of Pd/C Catalysts in Aqueous-Phase Hydrodechlorination Reactions. *Ind. Eng. Chem. Res.*, **44**, **2005**, 6661-6667.

- Campos-Martin, J.M.; Fierro, J.L.; Guerrero-Ruiz, A.; Herman, R.G.; Klier, K. Promoter Effect of Cesium on C–C Bond Formation during Alcohol Synthesis from CO/H₂ over Cu/ZnO/Cr₂O₃ Catalysts. *J. Catal.*, 163, **1996**, 418-428.
- Cançado, L.G.; Jorio, A.; Martins Ferreira, E.H.; Stavale, F.; Achete, C.A.; Capaz, R.B.; Moutinho, M.V.O.; Lombardo, A.; Kulmala, T.S.; Ferrari, A.C. Quantifying Defects in Graphene via Raman Spectroscopy at Different Excitation Energies. *Nano Lett.*, 11, **2011**, 3190-3196.
- Chaumette, P.; Courty, P.; Barbier, J.; Fortin, T.; Lavalley, J.C.; Chauvin, C.; Kiennemann, A.; Idriss, H.; Sneed, R.P.A.; Denise, B. Carbonates, a key for selecting methanol synthesis catalysts. In: *Catalysis: Theory to Practice. Proceedings: 9th international congress on catalysis. Vol. 2. C1 chemistry.* Ottawa, Ontario, Canada, Chemical Institute of Canada, **1988**, 585-593.
- Chen, X.; Faber, M.; Gao, Y.; Kulaots, I.; Suuberg, E.M.; Hurt, R.H. Mechanisms of Surfactant Adsorption on Non-polar, Air-oxidized and Ozone-treated Carbon Surfaces. *Carbon* 41, **2003**, 1489-1500.
- Cheng, P.-Z.; Teng, H. Electrochemical Responses from Surface Oxides present on HNO₃ treated Carbons. *Carbon* 41, **2003**, 2057-2063.
- Che, G.; Lakshmi, B.B.; Martin, C.R.; Fisher, E.R. Metal-Nanocluster-Filled Carbon Nanotubes: Catalytic Properties and Possible Applications in Electrochemical Energy Storage and Production, *Langmuir*, 15, **1999**, 750-758.
- Che, M.; Clause, O.; Marcilly, C. Impregnation and Ion exchange, in J. Weitkamp (Ed.) *Handbook of Heterogeneous Catalysis*, Vol. 1, Wiley-VCH: Weinheim, **1997**, 191-207.
- Chiang S-W, Chang C-C, Shie J-L, Chang C-Y, Ji D-R, Tseng J-Y, Chang C-F, Chen Y-H Synthesis of Alcohols and Alkanes from CO and H₂ over MoS₂/γ-Al₂O₃ Catalyst in a Packed Bed with Continuous Flow. *Energies* 5, **2012**, 4147-4164.

- Christensen, J. M.; Mortensen, P. M.; Trane, R.; Jensen, P. A.; Jensen A. D. Effects of H₂S and Process Conditions in the Synthesis of Mixed Alcohols from Syngas over Alkali-promoted Cobalt-Molybdenum Sulfide. *Appl. Catal., A*. **2009**, 366, 29-43.
- Christensen, J.M. Catalytic Synthesis of Long-Chained Alcohols from Syngas, PhD-Thesis, Department of Chemical and Biochemical Engineering, Technical University of Denmark, **2011**.
- Courty, P.; Chaumette, P., Syngas: A Promising Feedstock in the Near Future, *Energy Prog.* **1987**, 23-30.
- Datsyuk, V.; Kalyva, M.; Papagelis, K.; Parthenios, J.; Tasis, D.; Siokou, A.; Kallitsis, I.; Galiotis, C. Chemical Oxidation of Multi-walled Carbon Nanotubes. *Carbon* 46, **2008**, 833-840.
- Davidson, S.D.; Sun, J.; Hong, Y.; Karim, A.M.; Datye, A.K.; Wang, Y. The Effect of ZnO Addition on Co/C Catalyst for Vapor and Aqueous Phase Reforming of Ethanol. *Catalysis Today*, 233, **2014**, 38-45.
- DeCanio, E.C.; Storm, D.A. Carbon Monoxide Adsorption by K/Co/Rh/Mo/Al₂O₃ Higher Alcohols Catalysts. *J. Catal.* **1991**, 132, 375-387.
- de Klerk, A. Fischer-Tropsch Refining, Wiley-VCH Verlag GmbH & Co., **2011**.
- Devore, Jay L. Probability and Statistics for Engineering and the Sciences (8th ed.). Boston, MA: Cengage Learning. **2011**, 508-510.
- Dhaundiyal, A. Influence of Blending on the Engine Parameters and the Reynolds Number. *Int. J. Appl. Sci. Eng. Res.*, 3, **2014**, 130-152.
- Ding, M.; Yang, Y.; Xu, J.; Tao, Z.; Wang, H.; Xiang, H.; Li, Y. Effect of Reduction Pressure on Precipitated Potassium-promoted Iron-Manganese Catalyst for Fischer-Tropsch Synthesis. *Appl. Catal., A: Gen.*, 345, **2008**, 176-184.
- Dresselhaus, M.S.; Dresselhaus, G.; Saito, R.; Jorio, A. Raman Spectroscopy of Carbon Nanotubes. *Phys. Rep.* 409, **2005**, 47-99.

- Dry, M.E. The Fischer-Tropsch Process: 1950-2000. *Catal. Tod.*, 71, **2002**, 227-241.
- Dry, M.E. Chemical Concepts used for Engineering Purposes. *Stud. Surf. Sci. Catal.*, 152, **2004**, 196-257.
- Duchet, J.C.; van Oers, E.M.; de Beer, V.H.J.; Prins, R., “Carbon-Supported Sulfide Catalysts”, *J. Catal.*, **1983**, 80, 386-402.
- Eswaramoorthi, I.; Sundaramurthy, V.; Das, N.; Dalai, A.K.; Adjaye, J. Application of Multi-walled Carbon Nanotubes as Efficient Support to NiMo Hydrotreating Catalyst. *Appl Catal A Gen*, 339, **2008**, 187-195.
- Faraj, A.A.; Tahar, L.; Mamdouh, A-H.; Muataz, A.A. Modification and Functionalization of Multi-walled Carbon Nanotube (MWCNT) via Fischer Esterification. *Arab J. Sci. Eng.*, 35, **2010**, 37–48.
- Fei, Q.; Guarnieri, M.T.; Tao, L.; Laurens, L.M.L.; Dowe, N.; Pienkos, P.T. Bioconversion of Natural Gas to Liquid Fuel: Opportunities and Challenges. *Biotech. Adv.*, 32, **2014**, 596-614.
- Ferencz, Z.; Erdohelyi, A.; Baan, K.; Oszko, A.; Ovari, L.; Konya, Z.; Kiss, J. Effects of Support and Rh Additive on Co-based Catalysts in the Ethanol Steam Reforming Reaction. *ACS Catal.*, 4, **2014**, 1205-1218.
- Ferrari, A.C.; Robinson, J. Interpretation of Raman spectra of disordered and amorphous carbon. *Phys. Rev. B*, 61, **2000**, 14095-14107.
- Ferreira, M.; E.H., Moutinho, M.V.O.; Stavale, F.; Lucchese, M.M.; Capaz, R.B.; Achete, C.A.; Jorio, A. Evolution of the Raman Spectra from Single-, Few-, and Many-Layer Graphene with Increasing Disorder. *Phys. Rev. B*, 82, **2010**, 125429-125437.
- Filikov, A.V.; Myasoedov, N.F. Hydrogen Spillover and the Rate of Heterogeneous Catalytic Hydrogenation: Quantitative Model. *J. Phys. Chem.*, 90, **1986**, 4915-4916.
- Fischer, F.; Tropsch, H. *Brennstoff-Chem.*, 5, **1923**, 217-232.

- Fischer, F.; Tropsch, H. On the Preparation of Synthol by Construction: Oxyd and Hydrogen (II Communication). *Brennstoff-Chem.*, 5, **1924**, 201-208.
- Flory, P.J. Molecular Size Distribution in Linear Condensation Polymers. *J. Am. Chem. Soc.*, 58, **1936**, 1877-1885.
- Fogler, H. S. Elements of Chemical Reaction Engineering, Prentice Hall PTR, USA, 3rd ed., **1999**.
- Fogler, S.H. Elements of Chemical Reaction Engineering. 4th ed. Pearson Education, Inc., New Jersey, **2006**, 813-838.
- Forzatti, P.; Tronconi, E.; Pasquon, I. Higher Alcohol Synthesis. *Catal. Rev. - Sci. Eng.*, 33, **1991**, 109-168.
- Friedel, R.A.; Anderson, R.B. Composition of Synthetic Liquid Fuels. I. Product Distribution and Analysis of C₅-C₈ Paraffin Isomers from Cobalt Catalyst. *J. Am. Chem. Soc.*, 72, **1950**, 1212-1215.
- Frolich, P.; Cryder, D. Catalysts for the Formation of Alcohols from Carbon Monoxide and Hydrogen. *Ind. Eng. Chem.*, 22, **1930**, 1051-1057.
- Frössling N. The Evaporation of Falling Drops. *Gerlands Beitr. Geophys.* 52, **1938**, 170-216.
- Gandia, L. M.; Montes, M. Effect of Thermal Treatments on the Properties of Nickel and Cobalt Activated-Charcoal-Supported Catalysts. *J. Catal.*, 145, **1994**, 276-288.
- Gang, L.; Zhang, C. F.; Chang, Y.; Zhu, Z.; Ni, Y.; Cheng, L.; Yu, F. Synthesis of Mixed Alcohols from CO₂ Contained Syngas on Supported Molybdenum Sulfide Catalysts. *Appl. Catal., A* 150, **1997**, 243-252.
- Gardziella, A.; Pilato, L.A.; Knop, A. Phenolic Resins: Chemistry, Applications, Standardization, Safety and Ecology. New York: Springer; **2000**, 27-36.
- Geus, J.W.; van Dillen, A.J. Preparation of Supported Catalysts by Deposition Precipitation. In G. Ertl, H. Knözinger and J. Weitkamp (Eds.), *Handbook of Heterogeneous Catalysis*, Vol. 1, Wiley-VCH: Weinheim, **1997**, 240-257.

- Gherardi, P.; Ruggeri, O; Trifiro, F; Vaccari, A. Preparation of Catalysis III. (Poncelet, G; Grange, P.; Eds.) Elsevier Science: USA, **1983**, 723-726.
- Göransson, K.; Söderlind, U.; He, J.; Zhang, W. Renewable and Sustainable Energy Reviews. 15, **2011**, 482-492.
- Guglielminotti, E.; Giamello, E.; Pinna, F.; Strukul, G.; Martinengo, S.; Zanderighi, L. Elementary Steps in CO Hydrogenation on Rh Catalysts Supported on ZrO₂ and Mo/ZrO₂. J. Catal., 146, **1994**, 422-436.
- Guglielminotti, E.; Pinna, F.; Rigoni, M.; Strukul, G.; Zanderighi, L. The effect of iron on the activity and the selectivity of Rh/ZrO₂ catalysts in the CO hydrogenation. J. Mol. Catal. A: Chem., 103, **1995**, 105-116.
- Gunturu, A.K. Higher Alcohol Synthesis from Carbon Monoxide and Hydrogen: Kinetic Studies over MoS₂-Based Catalysts. M.Sc. Thesis, West Virginia University, **1997**.
- Gunturu, A. K.; Kugler, E. L.; Cropley, J. B.; Dadyburjor, D. B. A kinetic model for the synthesis of high-molecular-weight alcohols over a sulfided Co-K-Mo/C catalyst. Ind. Eng. Chem. Res. **1998**, 37, 2107-2115.
- Gupta, M.; Smith, M.L.; Spivey, J.J. Heterogeneous Catalytic Conversion of Dry Syngas to Ethanol and Higher Alcohols on Cu-Based Catalysts. ACS Catal., 1, **2011**, 641-656.
- Haber, J. Manual on Catalyst Characterization. Pure Appl. Chem., 63, **1991**, 1227-1246.
- Haber, J.; Block, J.H.; Delmon, B. Manual of Methods and Procedures for Catalyst Characterization (Technical Report). Pure Appl. Chem., 67, **1995**, 1257-1306.
- Haensel, V.; Jones, J.P.; Horne, W.A. Ministry of Fuel and Power, Report on Investigations by Fuels and Lubricants Teams at the I.G. Farbenindustrie AG Works at Leuna, **1947**, 93-97.
- Haifeng, X.; Jewell, L.L.; Coville, N.J. Shaped Carbons as Supports for the Catalytic Conversion of Syngas to Clean Fuels. ACS Catal., 5, **2015**, 2640-2658.

- Herman, R.G. Advances in Catalytic Synthesis and Utilization of Higher Alcohols. *Catal. Today*, **55**, **2000**, 233-245.
- Hirschfelder, J.; Curtis, C.; Bird, R. *Molecular Theory of Gases and Liquids*. John Wiley and Sons: New York, USA, **1954**.
- Hindermann, J.P.; Deluzarche, A.; Kieffer, R.; Kiennemann, A. Characterization of Chemisorbed Species in CO/H₂ and CO₂/H₂ Reactions: Evolutive Behaviour of the Species”, *Can. J. Chem. Eng.*, **1983**, 61, 21-28.
- Hussain, M.; Son-Ki, I. Synthesis, Characterization, and Hydrodesulfurization Activity of New Mesoporous Carbon Supported Transition Metal Sulfide Catalysts. *Ind. Eng. Chem. Res.*, **48**, **2009**, 698-707.
- Iijima, S.; Yudasaka, M.; Yamada, R.; Bandow, S.; Suenaga, K. Nano-aggregates of Single-Walled Graphitic Carbon Nano-horns. *Chem. Phys. Lett.*, 309, **1999**, 165-170.
- Iranmahboob, J.; Hill, D.O. Alcohol Synthesis from Syngas over K₂CO₃/CoS/MoS₂ on Activated Carbon. *Catal. Lett.*, **2002**, 49-55.
- Iranmahboob, J.; Hill, D. O.; Toghiani H. K₂CO₃/Co-MoS₂/clay Catalyst for Synthesis of Alcohol: Influence of Potassium and Cobalt. *Appl. Catal., A*. 231, **2003**, 99-108.
- Jang, S-R.; Vittal, R.; Kim, K-J. Incorporation of Functionalized Single-Wall Carbon Nanotubes in Dye-Sensitized TiO₂ Solar Cells. *Langmuir*, 20, **2004**, 9807-9810.
- Jawhari, T.; Roid, A.; Casado, J. Raman Spectroscopic Characterization of Some Commercially Available Carbon Black Materials. *Carbon* 33, 11, **1995**, 1561-1565.
- Jensen, K.L.; Menard, R.J.; English, B.C. *Market Analysis for Fischer-Tropsch waxes*, 2014, 1-36.
- Jie, S.; Wan, S.; Lin, J.; Wang, Y. Advances in Catalytic Conversion of Syngas to Ethanol and Higher Alcohols. In *Petrochemical Catalyst Materials, Processes, and Emerging Technologies*, **2016**, 177-215.

- Jun, S.; Choi, M.; Ryu, S.; Lee, H.Y.; Ryoo, R. Ordered Mesoporous Carbon Molecular Sieves with Functionalized Surfaces. *Stud. Surf. Sci. Catal.* 146, **2003**, 37-40.
- Kalamaras, C.M.; Efstathiou, A.M.; Hydrogen Production Technologies: Current State and Future Developments. *Conference Papers in Energy*, **2013**, 1-9.
- Kasuya, D.; Yudasaka, M.; Takahashi, K.; Kokai, F.; Iijima, S. Selective Production of Single-Walled Carbon Nanohorn Aggregates and Their Formation Mechanism. *J. Phys. Chem. B* **2002**, 106, 4947-495.
- Kent, J.E. Steam Reforming of Biodiesel By-Product Glycerol: A Major Qualifying Project Report, Bsc. Thesis, Worcester Polytechnic Institute, **2013**, 1-81.
- Key World Energy Statistics 2016, International Energy Agency, Paris, **2016**.
- Kim, D. S.; Wachs, I.E.; Segawa, K. Molecular Structures and Reactivity of Supported Molybdenum Oxide Catalysts. *J. Catal.* **1994**, 149, 268-277.
- Kinkade, N.E. Catalytic process for the production of alcohols from carbon monoxide, hydrogen and olefins. **1986**, Patent US4590314.
- Khodakov, A.Y.; Griboval, A.; Bechara, R.; Villain, F.J. Pore-Size Control of Cobalt Dispersion and Reducibility in Mesoporous Silicas. *Phys. Chem. B.* 105, **2001**, 9805-9811.
- Knowles, W.V.; Nutt, M.O.; Wong, M.S. Supported Metal Oxides and the Surface Density Metric; In: *Catalyst Preparation: Science and Engineering*, **2007**, 251-281.
- Kohl, A.; Linsmeier, C.; Taglauer, E.; Knozinger, H. Influence of Support and Promotor on the Catalytic Activity of Rh/VO_x/SiO₂ Model Catalysts. *Phys. Chem. Chem. Phys.* **2001**, 3, 4639-4643.
- Korodi, G. Application of Humic Acids and their Derivatives in Environmental Pollution Control. *Tech.*, 11, **2012**, 61-65.
- Kumar, A.; Jones, D.D.; Hanna, M.A. Thermochemical Biomass Gasification: A Review of the Current Status of the Technology Energies. 2, **2009**, 556-581

- Lazaro, M.J.; Calvillo, L.; Bordeje, E.G.; Moliner, R.; Juan, R.; Ruiz, C.R. Functionalization of Ordered Mesoporous Carbons Synthesized with SBA-15 Silica as Template. *Micropor. Mesoporous Mat.*, 103, **2007**, 158-165.
- Lazic, Z. R. *Design of Experiments in Chemical Engineering*, 1st ed.; Wiley-VCH Verlag GmbH: Weinheim, Germany, **2004**.
- Li, B. *Fourier Transform-Materials Analysis*. Intech, Shanghai, **2012**, 165-190.
- Li, X.; Feng, L.; Zhang, L.; Dadyburjor, D. B.; Kugler, E. L. Alcohol Synthesis over Pre-reduced Activated Carbon-Supported Molybdenum-based Catalysts. *Molecules*, 8, **2003**, 13-30.
- Li, Z.-R.; Fu, Y.-L.; Jiang, M. Structures and Performance of Rh-Mo-K/Al₂O₃ Catalysts used for Mixed Alcohol Synthesis from Synthesis Gas. *Appl. Catal. A*. 187, **1999**, 187-198.
- Li, Z.; Yan, W.; Dai, S. Surface Functionalization of Ordered Mesoporous Carbons: A Comparative Study. *Langmuir*, 21, **2005**, 11999-12006.
- Liu, L.; Wang, F-Y.; Shao, G-S.; Ma, T-Y.; Yuan, Z-Y. Synthesis of Ultra-Large Mesoporous Carbons from Triblock Copolymers and Phloroglucinol/Formaldehyde Polymer. *Carbon* 48, 9, **2010**, 2660-2664.
- Liu, Z. Y.; Li, X. G.; Close, M. R.; Kugler, E. L.; Petersen, J. L.; Dadyburjor, D. B. Screening of Alkali-Promoted Vapor-Phase-Synthesized Molybdenum Sulfide Catalysts for the Production of Alcohols from Synthesis Gas. *Ind. Eng. Chem. Res.*, 36, **1997**, 3085-3093.
- Liu, Z.; Yang, Y.; Mi, J.; Tan, X.; Song, Y. Synthesis of Copper-containing Ordered Mesoporous Carbons for Selective Hydrogenation of Cinnamaldehyde. *Catal. Comm.*, 21, **2012**, 58-62.
- Lox, E.S.; Marin, G.B.; de Graeve, E.; Bussier, P. Characterization of a Promoted Precipitated Iron Catalyst for Fischer-Tropsch Synthesis. *Appl. Catal., A: Gen.*, 40, **1988**, 197-218.
- Lu, A.H.; Li, W.-C.; Muratova, N.; Spliethoff, B.; Schuth, F. Evidence of C=C Bond Cleavage by H₂O₂ in a Mesoporous CMK-5 Type Carbon at Temperature. *Chem. Comm.*, **2005**, 5184-5186.

- Lucchese, M.M.; Stavale, F.; Ferreira, E.H.; Vilani, C.; Moutinho, M.V.O.; Capaz, R.B.; Achete, C.A.; Jorio, A. Quantifying Ion-Induced Defects and Raman Relaxation Length in Graphene. *Carbon* 48, **2010**, 1592-1597.
- Luk, H. T.; Mondelli, C.; Ferré, D.C.; Stewart, J.A.; Pérez-Ramírez, J. Status and Prospects in Higher Alcohols Synthesis from Syngas. *Chem. Soc. Rev.*, 46, **2017**, 1358-1426.
- Madon, R.J.; Iglesia, E.; Reyes, S.C. ACS Symposium Series: Selectivity in Catalysis. **1993**, 383-396.
- Mahdavi, V.; Peyrovi, M. H.; Islami, M.; Mehr, J.Y. Synthesis of Higher Alcohols from Syngas over Cu-Co₂O₃/ZnO, Al₂O₃ Catalyst. *Appl. Catal. A*, 281, **2005**, 259-265.
- Majocchi, L.; Lietti, L.; Beretta, A.; Forzatti, P.; Micheli, E.; Tagliabue, L. Synthesis of Short Chain Alcohols over a Cs-promoted Cu/ZnO/Cr₂O₃ Catalyst. *Appl. Catal. A* **1998**, 166, 393-405.
- Mao, Y.; Duan, H.; Xu, B.; Zhang, L.; Hu, Y.; Zhao, C.; Wang, Z.; Chen, L.; Yang, Y. Lithium Storage in Nitrogen-rich Mesoporous Carbon Materials. *Energy Environ. Sci.*, 5, **2012**, 7950-7955.
- Mawson S, McCutchen MS, Lim PK, Roberts G.W. Thermodynamics of Higher Alcohol Synthesis. *Energy Fuels* 7, **1993**, 257-267.
- McCutchen, M. S. Synthesis of Higher Alcohols from Carbon Monoxide and Hydrogen in a Slurry Reaction, Ph.D. Dissertation, North Carolina State University, Raleigh, NC, **1992**.
- Mills, G.A. Summary of the Higher Alcohol Synthesis Workshop, B. R. Service Corporation, **1992**.
- Mills, G. Status and Future Opportunities for Conversion Synthesis Gas to Liquid Energy Fuels: Final Report, NREL/TP-421-5150, **1993**, 1-62.
- Minahan, D.M.; Epling, W.S.; Hoflund, G.B.; Higher Alcohol Synthesis Reaction Study V. Effect of Excess ZnO on Catalyst Performance. *Appl. Catal., A* **1998**, 166, 375-385.

- Montgomery, D.C. Design and Analysis of Experiments, 4th ed.; John Wiley and Sons: New York, USA, **1997**.
- Muramatsu, A.; Tatsumi, T.; Tominaga, H. Active Species of Molybdenum for Alcohol Synthesis from Carbon Monoxide-Hydrogen. *J. Phys. Chem.*, 96, **1992**, 1334-1340.
- Murata, K.; Kaneko, K.; Kokai, F.; Takahashi, K.; Yudasaka, M.; Iijima, S. Pore Structure of Single-Walled Carbon Nanohorn Aggregates. *Chem. Phys. Lett.*, 331, **2000**, 14-20.
- Murchison, C.B., Conway, M.M., Stevens, R.R. Quarderer, G.J. in: M.J. Phillips, M. Ternan (Eds.), Proceedings of the 9th International Congress of Catalysis, Vol. 2, Calgary, Chemical Institute of Canada, Ottawa, **1988**, 626-633.
- Narayanasarma, P.; Dalai, A.K.; Adjaye, J. Mesoporous Carbon Supported NiMo Catalyst for the Hydrotreating of Coker Gas Oil. *Appl. Catal. A: Gen.* 40, **2011**, 1-11.
- Natta, G.; Colombo, U.; Pasquon, I. Direct catalytic synthesis of higher alcohols from carbon monoxide and hydrogen. In *Catalysis*; Emmett, P. H., Ed.; Reinhold: New York, **1957**; Vol. 5, Chapter 3, 131-174.
- National Resources Canada, Ethanol Facts Sheet, **2016**.
- Naumann, A.W.; Behan, A.S.; Thorsteinson, E. M. 4th International conference on the chemistry and uses of molybdenum, Golden, Colorado, **1982**, 313-318.
- Nylund, N-O.; Aakko-Saksa, P.; Sipilä, K. VTT Research Notes 2426. **2008**.
- Park, T.Y.; Nam, I.-S.; Kim, Y.G. Kinetic Analysis of Mixed Alcohol Synthesis from Syngas over K/MoS₂ Catalyst. *Ind. Eng. Chem. Res.*, 36, **1997**, 5246-5257.
- Portillo, M.A.; Villanueva-Perales A.L.; Vidal-Barrero, F.; Campoy, M. A kinetic Model for the Synthesis of Ethanol from Syngas and Methanol over an Alkali-Co Doped Molybdenum Sulfide Catalyst: Model Building and Validation at Bench Scale. *Fuel Proc. Tech.* 151, **2016**, 19-30.

- Pradhan, B.K.; Sandle, N.K. Effect of Different Oxidizing Agent Treatments on the Surface Properties of Activated Carbons. *Carbon* 37, **1999**, 1323-1332.
- Qi, H.; Li, D.; Yang, C.; Ma, Y.; Li, W.; Sun, Y.; Zhong, B. Nickel and Manganese Co-modified K/MoS₂ Catalyst: High Performance for Higher Alcohols synthesis from CO Hydrogenation. *Catal. Comm.*, **2003**, 4, 339-342.
- Quarderer, G.; K. Cochran. Catalytic Process for Producing Mixed Alcohols from Hydrogen and Carbon Monoxide. In European Patent 0119609, **1984**, WO 84/03696.
- Quarderer, G.J., Stevens, R.R., Cochran, G.A., Murchison, C.B. Preparation of Ethanol and Higher Alcohols from Lower Carbon Number Alcohols. US Patent 4825013, **1989**.
- Ratnasamy, P.; Sivasanker, S. Structural Chemistry of Co-Mo/Alumina Catalysts. *Cat. Rev.*, **1980**, 22, 401-429.
- Rostrup-Nielsen, J.; Christiansen, L.J. Concepts in Syngas Manufacture, Imperial College Press, London, **2011**.
- Ryoo, R.; Joo, S.H.; Kruk, M.; Jaroniec, M. Ordered Mesoporous Carbons. *Adv. Mater.*, 13, **2001**, 677-681.
- Ryoo, R.; Joo, S.H.; Jun, S.; Tsubakiyama, T.; Terasaki, O. Ordered Mesoporous Carbon Molecular Sieves by Templated Synthesis: The Structural Varieties. *Stud. Surf. Sci. Catal.* 135, **2001**, 1121-1128.
- Sachtler, W.M.H.; Ichikawa, M. Catalytic Site Requirements for Elementary Steps in Syngas Conversion to Oxygenates over Promoted Rhodium. *J. Phys. Chem.*, 90, **1986**, 4752-4758.
- Saito, M.; Anderson, R.B. The Activity of Several Molybdenum Compounds for the Methanation of CO. *J. Catal.* 63, **1980**, 438-446.
- Saito, R.; Hofmann, M.; Dresselhaus, G.; Jorio, A.; Dresselhaus, M.S. Raman Spectroscopy of Graphene and Carbon Nanotubes. *Adv. Phys.* 30, **2011**, 413-450.

- Saito, T.; Matsushige, K.; Tanaka, K. Chemical Treatment and Modification of Multi-Walled Carbon Nanotubes. *Phy. B: Condensed Matter*. 323, **2002**, 280-283.
- Satterfield, C.N. *Mass Transfer in Heterogeneous Catalysis*. MIT Press: Cambridge, England, **1970**.
- Satterfield, C.N. *Heterogeneous Catalysis in Industrial Practice*, 2nd ed., McGraw Hill: New York, USA, **1991**, 471-539.
- Sano, N.; Kikuchi, T.; Wang, H.; Chhowalla, M.; Amaratunga, G.A.J. Carbon Nanohorns Hybridized with a Metal-included Nanocapsule. *Carbon*, 2, 1, **2004**, 95-99.
- Santiesteban, J.G.; Bogdan, C.E.; Herman, R.G.; Klier, K.; Mechanism of C₁-C₄ Alcohol Synthesis over Alkali/MoS₂ and Alkali/Co/MoS₂ Catalysts. In *Catalysis: Theory to Practice, C₁ Chemistry*; Phillips, M. J., Ternan, M., Eds.; 9th International Congress on Catalysis: Calgary, 2, **1988**, 561-568.
- Santiesteban, J.G. Alcohol Synthesis from Carbon Monoxide and Hydrogen over MoS₂-based Catalyst, Ph.D. thesis, Lehigh University, Bethlehem, PA, USA, **1989**.
- Schulz, H. Short history and present trends of Fischer–Tropsch synthesis. *Appl. Catal. A.*, 186, **1999**, 3-12.
- Schwan, J.; Ulrich, S.; Batori, V.; Silva, S.R.P.; Ehrhardt, H. Raman Spectroscopy on Amorphous Carbon Films. *J. Appl. Phys.* 80, **2001**, 440-447.
- Serp, P.; Machado, B. Carbon Nanomaterials for Catalysis, in *Nanostructured Carbon Materials for Catalysis*, **2015**, 1-45.
- Shen, Y. Synthesis of Higher Alcohols from Syngas over MoS₂-based Catalysts. M.Sc. Dissertation, Mississippi State University, Mississippi, MI, **1997**.
- Shimodaira, N.; Masui, A.J. Raman Spectroscopic Investigations of Activated Carbon Materials. *Appl. Phys.* 92, **2002**, 902-909.

- Shuihua, T.; Gongquan, S.; Jing, Q.; Shiguo, S.; Junsong, G.; Qin, X.; Haarberg, G.M. Review of New Carbon Materials as Catalyst Supports in Direct Alcohol Fuel Cells. *Chin. J. Catal.*, **2010**, 31, 12-17.
- Siedlecki, M.; de Jong, W.; Verkooijen, A.H.M. Fluidized Bed Gasification as a Mature and Reliable Technology for the Production of Bio-Syngas and Applied in the Production of Liquid Transportation Fuels-A Review. *Energies*, 4, **2011**, 389-434.
- Sigurdson S.K. Hydrotreating of Light Gas Oil Using Carbon Nanotube Supported NiMoS. M.Sc. Thesis, University of Saskatchewan, Saskatoon, Canada, **2010**.
- Sikarwar, V.S.; Zhao, M.; Clough, P.; Yao, J.; Zhong, X.; Memon, M.Z.; Shah, N.; Anthony, E.J.; Fennell, P.S. An Overview of Advances in Biomass Gasification. *Energy Env. Sci.*, **2016**, 9, 2939-2977.
- Silva, R.; Al-Sharab, J.; Asefa, T. Edge-plane-Rich Nitrogen-doped Carbon Nanoneedles and Efficient Metal-free Electrocatalysts. *Angew. Chem., Int. Ed.*, 51, **2012**, 7171-7175.
- Smith, K.J.; Herman, R.G.; Klier, K. Kinetic Modelling of Higher Alcohol Synthesis Alkali-Promoted Cu/ZnO and MoS₂ Catalysts. *Chem. Eng. Sci.*, 45, **1990**, 2639-2646.
- Smith, K.J.; Anderson, R. B. The Higher Alcohol Synthesis over Promoted Cu/ZnO Catalysts. *Can. J. Chem. Eng.*, 61, **1983**, 40-45.
- Smith, K.J.; Anderson, R.B. A chain growth scheme for the higher alcohols synthesis. *J. Catal.*, 85, **1984**, 428-436.
- Smith, J.L.; Workman, J.P. Alcohols for Motor Fuels, Colorado State University Extension, Fact Sheet No. 5.010, **2014**, 1-3. [<http://www.ext.colostate.edu/pubs/farmmgmt/05010.pdf>].
- Song-bai, Q.; Wei-wei, H.; Yong, X.; Lu, L.; Quan-xin, L. Production of Mixed Alcohols from Bio-syngas over Mo-based Catalyst. *Chin. J. Chem. Phys.*, **2011**, 77-84.
- Speight J.G. The desulfurization of heavy oils and residua. Marcel Dekker, New York, **2000**.

- Spivey, J.J.; Egbebi, A. Heterogeneous Catalytic Synthesis of Ethanol from Biomass-derived Syngas. *Chem. Soc. Rev.*, 36, **2007**, 1514-1528.
- Stagnaro, S.Y.M.; Volzoneb, C.; Rueda, M.L. Influence of Thermal Treatment on Bentonite used as Adsorbent for Cd, Pb, Zn Retention from Mono-Solute and Poly-Solute Aqueous Solutions. *Mater. Res.*, 15, **2012**, 549-553.
- Stevens, R.R. Process for Producing Alcohols from Synthesis Gas. **1988**, Patent US4752622.
- Stevens, R.R.; Conway, M.M. Mixed Alcohols Production from Syngas. **1988**, Patent US4752623.
- Steynberg, A.P. Introduction to Fischer-Tropsch technology. *Stud. Surf. Sci. Catal.* **2004**, 152, 1-63.
- Storm, D.A. The Production of Higher Alcohols from Syngas Using Potassium-promoted CoMo/Al₂O₃ and Rh-Co-Mo/Al₂O₃. *Top. Catal.*, 2, **1995**, 99-101.
- Su, J.; Mao, W.; Xu, X-C.; Yang, Z.; Li, H.; Xu, J.; Yi-Fan, H. Kinetic Study of Higher Alcohol Synthesis Directly from Syngas CoCu/SiO₂ Catalysts. *AIChE J.* vol. 60, **2014**, 1797-1809.
- Subramani, V.; Gangwal, S.K., "A Review of Recent Literature to Search for an Efficient Catalytic Process for the Conversion of Syngas to Ethanol", *Energy & Fuels*, 22, **2008**, 814-839.
- Sudhakar, C.; Bhore, N. A.; Bischoff, K. B.; Manogue, W. H.; Mills, G. A. Molybdena Enhanced Rh/Al₂O₃ Catalysts. In *Proc. of the 10th Meeting of the Catalysis Society of North America*, San Diego, CA, **1987**.
- Suehiro, J; Sano N; Zhou G.B.; Zhou, G.; Imakiire, H.; Imasaka, K.; Hara, M. Application of Dielectrophoresis to Fabrication of Carbon Nanohorn Gas Sensor. *Journal of Electrostatics*, 64, **2006**, 408-415.
- Surisetty, V.R.; Tavasoli, A.; Dalai, A.K. Synthesis of Higher Alcohols from Syngas over Alkali-promoted MoS₂ Catalysts Supported on Multi-Walled Carbon Nanotubes. *Appl. Catal. A. Gen.*, 365, **2009**, 243-251.

- Surisetty V.R.; Dalai, A.K.; Kozinski, Alkali-promoted Trimetallic Co-Rh-Mo Sulfide Catalysts for Higher Alcohols Synthesis from Synthesis Gas: Comparison of MWCNT and Activated Carbon Supports. *J. Ind. Eng. Chem. Res.*, 49, **2010**, 6956-6963.
- Surisetty, V. R.; Dalai, A. K.; Kozinski, J. Intrinsic Reaction Kinetics of Higher Alcohols Synthesis from Synthesis Gas over Sulfided Alkali-promoted Co-Rh-Mo Trimetallic Catalyst Supported on MWCNTs. *Energy. Fuel.* 24, **2010**, 4130-4137.
- Surisetty, V.R. Research and Development of Co and Rh-promoted Alkali-modified Molybdenum Sulfide Catalysts for Higher Alcohols Synthesis from Synthesis Gas. Ph.D Thesis, University of Saskatchewan, Saskatoon, **2010**.
- Surisetty, V.R.; Tavasoli, A.; Dalai, A.K., "Influence of Porous Characteristics of the Carbon Support on Alkali-modified Trimetallic Co-Rh-Mo Sulfided Catalysts for Higher Alcohols Synthesis from Synthesis Gas", *Appl. Catal. A.*, **2011**, 393, 50-58.
- Surisetty, V.R.; Dalai, A.K.; Kozinski, J. Deactivation Studies of Alkali-Promoted Trimetallic Co-Rh-Mo Sulfide Catalysts for Higher Alcohols Synthesis from Synthesis Gas, *Energy Fuels*, **2011**, 25, 580-590.
- Surisetty, V.R.; Kozinski, J.; Dalai, A.K. Novel Ni-Co-Mo-K Catalysts Supported on Multi-walled Carbon Nanotubes for Higher Alcohols Synthesis, *J. Catal.*, **2013**, 1-7.
- Tanev, T.P.; Pinnavaia, T.J. Mesoporous Silica Molecular Sieves Prepared by Ionic and Neutral Surfactant Templating: A Comparison of Physical Properties. *Chem. Mater.*, 8, **1996**, 2068-2079.
- Tauster, S.J.; Fung, S.C.; Baker, R.T.K.; Horsley, J.A. Strong Interactions in Supported-Metal Catalysts. *Science*, 211, **1981**, 1121-1125.
- Tatsumi, T.; Muramatsu, A.; Yokota, K.; Tominga, H. Mechanistic study on the alcohol synthesis over molybdenum catalysts: Addition of probe molecules to CO-H₂. *J. Catal.* 115, **1989**, 388-398.

- Teng, H.; Suuberg, E.M. Chemisorption of Nitric Oxide on Char. 1. Reversible Nitric Oxide Sorption. *J. Phys. Chem.* 97, **1993**, 478-483.
- Tien-Thao, N.; Alamdari, H.; Zahedi-Niaki, M.H.; Kaliaguine, S. $\text{LaCo}_{1-x}\text{Cu}_x\text{O}_{3-\delta}$ Perovskite Catalysts for Higher Alcohol Synthesis. *Appl. Catal. A*, 311, **2006**, 204-212.
- Tronconi, E.; Forzatti, P.; Pasquon, I.I. An Investigation of the Thermodynamic Constraints in Higher Alcohol Synthesis over Cs-promoted ZnCr-Oxide Catalyst. *J. Catal.*, 124, **1990**, 376-390.
- Tsang, S.C.; Chen, Y.K.; Harris, P.J.F.; Green, M.L.H. A Simple Chemical Method of Opening and Filling Carbon Nanotubes. *Nature*, 372, **1994**, 159-162.
- Urita, K.; Seki, S.; Utsumi, S.; Noguchi, D.; Kanoh, H.; Tanaka, H.; Hattori, Y.; Ochiai, T.; Aoki, N.; Yudasaka, M.; Iijima, S.; Kaneko, K. Effects of Gas Adsorption on the Electrical Conductivity of Single-Wall Carbon Nanohorns. *Nano Letters*, 6, **2006**, 1325-1328.
- Utsumi, S.; Urita, K.; Kanoh, H.; Yudasaka, M.; Suenaga, K.; Iijima, S.; Kaneko, K. Preparing a Magnetically Responsive Single-Wall Carbon Nanohorn Colloid by Anchoring Magnetite Nanoparticles. *J. Phys. Chem. B*, 110, **2006**, 7165-7170.
- Van der Laan, G.P.; Beenackers, A.A.C.M. Kinetics and Selectivity of the Fischer-Tropsch Synthesis: A Literature Review. *Catal. Rev. Sci. Eng.*, 41, **2011**, 255-318.
- Van Steen, E.; Schulz, H. Polymerization Kinetics of the Fischer-Tropsch CO Hydrogenation using Iron and Cobalt-based Catalysts, *Applied Catalysis A: General* 186, **1999**, 309-320.
- Vinu, A.; Srinivasu, P.; Takahashi, M.; Mori, T.; Balasubramanian, V.V.; Ariga, K. Microporous Mesoporous Mater 100, **2007**, 20-26.
- Vradman, L.; Landau, M. V.; Herskowitz, M.; Ezersky, V.; Talianker, M.; Nikitenko, S.; Kolytyn, Y.; Gedanken, A. High Loading of Short WS_2 Slabs Inside SBA-15: Promotion with Nickel and Performance in Hydrodesulfurization and Hydrogenation. *J. Catal.*, 213, **2003**, 163-175.

- Vradman, L.; Landau, M.V.; Kantorovich, D.; Koltypin, Y.; Gedanken, A. Evaluation of Metal Oxide Phase Assembling Mode inside the Nanotubular Pores of Mesostructured Silica. *Micro. Meso. Mater.*, 70, **2005**, 307-318.
- Wang, H.; Chhowalla, M.; Sano, N.; Jia, S.; Amaratunga, G. Large-Scale Synthesis of Single-Walled Carbon Nanohorns by Submerged Arc. *Nanotechnology*, 15, **2004**, 546-550.
- Wang, Y.; Li, J.; Mi, W. Probing Study of Rh Catalysts on Different Supports in CO Hydrogenation. *React. Kinet. Catal. Lett.* **2002**, 76, 141-150.
- Weisz, P. B.; Prater, C. D. Interpretation of Measurements in Experimental Catalysis. *Adv. Catal.* 6, **1954**, 143-196.
- Woo, H.C.; Park, K.Y. Mixed Alcohols Synthesis from Carbon Monoxide and Dihydrogen over Potassium-promoted Molybdenum Carbide Catalysts. *Appl. Catal. A.*, 75, **1991**, 267-280.
- World Energy Outlook 2016, International Energy Agency, Paris, **2016**.
- World Population Prospects: The 2015 Revision, Department of Economic and Social Affairs/Population Division, United Nations, New York, **2017**.
- Xiao, B.; Thomas, K. Competitive Adsorption of Aqueous Metal Ions on an Oxidized Nanoporous Activated Carbon. *Langmuir* 20, **2004**, 4566-4578.
- Xiaoding, X.; Doesburg, E.B.M.; Scholten, J.J.F. Synthesis of Higher Alcohols from Syngas - Recently Patented Catalysts and Tentative Ideas on the Mechanism. *Catal. Tod.*, 2, **1987**, 125-170.
- Xiong, H.; Jewell, L.L.; Coville, N.J. Shaped Carbons as Supports for the Catalytic Conversion of Syngas to Clean Fuels. *ACS Catal.*, 5, **2015**, 2640-2658.
- Yang, S.; Gong, Y.; Zhang, J.; Zhan, L.; Ma, L.; Fang, Z.; Vajtai, R.; Wang, X.; Ajayan, P.M. Exfoliated Graphitic Carbon Nitride Nanosheets as Efficient Catalysts for Hydrogen Evolution under Visible Light. *Adv. Mater.*, 25, **2013**, 2452-2456.

- Yang, W.; Alsmeyer, D.C.; McCreery, R.L. Raman Spectroscopy of Carbon Materials: Structural Basis of Observed Spectra. *Chem. Mater.*, 2, **1990**, 557-563.
- Yang, Y.; Chiang, K.; Burke, N. Porous Carbon-Supported Catalysts for Energy and Environmental Applications: A Short Review, *Catal. Tod.*, 178, **2011**, 197-205.
- Yin, H.; Ding, Y.; Luo, H.; Yan, L.; Wang, T.; Liwu, L. The Performance of C₂ Oxygenates Synthesis from Syngas over Rh-Mn-Li-Fe/SiO₂ Catalysts with Various Rh Loadings. *Energy & Fuels*, 17, **2003**, 1401-1406.
- Yurum, Y.; Taralp, A.; Veziroglu, T.N. Review Paper: Storage of Hydrogen in Nanostructured Carbon Materials, *Int. J. Hydrogen Energy*, 34, **2009**, 3784-98.
- Zhang, H-B.; Dong, X.; Lin, G-D.; Liang, X-L.; Li, H-Y. Carbon Nanotube-promoted Co-Cu Catalyst for Highly Efficient Synthesis of Higher Alcohols from Syngas. *Chem. Comm.*, 40, **2005**, 5094-5096.
- Zhang, P.; Gong, Y.; Li, H.; Chen, Z.; Wang, Y. Solvent-free Aerobic Oxidation of Hydrocarbons and Alcohols with Pd@N-doped Carbon from Glucose. *Nat. Comm.*, 4, **2013**, 1593-1603.
- Zhongren, Y., Economy, J. Synthesis of Highly Mesoporous Carbon Pellets from Carbon Black and Polymer Binder by Chemical Activation. *Microporous Mesoporous Mater* 96 (1-3), **2006**, 314-320.
- Zurita, M.J.P.; Cifarelli, M.; Cubeiro, M.L.; Goldwasser, J.A.M.; Pietri, E.; Garcia, L.; Aboukais, A.; Lamonier, J.-F. Palladium-based Catalysts for the Synthesis of Alcohols. *J. Mol. Catal. A: Chem.* 206, **2003**, 339-351.

APPENDIX A

Research Outcome

A.1. Publications from Results of the Thesis

1. Philip E. Boahene, Ajay K. Dalai, “Higher Alcohols Synthesis: Experimental and process parameters study over CNH-supported KCoRhMo catalyst, *Ind. Eng. Chem. Res.*, **2017**, 56 (46), 13552–13565.
2. Philip E. Boahene, Ajay K. Dalai, “Sustainable production and utilization technologies of biojet fuels”, *Sustainable Utilization of Natural Resources*, **2017**, 595-606.
3. Philip E. Boahene, Ramaswami Sammynaiken, Ajay K. Dalai, “Syngas conversion to higher alcohols: Application of novel K-promoted CoRhMo catalysts supported over carbon nanohorns (CNHs) and its by-products (OCP & OCP_f)”, *Int. J. Petrochem. Sci. Eng.* 2, 1, **2017**, 1-14.
4. Philip E. Boahene, R. Sammynaiken, A.K. Dalai, “Syngas conversion to higher alcohols: A comparative study of acid and base-treated mesoporous carbon-supported KCoRhMoS₂ catalysts”, *Catal. Tod.*, Vol. 291, **2017**, 106-123.
5. Philip E. Boahene, R. Sammynaiken, A.K. Dalai, “Syngas Conversion to Higher Alcohols: A Comparative Study of Large-pore OMC and MWCNT-supported K-CoRhMoS₂ Catalysts”, *Fischer-Tropsch Synthesis, Catalysts, and Catalysis*, 15, **2016**, 275-294.
6. James Aluha, Philip E. Boahene, Ajay Dalai, Yongfeng Hu, Kossi Bere, Nadi Braidy, Nicolas Abatzoglou, “Synthesis and Characterization of Co/C and Fe/C Nanocatalysts for Fischer–Tropsch Synthesis: A Comparative Study Using a Fixed-Bed Reactor”, *Ind. Eng. Chem. Res.*, **2015**, 54 (43), pp 10661–10674.

7. Philip E. Boahene, V.R. Surisetty, R. Sammynaiken, A.K. Dalai, “Higher alcohol synthesis using K-doped CoRhMoS₂/MWCNT catalysts: Influence of pelletization, particle size and incorporation of binders”, *Top Catal.*, **57**, **2014**, 538-549.
8. Philip E. Boahene, Ajay K. Dalai, “Higher alcohols synthesis over CNH-supported KCoRhMo catalyst: Pelletization and kinetic modelling (Submitted to *Industrial & Engineering Chemistry Research* – **Under review**).
9. Philip E. Boahene, Ramaswami Sammynaiken, Ajay K. Dalai, “Synthesis and utilization of supported nano-transition metal catalysts for clean transportation fuels application: A short review” (**Under preparation**).

A.2. Refereed Conference Presentations

1. Philip E. Boahene, Ramaswami Sammynaiken, Ajay K. Dalai, “Syngas conversion to higher alcohols: Application of novel K-promoted CoRhMo catalysts supported over carbon nanohorns (CNHs) and its by-products (OCP & OCP_f)” (Oral presentation at the 252nd ACS Meeting & Exposition, Philadelphia, PA, USA, August 21-25, **2016**).
2. Philip E. Boahene, Ramaswami Sammynaiken, Ajay K. Dalai, “Syngas conversion to higher alcohols: Application of novel K-promoted CoRhMo catalysts supported over carbon nanohorns (CNHs) and its by-products (OCP & OCP_f)” (Poster presentation at the 16th International Congress on Catalysis, Beijing, China, July 3-8, **2016**).
3. P.E. Boahene, R. Sammynaiken, A.K. Dalai, “Syngas conversion to higher alcohols: A comparative study of acid and base-treated mesoporous carbon-supported KCoRhMoS₂ catalysts” (Oral presentation at the 24th North American Catalysis Society Meeting, Pittsburgh, PA, USA, June 14-19, **2015**).

4. Boahene, P.E.; Sammynaiken, R.; Dalai, A.K.; “Syngas Conversion to Higher Alcohols: A Comparative Study of Large-pore OMC and MWCNT-supported K-CoRhMoS₂ Catalysts” (Accepted for Oral presentation at the 23rd Canadian Symposium on Catalysis, Edmonton, Canada, May 11-14, **2014**).
5. Boahene, P.E.; Vosoughi, V.; Dalai, A.K. “Bio-syndiesel and alcohol production from synthesis gas”, (Presented at the Advanced Biofuel Symposium, Ottawa, May 27-29, **2014**).
6. Boahene, P.E.; Sammynaiken, R.; Dalai, A.K.; “Conversion of Syngas to Higher Alcohols: Influence of bentonite clay as a binder and its variable loadings on KCoRhMoS₂/MWCNT catalysts formulation” (Presented in an Oral session at the 248th ACS National Meeting & Exposition, San Francisco, CA, USA, August 10-14, **2014**).
7. Boahene, P.E.; Dalai, A.K.; “Comparative study of large-pore ordered mesoporous carbon and MWCNT-supported K-doped dual-promoted MoS₂ catalysts for higher alcohol synthesis”, (Presented in a Poster session at the 23rd North American Catalysis Society Meeting, June 2-7, **2013**, Louisville, Kentucky, USA).
8. Boahene, P.E.; Surisetty, V.R.; Dalai, A.K.; “Higher alcohol synthesis using K-doped CoRhMoS₂/MWCNT catalysts: Influence of pelletization, particle size, and incorporation of binders”, (Presented in an Oral session at the 245th ACS National Meeting, April 7-11, **2013**, New Orleans, Louisiana, USA).

APPENDIX B

Experimental Calibrations

This section provides the details about the temperature calibrations of the downward flow reactor as well as the calibrations of mass flow controllers used in the higher alcohols synthesis experiments.

B.1. Reactor temperature calibration

The reactor was packed with silicon carbide (SiC) of 90 μm grain size first without catalyst and subsequently with catalyst as part of the loading scheme. The temperature calibration was accomplished by pressurizing the reactor to 1400 psig with helium gas. Temperature of the furnace was varied from 200 to 350°C and the corresponding reactor temperature was measured using a single thermocouple inserted in a thermowell to enhance the variation of the thermocouple. The position of the thermocouple was then varied by 2 cm from the bottom to measure the temperature in the axial direction of the reactor after allowing 5 minutes each time for the temperature to equilibrate. Temperature profiles along the reactor bed are shown in Figure B.1 and the calibration curve for the temperature controller is presented in Figure B.2.

B.2. Mass flow controller calibration

Calibration of the mass flow controllers were performed at the experimental operating conditions for the flow of gaseous mixtures: 10 mol % $\text{H}_2\text{S}/\text{H}_2$ and 0 mol % Ar in syngas mixture. A bubble flow meter was connected at the outlet of the back-pressure regulator and outlet flow rates were measured at atmospheric conditions. Calibration curves for the two mass flow controllers are given in Figures B3 and B4. The following equation was used to calculate the flow rates at operating conditions (Surisetty, 2010).

$$\frac{P_0 * V_0}{T_0} = \frac{P_s * V_s}{T_s} \rightarrow V_0 = \frac{P_s * V_s}{T_s} \left(\frac{T_0}{P_0} \right) \dots\dots\dots (B.1)$$

where V = flow rate in mL/hr; T = temperature; P = pressure; subscripts “s” and “o” represent standard and operating conditions, respectively.

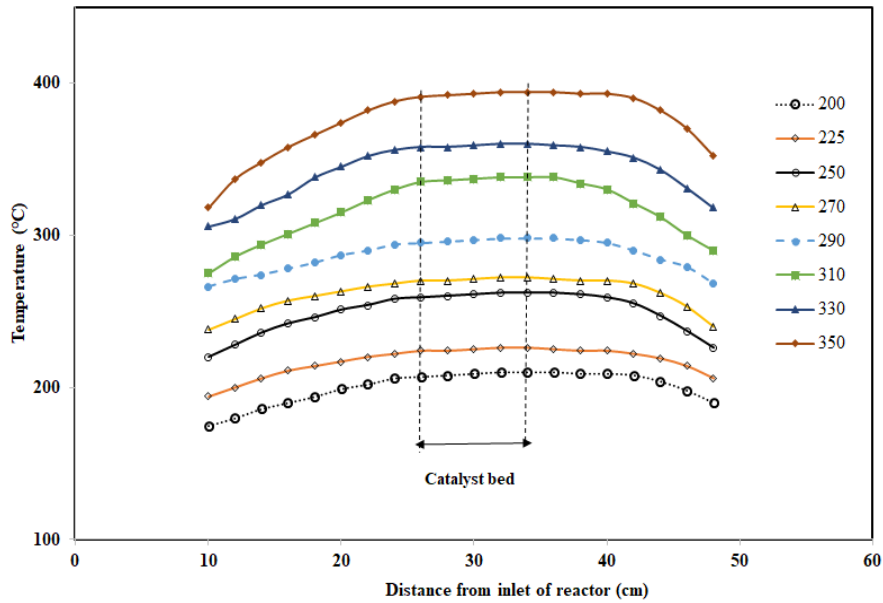


Fig. B.1: Axial temperature profiles for downward flow reactor

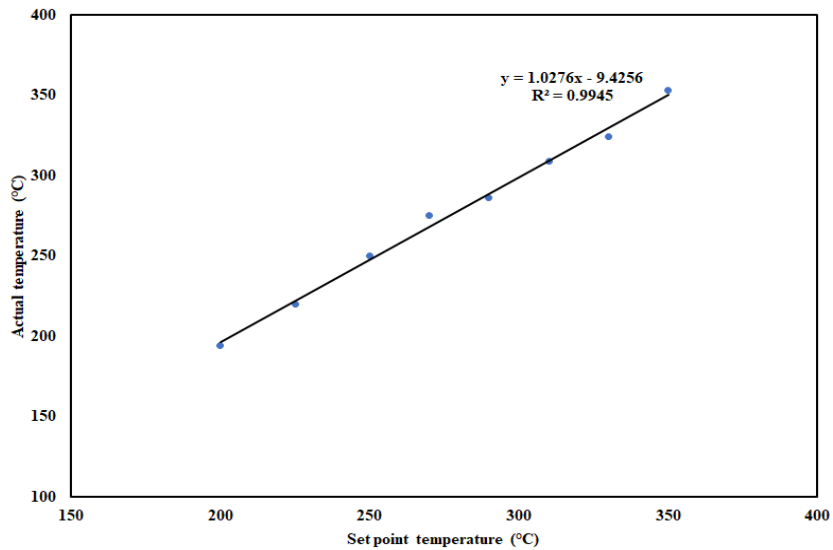


Fig. B.2: Calibration curve for temperature controller

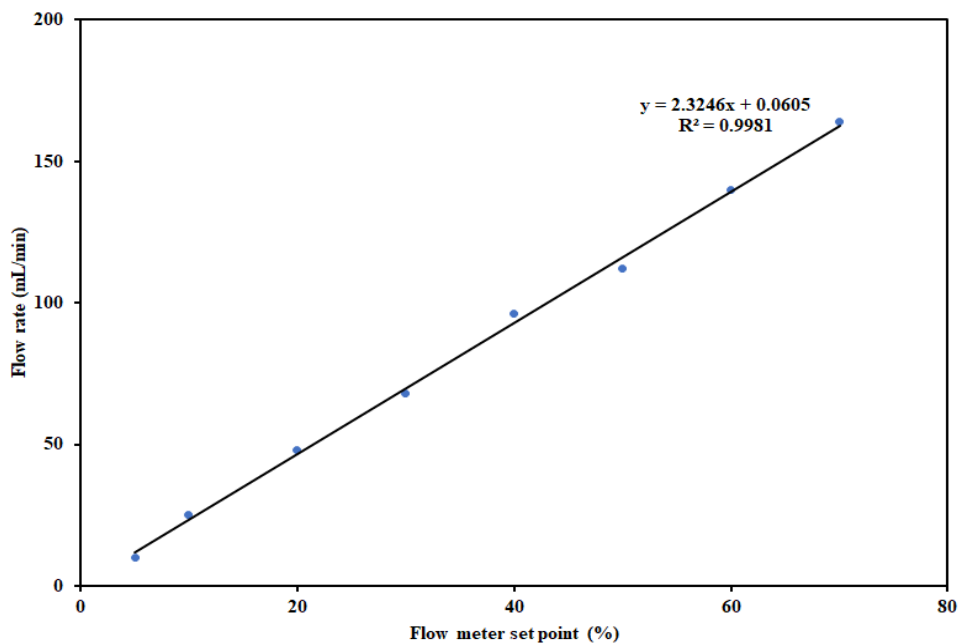


Fig. B.3: Calibration curve - mass flow controller for 10 mol% Ar in syngas

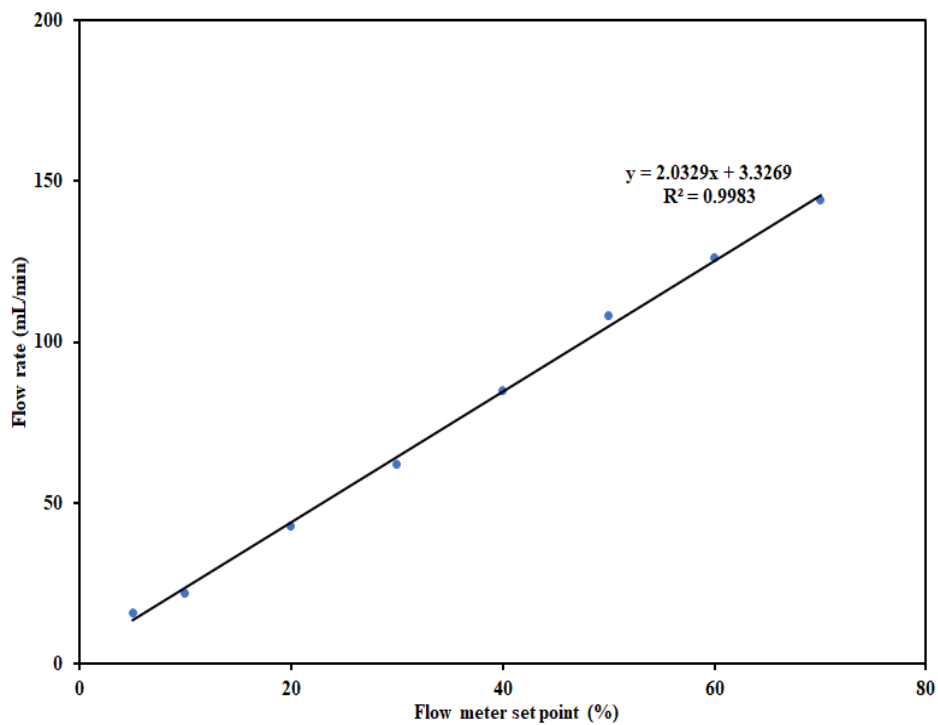


Fig. B.4: Calibration curve - mass flow controller for 10 mol% H₂S balance hydrogen

APPENDIX C

Material Balance Data

Catalyst	KCoRhMo/MWCNT
Mass of catalyst (g)	2
Process pressure (psi)	1200
Process temperature (°C)	320
Volumetric flow rate of syngas (mL/min)	120
Inlet moles of syngas (mol/h)	0.3214
Inlet H ₂ flowrate (mol/h)	0.16071
Inlet CO flowrate (mol/h)	0.1286
Inlet Ar flowrate (mol/h)	0.0321
H ₂ /CO	1.25
Outlet gas flowrate (mL/min)	108
Outlet gas temperature	0
Barometric pressure (psi)	760
Outlet gas molar density (gmol/L)	0.045
Mass of liquid collected (g)	2.652
Duration of run (min)	1440

Outlet gas compositions	
Component	Volume (%)
H ₂	57.598
CO	27.927
Ar	10.865
CO ₂	1.963
Methane	1.532
Ethane	0.095
Ethylene	0.006
Propane	0.012
Propylene	0.001
n-butane	0.001
TOTAL	100
Liquid compositions	
Component	Mass (%)
Water	0.68
Methanol	58.68
Ethanol	33.96
n-propanol	5.68
n-butanol	0.92
n-pentanol	0.08
TOTAL	100

Component	Inlet (g/min)	Outlet (g/min)	%Difference
Carbon	0.0168	0.0164	2.38
Hydrogen	0.0064	0.0062	3.12
Oxygen	0.0208	0.0205	1.44
Argon	0.0243	0.0243	0.00
OVERALL	0.0680	0.0674	6.94

Appendix D

Mass transfer resistance calculations

D.1. External mass-transfer limitation

The Frössling correlation (Frössling, 1938) was used to calculate the mass transfer coefficient as well as the boundary layer thickness around the catalyst particle. The KCoRhMo/CNH catalyst of particle size 210-297 μm was used.

Catalyst particle size = 210-297 μm

$$\text{Average particle size, } d_p = \frac{210+297}{2} = 254 \mu\text{m} = 254 * 10^{-6}\text{m} = 2.54 * 10^{-4} \text{ m}$$

Calculation of free stream velocity of gas (u):

$$\begin{aligned} \text{Free stream velocity (} u \text{)} &= \frac{\text{volumetric flowrate of gas (} Q \text{)}}{\text{Cross sectional area of reactor (} A_c \text{)}} = \frac{Q}{\pi * (\frac{d}{2})^2} \\ &= \frac{60 \frac{\text{mL}}{\text{min}} * \frac{1 \text{ m}^3}{10^6 \text{ mL}} * \frac{1 \text{ min}}{60 \text{ s}}}{\pi * (\frac{22 * 10^{-3}}{2})^2 \text{ m}^2} = 2.63 * 10^{-3} \text{ m/s} \dots\dots\dots (D1.1) \end{aligned}$$

Calculation of density and dynamic viscosity of gas (ρ):

In the computation of the average density and dynamic viscosity of gas, it was assumed that the syngas mixture to behave like an ideal gas under the HAS reaction conditions. Also, the densities and dynamic viscosities of the individual components in the syngas mixture was looked up online at the following websites: <http://www.globalspec.com/calculators/gas-density> and <http://www.lmnoeng.com/Flow/GasViscosity.php> (Date accessed: July 04, 2017).

Syngas compositions used for the HAS reaction:

$$\text{H}_2 = 50 \text{ mol\%}; \text{CO} = 40 \text{ mol\%}; \text{and Ar} = 10 \text{ mol\%}$$

Density of hydrogen at 1320 psig and 325°C = 3.7 kg/m³

Density of carbon monoxide at 1320 psig and 325°C = 51.82 kg/m³

Density of argon at 1320 psig and 325°C = 73.85 kg/m³

Hence, the average density of syngas = $(0.5 \times 3.86 + 0.4 \times 51.82 + 0.10 \times 73.85) / 3 = 10.01 \text{ kg/m}^3$

Similarly,

Dynamic viscosity of hydrogen at 1320 psig and 325°C = $1.39 \times 10^{-5} \text{ kg/(m-s)}$

Dynamic viscosity of carbon monoxide at 1320 psig and 325°C = $2.92 \times 10^{-5} \text{ kg/(m-s)}$

Dynamic viscosity of argon at 1320 psig and 325°C = $4.84 \times 10^{-5} \text{ kg/(m-s)}$

Hence, the average dynamic viscosity of syngas = $[(0.5 \times 1.39 \times 10^{-5}) + (0.4 \times 2.92 \times 10^{-5}) + (0.10 \times 4.84 \times 10^{-5})] / 3 = 7.82 \times 10^{-6} \text{ kg/(m-s)}$

Table D.1: Summary of calculated gas properties at 1320 psig.

T (°C)	Density, kg/m ³			
	H ₂	CO	Ar	Syngas
290	3.89	54.54	77.24	10.49
310	3.83	53.50	76.23	10.31
330	3.74	52.49	74.81	10.12
350	3.68	51.53	73.43	9.93
T (°C)	Dynamic viscosity*10 ⁻⁶ , kg/m-s			
	H ₂	CO	Ar	Syngas
290	1.34	2.80	4.94	7.61

310	1.37	2.87	4.89	7.74
330	1.39	2.93	4.79	7.82
350	1.42	3.00	4.63	7.91

Calculation of effective diffusivity (D_{eff}):

The effective diffusivity for binary gas mixtures was calculated based on the modern kinetic theory and the Lennard-Jones expression for intermolecular forces (Hirschfelder et al., 1954; Surisetty, 2010).

$$D_{AB} = \frac{0.001858 * T^{1.5} * [(M_1 + M_2)/(M_1 * M_2)]^{0.5}}{P * \sigma_{12}^2 * \Omega_D} \dots \dots \dots (D1.2)$$

where:

D_{AB} = diffusivity for a binary gas mixture

T = temperature (K)

M_i = molecular weight of species i

P = pressure (atm)

Ω_D = collision integral

σ = constant of Lennard-Jones potential function

Also, the collision integral is given by:

$$\Omega_D = \frac{k * T}{\epsilon_{12}} \dots \dots \dots (D1.3)$$

where:

ϵ = Lennard-Jones potential function

k = Boltzmann constant

$\Omega_D = 4.21$ (from Satterfield, 1970)

$M_1 = M_{CO} = 28.01$ g/mol

$M_2 = M_{H_2} = 2.02$ g/mol

$P = 1320$ psig = 89.82 atm

$T = 325^\circ\text{C} = 598.15$ K

The values of σ_1 and σ_2 were obtained for CO and H₂ from Table 1.3 (Satterfield, 1970) to represent species 1 and 2, respectively.

$$\sigma_{12} = \frac{\sigma_1 + \sigma_2}{2} = \frac{3.806 + 2.899}{2} = 3.353 \text{ \AA} \dots \dots \dots (D1.4)$$

Also,

$$\frac{\varepsilon_{12}}{kT} = \left(\frac{\varepsilon_1}{k}\right)^{0.5} * \left(\frac{\varepsilon_2}{k}\right)^{0.5} * \left(\frac{1}{T}\right) = (29.790)^{0.5} * (99.699)^{0.5} * \left(\frac{1}{598.15}\right) = 0.091$$

Thus,

$$\frac{kT}{\varepsilon_{12}} = (0.0911)^{-1} = 10.98$$

Hence,

$$D_{AB} = \frac{0.001858 * (598.15)^{1.5} * [(28.01 + 2.02)/(28.01 * 2.02)]^{0.5}}{92.81 * (3.353)^2 * 4.21} = 4.51 * 10^{-3} \text{ cm}^2/\text{s}$$

Similarly, $D_e = D_{AB} * \frac{\theta}{\tau} = 4.51 * 10^{-3} * \frac{0.5}{4} = 5.63 * 10^{-4} \text{ cm}^2/\text{s}$

where: θ = porosity of catalyst; τ = tortuosity factor.

Values of $\theta = 0.5$ and $\tau = 4$ are recommended for estimation purposes (Satterfield, 1991; Surisetty, 2010).

Calculation of Reynolds number

$$Re = \frac{\rho u d_p}{\mu} = \frac{10.01 \frac{kg}{m^3} * 2.63 * 10^{-3} \frac{m}{s} * 2.54 * 10^{-4} m}{7.82 * 10^{-6} \frac{kg}{m \cdot s}} = 0.855$$

Calculation of Schmidt number:

$$Sc = \frac{\mu}{\rho D_e} = \frac{7.82 * 10^{-6} \frac{kg}{m \cdot s}}{10.01 \frac{kg}{m^3} * 5.63 * 10^{-8} \frac{m^2}{s}} = 13.88$$

Calculation of Sherwood number:

$$Sh = 2 + 0.6 (Re)^{1/2} (Sc)^{1/3} = 2 + 0.6(0.855)^{1/2}(13.88)^{1/3} = 3.33$$

Calculation of mass transfer coefficient:

$$Sh = \frac{k_c d_p}{D_e} \dots \dots \dots (D1.5)$$

Thus,

$$k_c = \frac{Sh * D_e}{d_p} = \frac{3.33 * 5.63 * 10^{-8} \frac{m^2}{s}}{2.54 * 10^{-4} m} = 7.39 * 10^{-4} \frac{m}{s}$$

Hence, the boundary layer thickness:

$$\delta = \frac{D_e}{k_c} = \frac{5.63 * 10^{-8} \frac{m^2}{s}}{7.39 * 10^{-4} \frac{m}{s}} = 7.62 * 10^{-5} m = 0.0762 mm$$

Table D.2: Summary of computed dimensionless quantities and mass transfer parameters

T (°C)	Cat-CNH (Average particle size = 0.088 mm)				
	Re	Sc	Sh	k_c (m/s)	δ (mm)
290	0.14	14.08	2.82	1.65*10 ⁻³	3.12*10 ⁻²
310	0.31	13.85	2.78	1.72*10 ⁻³	3.16*10 ⁻²
330	0.30	13.56	2.78	1.80*10 ⁻³	3.16*10 ⁻²
350	0.29	13.28	2.77	1.89*10 ⁻³	3.18*10 ⁻²
T (°C)	Cat-CNH (Average particle size = 0.254 mm)				
	Re	Sc	Sh	k_c (m/s)	δ (mm)
290	0.92	14.08	3.39	6.87*10 ⁻⁴	7.49*10 ⁻²
310	0.89	13.85	3.36	7.17*10 ⁻⁴	7.56*10 ⁻²
330	0.86	13.56	3.33	7.47*10 ⁻⁴	7.63*10 ⁻²
350	0.84	13.28	3.30	7.80*10 ⁻⁴	7.69*10 ⁻²
T (°C)	Cat-5BC-CNH (Average particle size = 0.254 mm)				
	Re	Sc	Sh	k_c (m/s)	δ (mm)
290	0.92	15.64	3.44	6.28*10 ⁻⁴	7.38*10 ⁻²
310	0.89	15.27	3.40	6.59*10 ⁻⁴	7.46*10 ⁻²
330	0.86	15.06	3.38	6.82*10 ⁻⁴	7.52*10 ⁻²
350	0.84	14.78	3.35	7.10*10 ⁻⁴	7.59*10 ⁻²

D.2. Internal mass-transfer limitation

Estimation of the internal mass transfer resistance due to pore diffusion was estimated based on the Weisz-Prater criterion (C_{WP}) (Weisz, 1954; Fogler, 1999; Surisetty, 2010). If the criterion is satisfied, pore diffusion limitations during the HAS reaction can be considered negligible. For $C_{WP} \ll 1$, internal pore diffusion limits the overall rate of reaction; however, if $C_{WP} \gg 1$, internal pore diffusion severely limits the overall reaction (Weisz, 1954; Fogler, 1999; Surisetty, 2010).

Catalyst particle size = 210-297 μm

Average particle size, $d_p = \frac{210+297}{2} = 254 \mu m = 2.54 * 10^{-2} cm = 2.54 * 10^{-4} m$

$$C_{WP} = \frac{-(r_A)_{obs} * \rho_c * r^2}{C_{As} * D_e} \dots \dots \dots (D1.6)$$

where:

ρ_c = density of catalyst

r = catalyst particle radius

C_{As} = surface concentration of reactant A

D_e = effective diffusivity

$(r_A)_{obs}$ = reaction rate per unit mass of catalyst

Also, the surface concentration of reactant, C_{As} can be given by:

$$C_{As} = \frac{P_A}{RT} = \frac{0.4 * 92.81 \text{ atm}}{0.0821 \frac{\text{m}^3 \cdot \text{atm}}{\text{kgmol} \cdot \text{K}} * 598.15 \text{ K}} = 0.756 \frac{\text{kgmol}}{\text{m}^3}$$

$$r = 1.27 * 10^{-4} \text{ m}; \rho_c = 2864 \text{ kg/m}^3; D_e = 5.68 * 10^{-8} \text{ m}^2/\text{s}; -(r_A)_{\text{obs}} = 1.161 * 10^{-5} \text{ kgmol/kg}_{\text{cat}}\text{-s}$$

$$C_{WP} = \frac{1.161 * 10^{-5} \frac{\text{kgmol}}{\text{kg}_{\text{cat}}\text{-s}} * 2864 \frac{\text{kg}}{\text{m}^3} * (1.27 * 10^{-4})^2 \text{ m}^2}{0.756 \frac{\text{kgmol}}{\text{m}^3} * 5.68 * 10^{-8} \frac{\text{m}^2}{\text{s}}} = 1.25 * 10^{-2}$$

**SPRINGER LICENSE
TERMS AND CONDITIONS**

Aug 14, 2017

This Agreement between Mr. Philip Boahene ("You") and Springer ("Springer") consists of your license details and the terms and conditions provided by Springer and Copyright Clearance Center.

License Number	4167770789592
License date	Aug 14, 2017
Licensed Content Publisher	Springer
Licensed Content Publication	Topics in Catalysis
Licensed Content Title	Higher Alcohol Synthesis Using K-Doped CoRhMoS ₂ /MWCNT Catalysts: Influence of Pelletization, Particle Size and Incorporation of Binders
Licensed Content Author	Philip E. Boahene
Licensed Content Date	Jan 1, 2013
Licensed Content Volume	57
Licensed Content Issue	6
Type of Use	Thesis/Dissertation
Portion	Full text
Number of copies	1
Author of this Springer article	Yes and you are a contributor of the new work
Order reference number	
Title of your thesis / dissertation	Catalysts development for the conversion of syngas to higher alcohols using alkali-promoted mos ₂ -based catalysts over carbon supports
Expected completion date	Sep 2017
Estimated size(pages)	280
Requestor Location	Mr. Philip Boahene 57 Campus Drive Saskatoon, SK S7N5A9 Canada Attn: Mr. Philip Boahene
Billing Type	Invoice
Billing Address	Mr. Philip Boahene 57 Campus Drive Saskatoon, SK S7N5A9 Canada Attn: Mr. Philip Boahene
Total	0.00 USD
Terms and Conditions	

Introduction

The publisher for this copyrighted material is Springer. By clicking "accept" in connection with completing this licensing transaction, you agree that the following terms and conditions apply to this transaction (along with the Billing and Payment terms and conditions established by Copyright Clearance Center, Inc. ("CCC"), at the time that you opened your Rightslink account and that are available at any time at <http://myaccount.copyright.com>).

Limited License

With reference to your request to reuse material on which Springer controls the copyright, permission is granted for the use indicated in your enquiry under the following conditions:

- Licenses are for one-time use only with a maximum distribution equal to the number stated in your request.

- Springer material represents original material which does not carry references to other sources. If the material in question appears with a credit to another source, this permission is not valid and authorization has to be obtained from the original copyright holder.

- This permission

- is non-exclusive

- is only valid if no personal rights, trademarks, or competitive products are infringed.

- explicitly excludes the right for derivatives.

- Springer does not supply original artwork or content.

- According to the format which you have selected, the following conditions apply accordingly:

- **Print and Electronic:** This License include use in electronic form provided it is password protected, on intranet, or CD-Rom/DVD or E-book/E-journal. It may not be republished in electronic open access.

- **Print:** This License excludes use in electronic form.

- **Electronic:** This License only pertains to use in electronic form provided it is password protected, on intranet, or CD-Rom/DVD or E-book/E-journal. It may not be republished in electronic open access.

For any electronic use not mentioned, please contact Springer at permissions.springer@spi-global.com.

- Although Springer controls the copyright to the material and is entitled to negotiate on rights, this license is only valid subject to courtesy information to the author (address is given in the article/chapter).

- If you are an STM Signatory or your work will be published by an STM Signatory and you are requesting to reuse figures/tables/illustrations or single text extracts, permission is granted according to STM Permissions Guidelines: <http://www.stm-assoc.org/permissions-guidelines/>

For any electronic use not mentioned in the Guidelines, please contact Springer at permissions.springer@spi-global.com. If you request to reuse more content than stipulated in the STM Permissions Guidelines, you will be charged a permission fee for the excess content.

Permission is valid upon payment of the fee as indicated in the licensing process. If permission is granted free of charge on this occasion, that does not prejudice any rights we might have to charge for reproduction of our copyrighted material in the future.

-If your request is for reuse in a Thesis, permission is granted free of charge under the following conditions:

This license is valid for one-time use only for the purpose of defending your thesis and with a maximum of 100 extra copies in paper. If the thesis is going to be published, permission needs to be reobtained.

- includes use in an electronic form, provided it is an author-created version of the thesis on his/her own website and his/her university's repository, including UMI (according to the definition on the Sherpa website: <http://www.sherpa.ac.uk/romeo/>);

- is subject to courtesy information to the co-author or corresponding author.

Geographic Rights: Scope

Licenses may be exercised anywhere in the world.

Altering/Modifying Material: Not Permitted

Figures, tables, and illustrations may be altered minimally to serve your work. You may not alter or modify text in any manner. Abbreviations, additions, deletions and/or any other alterations shall be made only with prior written authorization of the author(s).

Reservation of Rights

Springer reserves all rights not specifically granted in the combination of (i) the license details provided by you and accepted in the course of this licensing transaction and (ii) these terms and conditions and (iii) CCC's Billing and Payment terms and conditions.

License Contingent on Payment

While you may exercise the rights licensed immediately upon issuance of the license at the end of the licensing process for the transaction, provided that you have disclosed complete and accurate details of your proposed use, no license is finally effective unless and until full payment is received from you (either by Springer or by CCC) as provided in CCC's Billing and Payment terms and conditions. If full payment is not received by the date due, then any license preliminarily granted shall be deemed automatically revoked and shall be void as if never granted. Further, in the event that you breach any of these terms and conditions or any of CCC's Billing and Payment terms and conditions, the license is automatically revoked and shall be void as if never granted. Use of materials as described in a revoked license, as well as any use of the materials beyond the scope of an unrevoked license, may constitute copyright infringement and Springer reserves the right to take any and all action to protect its copyright in the materials.

Copyright Notice: Disclaimer

You must include the following copyright and permission notice in connection with any reproduction of the licensed material:

"Springer book/journal title, chapter/article title, volume, year of publication, page, name(s) of author(s), (original copyright notice as given in the publication in which the material was originally published) "With permission of Springer"

In case of use of a graph or illustration, the caption of the graph or illustration must be included, as it is indicated in the original publication.

Warranties: None

Springer makes no representations or warranties with respect to the licensed material and adopts on its own behalf the limitations and disclaimers established by CCC on its behalf in its Billing and Payment terms and conditions for this licensing transaction.

Indemnity

You hereby indemnify and agree to hold harmless Springer and CCC, and their respective officers, directors, employees and agents, from and against any and all claims arising out of your use of the licensed material other than as specifically authorized pursuant to this license.

No Transfer of License

This license is personal to you and may not be sublicensed, assigned, or transferred by you without Springer's written permission.

No Amendment Except in Writing

This license may not be amended except in a writing signed by both parties (or, in the case of Springer, by CCC on Springer's behalf).

Objection to Contrary Terms

Springer hereby objects to any terms contained in any purchase order, acknowledgment, check endorsement or other writing prepared by you, which terms are inconsistent with these terms and conditions or CCC's Billing and Payment terms and conditions. These terms and conditions, together with CCC's Billing and Payment terms and conditions (which are incorporated herein), comprise the entire agreement between you and Springer (and CCC) concerning this licensing transaction. In the event of any conflict between your obligations

established by these terms and conditions and those established by CCC's Billing and Payment terms and conditions, these terms and conditions shall control.

Jurisdiction

All disputes that may arise in connection with this present License, or the breach thereof, shall be settled exclusively by arbitration, to be held in the Federal Republic of Germany, in accordance with German law.

Other conditions:

V 12AUG2015

Questions? customercare@copyright.com or +1-855-239-3415 (toll free in the US) or +1-978-646-2777.

**Taylor and Francis Group LLC Books LICENSE
TERMS AND CONDITIONS**

Aug 15, 2017

This is a License Agreement between Mr. Philip Boahene ("You") and Taylor and Francis Group LLC Books ("Taylor and Francis Group LLC Books") provided by Copyright Clearance Center ("CCC"). The license consists of your order details, the terms and conditions provided by Taylor and Francis Group LLC Books, and the payment terms and conditions.

All payments must be made in full to CCC. For payment instructions, please see information listed at the bottom of this form.

License Number	4170391393143
License date	Aug 15, 2017
Licensed content publisher	Taylor and Francis Group LLC Books
Licensed content title	Fischer-Tropsch Synthesis, Catalysts, and Catalysis : Advances and Applications
Licensed content date	Mar 14, 2016
Type of Use	Thesis/Dissertation
Requestor type	Author of requested content
Format	Electronic
Portion	chapter/article
Number of pages in chapter/article	20
Title or numeric reference of the portion(s)	pages 275-294 (entire chapter)
Title of the article or chapter the portion is from	Chapter 15
Editor of portion(s)	n/a
Author of portion(s)	Philip Boahene
Volume of serial or monograph.	n/a
Issue, if republishing an article from a serial	n/a
Page range of the portion	275-294
Publication date of portion	2016
Rights for	Main product
Duration of use	Life of current edition
Creation of copies for the disabled	no
With minor editing privileges	no
For distribution to	United States
In the following language(s)	Original language of publication
With incidental promotional use	no

The lifetime unit quantity of new product	Up to 499
Made available in the following markets	education
The requesting person/organization is:	Philip Boahene
Order reference number	cao2722
Author/Editor	Philip Boahene
The standard identifier of New Work	n/a
The proposed price	n/a
Title of New Work	CATALYSTS DEVELOPMENT FOR THE CONVERSION OF SYNGAS TO HIGHER ALCOHOLS USING ALKALI-PROMOTED MOS ₂ -BASED CATALYSTS OVER CARBON SUPPORTS
Publisher of New Work	University of Saskatchewan
Expected publication date	Sep 2017
Estimated size (pages)	285
Total (may include CCC user fee)	0.00 USD

Terms and Conditions

TERMS AND CONDITIONS

The following terms are individual to this publisher:

Taylor and Francis Group and Informa healthcare are division of Informa plc. Permission will be void if material exceeds 10% of all the total pages in your publication and over 20% of the original publication. This includes permission granted by Informa plc and all of its subsidiaries.

Other Terms and Conditions:

STANDARD TERMS AND CONDITIONS

1. Description of Service; Defined Terms. This Republication License enables the User to obtain licenses for republication of one or more copyrighted works as described in detail on the relevant Order Confirmation (the "Work(s)"). Copyright Clearance Center, Inc. ("CCC") grants licenses through the Service on behalf of the rightsholder identified on the Order Confirmation (the "Rightsholder"). "Republication", as used herein, generally means the inclusion of a Work, in whole or in part, in a new work or works, also as described on the Order Confirmation. "User", as used herein, means the person or entity making such republication.

2. The terms set forth in the relevant Order Confirmation, and any terms set by the Rightsholder with respect to a particular Work, govern the terms of use of Works in connection with the Service. By using the Service, the person transacting for a republication license on behalf of the User represents and warrants that he/she/it (a) has been duly authorized by the User to accept, and hereby does accept, all such terms and conditions on behalf of User, and (b) shall inform User of all such terms and conditions. In the event such person is a "freelancer" or other third party independent of User and CCC, such party shall be deemed jointly a "User" for purposes of these terms and conditions. In any event, User shall be deemed to have accepted and agreed to all such terms and conditions if User republishes the Work in any fashion.

3. Scope of License; Limitations and Obligations.

3.1 All Works and all rights therein, including copyright rights, remain the sole and exclusive property of the Rightsholder. The license created by the exchange of an Order Confirmation (and/or any invoice) and payment by User of the full amount set forth on that

document includes only those rights expressly set forth in the Order Confirmation and in these terms and conditions, and conveys no other rights in the Work(s) to User. All rights not expressly granted are hereby reserved.

3.2 General Payment Terms: You may pay by credit card or through an account with us payable at the end of the month. If you and we agree that you may establish a standing account with CCC, then the following terms apply: Remit Payment to: Copyright Clearance Center, 29118 Network Place, Chicago, IL 60673-1291. Payments Due: Invoices are payable upon their delivery to you (or upon our notice to you that they are available to you for downloading). After 30 days, outstanding amounts will be subject to a service charge of 1-1/2% per month or, if less, the maximum rate allowed by applicable law. Unless otherwise specifically set forth in the Order Confirmation or in a separate written agreement signed by CCC, invoices are due and payable on "net 30" terms. While User may exercise the rights licensed immediately upon issuance of the Order Confirmation, the license is automatically revoked and is null and void, as if it had never been issued, if complete payment for the license is not received on a timely basis either from User directly or through a payment agent, such as a credit card company.

3.3 Unless otherwise provided in the Order Confirmation, any grant of rights to User (i) is "one-time" (including the editions and product family specified in the license), (ii) is non-exclusive and non-transferable and (iii) is subject to any and all limitations and restrictions (such as, but not limited to, limitations on duration of use or circulation) included in the Order Confirmation or invoice and/or in these terms and conditions. Upon completion of the licensed use, User shall either secure a new permission for further use of the Work(s) or immediately cease any new use of the Work(s) and shall render inaccessible (such as by deleting or by removing or severing links or other locators) any further copies of the Work (except for copies printed on paper in accordance with this license and still in User's stock at the end of such period).

3.4 In the event that the material for which a republication license is sought includes third party materials (such as photographs, illustrations, graphs, inserts and similar materials) which are identified in such material as having been used by permission, User is responsible for identifying, and seeking separate licenses (under this Service or otherwise) for, any of such third party materials; without a separate license, such third party materials may not be used.

3.5 Use of proper copyright notice for a Work is required as a condition of any license granted under the Service. Unless otherwise provided in the Order Confirmation, a proper copyright notice will read substantially as follows: "Republished with permission of [Rightsholder's name], from [Work's title, author, volume, edition number and year of copyright]; permission conveyed through Copyright Clearance Center, Inc. " Such notice must be provided in a reasonably legible font size and must be placed either immediately adjacent to the Work as used (for example, as part of a by-line or footnote but not as a separate electronic link) or in the place where substantially all other credits or notices for the new work containing the republished Work are located. Failure to include the required notice results in loss to the Rightsholder and CCC, and the User shall be liable to pay liquidated damages for each such failure equal to twice the use fee specified in the Order Confirmation, in addition to the use fee itself and any other fees and charges specified.

3.6 User may only make alterations to the Work if and as expressly set forth in the Order Confirmation. No Work may be used in any way that is defamatory, violates the rights of third parties (including such third parties' rights of copyright, privacy, publicity, or other tangible or intangible property), or is otherwise illegal, sexually explicit or obscene. In addition, User may not conjoin a Work with any other material that may result in damage to the reputation of the Rightsholder. User agrees to inform CCC if it becomes aware of any infringement of any rights in a Work and to cooperate with any reasonable request of CCC or the Rightsholder in connection therewith.

4. Indemnity. User hereby indemnifies and agrees to defend the Rightsholder and CCC, and their respective employees and directors, against all claims, liability, damages, costs and

expenses, including legal fees and expenses, arising out of any use of a Work beyond the scope of the rights granted herein, or any use of a Work which has been altered in any unauthorized way by User, including claims of defamation or infringement of rights of copyright, publicity, privacy or other tangible or intangible property.

5. **Limitation of Liability.** UNDER NO CIRCUMSTANCES WILL CCC OR THE RIGHTSHOLDER BE LIABLE FOR ANY DIRECT, INDIRECT, CONSEQUENTIAL OR INCIDENTAL DAMAGES (INCLUDING WITHOUT LIMITATION DAMAGES FOR LOSS OF BUSINESS PROFITS OR INFORMATION, OR FOR BUSINESS INTERRUPTION) ARISING OUT OF THE USE OR INABILITY TO USE A WORK, EVEN IF ONE OF THEM HAS BEEN ADVISED OF THE POSSIBILITY OF SUCH DAMAGES. In any event, the total liability of the Rightsholder and CCC (including their respective employees and directors) shall not exceed the total amount actually paid by User for this license. User assumes full liability for the actions and omissions of its principals, employees, agents, affiliates, successors and assigns.

6. **Limited Warranties.** THE WORK(S) AND RIGHT(S) ARE PROVIDED "AS IS". CCC HAS THE RIGHT TO GRANT TO USER THE RIGHTS GRANTED IN THE ORDER CONFIRMATION DOCUMENT. CCC AND THE RIGHTSHOLDER DISCLAIM ALL OTHER WARRANTIES RELATING TO THE WORK(S) AND RIGHT(S), EITHER EXPRESS OR IMPLIED, INCLUDING WITHOUT LIMITATION IMPLIED WARRANTIES OF MERCHANTABILITY OR FITNESS FOR A PARTICULAR PURPOSE. ADDITIONAL RIGHTS MAY BE REQUIRED TO USE ILLUSTRATIONS, GRAPHS, PHOTOGRAPHS, ABSTRACTS, INSERTS OR OTHER PORTIONS OF THE WORK (AS OPPOSED TO THE ENTIRE WORK) IN A MANNER CONTEMPLATED BY USER; USER UNDERSTANDS AND AGREES THAT NEITHER CCC NOR THE RIGHTSHOLDER MAY HAVE SUCH ADDITIONAL RIGHTS TO GRANT.

7. **Effect of Breach.** Any failure by User to pay any amount when due, or any use by User of a Work beyond the scope of the license set forth in the Order Confirmation and/or these terms and conditions, shall be a material breach of the license created by the Order Confirmation and these terms and conditions. Any breach not cured within 30 days of written notice thereof shall result in immediate termination of such license without further notice. Any unauthorized (but licensable) use of a Work that is terminated immediately upon notice thereof may be liquidated by payment of the Rightsholder's ordinary license price therefor; any unauthorized (and unlicensable) use that is not terminated immediately for any reason (including, for example, because materials containing the Work cannot reasonably be recalled) will be subject to all remedies available at law or in equity, but in no event to a payment of less than three times the Rightsholder's ordinary license price for the most closely analogous licensable use plus Rightsholder's and/or CCC's costs and expenses incurred in collecting such payment.

8. Miscellaneous.

8.1 User acknowledges that CCC may, from time to time, make changes or additions to the Service or to these terms and conditions, and CCC reserves the right to send notice to the User by electronic mail or otherwise for the purposes of notifying User of such changes or additions; provided that any such changes or additions shall not apply to permissions already secured and paid for.

8.2 Use of User-related information collected through the Service is governed by CCC's privacy policy, available online here:

<http://www.copyright.com/content/cc3/en/tools/footer/privacypolicy.html>.

8.3 The licensing transaction described in the Order Confirmation is personal to User. Therefore, User may not assign or transfer to any other person (whether a natural person or an organization of any kind) the license created by the Order Confirmation and these terms and conditions or any rights granted hereunder; provided, however, that User may assign such license in its entirety on written notice to CCC in the event of a transfer of all or substantially all of User's rights in the new material which includes the Work(s) licensed under this Service.

8.4 No amendment or waiver of any terms is binding unless set forth in writing and signed by the parties. The Rightsholder and CCC hereby object to any terms contained in any writing prepared by the User or its principals, employees, agents or affiliates and purporting to govern or otherwise relate to the licensing transaction described in the Order Confirmation, which terms are in any way inconsistent with any terms set forth in the Order Confirmation and/or in these terms and conditions or CCC's standard operating procedures, whether such writing is prepared prior to, simultaneously with or subsequent to the Order Confirmation, and whether such writing appears on a copy of the Order Confirmation or in a separate instrument.

8.5 The licensing transaction described in the Order Confirmation document shall be governed by and construed under the law of the State of New York, USA, without regard to the principles thereof of conflicts of law. Any case, controversy, suit, action, or proceeding arising out of, in connection with, or related to such licensing transaction shall be brought, at CCC's sole discretion, in any federal or state court located in the County of New York, State of New York, USA, or in any federal or state court whose geographical jurisdiction covers the location of the Rightsholder set forth in the Order Confirmation. The parties expressly submit to the personal jurisdiction and venue of each such federal or state court. If you have any comments or questions about the Service or Copyright Clearance Center, please contact us at 978-750-8400 or send an e-mail to info@copyright.com.

v 1.1

Questions? customercare@copyright.com or +1-855-239-3415 (toll free in the US) or +1-978-646-2777.

**ELSEVIER LICENSE
TERMS AND CONDITIONS**

Aug 14, 2017

This Agreement between Mr. Philip Boahene ("You") and Elsevier ("Elsevier") consists of your license details and the terms and conditions provided by Elsevier and Copyright Clearance Center.

License Number	4167780074616
License date	Aug 14, 2017
Licensed Content Publisher	Elsevier
Licensed Content Publication	Catalysis Today
Licensed Content Title	Syngas conversion to higher alcohols: A comparative study of acid and base-treated mesoporous carbon-supported KCoRhMoS ₂ catalysts
Licensed Content Author	Philip E. Boahene,Ajay K. Dalai,Ramaswami Sammynaiken
Licensed Content Date	Aug 1, 2017
Licensed Content Volume	291
Licensed Content Issue	n/a
Licensed Content Pages	18
Start Page	106
End Page	123
Type of Use	reuse in a thesis/dissertation
Intended publisher of new work	other
Portion	full article
Format	both print and electronic
Are you the author of this Elsevier article?	Yes
Will you be translating?	No
Title of your thesis/dissertation	Catalysts development for the conversion of syngas to higher alcohols using alkali-promoted mos ₂ -based catalysts over carbon supports
Expected completion date	Sep 2017
Estimated size (number of pages)	280
Requestor Location	Mr. Philip Boahene 57 Campus Drive Saskatoon, SK S7N5A9 Canada Attn: Mr. Philip Boahene
Total	0.00 USD
Terms and Conditions	

1. The publisher for this copyrighted material is Elsevier. By clicking "accept" in connection with completing this licensing transaction, you agree that the following terms and conditions apply to this transaction (along with the Billing and Payment terms and conditions established by Copyright Clearance Center, Inc. ("CCC"), at the time that you opened your Rightslink account and that are available at any time at <http://myaccount.copyright.com>).

GENERAL TERMS

2. Elsevier hereby grants you permission to reproduce the aforementioned material subject to the terms and conditions indicated.

3. Acknowledgement: If any part of the material to be used (for example, figures) has appeared in our publication with credit or acknowledgement to another source, permission must also be sought from that source. If such permission is not obtained then that material may not be included in your publication/copies. Suitable acknowledgement to the source must be made, either as a footnote or in a reference list at the end of your publication, as follows:

"Reprinted from Publication title, Vol /edition number, Author(s), Title of article / title of chapter, Pages No., Copyright (Year), with permission from Elsevier [OR APPLICABLE SOCIETY COPYRIGHT OWNER]." Also Lancet special credit - "Reprinted from The Lancet, Vol. number, Author(s), Title of article, Pages No., Copyright (Year), with permission from Elsevier."

4. Reproduction of this material is confined to the purpose and/or media for which permission is hereby given.

5. Altering/Modifying Material: Not Permitted. However figures and illustrations may be altered/adapted minimally to serve your work. Any other abbreviations, additions, deletions and/or any other alterations shall be made only with prior written authorization of Elsevier Ltd. (Please contact Elsevier at permissions@elsevier.com). No modifications can be made to any Lancet figures/tables and they must be reproduced in full.

6. If the permission fee for the requested use of our material is waived in this instance, please be advised that your future requests for Elsevier materials may attract a fee.

7. Reservation of Rights: Publisher reserves all rights not specifically granted in the combination of (i) the license details provided by you and accepted in the course of this licensing transaction, (ii) these terms and conditions and (iii) CCC's Billing and Payment terms and conditions.

8. License Contingent Upon Payment: While you may exercise the rights licensed immediately upon issuance of the license at the end of the licensing process for the transaction, provided that you have disclosed complete and accurate details of your proposed use, no license is finally effective unless and until full payment is received from you (either by publisher or by CCC) as provided in CCC's Billing and Payment terms and conditions. If full payment is not received on a timely basis, then any license preliminarily granted shall be deemed automatically revoked and shall be void as if never granted. Further, in the event that you breach any of these terms and conditions or any of CCC's Billing and Payment terms and conditions, the license is automatically revoked and shall be void as if never granted. Use of materials as described in a revoked license, as well as any use of the materials beyond the scope of an unrevoked license, may constitute copyright infringement and publisher reserves the right to take any and all action to protect its copyright in the materials.

9. Warranties: Publisher makes no representations or warranties with respect to the licensed material.

10. Indemnity: You hereby indemnify and agree to hold harmless publisher and CCC, and their respective officers, directors, employees and agents, from and against any and all claims arising out of your use of the licensed material other than as specifically authorized pursuant to this license.

11. No Transfer of License: This license is personal to you and may not be sublicensed, assigned, or transferred by you to any other person without publisher's written permission.

12. **No Amendment Except in Writing:** This license may not be amended except in a writing signed by both parties (or, in the case of publisher, by CCC on publisher's behalf).

13. **Objection to Contrary Terms:** Publisher hereby objects to any terms contained in any purchase order, acknowledgment, check endorsement or other writing prepared by you, which terms are inconsistent with these terms and conditions or CCC's Billing and Payment terms and conditions. These terms and conditions, together with CCC's Billing and Payment terms and conditions (which are incorporated herein), comprise the entire agreement between you and publisher (and CCC) concerning this licensing transaction. In the event of any conflict between your obligations established by these terms and conditions and those established by CCC's Billing and Payment terms and conditions, these terms and conditions shall control.

14. **Revocation:** Elsevier or Copyright Clearance Center may deny the permissions described in this License at their sole discretion, for any reason or no reason, with a full refund payable to you. Notice of such denial will be made using the contact information provided by you. Failure to receive such notice will not alter or invalidate the denial. In no event will Elsevier or Copyright Clearance Center be responsible or liable for any costs, expenses or damage incurred by you as a result of a denial of your permission request, other than a refund of the amount(s) paid by you to Elsevier and/or Copyright Clearance Center for denied permissions.

LIMITED LICENSE

The following terms and conditions apply only to specific license types:

15. **Translation:** This permission is granted for non-exclusive world **English** rights only unless your license was granted for translation rights. If you licensed translation rights you may only translate this content into the languages you requested. A professional translator must perform all translations and reproduce the content word for word preserving the integrity of the article.

16. **Posting licensed content on any Website:** The following terms and conditions apply as follows: Licensing material from an Elsevier journal: All content posted to the web site must maintain the copyright information line on the bottom of each image; A hyper-text must be included to the Homepage of the journal from which you are licensing at <http://www.sciencedirect.com/science/journal/xxxxx> or the Elsevier homepage for books at <http://www.elsevier.com>; Central Storage: This license does not include permission for a scanned version of the material to be stored in a central repository such as that provided by Heron/XanEdu.

Licensing material from an Elsevier book: A hyper-text link must be included to the Elsevier homepage at <http://www.elsevier.com>. All content posted to the web site must maintain the copyright information line on the bottom of each image.

Posting licensed content on Electronic reserve: In addition to the above the following clauses are applicable: The web site must be password-protected and made available only to bona fide students registered on a relevant course. This permission is granted for 1 year only. You may obtain a new license for future website posting.

17. **For journal authors:** the following clauses are applicable in addition to the above:

Preprints:

A preprint is an author's own write-up of research results and analysis, it has not been peer-reviewed, nor has it had any other value added to it by a publisher (such as formatting, copyright, technical enhancement etc.).

Authors can share their preprints anywhere at any time. Preprints should not be added to or enhanced in any way in order to appear more like, or to substitute for, the final versions of articles however authors can update their preprints on arXiv or RePEc with their Accepted Author Manuscript (see below).

If accepted for publication, we encourage authors to link from the preprint to their formal publication via its DOI. Millions of researchers have access to the formal publications on ScienceDirect, and so links will help users to find, access, cite and use the best available

version. Please note that Cell Press, The Lancet and some society-owned have different preprint policies. Information on these policies is available on the journal homepage.

Accepted Author Manuscripts: An accepted author manuscript is the manuscript of an article that has been accepted for publication and which typically includes author-incorporated changes suggested during submission, peer review and editor-author communications.

Authors can share their accepted author manuscript:

- immediately
 - via their non-commercial person homepage or blog
 - by updating a preprint in arXiv or RePEc with the accepted manuscript
 - via their research institute or institutional repository for internal institutional uses or as part of an invitation-only research collaboration work-group
 - directly by providing copies to their students or to research collaborators for their personal use
 - for private scholarly sharing as part of an invitation-only work group on commercial sites with which Elsevier has an agreement
- After the embargo period
 - via non-commercial hosting platforms such as their institutional repository
 - via commercial sites with which Elsevier has an agreement

In all cases accepted manuscripts should:

- link to the formal publication via its DOI
- bear a CC-BY-NC-ND license - this is easy to do
- if aggregated with other manuscripts, for example in a repository or other site, be shared in alignment with our hosting policy not be added to or enhanced in any way to appear more like, or to substitute for, the published journal article.

Published journal article (JPA): A published journal article (PJA) is the definitive final record of published research that appears or will appear in the journal and embodies all value-adding publishing activities including peer review co-ordination, copy-editing, formatting, (if relevant) pagination and online enrichment.

Policies for sharing publishing journal articles differ for subscription and gold open access articles:

Subscription Articles: If you are an author, please share a link to your article rather than the full-text. Millions of researchers have access to the formal publications on ScienceDirect, and so links will help your users to find, access, cite, and use the best available version.

Theses and dissertations which contain embedded PJAs as part of the formal submission can be posted publicly by the awarding institution with DOI links back to the formal publications on ScienceDirect.

If you are affiliated with a library that subscribes to ScienceDirect you have additional private sharing rights for others' research accessed under that agreement. This includes use for classroom teaching and internal training at the institution (including use in course packs and courseware programs), and inclusion of the article for grant funding purposes.

Gold Open Access Articles: May be shared according to the author-selected end-user license and should contain a [CrossMark logo](#), the end user license, and a DOI link to the formal publication on ScienceDirect.

Please refer to Elsevier's [posting policy](#) for further information.

18. **For book authors** the following clauses are applicable in addition to the above:

Authors are permitted to place a brief summary of their work online only. You are not allowed to download and post the published electronic version of your chapter, nor may you scan the printed edition to create an electronic version. **Posting to a repository:** Authors are permitted to post a summary of their chapter only in their institution's repository.

19. Thesis/Dissertation: If your license is for use in a thesis/dissertation your thesis may be submitted to your institution in either print or electronic form. Should your thesis be published commercially, please reapply for permission. These requirements include permission for the Library and Archives of Canada to supply single copies, on demand, of the complete thesis and include permission for Proquest/UMI to supply single copies, on demand, of the complete thesis. Should your thesis be published commercially, please reapply for permission. Theses and dissertations which contain embedded PJAs as part of the formal submission can be posted publicly by the awarding institution with DOI links back to the formal publications on ScienceDirect.

Elsevier Open Access Terms and Conditions

You can publish open access with Elsevier in hundreds of open access journals or in nearly 2000 established subscription journals that support open access publishing. Permitted third party re-use of these open access articles is defined by the author's choice of Creative Commons user license. See our [open access license policy](#) for more information.

Terms & Conditions applicable to all Open Access articles published with Elsevier:

Any reuse of the article must not represent the author as endorsing the adaptation of the article nor should the article be modified in such a way as to damage the author's honour or reputation. If any changes have been made, such changes must be clearly indicated.

The author(s) must be appropriately credited and we ask that you include the end user license and a DOI link to the formal publication on ScienceDirect.

If any part of the material to be used (for example, figures) has appeared in our publication with credit or acknowledgement to another source it is the responsibility of the user to ensure their reuse complies with the terms and conditions determined by the rights holder.

Additional Terms & Conditions applicable to each Creative Commons user license:

CC BY: The CC-BY license allows users to copy, to create extracts, abstracts and new works from the Article, to alter and revise the Article and to make commercial use of the Article (including reuse and/or resale of the Article by commercial entities), provided the user gives appropriate credit (with a link to the formal publication through the relevant DOI), provides a link to the license, indicates if changes were made and the licensor is not represented as endorsing the use made of the work. The full details of the license are available at <http://creativecommons.org/licenses/by/4.0>.

CC BY NC SA: The CC BY-NC-SA license allows users to copy, to create extracts, abstracts and new works from the Article, to alter and revise the Article, provided this is not done for commercial purposes, and that the user gives appropriate credit (with a link to the formal publication through the relevant DOI), provides a link to the license, indicates if changes were made and the licensor is not represented as endorsing the use made of the work. Further, any new works must be made available on the same conditions. The full details of the license are available at <http://creativecommons.org/licenses/by-nc-sa/4.0>.

CC BY NC ND: The CC BY-NC-ND license allows users to copy and distribute the Article, provided this is not done for commercial purposes and further does not permit distribution of the Article if it is changed or edited in any way, and provided the user gives appropriate credit (with a link to the formal publication through the relevant DOI), provides a link to the license, and that the licensor is not represented as endorsing the use made of the work. The full details of the license are available at <http://creativecommons.org/licenses/by-nc-nd/4.0>. Any commercial reuse of Open Access articles published with a CC BY NC SA or CC BY NC ND license requires permission from Elsevier and will be subject to a fee.

Commercial reuse includes:

- Associating advertising with the full text of the Article
- Charging fees for document delivery or access
- Article aggregation
- Systematic distribution via e-mail lists or share buttons

Posting or linking by commercial companies for use by customers of those companies.

20. Other Conditions:

v1.9

Questions? customercare@copyright.com or +1-855-239-3415 (toll free in the US) or +1-978-646-2777.



Welcome, Philip
Not you?

[Log out](#)
[Cart \(0\)](#)
[Manage Account](#)
[Feedback](#)
[Help](#)
[Live Help](#)
[Get Permission / Find Title](#)

[Advanced Search Options](#)

Fischer-Tropsch Synthesis, Catalysts, and Catalysis : Advances and Applications

ISBN: 9781466555303 **Language:** English
Publication year(s): 2016
Author/Editor: Davis, Burtron ; Ocelli, Mario
Publication type: e-Book
Publisher: CRC Press
Rightsholder: TAYLOR & FRANCIS GROUP LLC - BOOKS

Permission type selected: Republish or display content

Type of use selected: Thesis/Dissertation

[Select different permission](#)

Terms and conditions apply to this permission type
[View details](#)

Enter the following details to determine a price:

Describe who will republish the content (person or entity)...

I would like to use...

Chapter/Article Page range (Examples: ii, iv-vi or 3, 7-10; max. range of 100 pages)

Total Number of pages in chapter/article (Enter total number of pages (< 100))

Does the content being licensed represent 20.0% or more of the new work/product?

I want rights for...

My format is... Print Electronic

Duration of use...

Creation of copies for the disabled...

With minor editing privileges...

For distribution to...

In the following language(s)...

With incidental promotional use...

The lifetime unit quantity of new product...

Promo code... (optional)

[Get Price](#)

[About Us](#) | [Privacy Policy](#) | [Terms & Conditions](#) | [Pay an Invoice](#)

Copyright 2017 Copyright Clearance Center

International Journal of Petrochemical Science & Engineering

To Whom It May Concern,

We (IPCSE) are giving **Copy Rights** © to *Dr. Philip E Boahene, Dr. Ramaswami Sammynaike and Dr. Ajay K Dalai* for “*Syngas Conversion to Higher Alcohols: Application of novel K-Promoted CoRhMo Catalysts Supported over Carbon Nanohorns and its by-Products*” published in our Journal.



Vincent Oscar
Editorial Office-MedCrave Group